Mechanistic characterisation of the *Escherichia coli* ammonium transporter AmtB

by

Gordon Williamson

Supervisor 1: Dr Arnaud Javelle **Supervisor 2:** Prof. Iain Hunter

A thesis submitted in fulfilment of the requirements for the degree of Doctor of Philosophy at the University of Strathclyde.

Strathclyde Institute of Pharmaceutical and Biomedical Sciences

October 2020

Declaration

‘This thesis is the result of the author’s original research. It has been composed by the author and has not been previously submitted for examination which has led to the award of a degree.’

Signed:  Date: 16th October 2020

Publications

One paper has been published as a result of the work carried out through this project. Much of its contents have been presented as part of Chapter 4. The paper can be found in Appendix A of this thesis, and the reference is listed below.

Gordon Williamson, Giulia Tamburrino, Adriana Bizior, Mélanie Boeckstaens, Gaëtan Dias Mirandela, Marcus G Bage, Andrei Pisliakov, Callum M Ives, Eilidh Terras, Paul A Hoskisson, Anna Maria Marini, Ulrich Zachariae, and Arnaud Javelle. (2020) 'A two-lane mechanism for selective biological ammonium transport', *eLife*., 9, p. e57183.

In addition, the data presented in Chapter 5 will form the core of another paper which is currently in preparation.

Gordon Williamson, Giulia Tamburrino, Adriana Bizior, Mélanie Boeckstaens, Derek Hardie, Paul A Hoskisson, Anna Maria Marini, Ulrich Zachariae, and Arnaud Javelle 'The conserved twin-His motif governs a mechanistic switch in *E. coli* AmtB' *manuscript in preparation*

Acknowledgements

The purpose of this document is to encapsulate, chronicle, and explain three years of hard work in the laboratory. It is also supposed to attest that the experience and skills I've developed within that time are sufficient to be considered an expert in my field, and become a doctor. However, this is more than the culmination of just three years and my experiences reach far beyond the lab. I cannot understate the number of lives which have touched mine, and the influence they've had in forging the person I am today. Fortuitously, this is the only section of my thesis which is immune to red ink, so I can ramble and rave to my heart's content and express my thanks to all those people.

First and foremost, I have to thank Dr Arnaud Javelle, my primary supervisor, for being a guiding light. Arnaud believed that I could do a PhD before even I did, and his support and encouragement have been constant since our first meeting many years ago. He has always been willing to share his knowledge and he's taught me many lessons, personal and professional, over the last three years. I couldn't have picked a better mentor. I'd also like to thank Prof. Iain Hunter for being my secondary supervisor. Iain is a seemingly endless source of interesting questions, advice, and surprising anecdotes.

I'd like to thank both Prof. Gwyn Gould and Prof. Ian Collinson for agreeing to be my examiners. I'm certain they will make it an unforgettable experience, and I hope they have more fun reading this thesis than I did writing it.

I also express my gratitude to all our collaborators, as without their efforts and expertise, my work wouldn't have been possible. This includes Dr Giulia Tamburrino and Prof. Ulrich Zachariae from the University of Dundee for performing the Molecular Dynamic Simulations and providing their computational expertise. In addition, I thank Dr Mélanie Boeckstaens and Dr Anna-Maria Marini for carrying out all the yeast complementation work and for consistently providing constructive and insightful comments throughout our collaborations together. I was fortunate enough to work with Mélanie for a brief period during my project and was inspired by her work-ethic and intelligence.

It is my fondest hope that the future will present an opportunity for me to work with them again.

Now my attention turns to other members of the Javelle group. Gaëtan was entering his third year when I started in the lab. Despite the stress that entails, Gaëtan somehow found the time to teach me pretty much everything I needed to know about protein purification and SSME. I'll always be grateful for his help, his teaching, and his friendship. In my final year, this had come full circle and I found myself teaching our new first year: Adriana Bizior. I'd like to thank her for trusting me to teach, putting up with my puns, and for moving the project forward. It feels like passing the Olympic Torch, and I can't wait to see the flame burn brighter in her care.

On the topic of teaching, I've spent a lot of time supervising undergraduate and postgraduate students. I feel like I've been lucky, as all of my students have been kind, enthusiast, and have brought a lot of fun to the lab. I'd like to thank them all: Derek, Eilidh, Margarida, Nawal, Adriana, Harry, Barry, Cortlyn, Priya, Thomas, and Cameron.

If Hamnett wing level 6 is the stage upon which my PhD played out, then my colleagues were an all-star cast. I've made so many friends and happy memories on this floor, that to recount them all would require a separate thesis. For a decent chunk of my PhD, I was the sole student in the Javelle group, but it never felt that way. With Ally as a bay buddy and light in the darkness it would be hard to feel alone, even when she **Oban**doned me. Much to the chagrin of everyone within earshot, Parra has helped me practice the philosophy to go along with my doctorate. If a topic exists we have discussed, and probably disagreed, about it. When it comes to baking cakes and lifting weights, Ainsley just can't be Beaton. Whether spotting me in the gym or the lab, or laughing at a pun which didn't land, I'm glad she's always had my back. David has always hit the Mark with jokes and since he and I joined forces, there has been an ex**pun**entional increase in puns within the lab. We even started a pun book which I thought was a truly novel idea. I was also never lacking in recommendations for novels, films, or shows thanks to Jonny. Between

Haikyuu, *Hunter x Hunter,* and *Westworld* he might have salvaged my work-life balance. Follow-up discussions with Emily, Darren, and John (the world's best Postdoc/DM) made these all the sweeter. Finally, I have to mention the lab's soft-boiled egg: Stuart Woods. He's very kind, sweet, and completely non-threatening, and I think it's vital that this be noted in a formal document that he can't edit. I can't list all my happy memories, but I can list names because this section has no word limit: Adriana, Ainsley, Alemão, Ally, Anna, Arnaud, Bea, Becca, Charlie, Charlotte, Craig, David, Darren, Eilidh, Emily, Elmira, Florent, Gaëtan, Gareth, Gillian, Hafiz, Hannah, Iain, John, Jonny, Jordan, Josephine, Josi, Kate, Kerry, Kirsty, Laia, Liam, Lily, Lis, Nick, Maria, Meg, Molly, Morgan, Paul Herron, Paul Hoskisson, Stuart, Thaer, Tiago, Walid. I'm thankful to the entire floor for these memories and more, and for showing me kindness far beyond anything I deserve.

It's a little-known fact, but there was a pandemic in 2020 (my final year). I ended up in a new flat and living alone for the duration of lockdown. I want to thank Jonny, Adam, and Jordan for keeping me sane throughout, because whether we wanted it or not, we'd started a war with the Cabal on Mars. I also have to thank Adam, Maria, Lis, and Jonny for making my birthday so special amid the chaos. Thanks to them, Ainsley, and Molly (Bunny) there was a steady supply of baked goods to improve my mood. I may have been alone, but I never felt lonely.

I've written a lot about the friends I've made during my PhD, but it would be remiss of me not to include the friends that have been around since before. Special thanks to Martin, Ross, and Andrew for putting up with me for so many years and giving me so many memories. I'm also grateful to Andrea, Ben, Craig, and Starkey for proving that friendships can survive beyond university.

Finally, and most importantly, I want to thank my family. I've always had the full-support of my Mum (Anne), my Dad (Gordon), my brothers (George, Scott, William), and sister (Michelle). No matter what, they've had my back. They have seen me at my worst and still believe in me. For them, I do my best to be better every day. I wouldn't be here without them.

Table of Contents

List of Abbreviations

°C	Degrees Celsius
A solution	Activating solution
Å	A
*Af*Amt1	*Archaeoglobus fulgidus* ammonium transporter 1
Amt	Ammonium transporter
*Ca*Mep2	*Candida albicans* Methylpermease 2
CV	Column Volume
DDM	dodecyl-β-maltopyranoside
DNA	Deoxyribonucleic acid
*Ec*AmtB	*Escherichia coli* ammonium transporter
IMAC	Immobilised Metal Affinity Chromatography
KDa	KiloDalton
K_i	Inhibition constant
Km	Michaelis constant
Ks-Amt5	*Kuenenia stuttgartiensis* ammonium transporter 5
LB	Lysogeny Broth
LDAO	lauryldecylamine oxide
LPR	Lipid Protein Ratio
MeA	Methylammonium
Mep	Methylammonium permease
MDS	Molecular Dynamic Simulation
nA	NanoAmpere
NA solution	Non-activating solution
*Ne*Rh50	*Nitrosomonas europaea*
nF	NanoFaraday
nS	Nanoseconds
OG	*n*-octyl-β-D-glucopyranoside
PAGE	Polyacrylamide gel electrophoresis
PDB	Protein Database
pH	Power of hydrogen
PMSF	Phenylmethylsulfonyl fluoride

POPC	1-palmitoyl-2-oleoyl phosphatidylcholine
Rsat	Saturation Constant
Rsol	Solubilisation Constant
Rh	Rhesus
RMSD	Root Mean Square Deviation
*Sc*Mep	*Saccharomyces cerevisiae* Methylpermease
SDS	Sodium Dodecyl Sulfate
SEC	Size Exclusion Chromatography
SSME	Solid Supported Membrane Electrophysiology
TEMED	Tetramethylethylenediamine
Tris	Tris(hydroxymethyl)aminomethane
g	x gravity

Abstract

The exchange of ammonium across cellular membranes is a fundamental process in all domains of life. In plants, bacteria, and fungi, ammonium represents a vital nitrogen source, which they seek to scavenge from the external environment. In contrast, ammonium is a cytotoxic metabolic waste product in animal cells and must be excreted to prevent cell death. Transport of ammonium is facilitated by the ubiquitous Amt/Mep/Rh transporter superfamily. In addition to their function as transporters, Amt/Mep/Rh proteins play roles in a diverse array of biological processes. For example, Mep proteins signal the onset of pseudohyphal growth, a transition associated with virulence in pathogenic fungi. The human Rh proteins are also essential in maintaining acid-base homeostasis, and their malfunction can lead to various pathologies, including hereditary anaemias, overhydrated stomatocytosis, and early-onset depressive disorders. Despite this clear physiological importance, the mechanism of Amt/Mep/Rh proteins has remained elusive. Crystal structures of AmtB from *Escherichia coli,* the most intensely studied member of the family, suggest electroneutral transport, whilst functional evidence supports an electrogenic mechanism. The overall goal of this project was to combine electrophysiology, yeast functional complementation, and extended molecular dynamics simulations (MDS) to characterise the mechanism of ammonium transport in AmtB.

An *in vitro* assay based on Solid Supported Membrane Electrophysiology (SSME) was developed to confirm electrogenic activity in AmtB and characterise activity, selectivity, and kinetics of WT AmtB (**Chapter 3**).

MDS revealed two ordered water chains embedded within the pore of AmtB, representing a potential polar transfer network. Subsequent SSME and *in vivo* yeast complementation characterisation of AmtB variants demonstrated that these wires were vital for AmtB-mediated NH_4^+ transport. This led to the proposal of a novel mechanism wherein NH_4^+ is deprotonated and H^+ and NH_3 are carried separately across the membrane (**Chapter 4**)**.**

Disruption of the twin-His motif, a highly conserved histidine dyad within the pore of AmtB, had a significant impact on the kinetics of ammonium transport and a deleterious impact on selectivity, resulting in passage of potassium ions through AmtB. It is imperative that transporters maintain substrate selectivity, as uncontrolled entry of charged molecules can prove fatal to the cell, thus this explains the conservation of the twin-His motif within the Amt/Mep/Rh family (**Chapter 5**).

This work provides a novel model of AmtB-mediated electrogenic transport and offers valuable insight into the mechanism of the highly important Amt/Mep/Rh family. Given their physiological relevance, this work may form the foundation for future medical interventions and treatments.

Chapter 1: Introduction

Section 1: Introduction

1.1 Biological Importance of Ammonium Transport

Movement of ammonium across biological membranes is a fundamental process that underpins nitrogen metabolism in all domains of life. Alongside nitrate, ammonium is the major nitrogen source for most higher plants (Britto and Kronzucker, 2002) and is also the preferred nitrogen source for many bacteria and yeast species, including *Escherichia coli* and *Saccharomyces cerevisiae* (Reitzer, 2003). Conversely, in humans, ammonium is a cytotoxic metabolic waste product (Martinelle, Westlund and Häggström, 1996), and elevated concentrations have been associated with hormonal and neurological conditions (Häberle, 2011). As a result, ammonium excretion is essential in detoxifying erythrocytes, kidney, and liver cells (Nakhoul and Hamm, 2004).

Whilst it is generally accepted that small and non-polar molecules can freely move across the cell membrane, large, polar, or charged molecules cannot diffuse freely through the membrane and thus require specific transporters. The availability of ammonium can vary depending on the environment, local nutritional status is not static, and nitrogen states may fluctuate between starvation and surplus. For example, bacteria often inhabit ammonium-limited environments where ammonium exists in the µM range (Verhamme, Prosser and Nicol, 2011). In such circumstances, ammonium uptake has to occur against a concentration gradient, necessitating active uptake.

1.2 The Amt/Mep/Rh family of Ammonium Transporters

1.2.1 Preliminary Evidence for an Ammonium Transport System

The first evidence for dedicated ammonium transport systems was reported by Benko *et al*, whilst investigating the role of amino acid transport in the

nitrogen starvation response of *Penicillium chrysogenum*. Interestingly, a key non-specific amino acid permease was inhibited by ammonium, suggesting the presence of a dedicated ammonium transport system within *P. chrysogenum* (Benko, Wood and Segel, 1969).

Later, Hackette *et al*, measured the uptake of ^{14}C labelled methylammonium (MeA) as a substrate analogue to characterise the ammonium transport activity in *P. chrysogenum.* This work demonstrated that *P. chrysogenum* was able to grow on MeA as sole nitrogen source, and that the uptake of MeA exhibited characteristics consistent with a permease, including pH-dependency and temperature-dependency (Hackette *et al.*, 1970). Crucially, Hackette *et al*. showed that ammonium was a highly-competitive inhibitor of MeA uptake. As the K_i value for the ammonium inhibition of MeA transport activity (~0.25 µM) was an order of magnitude lower than the K_m for MeA (1 mM), this uptake system was identified as an ammonium, rather than MeA, transporter (Hackette *et al.*, 1970).

1.2.2 Identification of First Gene Encoding an Ammonium Transporter

The first genes encoding for *bona fide* ammonium transporters were simultaneously identified in the plant *Arabidopsis thaliana* (Ninnemann, Jauniaux and Frommer, 1994), named Amt for ammonium transporter, and in *S. cerevisiae* (Marini *et al.*, 1994), named Mep for methylammonium permease. A few years later, the first bacterial gene encoding an ammonium transporter was characterised in *Corynebacterium glutamicum* (Siewe *et al.*, 1996). In the following years, members of the Amt/Mep family have been reported in a plethora of organisms, including *E. coli*, *Archaeoglobus fulgidus*, and *Candida albicans* (Van Heeswijk *et al.*, 1996; Biswas and Morschhäuser, 2005; Andrade *et al.*, 2005)

1.2.3 Discovery of Mammalian Ammonium Transporter Expanded Family

In 1997, Marini *et al* reported that the human Rhesus (Rh) proteins were mammalian homologues of the Amt/Mep family (Marini *et al*, 1997). This was concluded on the basis of sequence similarity between existing Amt/Mep family members and the Rh proteins in humans and other primates. In 2000, Marini *et al* demonstrated that two human Rh protein were able to complement transport activity in a triple-*mepΔ S. cerevisiae* strain, which is deprived of its three endogenous Mep ammonium transporters. This proved that rhesus proteins represent the Amt/Mep family's orthologues in mammals (Marini *et al.*, 2000).

1.3 Evolution of the Amt/Mep/Rh Ammonium Transporters

Since their initial discovery, the Amt/Mep/Rh family have proven to be ubiquitous (For review, see Andrade and Einsle, 2007 and references therein). Despite this, our understanding of the evolution of the Amt/Mep/Rh family is limited, with only a small selection of literature available.

The first investigation into evolution within the family was carried out by the Peng lab in 2005 (Huang and Peng, 2005). Specifically, their work aimed to probe evolution and co-existence of Amt and Rh genes. They constructed a maximum likelihood tree using 111 non-redundant Rh genes and 260 non-redundant Amt genes. This analysis revealed a clear phylogenetic clustering and separation of Amt and Rh proteins (**Figure 1.1A**). A later analysis corroborated this, and demonstrated that whilst Mep proteins are phylogenetically closer to Amt, they still show distinct clustering (Pitts *et al.*, 2014) (**Figure 1.1B**). This highlighted that Rh was a distant relative of Amt and suggested that they had undergone divergence.

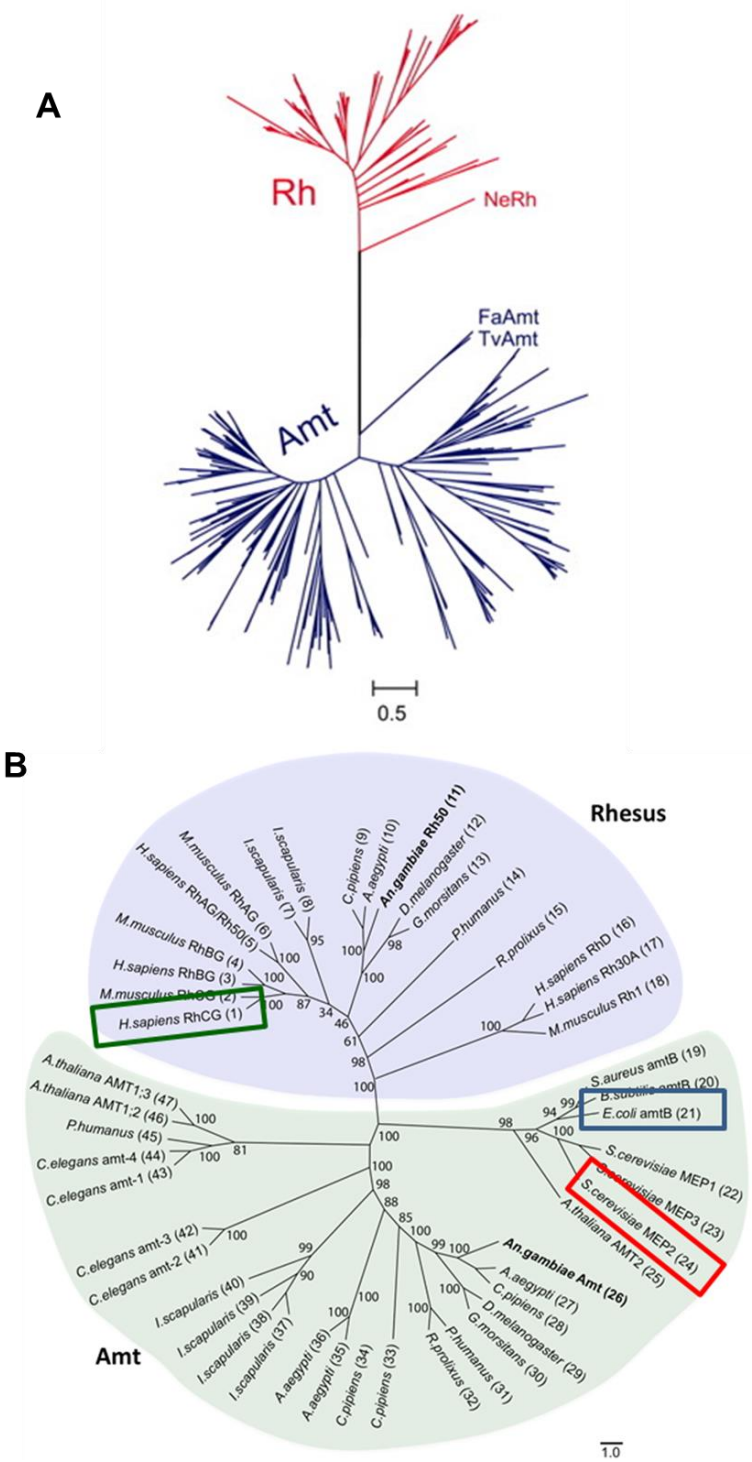

Figure 1.1 Relationship between Amt, Mep, and Rhesus: A) Maximum likelihood tree of Amt (blue) and Rh (red) proteins, *Ne*Rh (bacterial Rhesus), *Fa*AmtB/*Tv*AmtB (archaeal Amts) (Figure from Huang and Peng, 2005). B) Neighbour-joining tree comparing ammonium transporters. Rhesus and Amt separate into distinct clades, whilst Mep appears within the Amt grouping. One example each of Amt (blue), Mep (red), and Rh (green) have been highlighted. (Figure from Pitts *et al.* 2004) Scale bars are 0.5% and 1% corrected distance

Interestingly, Huang and Peng found that all vertebrates within the dataset possessed Rh but not Amt (Huang and Peng, 2005). In contrast, Rh proteins were not observed in vascular plants or archaea, but were found in 41 organisms, ranging from the chemolithoautotroph bacteria *Nitrosomonas europaea* to higher mammals. Within this group a diverse range of organisms, from unicellular eukaryotic microbes (including green algae and slime moulds) to invertebrates (including nematodes and ascidians), possessed both Rh and Amt proteins. From this, it is clear that Amt and Rh have co-existed over a long evolutionary period.

This coexistence of Amt and Rh in some species prompts an interesting question. If the two sub-families were exclusive, it would be possible that they diverged but still fulfil the same role. Alternatively, an ancient Amt may have been recruited and subjected to differential selective pressure, adopting a new function. In this instance, both vertebrates and vascular plants would then be examples of purifying selection. However, that some species contain a mix of the proteins, suggests there is an advantage to retaining both. As detailed in **Section 1.4.1**, Amt/Mep are scavengers, whilst Rh typically have been hypothesised to act as exporters, but it is unclear how they operate in mixed systems. To investigate this, the mechanism of ammonium transport in one family member must first be elucidated and then the conservation of that mechanism probed across the superfamily.

Whilst we know the current relationship between the Amt/Mep/Rh sub-families, we have limited understanding of their evolution. Two studies by McDonald *et al* highlight two separate modes of transmission: vertical gene transfer (parent-offspring) within the Amt and Mep sub-families, and horizontal gene transfer (HGT) from Amt to Mep (McDonald, Dietrich and Lutzoni, 2012; McDonald and Ward, 2016). Specifically, they found that eukaryotic Mep clades were not closely related to each other, but rather were the result of at least nine separate HGT events from at least three lineages of bacteria (McDonald, Dietrich and Lutzoni, 2012). While Huang and Peng suggest a prokaryotic origin for Rh, they also showed it diverged into 4 paralogous clusters: Rh30, RhAG, RhBG, and RhCG. RhBG and RhCG are transport competent and appear to have

diverged from a common ancestor to occupy different tissues. RhAG and Rh30 are erythrocyte specific and also share a common ancestor, however Rh30 is non-transporting. The authors concluded that this 4 gene framework did not arise until after vertebrate speciation (Huang and Peng, 2005). This surge in complexity and subsequent divergence of Rh from Amt/Mep raises the possibility that Rh have acquired a distinct functional role from Amt/Mep and even from prokaryotic Rh. Again, while these proteins are undoubtedly ubiquitous, the universality of their function and mechanism is unclear.

1.4 Biological Importance of the Amt/Mep/Rh Proteins

1.4.1 Amts

Generally, Amts are important in plants and bacteria due to their role in scavenging ammonium from the external environment. Of the seven putative Amt orthologues in the planctomycete *Kuenenia stuttgartiensis,* one (*Ks*-Amt5) was recently demonstrated to act as an ammonium sensor/transducer.(Pflüger *et al.*, 2018). The structure of *Ks*-Amt5 will be discussed in further detail in **Section 1.5.4.2**, but briefly, *Ks*-Amt5 has an elongated cytoplasmic domain with significant homology to histidine kinases. While the protein selectively binds NH_4^+, it does not complete the translocation cycle, instead triggering an increase in histidine kinase activity and subsequent transduction of information to a currently unidentified response regulator (Pflüger *et al.*, 2018).

1.4.2 Mep

The three Mep isoforms within *S. cerevisiae* allow for precise and adaptable control of ammonium uptake. Mep1-3 differ in terms of affinity and flux: Mep1 (Km, 1- 2 µM) and Mep2 (Km, 5- 10 µM) are high affinity transporters, whilst Mep3 is a lower affinity transporter (Km, 1.4 – 2.1 mM) (Marini *et al.*, 1997). As

with other Amt/Mep/Rh members, the Mep proteins are regulated in response to nitrogen availability, with their expression controlled at the gene-level. Specifically, they are subject to differential regulation *via* Gln3p and Nil1p, two general nitrogen regulatory factors (Marini *et al.*, 1997).

In addition to their role as ammonium scavengers Mep proteins signal the formation of pseudohyphae in some species of filamentous fungi (Michael C. Lorenz and Heitman, 1998). In *S. cerevisiae,* the formation of pseudohyphae is observed under nitrogen limitation (Gimeno *et al.*, 1992). In this example, nitrogen limitation drives the yeast to transition from a unipolar budding phase and form pseudohyphae which venture into the agar in search of environmental nutrients. *MEP2Δ S. cerevisiae* lose the ability to make this transition and do not form pseudohyphae, while deletion of *MEP1* or *MEP3* had no impact on filamentation (Lorenz and Heitman, 1998). In addition, ammonium transport in *MEP2Δ S. cerevisiae* was unaffected – likely by the contribution of Mep1 and Mep2 to overall transport (Lorenz and Heitman, 1998). Thus, Mep2 has been nominated as a transceptor; sensing nitrogen limitation and initiating a signalling cascade that culminates in filamentation (van den Berg *et al.*, 2016). This behaviour is associated with virulence of human pathogens *C. albicans*, *Cryptococcus neoformans,* and *Histoplasma capsulatam* (Maresca and Kobayashi, 1989; Rutherford *et al.*, 2008; Lo *et al.*, 2015), thus improved understanding of this process could aide disease treatment.

1.4.3 Rhesus

In contrast to the other members of the Amt/Mep/Rh family, the mammalian rhesus proteins facilitate ammonium excretion (Marini *et al.*, 2000). As such, their biological roles are distinct from those fulfilled by Amt and Mep proteins. Notably, rhesus proteins are key to the survival strategies of several species that encounter or persist within otherwise toxic levels of ammonium. Recent work revealed that the larvae of *Aedes aegypti* – a disease vector mosquito

which readily develops in ammonium-rich sewage water – upregulate expression of their native rhesus protein within a “physiological triad” of organs to efficiently excrete ammonium against a steep concentration gradient (Durant and Donini, 2019). Additionally, various species of amphibious fish possess cutaneous Rh proteins, which they upregulate when emersed, in order to avoid ammonium toxicity in the absence of water-flow over the gills (Livingston *et al.*, 2018).

In mammals, rhesus proteins are instrumental in detoxification of erythrocytes, maintaining pH balance, and reabsorption of ammonium through the renal tubule epithelial cells (Garvin, Burg and Knepper, 1988; Biver *et al.*, 2008). Accordingly, mutations in Rh are associated with numerous pathologies. The antigen-carrying rhesus proteins, RhD and RhCE, are clinically relevant in transfusion-incompatible immune responses, autoimmunity, and haemolytic diseases in neonates (Hadley and Kumpel, 1993; Lozano and Cid, 2003). RhAG malfunction is associated with Overhydrated Stomatocytosis, a rare hereditary haemolytic anaemia, that is characterised by uncontrolled entry of monovalent cations into erythrocytes (Bruce *et al.*, 2009). In mice, RhCG mutations disrupt homeostasis, which has been linked to Distal Renal Acidosis and male infertility (Biver *et al.*, 2008; Bourgeois *et al.*, 2018). Finally, RhCG has been identified as a potential contributor to early-onset depressive disorders (Verma *et al.*, 2008).

1.5 Structural characterisation

1.5.1 Membrane Topology and Secondary Structure

The topology of Amt/Mep/Rh proteins was first determined *in vivo* for the ammonium transporter AmtB from *E. coli* (Thomas and Mullins, 2000). Thomas *et al* fused AmtB to one of two reporter proteins: the alkaline phosphatase (PhoA) or the β–galactosidase (LacZ). Each of the reporter proteins were

fused to the C-terminus of the 12 transmembrane (TM) helices predicted previously (Van Heeswijk *et al.*, 1996). PhoA and LacZ are active in the periplasm and the cytoplasm respectively, therefore the activity of PhoA- and LacZ- fusions depends on the orientation of the associated helix. The AmtB-PhoA fusions had an alternating pattern of activity which supported an 11 TM model with the N-terminus extruding into the periplasm and the C-terminus located in the cytoplasm (**Figure 1.2**).

Prior sequence analysis had predicted a 12th helix (Van Heeswijk *et al.*, 1996), but these results suggested that the 1st theoretical helix was actually a signal peptide that would be cleaved following correct folding or insertion of the protein into the membrane. Further topological studies have since demonstrated that the 11 TM model and general topology observed in AmtB is conserved across Amt/Mep proteins. 3D crystal structures of bacterial and human Rhesus proteins however, have been shown to possess 12 TM helices with both the N-terminus and C-terminus located in the cytoplasm (Lupo *et al.*, 2007; Gruswitz *et al.*, 2010). This will be discussed later in **Section 1.5.4.5**.

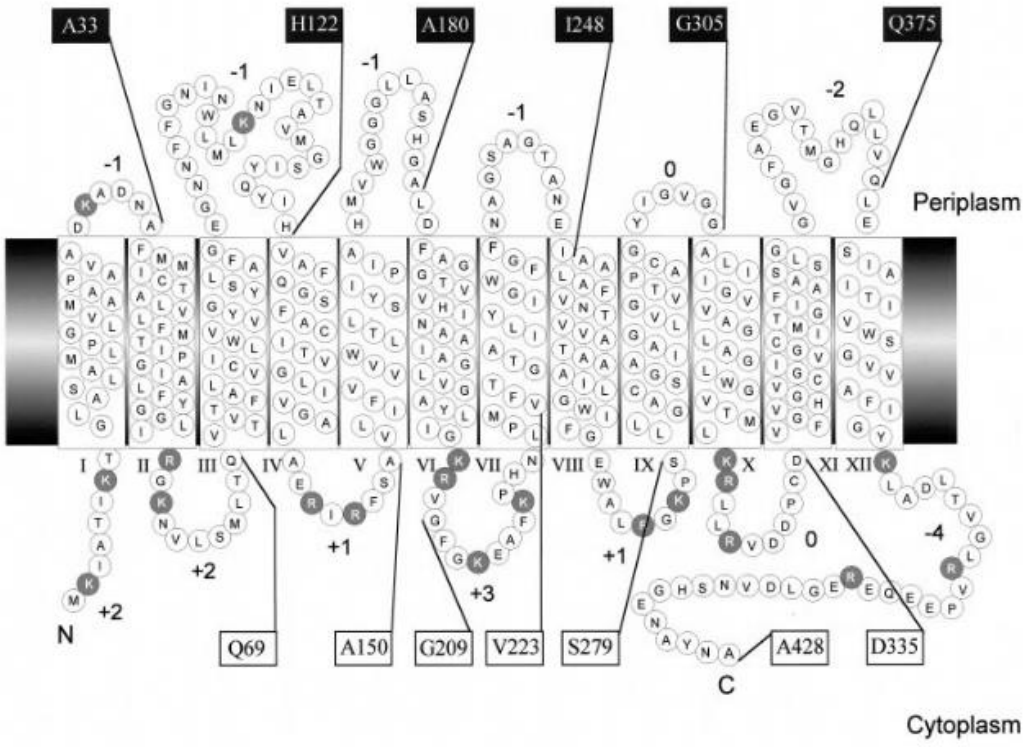

Figure 1.2. Topological model of AmtB for each of the loops, the overall charge is indicated and positively charged residues are highlighted in black. Boxes designate positions of AmtB+PhoA fusions, with boxes indicate positions of AmtB±PhoA fusions that were blue on indicator plates (between 1400 and 7160 AP units), whereas boxes that are white correspond to fusions that were white on indicator plates (between 20 and 120 units). Figure from Thomas *et al* 2000.

1.5.2 Tertiary and Quaternary Structure

Investigation into the oligomeric state of Amt/Mep/Rh was prompted by the observation of cross-talk between the different Mep isoforms in *S. cerevisiae*, where expression of an inactive Mep1 inhibited the activity of Mep2 and Mep3 (Marini *et al.*, 2000).

Subsequently *Ec*AmtB, the first Amt/Mep protein to be purified was subjected to a combination of analytical ultracentrifugation (AUC) and size-exclusion chromatography (SEC). Through these techniques it was determined that, when solubilised in dodecyl-β-maltopyranoside (DDM), AmtB purifies as a homotrimer with a molecular mass of ~140 kDa (Blakey *et al.*, 2002). This does not correspond to the expected mass of the trimer (~130 kDa), likely due to partial unfolding of hydrophobic domains following SDS-binding (Rath *et al.*, 2009). Shortly thereafter, Conroy *et al* obtained the first ordered 2D crystals of AmtB. From these, they used cryo-electron microscopy to generate a low resolution (12Å) projection map, and atomic force microscopy to obtain higher resolution topographs (Conroy *et al.*, 2004). Both methods supported the trimeric structure of AmtB, and suggested that each monomer exhibited pseudo-two-fold symmetry. The authors also speculated that each monomer would possess a translocation pathway and that the structure seen in AmtB might be conserved across other family members.

This speculation was later validated when the laboratories of Fritz Winkler and Robert Stroud independently reported the first high resolution crystal structures of AmtB (Khademi *et al.*, 2004; Zheng *et al.*, 2004). These structures confirmed the trimeric organisation of AmtB and provided an unprecedented insight into the structure of the translocation pathway: enabling investigation into the mechanism of ammonium transport. Over the last two decades, high resolution crystal structures have been solved across the Amt/Mep/Rh family, including; rhesus proteins from *N. europaea* and *Homo sapiens*; fungal Mep2 from *S. cerevisiae* and *Candida albicans*; and Amt from *Archaeoglobus*

fulgidus and *K. stuttgartiensis* (Andrade *et al.*, 2005; Lupo *et al.*, 2007; Gruswitz *et al.*, 2010; van den Berg *et al.*, 2016; Pflüger *et al.*, 2018).

As AmtB is the paradigmatic member of the family, with over 20 high-resolution structures in the Protein Databank (PDB) and the model used for the work presented in **Chapters 3-5**, its structure will first be discussed in detail, followed by a series of comparisons to other solved structures of Amt/Mep/Rh proteins.

1.5.3 Structure of EcAmtB

In line with previous predictions (Blakey *et al.*, 2002; Conroy *et al.*, 2004) AmtB crystalised as a homotrimer (**Figure 1.3A**), with each monomer conforming to the 11 TM helix model proposed by Thomas *et al*. (Thomas and Mullins, 2000). TM1-10 diverge from the central plane, forming a right-handed helical bundle around the centre of each monomer. Both Zheng and Khademi agreed that the fold of the protein was unusual and not-homologus to known membrane proteins (Khademi *et al.*, 2004; Zheng *et al.*, 2004). Specifically, TM1-5 and TM6-10 could be split into two α-helical bundles related by a two-fold axis, while TM11 is an extra-long extension laying perpendicular to the membrane interface and surrounding the lipid accessible portion of the monomer (Khademi *et al.*, 2004; Zheng *et al.*, 2004). Additionally, the subunit interface was notably hydrophobic - with hydrphobic side-chains from each TM1 forming a tight contact ~20Å into the membrane. Additional contact occurs between TM1-3 of one monomer and the TM-6-8 of another (Zheng *et al.*, 2004).

Crucially, these high resolution structures led to the indentifcation and characterisation of the potential substrate translocation pathway – located in the centre of each monomer. The crystollographic structures revealed four key features (**Figure 1.3B**) of mechanistic interest within the translocation pathway:

1. An NH_4^+ binding site within a vestibule in the periplasmic face of the protein named S1 site

2. A constriction imposed by two stacked phenyalanine residues that seperates the S1 site from the pore named the “Phe-gate”.
3. A narrow pore lined with hydrophobic residues
4. A cytoplasmic vestibule

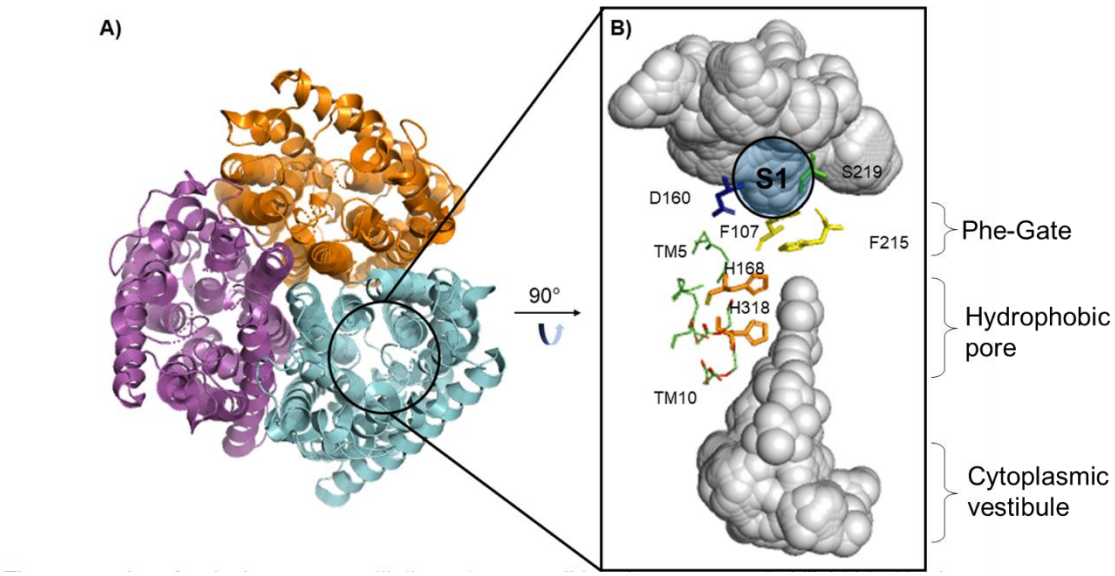

Figure 1.3 Structure of AmtB: A) View of the AmtB trimer from the periplasm, with each monomer represented in purple, orange, or cyan. B) Expanded view of the pore region of a single monomer with the water-accessible volume represented in grey. Highly conserved residues are shown in ball-and- stick representation for the ammonium binding site (green), phenylalanine gate (yellow) and central pore (orange), where parts of the two transmembrane helices TM5 (His168) and TM10 (His318) are also shown.

1.5.3.1 S1 binding Site

Zheng and Khademi both observed a putative NH_4^+ binding site, nestled within a periplasmic vestibule in each monomer. A binding site is consistent with the fact that the transporter is only expressed under ammonium-limited conditions, as it is necessary to ensure a high affinity for the substrate and confer efficient scavenging for ammonium (Wirén and Merrick, 2004). In AmtB, this binding site is delineated by the residues S219, W148, F107, and D160. At this site, NH_4^+ could be stabilised *via* π-cation interactions with the phenyl rings of W148 and F107 alongside hydrogen bonding with S219 (Khademi *et al.*, 2004; Zheng *et al.*, 2004). Javelle *et al.* demonstrated that thallium (which has a similar size and coordination as ammonium) can bind at this position, and that thallium competitively inhibits MeA uptake (Javelle *et al.*, 2008).

D160 lies in close proximity of the S1 site, and is highly conserved, implying a functional or structural role (Thomas and Mullins, 2000; Javelle *et al.*, 2004). Prior substitution of D160 to a A160 resulted in a loss of MeA uptake activity, which implied a mechanistically important role for D160 (Javelle *et al.*, 2004). However, the crystal structures rule out a role in binding as the carboxy function of D160 is buried too deep in the pore to directly contact ammonium (Khademi *et al.*, 2004). The potential role for D160 is further discussed in **Section 1.6.2.1**.

1.5.3.2 “Phe-Gate”

The second key structural feature of AmtB is the “Phe-gate”. Positioned immediately after the S1 binding site, the stacked phenyl rings of F107 and F215 form a constriction that completely blocks access to the pore from the S1 site (Khademi *et al.*, 2004). The arrangement of F107 and F215 was identical in all of the AmtB crystal structures, but the authors suggested that the rings would have to be dynamic to facilitate any conduction event.

1.5.3.3 Hydrophobic Pore & Twin-His motif

The Phe-gate is followed by a strongly hydrophobic pore that leads to the cytoplasm. The hydrophobicity of this pore represents a high energetic barrier against the movement of ions (Zheng *et al.*, 2004). Two highly conserved histidine residues, H168 and H318, protrude into the lumen of this pore, forming the family's characteristic "twin-His" motif (Javelle *et al.*, 2006). Whilst the hydrophobic residues in the pore can be variable, the twin-His motif is highly conserved, indicating a functionally important role (Javelle *et al.*, 2006, Zheng *et al.*, 2004).

Interestingly, Khademi *et al* observed a series of densities (denoted Am2, 3, and 4) within the hydrophobic pore (**Figure 1.4**). They only recorded these densities in the presence of 25 mM $(NH_4)_2SO_4$ and did not observe them in the absence of substrate, so concluded that they were ammonium molecules (Khademi *et al.*, 2004). Crucially, Zheng *et al* observed these densities regardless of the presence or absence of ammonium – allowing the hypothesis that the densities are water molecules (Zheng *et al.*, 2004). At 1.35Å a molecule of H_2O and NH_3 are not readily distinguished, thus the densities are equally likely to be water molecules.

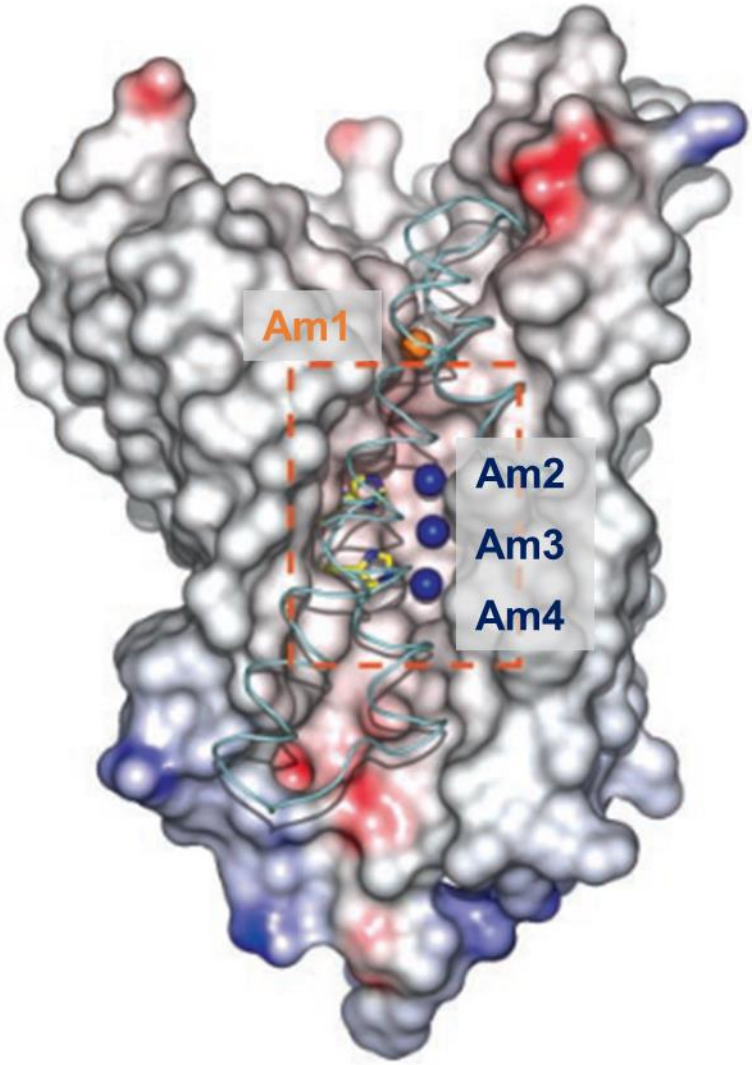

Figure 1.4 Densities in the Crystal Structure of AmtB. The surface of TM 9, and parts of TM 8 and 10 (whose backbones are represented by cyan lines) have been removed to permit a clear view of the lumen, and the surfaces coloured according to electrostatic potential. Am1 (denoted in orange) indicates a NH_4^+ ion in the periplasmic vestibule. Within the pore (highlighted by the orange dashed region) lie a further three densities, Am1-3 (represented by blue spheres). This figure is adapted from (Khademi *et al*., 2004), who speculated that these densities were ammonia.

1.5.3.4 Cytoplasmic vestibule

Khademi and Zheng also observed that the translocation pathway terminated at a vestibule in the cytoplasmic face of the protein (Khademi *et al.*, 2004; Zheng *et al.*, 2004). Unlike the periplasmic vestibule, no discernible binding site was detected. In addition, there was no barrier between the vestibule and the pore, resulting in a clear asymmetry between the periplasmic and cytoplasmic ends of the channel. Interestingly, Zheng *et al* crystallised AmtB in two different spatial groups, R3 and $P6_3$, and found the vestibule in different states in each crystal. In the $P6_3$ crystal, residues around the N-terminus of TM10 are positioned differently, such that they obstruct the cytoplasmic exit and create a purely hydrophobic environment (Zheng *et al.*, 2004). In the R3 structure, the residues do not obstruct the pore exit and result in a more polar "open" state (Zheng *et al.*, 2004). This evidence of conformational change within the vestibule suggested a functionally relevant role –which is still unknown.

1.5.4 Additional Amt/Mep/Rh Structures

1.5.4.1 *Archaeoglobus fulgidus* Amt1

The crystal structure of *Af*Amt1, an ammonium transporter from *Archaeoglobus fulgidus*, was first solved in 2005 by Andrade and colleagues (Andrade *et al.*, 2005). The general topology of *Af*Amt1 was highly similar to that shown for *Ec*AmtB, following the same 11 TM model – with only the signal sequence missing (**Figure 1.5**). In addition, *Af*Amt1 retains the pseudo-two-fold symmetry seen in *Ec*AmtB, loosely mirroring TM1-5 and TM6-10 (Khademi *et al.*, 2004; Andrade *et al.*, 2005).

Similarly, to the S1 binding site identified in AmtB, *Af*Amt1 also possessed a serine (S208) and tryptophan (W137) which could stabilise a molecule of NH_4^+ in the vestibule. Whilst Andrade *et al* observed a strong electron density in this

region – they were unable to correlate the density with the presence or absence of ammonium. The paired phenylalanine residues beneath the periplasmic vestibule were conserved in *Af*Amt1 and, as with AmtB, were positioned such that their rings occluded access to the channel. Interestingly, Andrade *et al* observed higher flexibility in the sidechain of F204, leading them to conclude that the residues much move during the translocation event. Where Khademi observed several density peaks within the hydrophobic pore after soaking the crystal in ammonium sulphate and Zheng observed the densities in both the absence and presence of ammonium – Andrade *et al* did not observe densities in either condition (Khademi *et al.*, 2004; Zheng *et al.*, 2004; Andrade *et al.*, 2005).

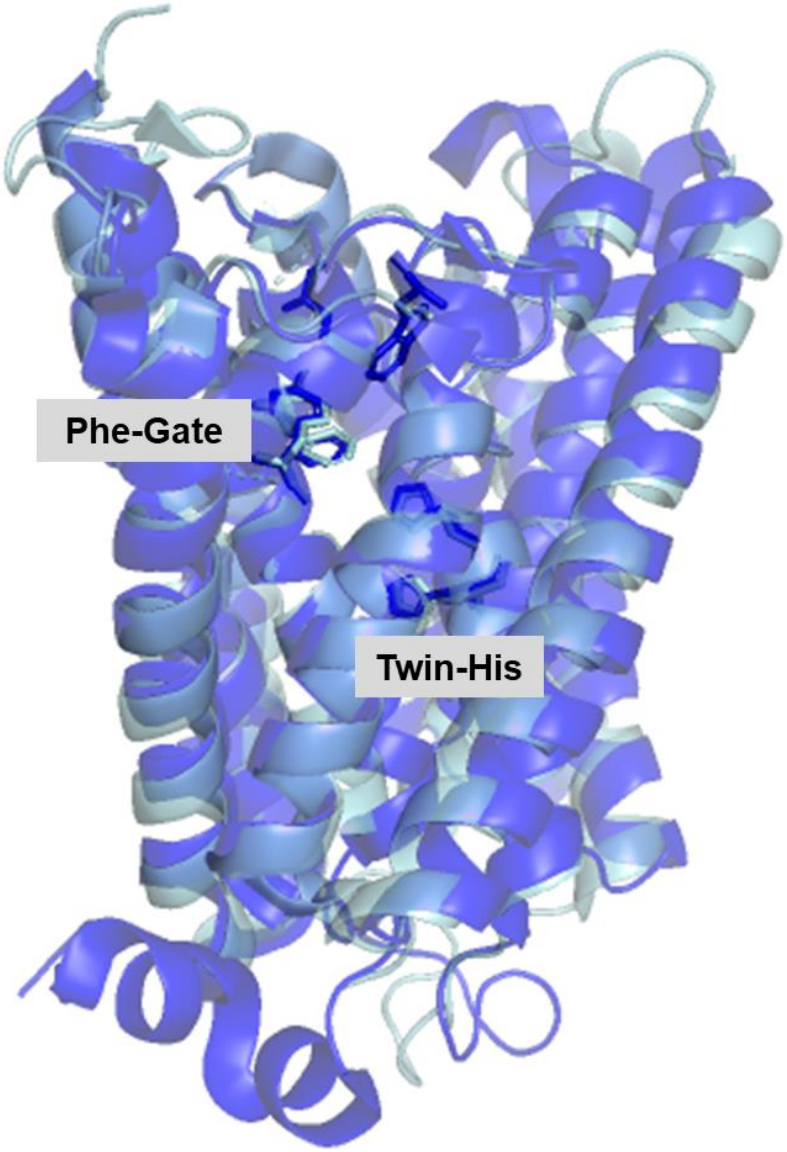

Figure 1.5 Comparison of AmtB and Amt1: Overlay of a single monomer of AmtB (cyan) or Amt1 (blue) as inserted into the membrane (A) or from the view of the periplasm (B). Residues of the binding site, Phe-gate, twin-his motif are displayed in the same colour as their respective monomer.

1.5.4.2 *Kuenenia stuttgartiensis* Amt5

In 2018, the crystal structure of *Ks*Amt5 from the bacterial species *Kuenenia. stuttgartiensis* was solved. While the general topology of *Ks*-Amt5 is similar to that previously described for *Ec*AmtB and *Af*Amt1 (Pflüger *et al.*, 2018), the structure differed in key ways.

Firstly, while the binding site (W144/S227), the Phe-gate (F103/F223), and the twin-His motif (H171/H326) are all conserved – the crystal structure revealed an additional three residues (F27, Y30, F34) present in the translocation pore. The large sidechains of these residues, combined with an inward shift of the twin-His motif, completely occludes the pore and prevents access for ammonium **Figure 1.6A**. Pflüger *et al* also used Surface Supported Membrane Electrophysiology (explained in **Section 2.5**) to demonstrate that *Ks*-Amt5 binds ammonium, but does not translocate it across the membrane. These marked structural and functional differences imply a distinct role for this Amt.

In addition, unlike *Ec*AmtB and *Af*Amt1, *Ks*-Amt5 features an extended C-terminal tail with high similarity to the histidine kinase (HK) domain observed in bacterial two-component systems (Pflüger *et al.*, 2018). Although the overall crystal structure obtained was high-resolution, the HK domain was highly disordered due to its relative flexibility and thus remained undefined. Despite this, Pflüger *et al* demonstrated HK-mediated phosphorylation to be concentration-dependent: with a significant increase under nitrogen limitation conditions (5-10 mM).

Thus, *Ks*-Amt5 represents a system wherein an Amt protein has been repurposed as a specific ammonium receptor which modulates signal transduction to its HK in response to NH_4^+ concentration. This unusual arrangement may have evolved to complement the unique physiology of anaerobic ammonium oxidation (anammox) bacteria where ammonium catabolism is highly dependent on the ammonium concentration within its unique organelle, the anammoxosome. Whilst Ks-Amt5 is the first to be characterised, other naturally occurring sequences combining Amt with other

protein domains have been observed (Tremblay and Hallenbeck, 2009). It's possible that similar examples will be observed in other bacteria.

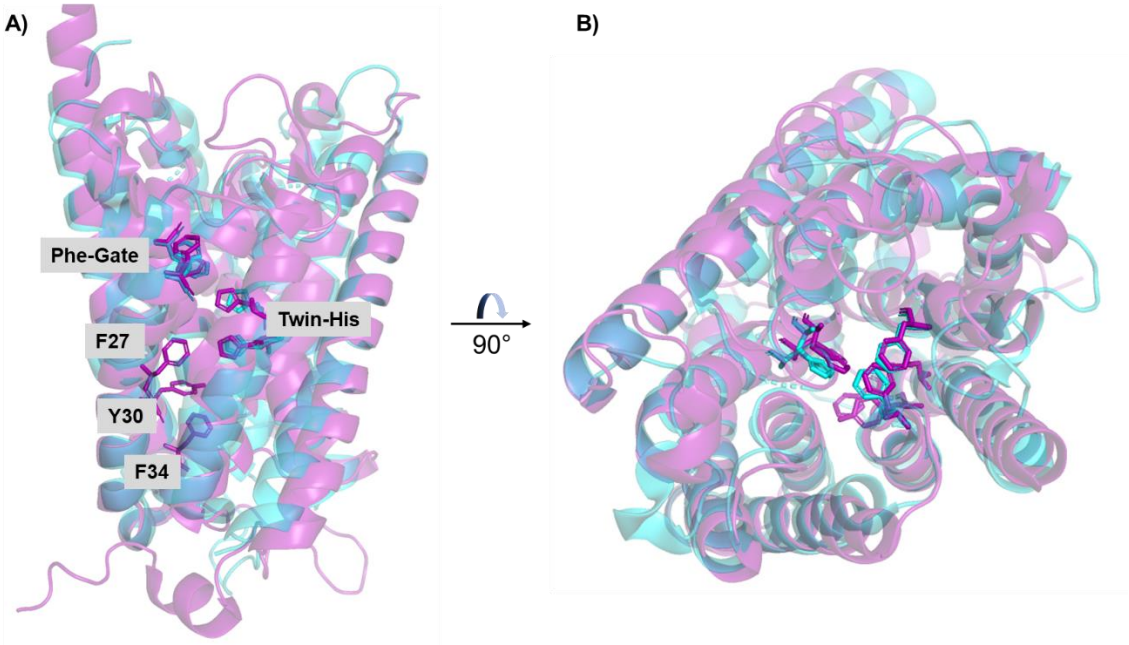

Figure 1.6 Comparison of AmtB and Ks-Amt5: Overlay of a single monomer of AmtB (cyan) or Ks-Amt5 (magenta) as inserted into the membrane (A) or from the view of the periplasm (B). Residues of the Phe-gate, twin-his motif, and the additional Ks-Amt5 pore occluding residues are displayed in the same colour as their respective monomer.

1.5.4.3 *Saccharomyces cerevisiae* and *Candida albicans* Mep2

In 2016, two separate crystal structures of fungal Mep proteins, Mep 2 from *S. cerevisiae* and Mep2 from *C. albicans,* were reported simultaneously (van den Berg *et al.*, 2016). Compared to each other, these proteins were highly similar (root mean square deviation of 0.7 Å) and thus will be discussed together.

The crystal structures revealed the general architecture of the fungal Mep proteins to be highly similar to their prokaryotic counterparts: conserving archetypal trimeric organisation and pseudo-two-fold similarity across the 11TM helices in the monomers. In addition, the key structural features of the translocation pathway (S1 binding site, Phe-gate, twin-His motif) are all conserved (**Figure 1.7B**). Significant deviation between Mep2 and previous bacterial structures was noted at 3 regions and could signify potential functional divergence.

The first of these divergent regions is the N-terminus, which is extended by 20-25 resides compared to bacterial Amt. This causes the N-terminus to contact the ECL5 (Extracellular Loop 5) of the neighbouring monomer, substantially widening the extracellular domain and creating a more distinct binding site (**Figure 1.8A**) (van den Berg *et al.*, 2016). The authors proposed that these changes would increase the stability of the Mep2 trimer however, as N-terminal mutants grew as well as WT on minimal media, they could not verify a functional role for the N-terminus.

The Mep2 structures also differ from other ammonium transporters at cytoplasmic exit of the translocation channel. In Mep2, the cytoplasmic end of TM2 is unwound, creating an extended intracellular loop 1 (ICL) that is shifted inwards compared to its bacterial counterparts (**Figure 1.8B**). This alters the positioning of a number residues, and ultimately results in a hydrogen bond interaction between Y49 (located at the C-terminus of TM1) and H342 of the twin-His motif which is not present in prokaryotic Amt. In addition, the ICL which links TM1-5 and TM6-10 is shifted by ~10 Å, blocking the channel on the cytoplasmic side (van den Berg *et al.*, 2016).

Finally, the C-terminal region of Mep2 differs from its bacterial counterparts. In AmtB, the C-terminal region contacts the N-terminal portion of TM1-5, resulting in a compact protein. In contrast, the Mep2 C-terminal region makes very few contacts the main core of the protein, resulting in elongated proteins.

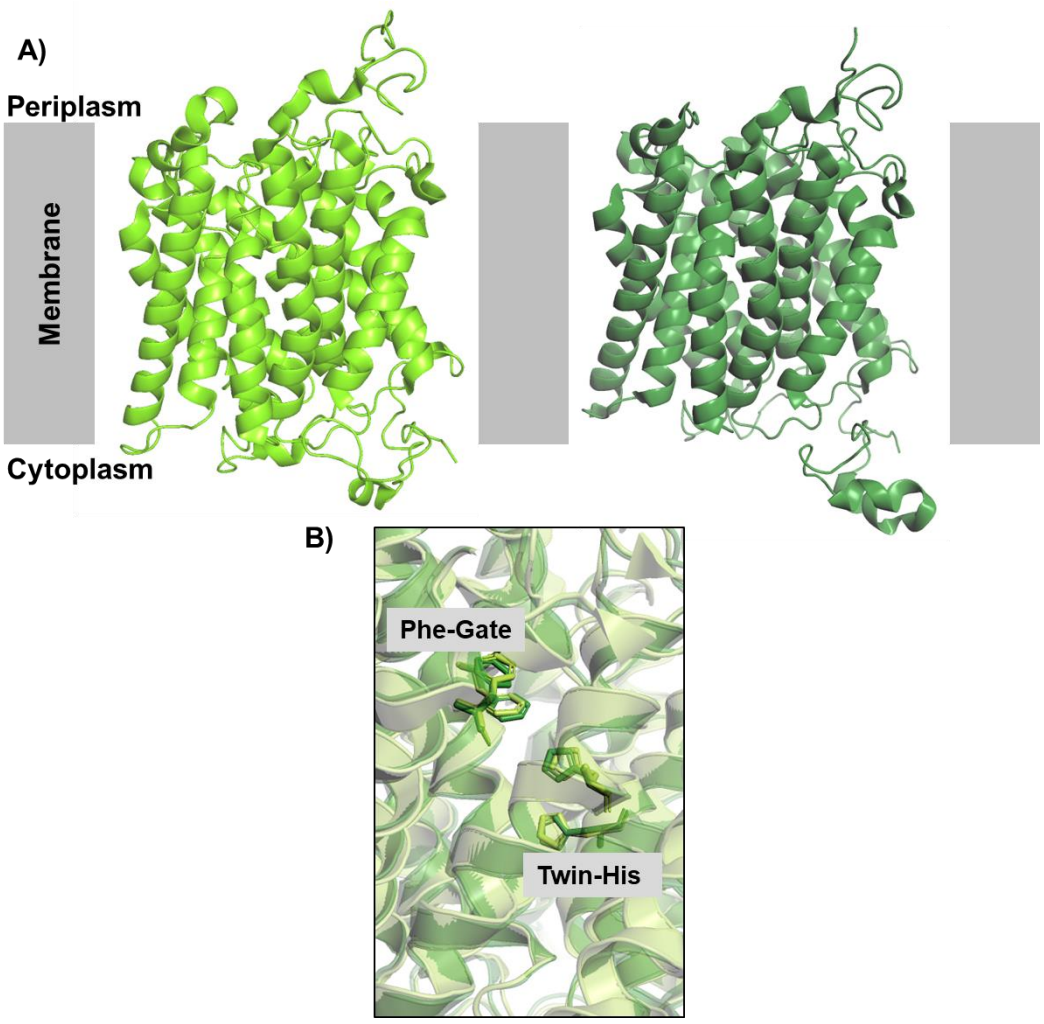

Figure 1.7 Comparison of *Sc*Mep2 and *Ca*Mep2. A) Cartoon models of X-ray crystal structures of Mep2 transceptors. viewed from the side for *S. cerevisiae* Mep2 (light green) and *C. albicans* Mep2 (dark green. **B)** Overlay of translocation pathway for *Sc*Mep2 (light green) and *Ca*Mep2 (dark green), showing the conservation of the Phe-gate and twin-His motif.

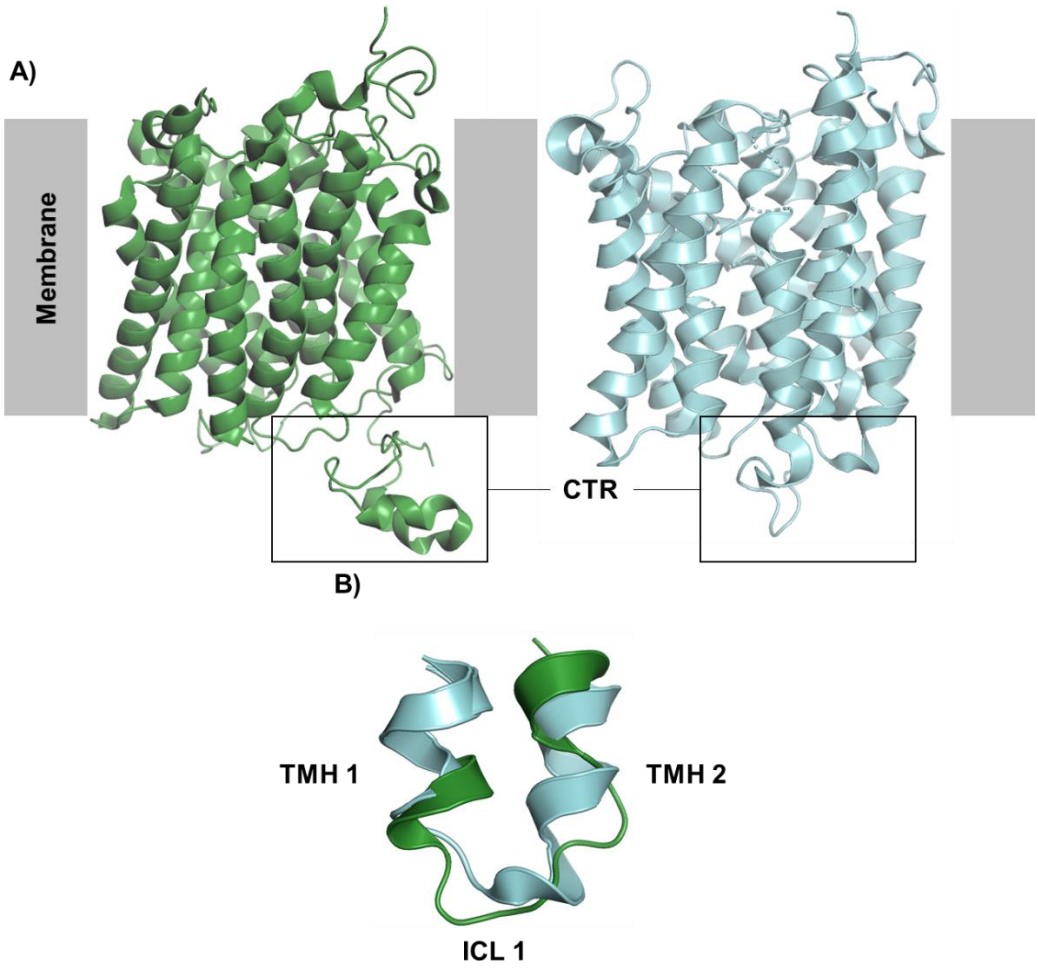

Figure 1.8 Comparison of fungal Mep2: A) Cartoon models of X-ray crystal structures of Mep2 transceptors. viewed from the side for *C. albicans* Mep2 (dark green) and AmtB (cyan) The extended CTR has been boxed for comparison. **B)**. ICL1 in AmtB (cyan) and *Ca*Mep2 (dark green), showing unwinding and inward position of the fungal protein.

1.5.4.4 *Nitrosomonas europaea* Rh50

In 2007 the first high resolution (1.3 Å) structures of a rhesus protein from the bacteria *Nitrosomonas europaea* was published by two groups (Li *et al.*, 2007; Lupo *et al.*, 2007). This was a milestone moment, as it allowed for structural insight into Rh50 itself but also enabled comparison to the pre-established structures of *Ec*AmtB (Khademi *et al.*, 2004; Zheng *et al.*, 2004) and *Af*Amt1 (Andrade *et al.*, 2005).

Previous *in silico* work predicted that Amt and Rh had 11 and 12 TM helices, respectively (Marini *et al.*, 1997). However, the crystal structure of *Ne*Rh50 revealed only 11 TM helices – leading Lupo *et al* to hypothesise that the 12th TM helix was cleaved off when expressed in *E. coli* (Lupo *et al.*, 2007).

Of the key residues seen in the AmtB S1 binding site (F107, W148, S219) only the phenylalanine is conserved in *Ne*Rh50. However, the vestibule structure is not conserved and no ammonium binding site is seen in Rh.

The Phe-gate is conserved but altered in comparison to that seen in AmtB. F86 is tilted in *Ne*Rh50, creating an opening for a water molecule 2Å deeper in the pore. A similar pocket is present directly above the first histidine of the twin-His motif, and contains 2 water molecules. Beyond this change, the twin-His motif is conserved and similar in both Rh and Amt (**Figure 1.9**). Interestingly, while residual electron densities have been seen in the hydrophobic pore of AmtB, they weren't observed here (Zheng *et al.*, 2004; Lupo *et al.*, 2007).The cytoplasmic vestibules of AmtB and Rh50 are very similar, but the asymmetry between the periplasmic and cytoplasmic vestibules in Rh50 is less pronounced due to the lack of the S1 binding site.

In contrast to prior speculation that the human Rhesus proteins would form heterotetramers (Eyers *et al.*, 1994), Lupo *et al* concluded that they should be trimeric (Lupo *et al.*, 2007). This was based on the trimeric structures of *Ec*AmtB and *Ne*Rh50, and comparative analysis of their respective monomer interface regions. Of course, this could not be proven without a crystal structure of a human rhesus protein.

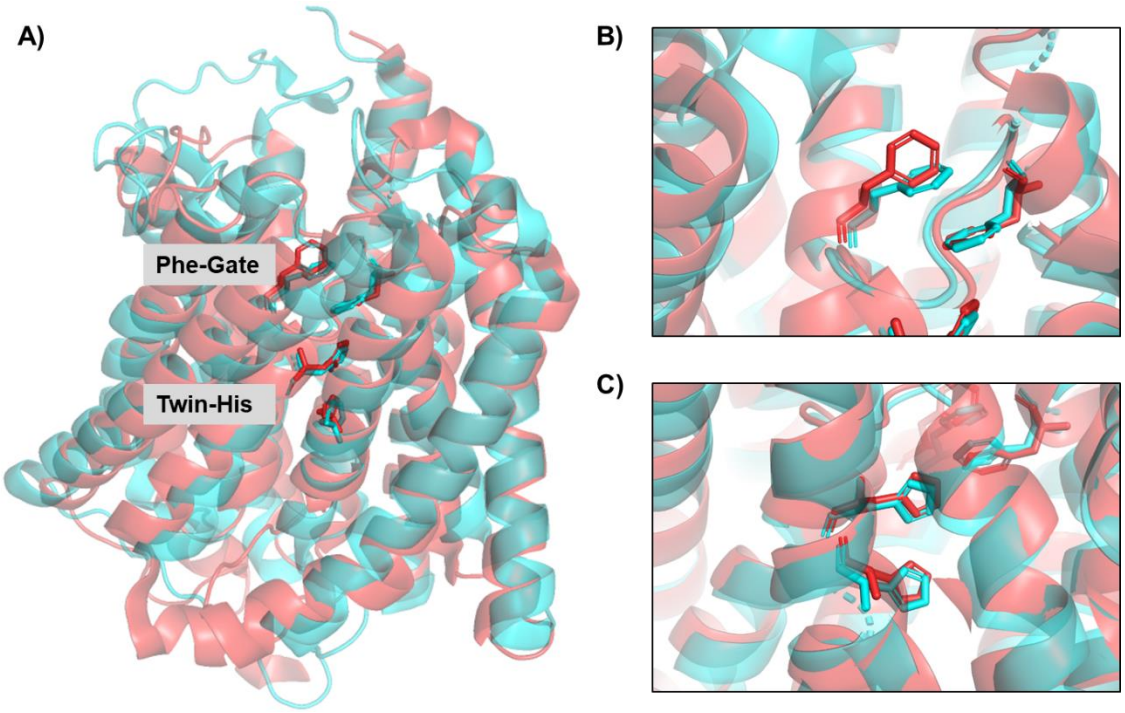

Figure 1.9 Comparison of AmtB and *Ne*Rh50: A) Overlay of a single monomer of AmtB (cyan) and NeRh50 (red) as inserted into the membrane. Residues of the Phe-gate and twin-His motif, are displayed in the same colour as their respective monomer. B) Enlarged view of tilt in the phenylalanine in NeRH50 compared to that in AmtB C) Enlarged view of the twin-His motif in each protein.

1.5.4.5 *Homo sapiens* RhCG

In 2010, the crystal structure of RhCG – found in epithelial cells of the renal collecting ducts - was resolved at 2.1 Å (Gruswitz *et al.*, 2010). This demonstrated that human Rh also adhered to a trimeric organisation and confirmed conservation of this conformation across the Amt/Mep/Rh superfamily (**Figure 1.10A**).

RhCG retains the pseudo-two-fold symmetry between TMH1-5 and TMH6-10 seen in bacterial Amt and Rh proteins, but also features a 12th N-terminal TMH. This helix, termed TM0, lies at the subunit interface of the trimer and varies in length across the different Rh isoforms, suggesting functional differentiation (Gruswitz *et al.*, 2010).

As with the bacterial *Ne*Rh50, no S1 binding site was observed in the structure of RhCG. However, the authors suggested that acidic residues within the extracellular vestibule (E166, D218, D278, and E329) could serve to recruit NH_4^+. The phenylalanines of the Phe-gate are conserved, but in RhCG the outer phenylalanine (F130) does not obstruct the pore, resulting in an “open” conformation with no barrier between the vestibule and the hydrophobic central pore (**Figure 1.10B**). As with previously discussed members of the family, the twin-His motif is conserved and protrudes into the centre of this pore.

Interestingly, Rh proteins share a common feature not seen in Amt or Mep proteins: a “shunt” on the cytoplasmic face of the proteins (**Figure 1.10C**). Whilst the function, if any, of the “shunt” is unclear, Grunswitz *et al*. hypothesised that it may represent an alternative path for NH_4^+ entry, and NH_3 delivery into the hydrophobic portion of the pore.

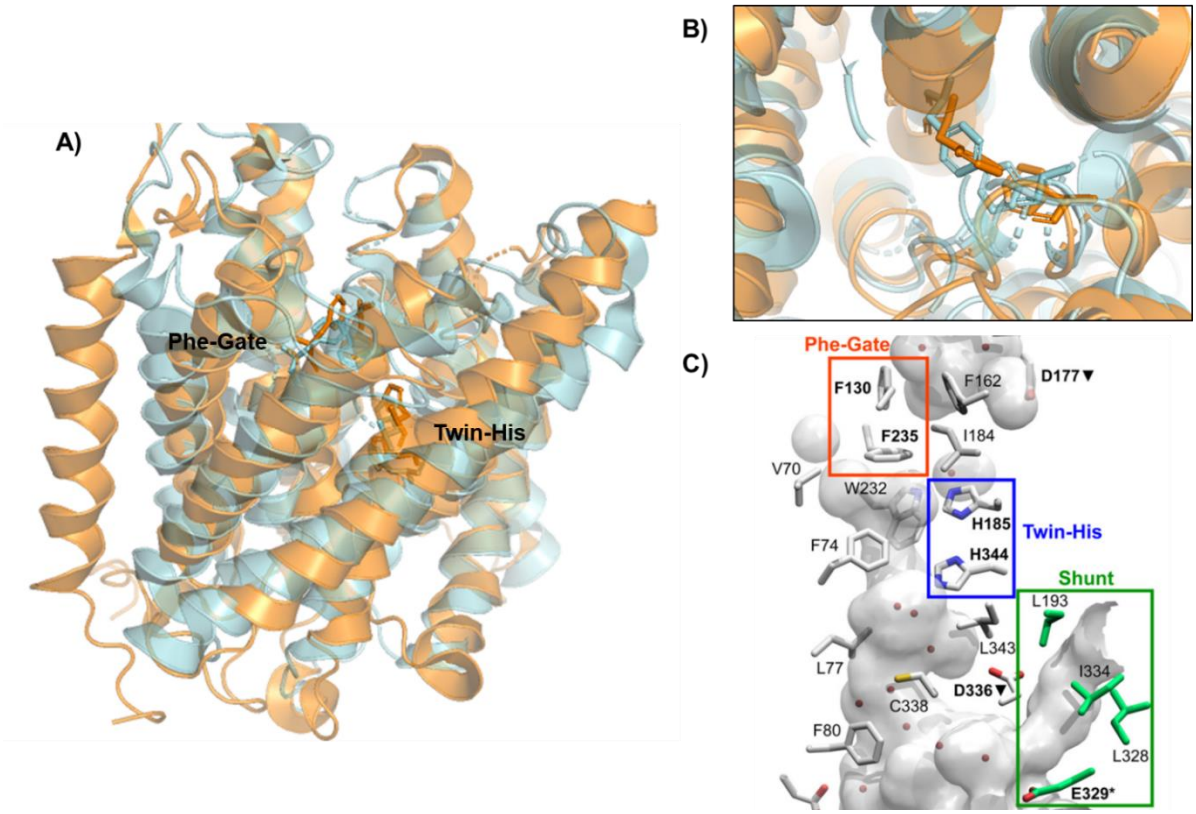

Figure 1.10 Comparison of AmtB and RhCG: Overlay of a single monomer of AmtB (cyan) or RhCG (orange) as inserted into the membrane (A) Residues of the Phe-gate, and twin-His motif are displayed in the same colour as their respective monomer. B) Comparison of the Phe-gate as viewed from the periplasm. C) Side-view of the RhCG channel and shunt, as presented by Gruswitz *et al*., 2010

1.6 General Mechanism of Amt/Mep/Rh

Thus far the expectation that 3D structures of Amt/Mep/Rh proteins would elucidate the transport mechanisms has not been met, due to all structures showing an identical inward-facing state of the protein. There are no significant differences in the crystal structures of Amt and Rh proteins that can clearly account for the functional differences between transporter-like (Amt) and channel-like (Rh) activity. While the crystal structures allow for hypotheses they provide no definitive answers and as such the mechanism of Amt/Mep/Rh proteins remains unclear and controversial. Throughout **Section 1.6** I will outline and discuss the literature surrounding the mechanism of Amt/Mep/Rh proteins.

1.6.1 General Mechanism of Amt/Mep/Rh

Despite the ubiquity and importance of the Amt/Mep/Rh family, their mechanism remains elusive. Questions persist concerning not only the nature of the transporters (passive channels *vs* active transporters), but also the transported species (NH_4^+ or NH_3), with a number of mechanisms proposed.

Early functional studies measured the uptake of an ammonium analogue, methylammonium, to characterise the transporters. These studies demonstrated that Amt/Mep/Rh proteins facilitate methylammonium uptake in *S. cerevisiae* and, through ammonium competition assays, that they are selective for ammonium (Marini *et al.*, 1994). They also enabled comparison of substrate capacity and transport rate between proteins, such as the three Mep proteins in *S. cerevisiae* (Marini *et al.*, 1997). However, these studies did little to remedy the lack of knowledge around the mechanism of transport. This was, in part, due to the lack of a robust *in vitro* assay that would allow for direct measurement of the true substrate, NH_4^+, and permit complete control over environmental conditions, thus enabling specific mechanistic questions to be asked. In addition, the lack of structural information hindered mechanistic

understanding. Therefore, it was expected that crystal structures would finally reveal the mechanism of transport.

In 2004, AmtB *E. coli* became the first ammonium transporter to have its crystal structure resolved. As detailed in **Section 1.5.3,** each monomer of AmtB possesses a potential periplasmic NH_4^+ binding site (S1, delineated by the residues S219, W148, F107, D160), followed by a strongly hydrophobic pore leading to the cytoplasm (Khademi *et al.*, 2004). The hydrophobicity of the pore acts as an energetic barrier for ions translocation. This structure is highly conserved across the family, being seen in the crystal structures of *S. cerevisiae* Mep proteins, and the rhesus proteins in both *N. europaea* and *Homo sapiens* (**Figure 1.11**) (Lupo *et al.*, 2007; Gruswitz *et al.*, 2010; van den Berg *et al.*, 2016). As a result of this conserved hydrophobic pore, it was concluded that the Amt/Mep/Rh family were electroneutral NH_3 transporters.

Since then, the view that Amt/Mep/Rh proteins conducted a neutral species has been experimentally challenged for some plant Amt and Rh proteins (Neuhäuser, Dynowski and Ludewig, 2014; Caner *et al.*, 2015), with charge translocation observed for both AMT1;1 from *Lycopersicon esculentum* and human RhAG expressed in *Xenopus laevis* oocytes in the presence of ammonium (Ludewig, Von Wirén and Frommer, 2002; Caner *et al.*, 2015). Additional *in vitro* studies have revealed that charged species are translocated across the membrane during the transport cycle of bacterial Amt proteins (Wacker *et al.*, 2014; Mirandela *et al.*, 2019).

Recent evidence has also been reported to support the importance of deprotonation of NH_4^+ as a major step in ammonium transport across the whole family (Ariz *et al.*, 2018). The apparent conflict between the crystal structures, which prohibit charge translocation, and functional observations of electrogenic transport reignited the controversies regarding the transport mechanism of Amt/Mep/Rh, centring on a new paradox: **how can a charge travel through a hydrophobic pore?**

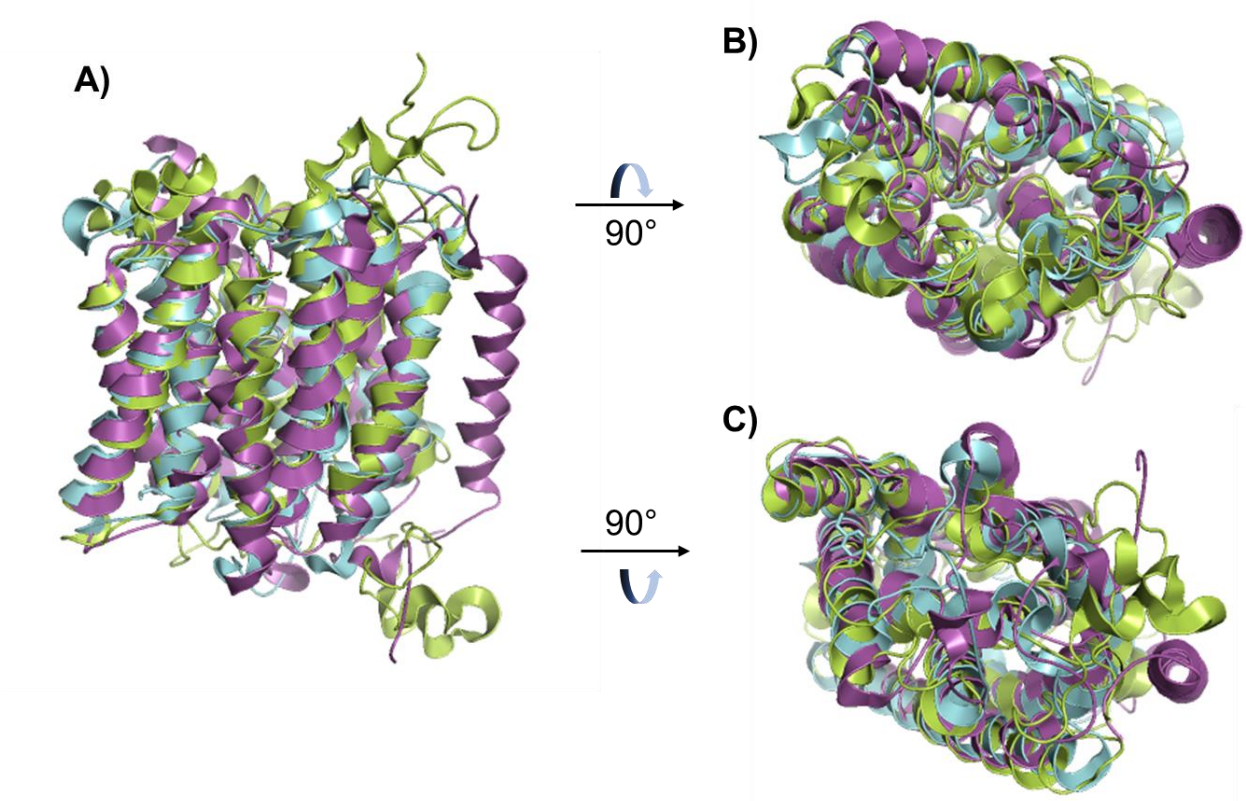

Figure 1.11 Structural Conservation of Amt/Mep/Rh protein: A monomer from *E. coli* AmtB (cyan), *S. cerevisiae* Mep2 (green), and *H. sapiens* RhCG (purple) shown from three orientations: A) Sideview of proteins as inserted in the membrane, with N-terminus at the top and C-terminus at the bottom. B) Top-down view of N-terminus. C) Top down view of C-terminus. Crystal structures for AmtB, Mep2, and RhCG were obtained from PDB (1u7g, 5af1, 3hd6 respectively) and aligned in pymol.

1.6.2 Functional Characterisation of AmtB

Over the course of the last 15 years, many studies have been conducted with the aim of elucidating the mechanism of AmtB-mediated ammonium conduction. However, there is now a clear conflict between the existing structural and functional evidence within the Amt/Mep/Rh family. As such, I will review the previous characterisation of AmtB in light of this conflict, discussing specific facets of the mechanism in turn.

1.6.2.1 Deprotonation

The hydrophobic pore seen in AmtB, and other members of the family, acts as an energetic barrier against movement of ions. Therefore, between the S1 binding site and the hydrophobic pore NH_4^+ must be deprotonated.

When initially reporting the crystal structure, Khademi *et al* hypothesised that NH_4^+ could be deprotonated by a water molecule (Khademi *et al.*, 2004). As they did not detect proton translocation, they concluded that following deprotonation the proton would be released into the bulk water in the periplasm. This view was echoed by Professor Fritz Winkler, who used a Michaelis-Menten model to argue that recruitment and deprotonation at the S1 site was vital to ensure sufficient conduction (Winkler, 2006). In the context of electroneutral transport, this mode of deprotonation is possible. However, as Mirandela *et al* have recently demonstrated that AmtB-mediated transport is electrogenic, this hypothesis can be rejected (Mirandela *et al.*, 2019). If the proton exited into the bulk solvent, then no charge would be measured on the Solid Supported Membrane Electrophysiology system (explained in **Section 2.5**) used by Mirandela *et al.*

Computational modelling suggested that S219 fulfils a dual role in ammonium transport: first coordinating NH_4^+ *via* H-bond formation between the hydroxyl oxygen of S219 and NH_4^+; before acting as a proton acceptor to facilitate

deprotonation (Ishikita and Knapp, 2007). This model has remained relatively untested – but Javelle *et al* showed that AmtB^{S219A} had enhanced, rather than reduced, MeA uptake compared to the WT (Javelle *et al.*, 2008). This increased MeA accumulation was observed for all single mutations of binding site residues (F107A, W148A, and S219A), suggesting that under the conditions in the study recruitment at S1 was not rate-limiting.

If deprotonation occurs at the S1 site, then D160 is another potential proton acceptor. As shown by sequence analysis of Amt/Mep/Rh proteins this aspartate (position 160 in AmtB) is highly conserved – suggesting a structural or functional role (Javelle *et al.*, 2004). A functional role was validated by methylammonium uptake assays, which demonstrated that a D160A variant of AmtB was inactive in MeA transport while D160E variants retained ~70% of WT activity (Javelle *et al.*, 2004). In addition, the equivalent residue in *Sc*Mep2 (D182) has been implicated in methylammonium binding affinity, strengthening the functional importance of D160 (Marini *et al.*, 2006).

When reporting the crystal structure of AmtB, Khademi *et al* noted that they did not observe a density against D160 in either the presence of NH_4^+ or MeA. Due to this and the orientation of the D160 in the crystal structure, they concluded that it could not interact with an NH_4^+ held within the binding site (Khademi *et al.*, 2004). However, a later molecular dynamic simulation (MDS) predicted that D160 was vital for binding and the carboxyl group of D160 would be available for interaction (Luzhkov *et al.*, 2006). Thus, a functional role of D160 remains viable and must be further elucidated.

Despite the different hypotheses, the basis for deprotonation in AmtB remains unclear. To elucidate the deprotonation events involved in AmtB-mediated transport, variants with substitutions in the discussed residues should be analysed using *in vitro* assays.

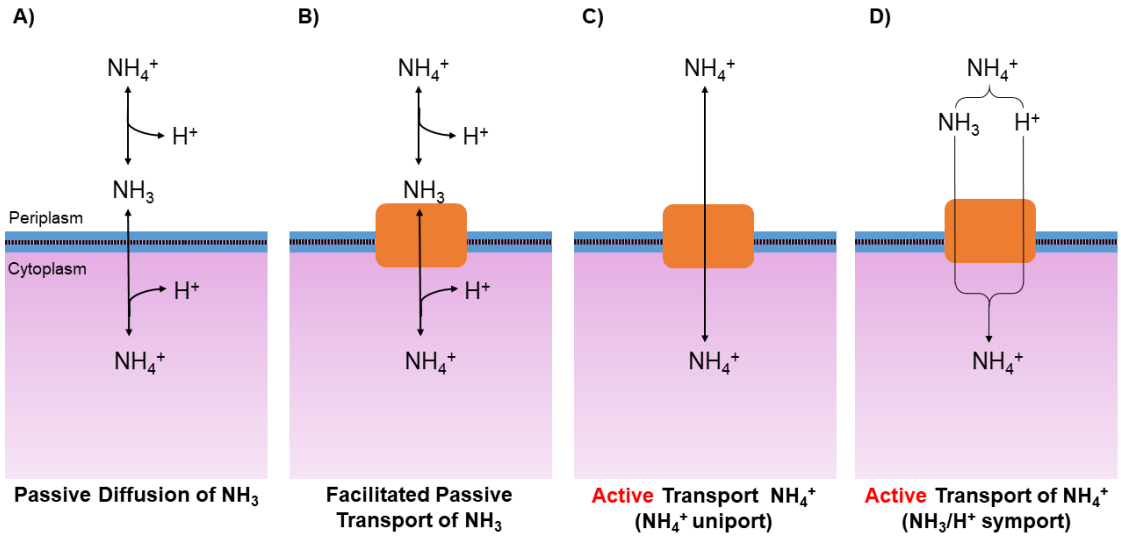

Figure 1.12 Mechanisms of Ammonium Transport. The rounded rectangle represents AmtB. Four modes (mechanisms) of transport are shown. A) Transport via passive diffusion of NH_3; B) facilitated transport of NH_3; C) active transport of NH_4^+, corresponding to facilitated transport of NH_4^+; D) active transport of NH_3, via NH_3/H^+ symport.

1.6.2.2 Substrate and Proton Conductance

As detailed previously, the substrate transported by AmtB has been a matter of controversy. The potential modes of transport included: passive diffusion of NH_3, facilitated NH_3 diffusion, active transport of NH_4^+, and active $NH_3 + H^+$ transport (**Figure 1.12**).

The former two, which nominate NH_3 as the sole substrate, are the result of early studies which viewed the AmtB as a passive gas channel (Soupene, Lee and Kustu, 2002). However, the S1 binding site observed in the crystal structures runs counter to the electrochemical gradient acting as the sole driving force (Khademi *et al.*, 2004). Soupene *et al* proposed facilitated diffusion of NH_3, following their finding that accumulation was due to acid trapping of MeA (Soupene, Lee and Kustu, 2002). Whilst this is consistent with the hydrophobicity of the pore, it is limited by the predominance of NH_4^+ at physiological pH.

To demonstrate this Boogerd *et al* employed a system biology approach, which concluded that passive transport of NH_3 would not be sufficient for observed growth in *E. coli* (Boogerd *et al.*, 2011). Thermodynamically, intracellular [NH_4^+] would not be able to exceed extracellular [NH_4^+] whilst maintaining an inward nitrogen flux. Therefore, if transport were passive it would be expected that in an ammonium limited environment with low pH, *E. coli* would be unable to grow. However, it can still grow and continues to use ammonium as a nitrogen source. In fact, Amt/Mep/Rh are expressed under nitrogen limiting conditions, when passive conductance would be insufficient.

Wacker ***et al's*** observation of electrogenic transport provided the final evidence required to exclude NH_3 uniport as a transport mechanism, but did not reveal the true mechanism (Wacker *et al.*, 2014). Three potential electrogenic mechanisms are possible: NH_4^+ uniport, NH_4^+/H^+ symport, deprotonation symport (NH_3/H^+). Of these, NH_4^+ uniport is the least likely, due to the aforementioned energetic barriers impeding ion conduction through a

hydrophobic pore. Additionally, it has been shown that “open-pore” mutants of AmtB (constructed with the phenylalanine gate removed) become inactive in transporting MeA, and does not gain permeability to neither H^+ nor K^+ (Javelle *et al.*, 2008). This demonstrates that widening access to the pore does not allow for ion conduction through AmtB, and suggests that another mechanism and/or residues must be implicated in transport.

The latter proposition of NH_3/H^+ is consistent with the hypothesis that NH_4^+ is recruited by AmtB, and subsequently deprotonated to NH_3 and H^+, and each individually conducted through the pore. Although this is contested by prior structural data, more recent molecular dynamic simulations suggested that a chain of water molecules can form at the twin-His motif, parallel to the central pore (Baday *et al.*, 2013). Such a chain could function as a water wire, facilitating the movement of protons via a Grothuss mechanism, in which a single proton is rapidly transported by “hopping” from one water molecule to another.

To date however, the presence of a water wire has not been verified experimentally, nor has proton-hopping been proven as a mechanistic feature of AmtB-mediated transport. Therefore, the fate of a proton following deprotonation must be elucidated to fully understand the mechanism of AmtB.

1.6.2.3 Specificity of Transport

Another important yet poorly understood element of AmtB-mediated ammonium transport is its specificity and selectivity. AmtB, as with other members of the superfamily, is expressed in response to nitrogen limitation. As a result, it is imperative that it maintains selectivity against other prevalent cations, such as K^+ and Na^+. Classical mechanisms of selectivity include size-exclusion, wherein the protein region which interacts with the substrate is of a precise or limited size. Thus larger molecules are sterically blocked from being transported (Kopec *et al.*, 2018). Within a solution, ions interact with the solvent

and become surrounded by a concentric ring of solvent. Prior to transport this shell has to be stripped away. The strength of the interactions holding the ring together will vary depending on the central ion, with stronger bonds requiring more energy to break. This can be exploited to enforce selectivity, with proteins able to desolvate certain ions but not others (Kopec *et al.*, 2018). These mechanisms, however, do not explain the selectivity we observe in AmtB as K^+ and Na^+ have similar ionic radii and charge to NH_4^+.

Different features of AmtB have been suggested to account for selectivity.

S1: Molecular Dynamic Simulations (MDS) have reported binding free energies which heavily favour NH_4^+ over other ions (Luzhkov *et al.*, 2006). Javelle *et al.* suggest that this is due to the unusual combination of hydrogen bonding and pi-cation stabilisation in the S1 site, which creates a tetrahedral coordination preferred by NH_4^+. In contrast, Na^+ and K^+ favour octahedral coordination (Javelle *et al.*, 2008). This has not been tested directly, but when co-crystallised with K^+ or Na^+, no density is observed, while a density is observed with thallium (Javelle *et al.*, 2008). Thallium has previously been shown to bind to the ammonium binding site of glutamine synthetase (Liaw, Kuo and Eisenberg, 1995), so it's binding suggests that the S1 site is selective. In addition, S219A has been demonstrated to retain transport activity *in vivo* (Javelle *et al.*, 2008). If it's selectivity was impaired such that K^+ could permeate AmtB then it is likely that cytotoxicity would have been observed by the authors.

Due to its position as a blockade between the periplasmic vestibule and the hydrophobic pore, movement of Phe-gate would be required for substrate translocation and could contribute to selectivity (Khademi *et al.*, 2004). This role was challenged however, by the characterisation of an "open-pore" mutant (F107A/F215A). Compared to the WT this open-pore variant should have increased permeability to NH_4^+, NH_3, protons, and physiologically relevant ions. However, Javelle *et al* demonstrated that this variant did not conduct either K^+, H^+, or water, and was inactive in the transport of MeA (Javelle *et al.*, 2008). While this supports a functional role for the Phe-gate in translocation, it

also suggests that selectivity is independent of the Phe-gate and is achieved *via* a specific mechanistic feature, not *via* steric hindrance.

Despite the almost complete conservation of the histidines that comprise the twin-His motif, Hall *et al* demonstrated that AmtB could tolerate substitution of acidic residues at H168 and/or H318 while retaining activity (Hall and Kustu, 2011). This prompted them to question why the motif was conserved, if it was apparently non-essential for function. Further work demonstrated that the double mutation of H168D/H318E led to a loss of selectivity and to measurable transport of K^+ (Hall and Yan, 2013). This suggests a role for the twin-His motif in selectivity, however it is unclear how this is achieved and its place within the overall translocation cycle.

Many of these studies incorporate methylammonium uptake experiments, as it is the classical substrate analogue for ammonium. Therefore, it is important to question the suitability of MeA as an analogue, particularly as it pertains to elucidating discrete mechanistic details. A 2013 study observed various single His variants (in both *Ec*AmtB and *Sc*Mep2) used in this study were unable to uptake MeA, however they retained their ability to grow on minimal media supplemented with 1 mM NH_4^+ as a sole nitrogen source (Wang *et al.*, 2013). The authors explained this discrepancy with molecular dynamic simulations, which suggested that the substitutions created space for ammonium to pass through the pore, but not MeA (Wang *et al.*, 2013). This highlights the need for awareness of the limitations of MeA as an analogue, as well as the importance of a robust *in vitro* assay for the investigation of the mechanism of ammonium transport.

1.6.3 Mechanistic Insights in Other Members of the Amt/Mep/Rh family

As with AmtB, the mechanism of other members of the Amt/Mep/Rh family are poorly understood. In addition, it is unclear if there is a conserved mechanism across the superfamily or if different mechanisms have evolved within it. Here

follows a brief summary of mechanistic information acquired from other Amt/Mep/Rh and their implications.

The Mep proteins have been shown to be closely related to prokaryotic Amt proteins, both phylogenetically and functionally. They cluster together in phylogenetic trees and bacterial AmtB can replace the function of Mep in triple-*mep1-3Δ S. cerevisiae.* Based on this, it is likely that they share a similar mechanism. However, the transceptor/signalling function of Mep2 (explored in **Section 1.4.2**) may hint at a different mechanism. Currently, it is unknown how the signal is initiated but there are two possibilities: 1) Mep2 binds to a partner protein to illicit the signal, or 2) Mep2 conducts ammonium *via* a separate mechanism in order to transduce the signal.

Whilst AmtB is the paradigm of the family, plant Amts are also the subject of much research. In plants, the mechanism of ammonium transport is best understood in *Arabidopsis thaliana*. The *Arabidopsis* genome encodes for 6 AMT genes, divided into two sub-families. The larger of these families AMT1, has been demonstrated to facilitate electrogenic transport in *Arabidopsis* and in other plants (Neuhäuser, Dynowski and Ludewig, 2014). However, it has been suggested that the AMT2 family is are electroneutral NH_3 transporters (Neuhauser, Dynowski and Ludewig, 2009). If this is true, it remains unclear what drives the differences in the mechanism between the two subfamilies.

As the most distant member of the Amt/Mep/Rh family, distinct functions have repeatedly hypothesised for the rhesus proteins. It is clear that a subset of the family (Rh30) has evolved to lose transport activity and instead act as antigens on the surface of erythrocytes. Rh50 proteins are known to be transporters but their substrate and mechanism remains debated. The Rh50 protein from *N. europaea* and the human RhAG and RhCG complement *mep1-3Δ S. cerevisiae* (Marini *et al.*, 2000; Cherif-Zahar *et al.*, 2007), suggesting they also transport ammonium. Attempts to elucidate the mechanism however, have been conflicting. An initial patch-clamp physiology experiments wherein RhAG expressed in *Xenopus* oocytes lead the authors to propose that RhAG is an NH_4^+/H^+ antiporter (Westhoff *et al.*, 2002). Contemporaneous studied revealed

that RhAG and RhBG were electroneutral, and RhCG was an electrogenic NH_4^+ uniporter (Ludewig, Von Wiren and Frommer, 2002). However, later work using stopped-flow spectrophotometry to measure changes in pH in erythrocyte vesicles and liposomes containing RhCG concluded that it was an electroneutral (NH_3) channel (Ripoche *et al.*, 2004; Mouro-Chanteloup *et al.*, 2010). This is supported by more recent oocyte experiments, wherein no significant difference in current was observed in RhCG-expressing oocytes compared to control (Caner *et al.*, 2015). Despite this lack of current, RhCG resulted in increased surface-acidification leading the authors to conclude that RhCG transported NH_3 but not NH_4^+.

1.7 Aims of the PhD Project

Currently, there is a clear conflict between the structural and functional evidence surrounding AmtB-mediated ammonium transport. Despite the hydrophobic pore reported in the crystal structure representing an energetic barrier for charge translocation, electrogenic transport has been experimentally reported. In this context, the overall aim of this PhD project is to establish the mechanism of AmtB-mediated transport at the molecular level, using a combinatorial approach (molecular dynamic simulations, *in vivo* assays, and *in vitro* electrophysiology assays). In particular, solid supported membrane electrophysiology (SSME) represents a powerful tool for probing the mechanistic detail of ammonium transport (detailed in **Section 2.5**). Once established, the conservation of this mechanism in other family members could be investigated. The specific aims are to:

1. Characterise the kinetics, energetics and specificity of *Ec*AmtB
2. Demonstrate importance of deprotonation in the transport mechanism.
3. Determine how H^+ is subsequently translocated.
4. Understand the mechanism underlying AmtB's strict selectivity.

Chapter 2:
Materials and Methods

Chapter 2: Materials and Methods

2.1 Molecular Biology

2.1.1 Strains and Media Preparation

A list of all strains and media compositions used throughout this work can be found in **Table 2.1** and **2.2** respectively.

All media and buffers were filtered through a 0.22 µm pore filter and autoclaved at 121°C for 15 minutes to sterilise.

2.1.2 Preparation of Chemically Competent Cells

A single colony of *E. coli* was used to inoculate 5 mL of LB media in a sterile 20 mL universal, and incubated overnight at 37°C. This was then used to inoculate 100 mL of sterile LB in a 250 mL Erlenmeyer flash and subsequently incubated at 37°C for between 1.5 and 3 hours, or until the OD_{600} reached 0.5.

The culture was then transferred to sterile 50 mL centrifuge tubes and rested on ice for 10 minutes. The cells were pelleted by centrifugation at 4000 *g* at 4°C for 10 minutes. The supernatant was discarded and the cells gently suspended in 10 mL of ice-cold sterile 0.1M CaCl, before being rested on ice for a further 20 minutes. Following this rest, the centrifugation was repeated and the cells resuspended in 5 mL of ice-cold sterile 0.1M CaCl + 15% glycerol (w/v). Competent cells were dispensed in 300 µL aliquots and flash-frozen in liquid nitrogen prior to storage at -80°C.

Table 2.1 Strains Used in This Work

Strain	Genotype	Reference
E. coli		
DH5α	F⁻ φ80*lac*ZΔM15 Δ(*lac*ZYA-*arg*F) U169 *rec*A1 *end*A1 *hsd*R17(r_K^-, m_K^+) *pho*A *sup*E44 λ⁻ t*hi*-1 *gyr*A96 *rel*A1	(Hanahan, 1985)
C43 (DE3)	F⁻ ompT gal dcm hsdS_B(r_B^- m_B^-)(DE3)	(Miroux and Walker, 1996)
GT1000	rbs lacZ::IS1 gyrA hutCK glnKamtB	(Coutts *et al.*, 2002)
S. cerevisiae		
31019b	*MATa ura3 mep1Δ mep2Δ::LEU2 mep3Δ::KanMX2*	(Marini *et al.*, 1997)
228	*mep1Δ mep2Δ mep3Δ trk1Δ trk2Δ leu2*	(Hoopen *et al.*, 2010)

Table 2.2 Media Preparation

Name of Media	Composition	Reference
Lysogeny Broth	10 g/L Tryptone	(Bertani, 1951)
	5 g/L Yeast Extract	
	5 g/L NaCl	
ZY	10 g/L Tryptone	(Studier, 2005)
	5 g/L Yeast Extract	
50X5052	1.4 M Glucose	(Studier, 2005)
	270 mM Glycerol	
	300 mM α-Lactose	
20XNPS	0.5 M $(NH_4)_2SO_4$	(Studier, 2005)
	1 M KH_2PO_4	
	1 M Na_2HPO_4	
ZYP-5052	928 mL ZY	(Studier, 2005)
	1 mM $MgSO_4$	
	25 mM $(NH_4)_2SO_4$	
	50 mM KH_2PO_4	
	50 mM Na_2HPO_4	
	28 mM Glucose	
	5.4 mM Glycerol	
	6 mM α-Lactose	
M9 Salt Solution	6 g/L Na_2HPO_4	(Elbing and Brent, 2002)
	3 g/L KH_2PO_4	
	0.5 g/L NaCl	
M9 Minimum	0.2% (v/v) glucose	(Elbing and Brent, 2002)
Media	0.2 mg/mL glutamine	
	1 mM $MgSO_4$	
Ampicillin	100 µg/mL	
Chlromaphenichol	34 µg/mL	

2.1.3 Heat-Shock Transformation of E. coli

0.1 µg of plasmid DNA was added to 50 µL of thawed chemically competent cells and incubated on ice for 30 minutes. Following this, the cells were heat-shocked at 42°C for 45 seconds and transferred to ice for 5 minutes. 300 µL of sterile LB was added and the cells incubated at 37°C for at least 1 hour, before spreading 100 µL on LB plates containing the appropriate antibiotic for selection.

2.1.4 Plasmid Purification

Cells were grown overnight in 5 mL of LB supplemented with the appropriate antibiotic and plasmids purified with a QIAGEN Miniprep kit [Qiagen], according to the provided instructions. Briefly, cells were pelleted *via* centrifugation and chemically lysed under alkaline conditions. Cellular debris was separated *via* centrifugation and DNA subsequently bound to a provided QIAGEN silica column. RNA and protein contaminants were washed off with a high salt buffer, and the DNA eluted in sterile ddH_2O. DNA concentration was subsequently quantified using Nanodrop 2000.

2.1.5 Site Directed Mutagenesis

amtB mutants were generated using the Quikchange XL site directed mutagenesis kit (Agilent Technologies), according to manufacturer's instructions. Following a PCR step, 1 µL of DpnI was added to the PCR product and the sample incubated for at least one hour at 37°C, before being transformed into chemically competent *E. coli* DH5α. Plasmid DNA was purified from candidate colonies and successful mutagenesis verified by Sanger sequencing (carried out by Eurofins Genomics). The primers used for the mutagenesis are listed in **Table 2.3** and the template was the *amtB* gene cloned into the plasmid pET22b(+)(Zheng *et al.*, 2004)(**Table 2.4**).

Table 2.3: Primers*

Primer	Direction	Sequence
Mutagenesis:		
AmtB^{S219A}	Forward	GGTGGCACCGTGGTGG**ATA**TTAACGCCGCAATC
AmtB^{D160A}	Forward	CTCACGGTGCGCTGG**CC**TTCGCGGGTGGCACC
AmtB^{D160E}	Forward	CTCACGGTGCGCTGG**AG**TTCGCGGGTGGCACC
AmtB^{H168E}	Forward	GGTGGCACCGTGGTGG**AGA**TTAACGCCGCAATC
AmtB^{H168D}	Forward	GGTGGCACCGTGGTGG**ATA**TTAACGCCGCAATC
AmtB^{H168A}	Forward	GGTGGCACCGTGGTGG**CCA**TTAACGCCGCAATC
AmtB^{H318A}	Forward	TGTCTTCGGTGT**GGC**CGGCGTTTGTGGCATT
AmtB^{H318E}	Forward	TGTCTTCGGTGT**GGA**GGGCGTTTGTGGCATT
Expression in Yeast:		
AmtB XhoI	Forward	AGTC**CTCGAG**ATGAAGATAGCGACGATAAAA
AmtB BamHI	Reverse	AGTC**GGATCC**TCACGCGTTATAGGCATTCTC
P5'NeRh	Forward	GCC**ACTAGT**ATGAGTAAACACCTATGTTTC
P3'NeRh	Reverse	GCC**GAATTC**CTATCCTTCTGACTTGGCAC

*Nucleotides in bold have been changed to introduce the mutations/restriction sites

Table 2.4: Plasmids used in this study

Plasmid	Description	Reference
pET22b (+)	High copy bacterial expression vector	Novagen
pDR195	High copy yeast expression vector	(Rentsch *et al.*, 1995)
pAD7	pESV2-Rh50$(His)_6$	(Cherif-Zahar *et al.*, 2007)
p426MET25	High copy shuttle expression vector	(Mumberg *et al* 2012)
pZheng	pET22b-AmtB$(His)_6$	(Zheng *et al.*, 2004)
pAJ2024	pET22b-AmtB$(His)_6^{S219A}$	(Javelle *et al.*, 2008)
pGDM2	pET22b-AmtB$(His)_6^{H168AH318A}$	This study
pGDM4	pET22b-AmtB$(His)_6^{D160A}$	This study
pGDM5	pET22b-AmtB$(His)_6^{D160E}$	This study
pGDM6	pET22b-AmtB$(His)_6^{S219AH168AH318A}$	This study
pGW1	pET22b-AmtB$(His)_6^{H168E}$	This study
pGW2	pET22b-AmtB$(His)_6^{H168A}$	This study
pGW3	pET22b-AmtB$(His)_6^{H318A}$	This study
pGW4	pET22b-AmtB$(His)_6^{H318E}$	This study
pGDM7	pDR195-AmtB^{S219A}	This study
pGDM9	pDR195-AmtB^{D160A}	This study
pGDM12	pDR195-AmtB^{H168AH318A}	This study
pGDM13	pDR195-AmtB^{S219AH168AH318A}	This study
pGW6	pDR195-AmtB^{H168E}	This study
pGW7	pDR195-AmtB^{H168A}	This study
pGW8	pDR195-AmtB^{H318A}	This study
pGW9	pDR195-AmtB^{H318E}	This study

2.1.6 Sub-cloning for Yeast Expression

In order to express our variants in *Saccharomyces cerevisiae* we used the plasmid PDR195 (Rentsch *et al.*, 1995). In this plasmid, *amtB* expression is controlled by the promoter of *PMA1*, a housekeeping plasma membrane ATPase gene.

20 ng of plasmid DNA from each construct was amplified by PCR reaction using Q5 High Fidelity DNA Polymerase (NEB), according to the manufacturer's instructions. The primers (**Table 2.3**) were designed to add XhoI and BamHI restriction sites to the end of *amtB.* After the PCR, 1 µg of amplified DNA products and 2 µg of pDR195 vector (**Table 2.4**) were digested with XhoI and BamHI (Promega Corporation) (5 units of enzyme/µg of DNA) at 37°C for 2 hours. Digested DNA samples were run on 2% agarose gels in TAE buffer (**Table 2.2**) at $100V*cm^{-1}$ for 1 hour. DNA was extracted from the gel using the kit Wizard® SV Gel and PCR clean-up system (Promega Corporation), following the provided protocol.

For ligation, 50 ng of digested insert DNA was mixed with linearised pDR195 to an insert: vector molar ratio of 5:1. The ligations were carried out in a reaction volume of 10 µL and incubated overnight at 4°C to increase ligation efficiency. Finally, 10 µL of the ligation reaction was transformed into *E. coli* DH5α *via* heat-shock transformation (see **Section 2.1.3**)

2.2 AmtB and NeRh50 expression in yeast and complementation test

The different variants of *amtB* were amplified using *amtB* cloned into pET22b(+) (**Table 2.4**) as a template, the primers AmtB XhoI and AmtB BamHI and sub-cloned into the plasmid pDR195 (**Table 2.4**). The NeRh50 gene was amplified from *N. europaea* genomic DNA (gift from Daniel J. Arp and Norman G. Hommes, Department of Botany and Plant Pathology, Oregon State University, Corvallis, USA) using the primers P5'NeRh and P3'NeRh (**Table 2.3**) and was cloned into the SpeI and EcoRI restriction sites of the high-copy

vector p426Met25 (**Table 2.4**) allowing controlled-expression of NeRh50 by the yeast methionine repressible MET25 promoter.

Two *S. cerevisiae* strains were used in this work: 31019b (*MATa ura3 mep1Δ mep2Δ::LEU2 mep3Δ::KanMX2*), and 228 (*mep1Δ mep2Δ mep3Δ trk1Δ trk2Δ leu2)*(Marini *et al.*, 1997; Hoopen *et al.*, 2010)**.** Plasmids (listed in **Table 2.3)** were transformed into these strains as described previously (Gietz *et al.*, 1992). For growth tests on limited ammonium, *S. cerevisiae* cells were grown in a minimal buffered (pH 6.1) medium with 3% glucose as the carbon source and 0.1% (7 mM) glutamate, or $(NH_4)_2SO_4$ at the specified concentrations, as the sole nitrogen sources. For growth tests on limiting potassium concentrations, a minimal buffered (pH 6.1) medium deprived of potassium salts was used.

2.3 Protein Expression and Purification

2.3.1 AmtB

2.3.1.1 Overexpression

AmtB(His)$_6$ cloned into the pET22b(+) vector (**Table 2.4**) was overexpressed in the C43 strain of *E. coli*. A single colony of C43 transformed with pET22b-AmtB(His)$_6$ fusion was used to inoculate 1 litre of LB broth (+ 100 µg/mL ampicillin) and incubated for ~8 hours at 37°C with 300 rpm shaking to provide a starter culture for overexpression. This starter culture was then used to inoculate up to 12 litres of ZYP-5052 auto-induction media (**Table 2.2**).

These cultures were placed in a 30°C incubator with 300 rpm orbital shaking overnight. The following morning, the cells were collected by centrifuging the cultures at 7,439 *g* for 1 hour (JLA 9.100, Beckman Avanti JXN-26). The cell pellet was suspended in solubilisation buffer (**Table 2.5**) at a ratio of 1g of pellet: 10 mL buffer. DNase and PMSF were added, at respective final concentrations of 10 ng/mL and 200 µM, to reduce viscosity and to inhibit proteolytic activity respectively, before the suspension was separated into 50 mL aliquots, and stored at -20°C.

2.3.1.2 Membrane Preparation

Prior to purification, the *E. coli* cells first had to be lysed and the cellular membrane isolated. This was achieved via the French press: a hydraulic pump system that places cells under high pressure and forces them to rupture, thus fragmenting the membrane (Simpson *et al.*, 1963). Collected cells were allowed to thaw on ice and broken by three passages through a French Press maintained at 20, 000 psi. Remaining intact cells were pelleted by centrifugation at 23, 000 *g,* 4°C for 30 minutes (JA 25-50, Beckman Avanti JXN-26). The supernatant was retained, and subsequently subjected to ultracentrifugation at 200,000 *g* at 4°C for 1 hour (Ti 45, Beckman Optima XPN-100)., in order to pellet fragmented membrane, separating it from other cellular debris. The collected membrane was transferred to a 50 mL tube, weighed, and stored at -20°C.

2.3.1.3 Immobilised Metal Affinity Chromatography

E. coli membrane was solubilised by suspending the membrane in IMAC A buffer (**Table 2.5**) to a ratio of 1 g membrane: 10 mL buffer. This buffer contains DDM at 2%, which solubilises AmtB from the membrane whilst helping preserve its structure (**Figure 2.1**). The suspension was incubated at 4°C and agitated gently with a magnetic stirrer for a minimum of 2 hours, then the suspension was centrifuged at 200,000 *g* at 4°C for 30 minutes to pellet remaining insoluble membrane. Finally, the membrane suspension was diluted two-fold in IMAC A buffer to reduce the final DDM concentration to 1%.

The diluted solution was passed through 1 ml HiTrap HP column [GE Healthcare] using the ÄKTA Pure FPLC platform [GE Healthcare]. The column had previously been loaded with cobalt and equilibrated in IMAC A buffer + 0.033% DDM (**Table 2.5**). The $(His)_6$ tag on AmtB is coordinated by the cobalt bound to the resin, whilst other proteins within the solution flow through the column unabated. After sample loading was complete, non-specifically bound

proteins were eluted by washing the column in 10 column volumes (CV) of IMAC A containing 40 mM imidazole.

AmtB was eluted from the column using an imidazole gradient, gradually increasing from 40 mM to 500 mM over 20 column volumes. The eluent was collected in a 96-well deep well plate in 2 mL fractions. Protein size and purity was verified via SDS-PAGE electrophoresis (**Section 2.3.3**). Elution fractions containing AmtB were pooled together and concentrated to ~5 mg/mL using an Amicon centrifugal filter with a 100 kDa cut-off. The concentrated protein solution was then injected into a Superdex 200 increase (10/300) size exclusion column for polishing (**Section 2.3.1.5**).

n-dodecyl-β-D-maltopyranoside
(**DDM**)

CMC: 0.2 mM (0.01% w/v)

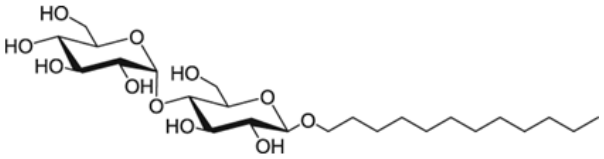

Lauryldimethylamine-N-oxide
(**LDAO**)

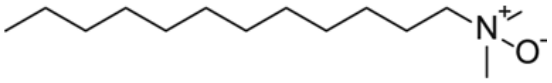

CMC: 2 mM (0.023% w/v)

Figure 2.1 Molecular Structure of Detergents. Chemical structure of detergents used in the purification of AmtB and Rh50. Structures were drawn in ChemDraw and the CMC (critical micelle concentration) values obtained from product documentation supplied by Avanti Polar Lipids.

2.3.1.4 Column regeneration

Following IMAC, the column was regenerated according the manufacturer's instructions. Briefly, the column was regenerated by sequentially passing 5 CV of water, stripping solution, water, cobalt solution, and water. The columns were stored in 20% ethanol to prevent bacterial growth and/or degradation of the resin. The composition of the solutions is detailed in **Table 2.5**.

2.3.1.5 Size Exclusion Chromatography

Elution fractions from IMAC containing AmtB were pooled and the concentration increased to a maximum of 5 mg/mL using an Amicon centrifugal filter unit [Merck] with a 100 kDa cut-off. This was subsequently injected into an ÄKTA PURE mounted with a Superdex 200 increase 10/300 size exclusion column [GE Healthcare]. 300 µL of AmtB at 5 mg/mL was injected into the system for each run, with size exclusion buffer (**Table 2.5**) passed through at a flow rate of 0.5 mL/min**.** The elution fractions were analysed on SDS-PAGE gel to confirm the presence of AmtB and assess the purity of the samples. AmtB was concentrated to 5 mg/mL using an Amicon centrifugal filter unit and stored at 4°C.

2.3.2 Purification of NeRh50

The plasmid pAD7 (**Table 2.4**) was used to overexpress *Ne*Rh50 in the *E. coli* strain GT1000 (Javelle *et al.*, 2004). GT1000 was transformed with pAD7 and grown in M9 medium (Elbing and Brent, 2002) in which ammonium was replaced by 200 µg/ml glutamine as the sole nitrogen source. *Ne*Rh50 was purified as described by Lupo *et al.*(Lupo *et al.*, 2007), with minor modifications: the membrane was solubilised using 2% lauryldecylamine oxide (LDAO) instead of 5% *n*-octyl-β-D-glucopyranoside (OG), and 0.09% LDAO was used in place of 0.5% β-OG in the final size exclusion chromatography buffer (50 mL Tris pH 7.8, 100 mL NaCl, 0.09% LDAO).

2.3.3 SDS-PAGE

The principle of SDS-PAGE was previously described by (Laemmli, 1970) In summary, sodium dodecyl sulfate (SDS) is an anionic detergent which linearises and confers a negative charge to proteins. The charge applied is uniform, thus proteins linearised by SDS separate according to their molecular mass. Unless otherwise stated, 15 µL of sample was mixed with 5 µL of loading buffer and loaded onto the gel. The gels were run at 27 V/cm for 1 hour, stained in Coomassie Brilliant Blue for 30 min and destained for 3 hours prior to visualisation. The buffer compositions are described in **Table 2.5**.

2.3.4 Determination of Protein Concentration

Protein concentration was determined using the relationship between aromatic residues and absorbance at 280 nm. The molar extinction coefficient (ε) was calculated from the amino acid sequence using the ExPASy ProtParam tool (Gasteiger *et al.*, 2005). Absorbance at 280 nm was measured using a Nanodrop 2000c (ThermoFisher Scientific) and protein concentration subsequently calculated *via* the Beer-Lambert Law. The amino acid sequences and extinction coefficients used are provided in **Table 2.6**.

Table 2.5 Composition of Buffers in This Study

Buffer Name	Composition
Protein Purification	
Resuspension buffer	50 mM Tris-HCl pH8 500 mM NaCl 10% glycerol 160 µM phenylmethylsulphonyl fluoride 10 µg/ml DNase
Solubilisation buffer	50 mM Tris-HCl pH8 500 mM NaCl 10% (w/v) Glycerol 2% (w/v) DDM or 2% (w/v) LDAO
IMAC A buffer	50 mM Tris- HCl pH8 500 mM NaCl 10% (w/v) glycerol 0.03% DDM or 0.09% LDAO
IMAC B buffer	50 mM Tris- HCl pH8 500 mM NaCl 10% (w/v) glycerol 500 mM Imidazole 0.03% (w/v) DDM or 0.09% (w/v) LDAO
Stripping solution	100 mM EDTA 500 mM NaCl
Cobalt solution	100 mM $CoCl_2$
SEC buffer	50 mM Tris-HCl pH7.8 100 mM NaCl 0.03% DDM (w/v) or 0.09% (w/v) LDAO
SDS-PAGE	
10%SDS-PAGE Resolving gel	32.5% (v/v) 30% Acrylamide 25% (v/v) solution 2 SDS-PAGE 1% (v/v) of 10% APS 0.1% (v/v) TEMED
10% SDS-PAGE Stacking gel	15% (v/v) 30% Acrylamide 30% (v/v) solution 3 SDS-PAGE 60% (v) H_2O 1% (v/v) of 10% APS 0.1% (v/v) TEMED

SDS-PAGE Solution 2	1.5M Tris-HCl pH8.8 0.3% (w/v) SDS
SDS-PAGE Solution 3	0.5M Tris-HCl pH6.8 0.3% (w/v) SDS
10x Running Buffer pH 8.3	30 g/L Tris-base 144 g/L glycine 1% (w/v) SDS
Loading blue 6x	2% (w/v) SDS 10% (w/v) glycerol 0.001% (w/v) bromophenol blue 0.0625 M Tris-HCl pH6.8 5% β-mercaptoethanol
Staining Buffer	0.1% Coomassie Brilliant Blue R-250 50% methanol 10% acetic acid
Destining Buffer	40% (v/v) methanol 10% (v/v) acetic acid 50% (v/v) water
Agarose Gel Electrophoresis	
2% agarose gel	10 g/L agarose TAE buffer 1 µg/mL ethidium bromide
TAE Buffer	40 mM Tris-HCl 20 mM acetic acid 1 mM EDTA
Reconstitution into Liposomes	
Liposome Buffer	100 mM potassium phosphate pH7.6 ; 300 mM KCl

Table 2.6 Amino Acid Sequence and Properties of Proteins in This Study

Protein	Amino Acid Sequence	MW (kDa)	ε ($M^{-1}cm^{-1}$)	Reference
*Ec*AmtB	MKIATIKTGLASLAMLPGLVMAAP AVADKADNAFMMICTALVLFMTIP GIALFYGGLIRGKNVLSMLTQVTV TFALVCILWVVYGYSLAFGEGNNF FGNINWLMLKNIELTAVMGSIYQY IHVAFQGSFACITVGLIVGALAER IRFSAVLIFVVVWLTLSYIPIAHM VWGGGLLASHGALDFAGGTVVHIN AAIAGLVGAYLIGKRVGFGKEAFK PHNLPMVFTGTAILYIGWFGFNAG SAGTANEIAALAFVNTVVATAAAI LGWIFGEWALRGKPSLLGACSGAI AGLVGVTPACGYIGVGGALIIGVV AGLAGLWGVTMLKRLLRVDDPCDV FGVHGVCGIVGCIMTGIFAASSLG GVGFAEGVTMGHQLLVQLESIAIT IVWSGVVAFIGYKLADLTVGLRVP EEQEREGLDVNSHGENAYNA	44.4	66390	Uniprot: C3TLL2
*Ne*Rh50	MSKHLCFTAFSSIALFLLCFSSWA SAVAPAEINEARLVAQYNYSINIL AMLLVGFGFLMVFVRRYGFSATTG TYLVVATGLPLYILLRANGIFGHA LTPHSVDAVIYAEFAVATGLIAMG AVLGRLRVFQYALLALFIVPVYLL NEWLVLDNASGLTEGFQDSAGSIA IHAFGAYFGLGVSIALTTAAQRAQ PIESDATSDRFSMLGSMVLWLFWP SFATAIVPFEQMPQTIVNTLLALC GATLATYFLSALFHKGKASIVDMA NAALAGGVAIGSVCNIVGPVGAFV IGLLGGAISVVGFVFIQPMLESKA KTIDTCGVHNLHGLPGLLGGFSAI LIVPGIAVAQLTGIGITLALALIG GVIAGALIKLTGTTKQAYEDSHEF IHLAGPEDEHKAERLVLEAKTEIQ GLKNRIDAAVLSAKSEG	44.6	38515	Uniprot Q82X47

2.4 Preparation of Proteoliposomes

2.4.1 Liposome Preparation

Proteoliposomes were prepared by mixing *E. coli* Polar lipids and POPC lipids (dissolved in chloroform) at a 2:1 in a glass tube and evaporating the chloroform off via N_2 flux. To ensure the complete removal of chloroform, the lipids were dried further by placing in a vacuum desiccator for approximately 2 hours. Once dry, the lipid cakes were suspended in 4 mL of liposome buffer (**Table 2.2**) at 5 mg/mL multilamellar liposome solution. This solution was then passed through a mini-extruder (Avanti Polar Lipids) 13 times to obtain an uninominal and unilamellar liposome solution.

2.4.2 Rsat and Rsol Determination

Insertion of membrane proteins into liposomes requires destabilisation of the liposomes with detergent (Triton X-100 in this work). The addition of detergent disrupts lipid-lipid interactions, resulting in a more permeable bilayer which is more receptive to protein insertion. Optimal insertion occurs at a detergent: lipid between the onset of solubilisation (R_{sat}) and complete solubilisation (R_{sol}) of the lipids. The addition of detergent disrupts lipid-lipid interactions, which results in a more permeable bilayer which is more receptive to protein insertion. As the liposomes are saturated with detergent, the liposome solution becomes increasingly turbid until R_{sat} is reach, then the turbidity decreases until the lipids solubilise completely (R_{sol}). Hence, to determine the R_{sat} and R_{sol} of the polar/POPC 2:1 liposomes, 25% Triton X-100 was incrementally added to 500 µL of liposomes (5 mg/mL) and the absorbance at 400, 500, 550 and 600 nm was measured. The optimum amount of Triton X-100 for protein insertion was determined to be 2.5 µL of Triton X-100 at 25% (w/v) per mg of lipid.

2.4.3 Reconstitution into Proteoliposomes

500 µL of liposome (5 mg*ml^{-1}) was destabilised by incubating with 2.5 µL of 25% Triton X-100 at room temperature for 5 minutes with 300 rpm orbital shaking. Then purified AmtB was added to either a lipid-protein ratio of 5:1, 10:1, or 50:1 and the tube incubated for a further 30 minutes at room temperature at 300 rpm on an orbital shaker.

Detergent was removed from the solution via the addition of ~200 mg of SM-2 Biobeads (BioRad) to each tube and the microcentrifuge tubes followed by an incubation at 4°C on a rotary wheel for 2 hours. The solution was then transferred to a clean microcentrifuge tube containing a fresh batch 200 mg of SM-2 Biobeads and incubated overnight at 4°C.

2.4.4 Proteoliposome Wash Step

Immediately following reconstitution, proteoliposomes were subjected to three successive wash steps in order to remove excess protein or detergent. Proteoliposomes were transferred to centrifuge tubes. The original volume was noted and the volume in each tube was completed to 9 mL using liposome buffer. The proteoliposomes were pelleted by centrifuged at 200,000 *g* and 4°C for 1 hour (Ti 90, Beckman Optima XPN-100). 100 µL of supernatant was collected and the rest discarded. The liposome pellet was then suspended in a fresh 9 mL of liposome buffer (**Table 2.5**) and centrifuged again. This operation was repeated for three centrifugation cycles. Finally, the proteoliposomes were suspended in liposome buffer (**Table 2.5**) to match their starting volume, dispensed into microcentrifuge tubes in 100 µL aliquots and stored at -80°C.

The size distribution of proteoliposomes was measured *via* dynamic light scattering (DLS) using a Zetasizer Nano ZS (Malvern Instruments). This showed that the proteoliposomes had an average diameter of 110 nm. Proteoliposomes were divided into 100 µL aliquots and stored at -80°C.

The quantity of protein inserted in liposomes was assessed *via* SDS-PAGE analysis.15 µL of proteoliposomes (5mg/ml) containing each variant at a LPR of 5:1, 10:1, or 50:1 (w/w) or wild-type AmtB at LPR 10 (WT-AmtB), were run on 10% SDS-PAGE gels alongside proteoliposomes containing WT-AmtB at LPR 10, demonstrating that the quantity of protein inserted is similar for all variants and varied according to LPR. It was noted that $AmtB^{D160A}$ ran as a monomer in SDS-PAGE gel, rather than the trimer seen for the WT and other variants. To ensure that $AmtB^{D160A}$ was correctly inserted in the proteoliposome, the proteoliposomes were solubilised in 2% DDM and the proteins analyse by size exclusion chromatography using a Superdex 200 (10/300) increase column. The elution profile of all variants and wild type were identical showing a single monodisperse peak eluting at 10.4-10.6 mL, showing that all proteins were correctly folded as trimers into the proteoliposomes.

2.5 Solid Supported Membrane Electrophysiology

Solid supported membrane electrophysiology (SSME) is a technique that allows for investigation of electrogenic transporters, particularly those that cannot be assessed via patch clamp or voltage clamp methods (Bazzone *et al.*, 2013). The resultant output can be used to assess: activity (+/-), transport flux and kinetics. In simple terms, an SSME trace results from the measurement of i) a pre-steady state current which represents the interaction between the protein and transport substrate (i.e. binding); and ii) a steady state current which describes the entire translocation cycle activity of the transporter. The technology is composed of a gold sensor chip that is thiolated and subsequently coated with a phosphatidylcholine monolayer. Proteoliposomes containing purified transporter are then adsorbed to this monolayer and transport induced via solution exchange.

2.5.1 Sensor preparation

3 mm gold plated sensors (Nanion Technologies) were prepared as described previously (Bazzone, Barthmes and Fendler, 2017). Briefly, sensors were coated with 50 µL of 0.5 mM 1-octadecanethiol (in isopropanol) and incubated for at least one hour at 4°C. The solution was removed by tapping the sensor on paper, and the sensors subsequently rinsed three times with 10 mL isopropanol and 10 mL deionised water. Dry sensors were subsequently coated with 1.5 µL of 1,2-diphytanol-sn-glycerol-3-phosphocholin solution and 100 µL of non-activated (NA) buffer (**Table 2.7**) was immediately added to form the solid supported membrane (SSM).

Proteoliposomes/empty liposomes were defrosted and sonicated in a sonication bath at 35 W for 10 seconds and diluted 10-fold in non-activating (NA) solution (**Table 2.7**), and 10 µL was added at the surface of the solid-supported membrane (SSM) on the sensor. Sensors were centrifuged at 2500*g* for 30 minutes and stored at 4°C for a maximum of 48 hours before electrophysiological measurements.

All measurements were made at room temperature (21ºC) using a SURFE^{2}R N1 apparatus (Nanion Technologies) with default parameters (Bazzone, Barthmes and Fendler, 2017). Unless otherwise stated, all measurements were carried out using pH 7 buffers. Prior to any measurements, the quality of the sensors was determined by measuring capacitance (should be 15-30 nF) and conductance (should be <5 nS) and comparing to reference values provided by the manufacturer.

2.5.2 Single Solution Exchange

For functional measurements at a fixed concentration, a single solution exchange protocol was used, with each phase lasting 1 second (Bazzone, Barthmes and Fendler, 2017). Firstly, non-active (NA) solution is injected onto the sensor, followed by activating (A) solution containing the substrate at the chosen concentration, and finally NA solution. Measurements were recorded

on six sensors from two independent protein purification batches, with three measurements recorded for each sensor. Figures present individual traces representative of these datasets.

2.5.3 Proton conduction

A pH gradient was generated by sequential passage of NA solution and A to establish the external pH, followed by a 15-minute incubation time in resting (R) NA solution (**Figure 2.3**). This incubation adjusts the internal pH of the proteoliposomes to the pH of (R) and creates the pH gradient. The same programme was used to measure H^+ conduction, using solutions without NH_4^+. NH_4^+ activity under an inward proton gradient is not diminished compared to static pH 7, demonstrating that activity is not driven by the electrochemical gradient.

2.5.4 Analysis

The kinetic parameters were calculated using Graphpad Prism 6 and fitted according to the Michaelis-Menten equation.

Lifetime analysis of the current (decay time of the transient current) was performed to differentiate small pre-steady state currents, which arise due to the binding of a charged species to membrane proteins, from currents reflecting full transport cycles, which show faster decay rates under raised liposomal lipid-to-protein ratio (LPR) (Bazzone, Barthmes and Fendler, 2017). The decay time of the transient current was calculated by fitting the raw transient current between the apex of the peak and the baseline (after transport) with a non-linear regression using OriginPro 2017 (OriginLab). The regression was done using a one-phase exponential decay function with time constant parameter (equation below) and the fit obtained using the Levenberg Marquardt iteration algorithm.

$$y = y_0 + A_1 e^{-x/t_1}$$

Where *x* and *y* represent coordinates on the respective axis, y_0 represents the offset at a given point, *A* represents the amplitude, and *t* is the time constant.

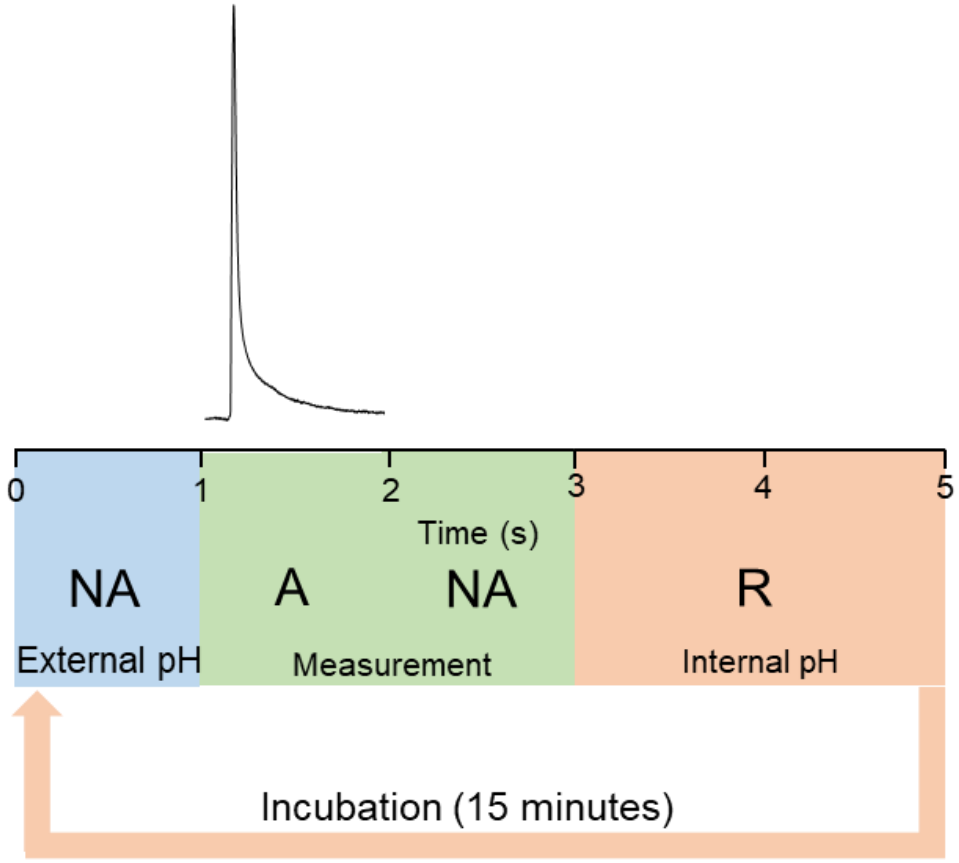

Figure 2.2. Schematic Protocol for Double Solution Exchange The coloured segments represent the distinct blocks in the flowtime sequence. First the sensor is rinsed with a resting solution (R) for 2 seconds and allowed to incubate for 15 minutes (red section) This allows the solution to equilibriate and adjusts the intraliposomal pH to the pH of R. Following the incubation, the pulse of non-activating (NA) solution sets the external pH and establishes a pH gradient across the liposome (blue). Then an activating solution (A) of the same pH provides ammonium and initiates a symport activity under pH gradient conditions and the transient current is recorded (Bazzone et. al., 2016).

Table 2.7: Solid-Supported Membrane Electrophysiology Solutions*

Substrate	Activating	Non-Activating
Ammonium	100 mM KPho 100 mM KCl 200 mM NH_4Cl	100 mM KPho 300 mM KCl
Potassium	100 mM NaPho 100 mM NaCl 200 mM KCl	100 mM NaPho 300 mM NaCl

*All solutions adjusted to pH 7. KPho: potassium phosphate buffer, NaPho: sodium phosphate buffer.

Chapter 3:

Characterisation and Deprotonation

Chapter 3: Characterisation and Deprotonation

Aims and Objectives

The focus of this PhD thesis is to unravel the mechanism of ammonium transport used by the *E. coli* ammonium transporter AmtB. The principle technique used to elucidate this is Solid-Supported Membrane Electrophysiology (SSME). As this is a relatively novel technique, the activity of wild-type (WT)- AmtB was first fully characterised. Following this, I could investigate the effect of variant proteins on observed activity and relate this back to mechanistic steps. In parallel to the *in vitro* SSME experiments, I also conducted *in vivo* yeast complementation experiments in collaboration with Dr. Mélanie Boeckstaens and Dr. Anna-Maria Marini (Free University of Brussels).

Our aims were to:

1) Characterise the electrogenic activity of AmtB *via* SSME
2) Characterise selectivity of AmtB
3) Investigate residues associated with deprotonation in AmtB

3.1 Introduction

AmtB (the native *Escherichia coli* ammonium transporter) is the paradigmatic member of the ubiquitous Amt/Mep/Rh family, and is widely used as a model system to study ammonium uptake by these proteins. Structurally, AmtB is well understood, with over 20 high-resolution structures deposited in the Protein Data Bank (PDB). Initially, it was expected that the advent of high-quality crystal structures would finally elucidate the controversial mechanism of AmtB. However, these expectations have yet to be met, as the structures share a similar conformation irrespective of the presence or absence of ammonium. Due to the presence of a strongly hydrophobic pore in each monomer of the protein, it was concluded that NH_3 was the transported species.

Recently, however, Wacker *et al* demonstrated electrogenic transport in Amt1 from *A. fulgidus* (Wacker *et al.*, 2014). The apparent conflict between the crystal structures, which prohibit charge translocation, and functional observations of electrogenic transport reignited the controversies regarding the transport mechanism of Amt/Mep/Rh, and suggested either NH_4^+ uniport or NH_3/H^+ symport. Recent evidence has also been reported to support the importance of NH_4^+ deprotonation as a major step in ammonium transport across the whole family (Ariz *et al.*, 2018).

To confirm that Amt proteins are electrogenic transporters and begin investigating the potential role of deprotonation, I have purified and characterised the activity of *Ec*AmtB and select variants using SSME technology.

3.2 Purification of AmtB

3.2.1 Immobilised Metal Affinity Chromatography

AmtB was overexpressed in C43(DE3) *E. coli* and purified as described in **Section 2.3** The membrane fraction of *E. coli* containing AmtB was isolated and solubilised in 2% DDM, before being diluted to a final concentration 1% DDM. This sample was then loaded onto a 1 mL Histrap column packed with cobalt-charged sepharose and the column washed with 10 mL with IMAC A buffer supplemented with 40 mM imidazole to remove non-specifically bound protein. AmtB was eluted using an imidazole gradient, increasing from 40-500 mM over 20 column volumes. Throughout the purification process, the protein was continuously monitored by absorbance at 280 nm.

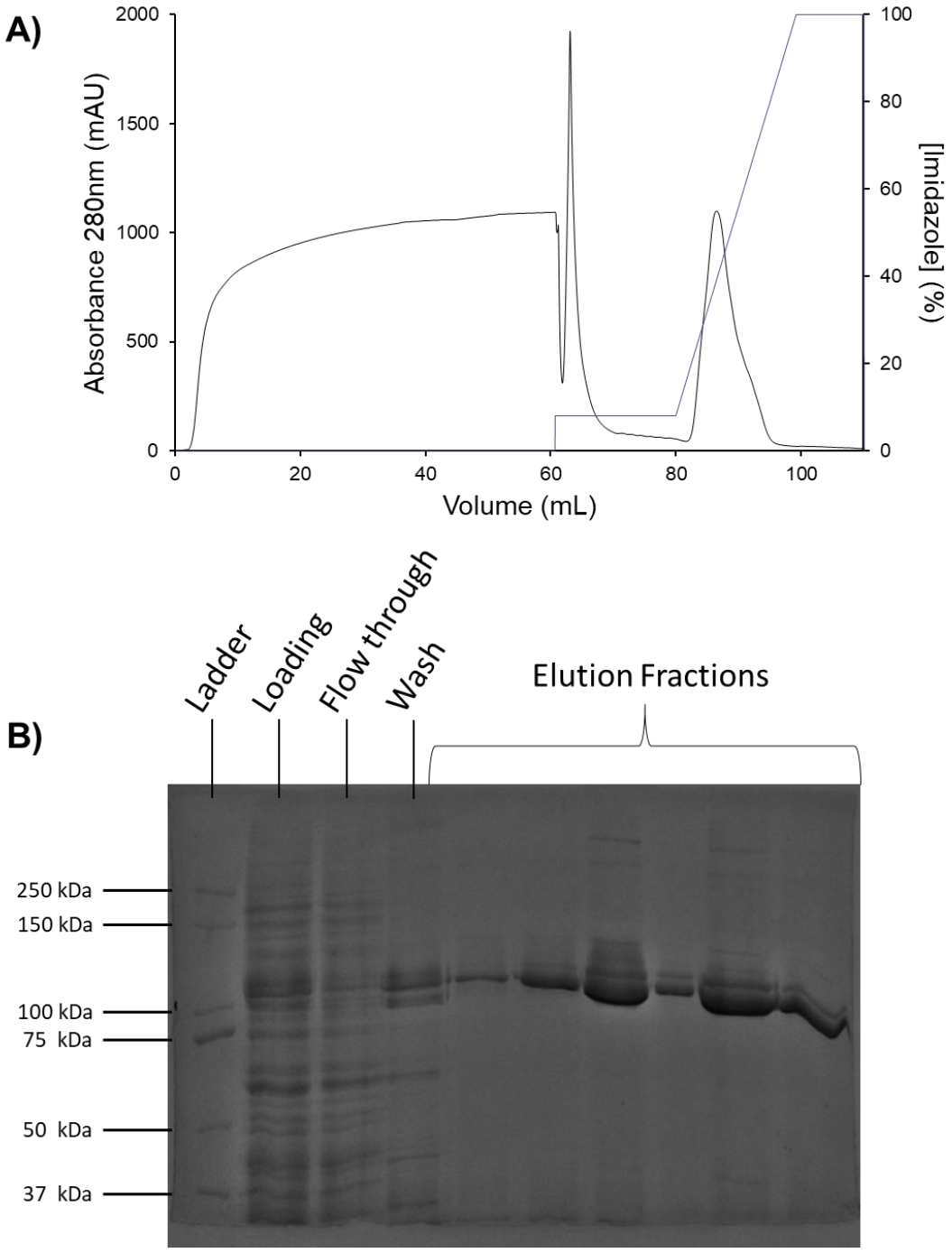

Figure 3.1 Purification of AmtB A) IMAC profile of the wash and elution of *EcAmtB* from solubilised *E. coli* membrane. The black line represents A_{280nm} and the purple line represents the concentration of imidazole as a percentage (100% = 500 mM). B) 10% SDS-PAGE of the membrane solution loaded, the flow through, the wash, and elution fractions across the peak.

The absorbance at 280nm shows that AmtB eluted between 100 and 200 mM imidazole (**Figure 3.1A**). However, this elution profiles do not provide any information on the relative purity or size of the protein. To address this, the elution fractions were analysed *via* SDS-PAGE. AmtB presented with a single major band of ~130 kDa (**Figure 3.1B**). The theoretical molecular weight for AmtB is ~44 kDa, so bands of this size indicate that, despite the presence of SDS, the variants retained their trimeric arrangement. To confirm the structural integrity of the variants and ensure the high-purity samples for insertion into proteoliposomes, the protein was subjected to a polishing step.

3.2.2 Size Exclusion Chromatography

After the IMAC, the elution fractions containing AmtB were pooled together and concentrated to 5 mg/mL. The sample was injected (300 µL) on a Superdex S200 10/300 size exclusion chromatography (SEC) column. Throughout the purification process, the protein was continuously monitored by absorbance at 280 nm. The WT eluted between 10.5 -11.6 mL as a single symmetrical peak without any protein present in the void-volume (**Figure 3.2**). This indicates that the protein did not aggregate and that the variants shared the same hydrodynamic radius so were likely structurally intact. Fractions of the elution peak were analysed *via* SDS-PAGE and revealed that the samples were pure (**Figure 3.2, insert**).

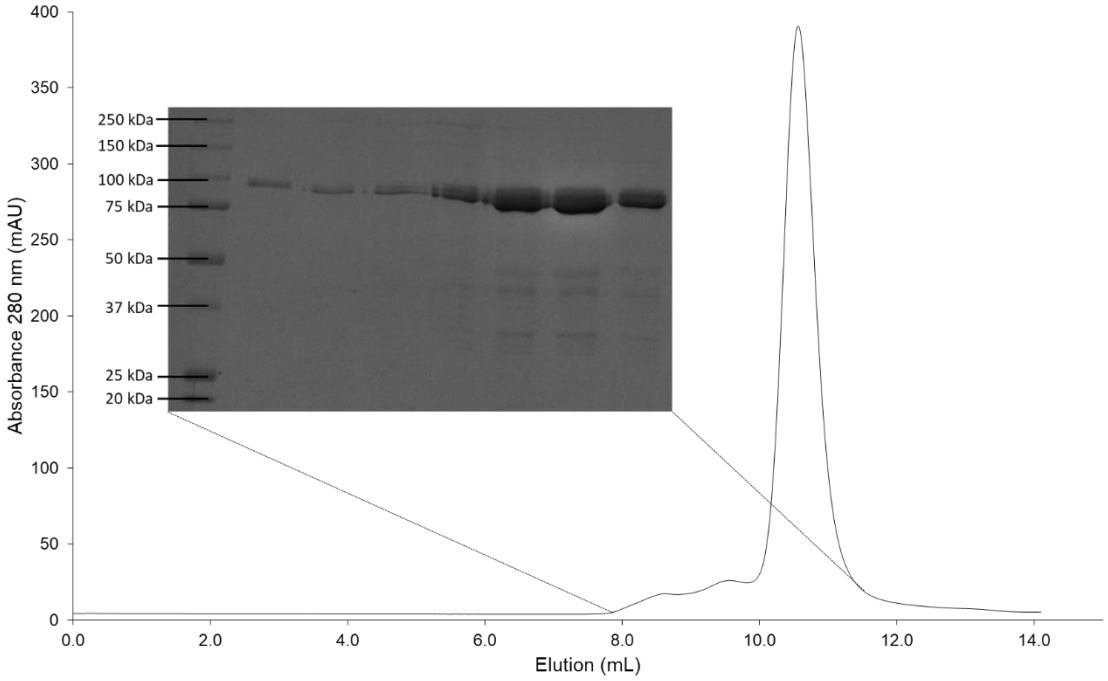

Figure 3.2 Size Exclusion Chromatography of AmtB: Chromatogram of *Ec*AmtB solubilised in 0.033% DDM and injected onto a Superdex 200 increase (10/300) column. (Insert) 10% SDS-PAGE of fractions within the elution peak.

3.3 Proteoliposome Formation and Characterisation

3.3.1 Determination of Rsat and Rsol Coefficients

E. coli polar lipids and phosphatidylcholine (POPC) at a 2:1 mass ratio to prepare liposomes with a similar lipid composition to the *E. coli* membrane. Optimal insertion of AmtB into liposomes first requires that the liposomes be destabilised with a detergent. Optimal insertion occurs when the liposomes are at the onset of solubilisation and are saturated with detergent (R_{sat}), as further addition of detergent results in total solubilisation of the liposomes (R_{sol}). To determine the R_{sat} and R_{sol} experimentally, 1 µL of 25% Triton X-100 was added sequentially to 500 µl of liposomes and the absorbance monitored across different wavelengths to track the change in liposome stability. As detergent is added, the liposomes become increasingly saturated with detergent and begin to swell: increasing the turbidity of the solution and thus its absorbance. After R_{sat}, the absorbance decreased with the addition of detergent, reaching a baseline after 7 µL of 25% Triton X-100 was added (**Figure 3.3**). Based on these results, the optimal amount of Triton X-100 to destabilise liposomes for protein insertion was 1.56 µM per mg of lipid.

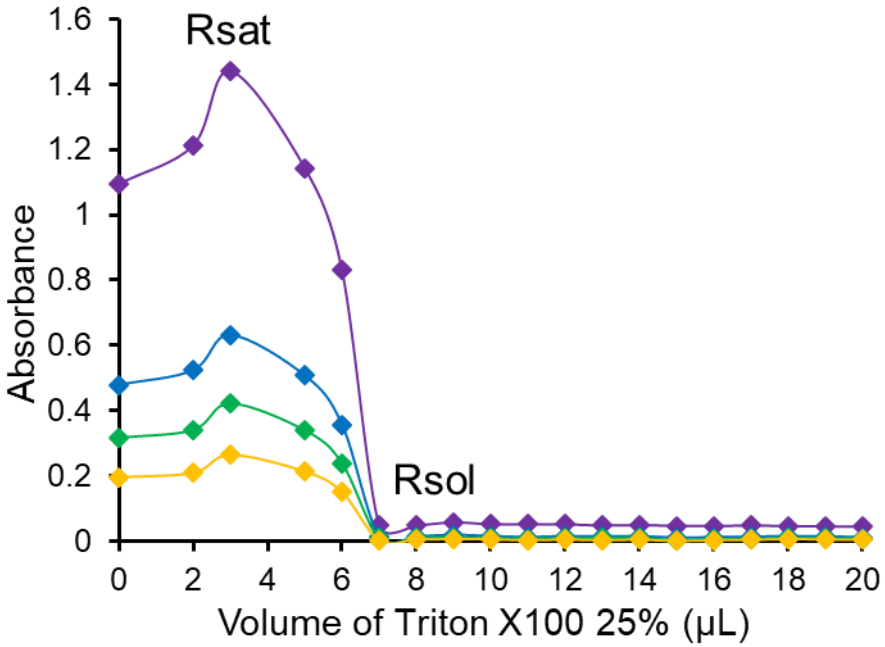

Figure 3.3: Determination of Rsat and Rsol: Absorbance at 400 (purple), 500 (blue), 550 (green), and 600 (yellow) nm following sequential addition of 1 µL 25% Triton X-100 (represented by data points) The measured sample contained 500 µL Polar/POPC 2/1 liposomes at 5 mg/mL and 100 µL of size exclusion buffer to emulate the presence of purified protein during reconstitution.

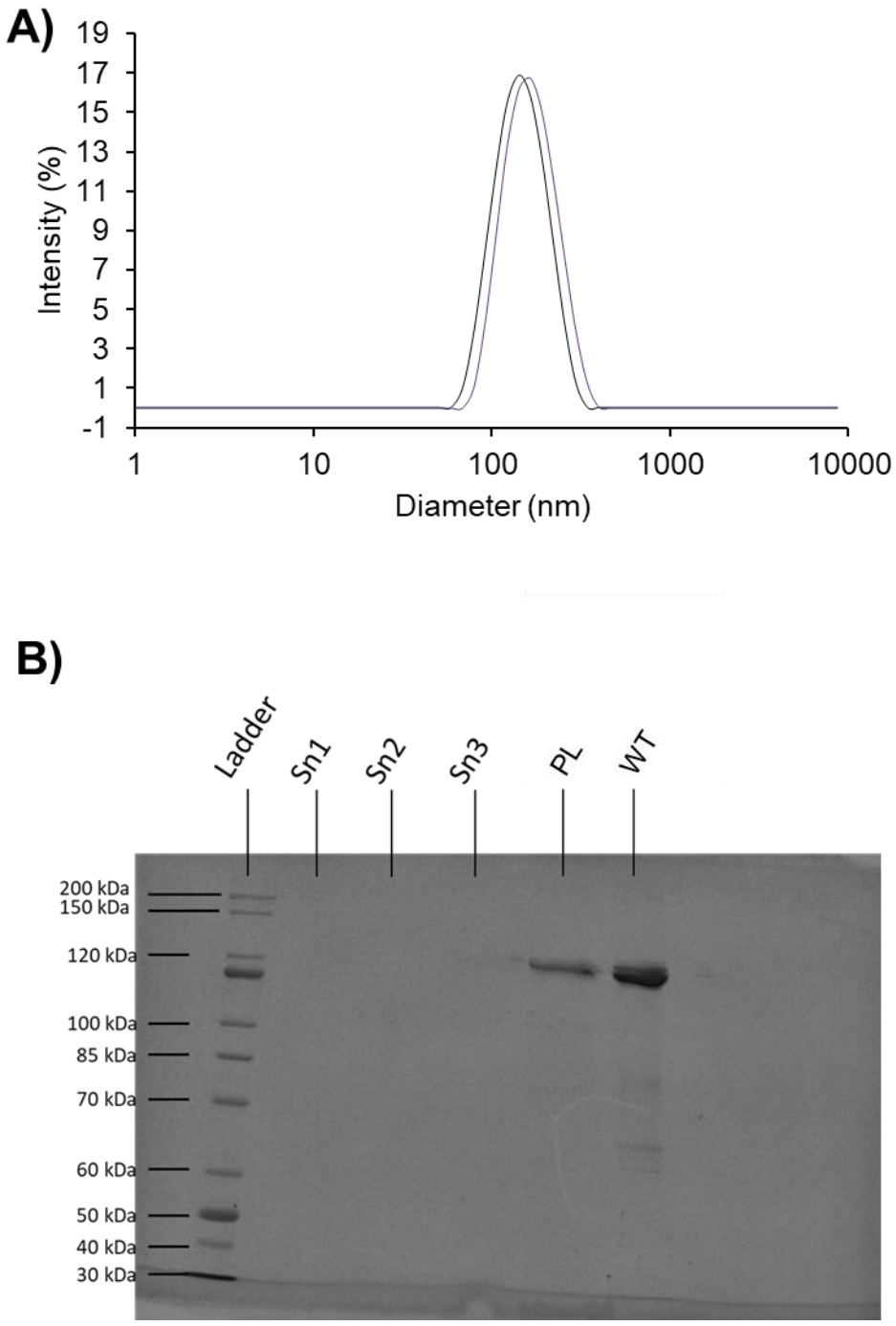

Figure 3.4 Insertion of AmtB into Liposomes: A) Comparison of size distribution of empty polar/POPC 2/1 liposomes (purple) and AmtB Polar/POPC 2/1 proteoliposomes (black) via DLS analysis. B) 10% SDS-PAGE gel monitoring the wash protocol. Sn1-3 = supernatant from each wash step, PL = a proteoliposomes at LPR 10. The WT lane contains 5 µg of pure AmtB used for the reconstitution in the proteoliposomes.

3.3.2 Insertion of AmtB into proteoliposomes

To ensure the correct insertion of AmtB into liposomes, the proteoliposomes were analysed by SDS-PAGE. As detailed in **Chapter 2,** the proteoliposomes are subjected to a repeated wash step following the insertion protocol. This step consists of diluting the liposomes in liposome buffer (**Chapter 2, Table 2.5**), pelleting *via* ultracentrifugation, and removing the supernatant. This is repeated a further two times, and is intended to separate and remove any protein that has not successfully inserted into the liposome. A sample of the supernatant from each wash step was retained and analysed alongside the proteoliposomes on an SDS-PAGE gel. In the event of complete insertion, there should be no protein in the wash fractions, therefore we could expect there to be no visible band. In addition, successful insertion should result in a single band for the proteoliposome fraction, corresponding to AmtB. As shown in **Figure 3.4B** no protein was observed in any of the wash lanes, while a single band corresponding to AmtB was visible in the proteoliposome fraction. This indicated successful insertion of AmtB into the liposomes.

3.3.3 Size Distribution of Proteoliposomes

It was important to ensure that proteoliposomes (at different LPRs) and empty liposomes had a similar diameter and size distribution. This is important as the transient current observed *via* SSME is, in part, due to the accumulation of charge within the liposome creating a membrane potential and prohibiting further translocation. If the size of the liposomes differs, this will occur at different rates and obfuscate the impact of the transporter. Therefore, to assess the size of the liposomes and proteoliposomes, the average diameter was determined *via* dynamic light scattering (DLS).

As detailed in **Chapter 2**, DLS determines the size of liposomes within solution by recording the motion of particles in the solution *via* light scattering detectors at set angles. Based on the movement and scatter, an auto-correlation function

can be applied to derive the particle size distribution. DLS analysis of confirmed that the proteoliposomes followed a unimodal size distribution, with a mean diameter of ~110 nm (**Figure 3.4A**). In addition, comparison of the DLS profiles of empty liposomes and proteoliposomes indicates that the insertion of AmtB does not affect the size distribution nor does it lead to aggregation **(Figure 3.4A**). Taken together, these results validate direct comparison of transient charge displacement between: empty liposomes and proteoliposomes; and the different variant proteoliposomes. This allows for characterisation and mechanistic investigation *via* solid supported membrane electrophysiology.

3.4 Variant AmtB Purify Correctly

All AmtB variants were overexpressed, purified and reconstituted in liposomes following the procedure establish for wild-type AmtB. However, it is possible that the mutation introduced could destabilise, interfere with folding, or impact the reconstitution of the protein into the liposomes. To ensure that variants were structurally stable we compared their size-exclusion chromatograms to the WT (**Figure 3.5A**). All variants presented with the same unimodal peak as the WT and eluted over the same time frame, indicating that they retain the same hydrodynamic properties. The difference in peak height between the proteins is due to differing concentrations of the sample injected on the column.

In order to verify successful insertion into proteoliposomes, and thus ensure SSME measurements were viable, SDS-PAGE was used to monitor the wash-step following reconstitution. For all variants, bands were only observed in the proteoliposomes and each of their wash fractions ran empty (**Figure 3.5B**), indicating successful insertion. Notably, the size of the bands for AmtB and S219A matched the expected size of trimeric AmtB, whilst the major band observed for the D160 variants was ~44 kDa. This is closer to the size of the monomer, suggesting that these variants are unfolded in the presence of SDS. This indicates that AmtB, and its variants, were all successfully inserted into liposomes and that they remain undamaged by the process.

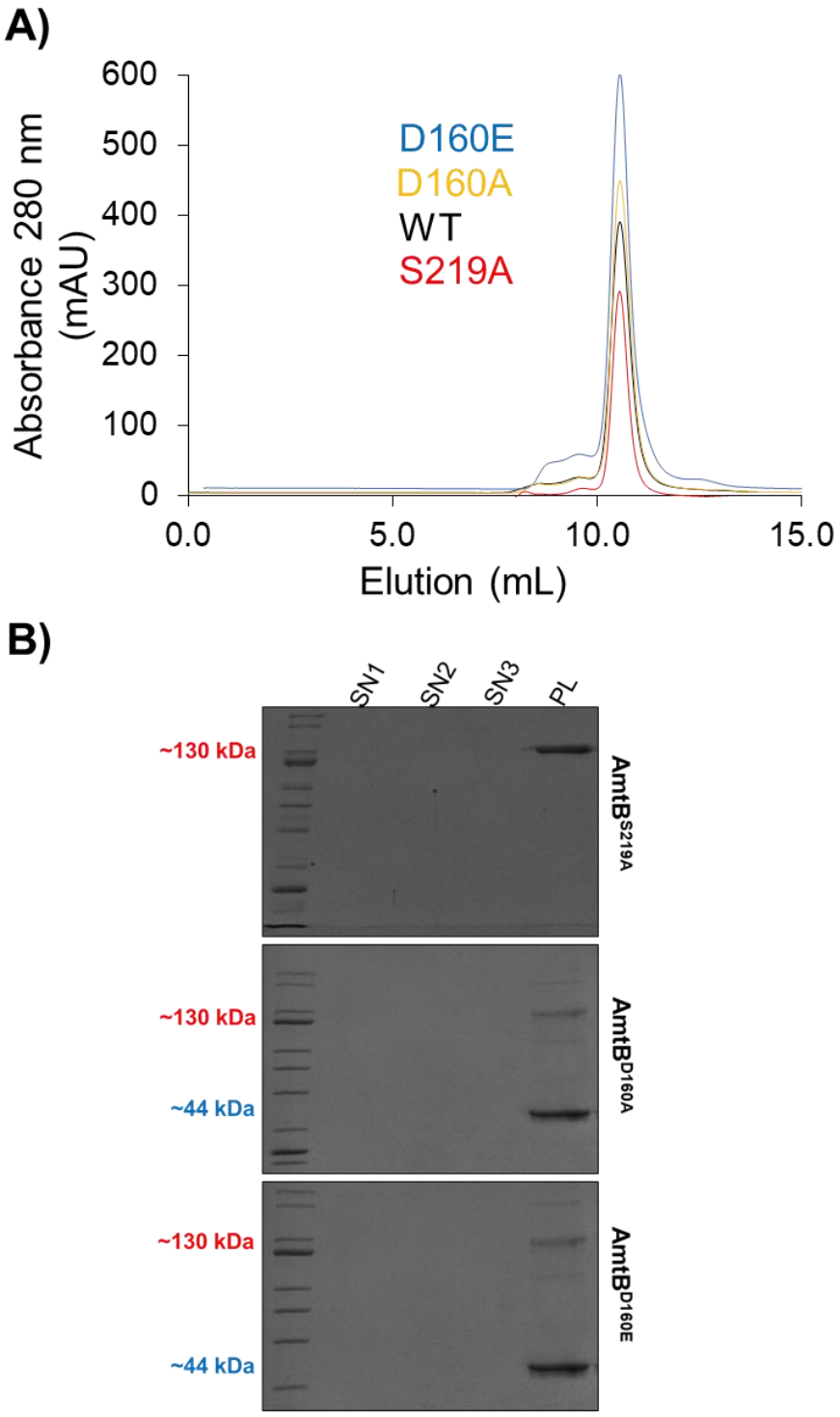

Figure 3.5 Verification of variant AmtB: A) Chromatogram of WT (black), S219A (red), D160A (yellow), or D160E (blue) AmtB solubilised in 0.033% DDM. B) 10% SDS-PAGE gel monitoring the wash protocol. S1-3 = supernatant from each wash step, PL is a sample of either $AmtB^{219A}$ (top), $AmtB^{D160A}$(middle), or $AmtB^{D160E}$(bottom) Polar/POPC 2/1 proteoliposomes at LPR 10.

3.5 AmtB activity is Electrogenic

The activity of AmtB was characterised *via* Solid-Supported Membrane Electrophysiology (SSME) to determine if AmtB activity was electrogenic or electroneutral. SSME allows charge translocation across a membrane to be measured like an electric circuit. The resultant output can be used to assess activity, measure transport flux, and obtain some kinetic parameters. The SSME traces contains two types of information regarding the mechanism; i) a pre-steady state current which represents the interaction between the protein and transport substrate (*i.e.* binding); and ii) a steady state current which describes the entire translocation cycle (both binding and transport of the substrate). It is difficult to separate these two forms of information, as measurement of an active transporter will be a combination of both.

A 200 mM NH_4^+ pulse on polar/POPC 2/1 liposomes containing AmtB at LPR 10 elicits a transient current that reaches a maximum amplitude of ~ 3.3 nA which decays back to the baseline (**Figure 3.6A**). As NH_4^+ is translocated into the proteoliposome the amplitude of the measured current increases. Eventually however, the concentration of positive charge inside the proteoliposome results in a membrane potential which repels further inward movement of charge. This results in a decay of the current back to baseline. As the liposomes are a fixed size, an increase in the concentration of protein means that their maximum capacity will be reached faster and thus the transient current will decay faster. If the protein was inactive, the decay rate would not change. Therefore, to verify that the observed current was due to transport activity, AmtB was reconstituted into proteoliposomes at various lipid-protein ratios (LPRs) of 5:1, 10:1, and 50:1. As shown in **Figure 3.6B**, there is the maximum amplitude observed is dependent on protein concentration, and is decreased at lower concentrations. This shows that the initial binding interaction is protein specific. In addition, the decay rate also depended on concentration, increasing from 9.5 ± 0.7 s^{-1} for LPR 50:1, to 13.4 ± 1.5 s^{-1} for LPR 10:1, to 18.7 ± 1.0 s^{-1} for LPR 5:1. This demonstrates that AmtB successfully translocates a charge, and that the activity is protein dependant.

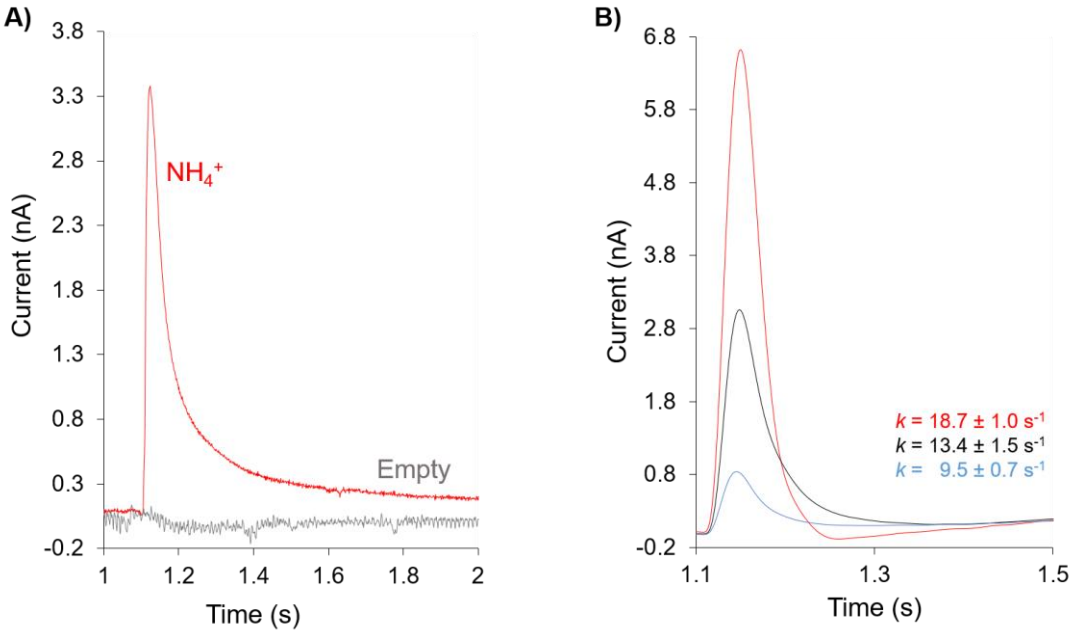

Figure 3.6 Characterisation of WT-AmtB Activity: A) Transient currents following a 200 mM pulse of NH_4^+ in empty Polar/POPC 2/1 liposomes (grey) or with AmtB reconstituted into Polar/POPC 2/1 proteoliposomes at a LPR of 10:1 (red). B) Transient currents following a 200 mM NH_4^+ pulse with AmtB reconstituted into Polar/POPC 2/1 proteoliposomes at a LPR of 5:1 (red), 10:1 (black), or 50:1 (blue).

3.6 AmtB activity is Ammonium Specific

To ensure the transient current we observed was specific to NH_4^+ translocation, the SSME measurements were repeated with other substrates. K^+ and Na^+ are similar in size and ionic radii to ammonium (Shannon, 1976; Sidey, 2016), thus if the interaction was nonspecific or the proteoliposomes were leaking a similar current would be expected. 200 mM pulses of K^+ and Na^+ yielded no observable current (**Figure 3.7A**). This demonstrates that AmtB is selective for NH_4^+ and its electrogenic activity is specific to NH_4^+.

In addition, the relative specificity of AmtB for ammonium versus methylammonium (MeA) was investigated. MeA has been prominently used as an ammonium analogue in the study of ammonium transport, due to the availability and stability of radiolabelled ^{14}C-MeA (Javelle *et al.*, 2007). Due to MeA's role as a substrate analogue, it would be expected to yield a similar current to NH_4^+. However, a 200 mM pulse of methylammonium elicits a current of only 0.7 nA, a ~5-fold reduction compared to NH_4^+ (**Figure 3.7A**). Further, the kinetics of ammonium and MeA were investigated by measuring transient currents in LPR 10 proteoliposomes following ammonium/MeA pulses ranging from [0.1-200 mM]. The peak amplitudes of these currents were recorded and fit according to the Michaelis-Menten equation (**Figure 3.7B**). This analysis revealed that the *Km* for MeA (55.8 ± 15.6 mM) was ~70-fold higher than that of ammonium (0.8 ± 0.1 mM). Taken together, these results show that MeA is a poor substrate for AmtB and thus is not well-suited for elucidating mechanistic details and confirms that AmtB is a highly selective electrogenic transporter.

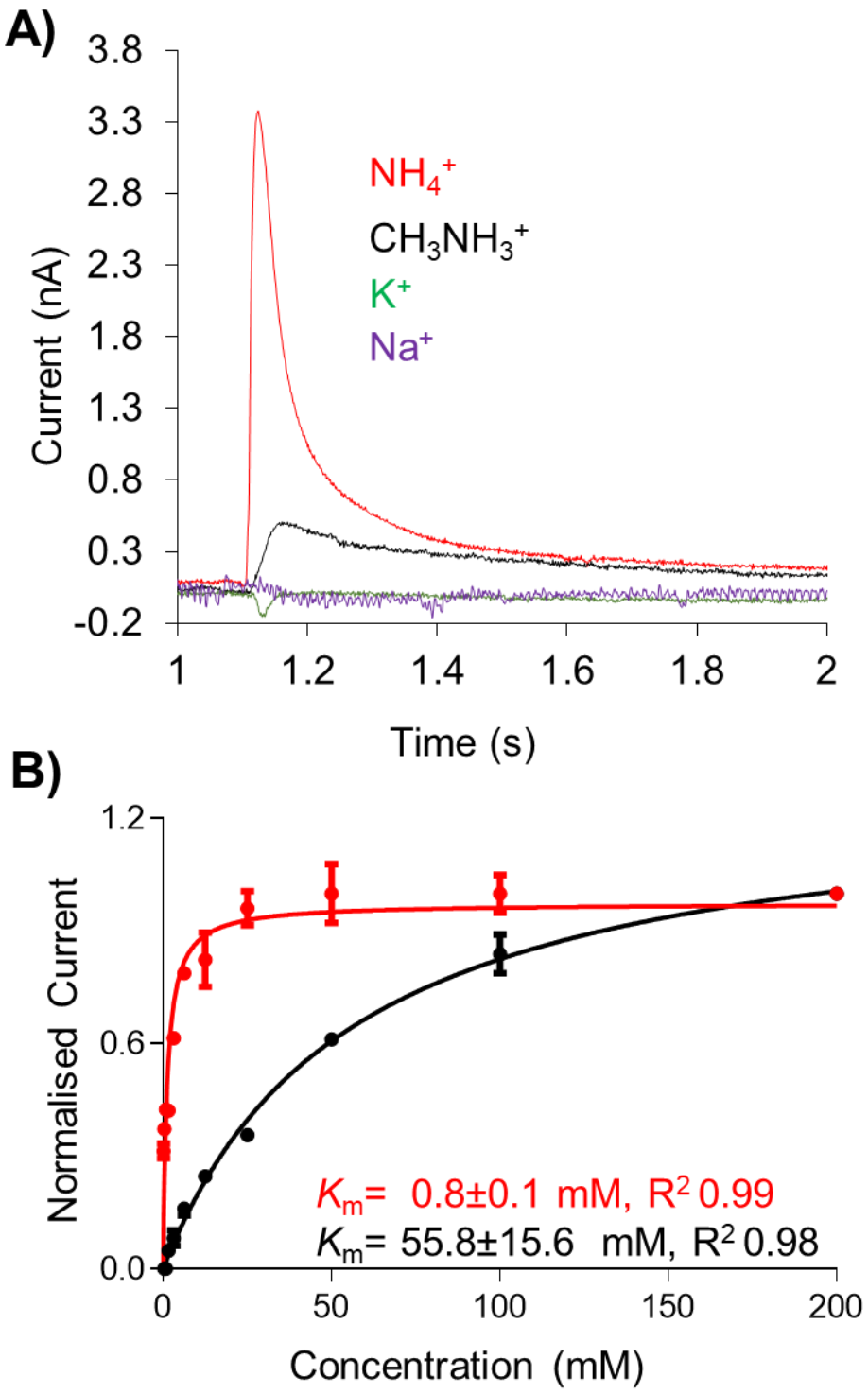

Figure 3.7 Selectivity of AmtB: A) Transient currents following a 200 mM pulse of NH_4^+ (red), $CH_3NH_3^+$ (black), K^+ (green), or Na^+ (purple) with AmtB reconstituted into Polar/POPC 2/1 proteoliposomes at a LPR of 10:1 B) Kinetics for WT AmtB at LPR 10 using NH_4^+ (red) or $CH_3NH_3^+$ (black). Maximum amplitudes have been normalised to 1.0 for comparison. Data points represent mean ± SD.

3.7 Activity is unaffected by a proton gradient

Having shown that AmtB is electrogenic and that it's activity is specific to ammonium, I wanted to determine what was contributing the charge. As discussed in **Section 1.6.2.2**, NH_4^+/H^+ symport and deprotonation symport (NH_3/H^+) represent the most likely electrogenic mechanisms in AmtB. Either of these mechanisms could give rise to the transient currents observed in SSME, however NH_4^+/H^+ symport would require recruitment and passage of a free proton, whilst NH_3/H^+ symport would rely on a deprotonation event. We tested this by setting up an inward proton gradient and measuring the impact on AmtB activity in the presence or absence of NH_4^+. If free protons could pass through the protein, an inward proton gradient would be expected to yield a current on the SSME.

There is no difference between the transient current measured after a 200 mM ammonium pulse at static pH 7 or under an inwardly orientated proton gradient (**Figure 3.8**). This suggests that NH_4^+/H^+ symport is not occurring, as the increased availability of H^+ would be expected to increase the observed activity in that system. In addition, a proton pulse alone does not elicit a measureable current demonstrating that free protons are not able to translocate through AmtB. Taken together, these results suggest that the transient current associated with AmtB activity is due to the translocation of the proton generated by NH_4^+ deprotonation rather than by a H^+ dependent symport mechanism. Therefore, I aimed to identify how this deprotonation occurs.

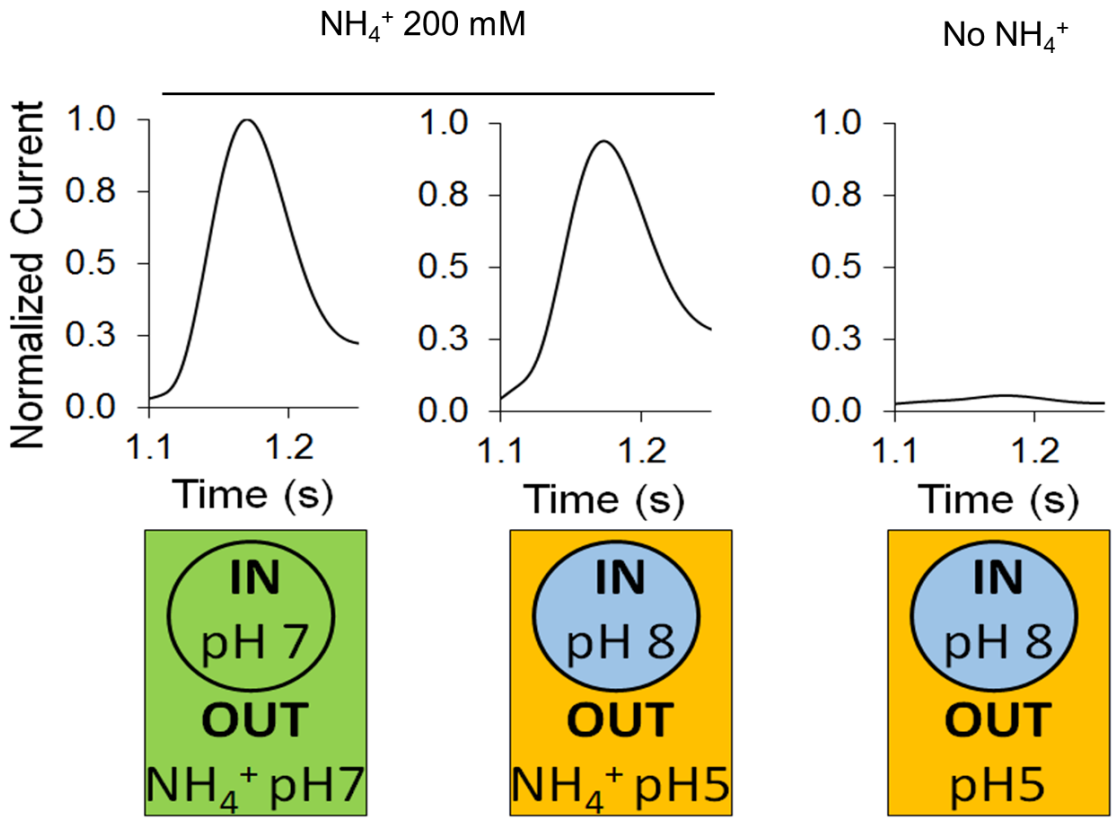

Figure 3.8 Effect of a proton gradient on AmtB activity. The transient currents were measured following an ammonium pulse at pH 7 (left) or under an inwardly directed pH gradient in the presence (centre) or absence (right) of ammonium.

3.8 Mechanism of Deprotonation

AmtB possesses a periplasmic vestibule followed by a hydrophobic pore, which represents a high energetic barrier to ion translocation (Khademi *et al.*, 2004; Zheng *et al.*, 2004). Therefore, NH_4^+ must be deprotonated before the entrance of the hydrophobic pore. Whilst some authors have proposed this occurs at the first histidine of the twin-His motif, it appears more likely that deprotonation occurs upon recruitment at the S1 site (**Section 1.6.2.1**). The twin-His motif is explored extensively in **Chapter 4** and **Chapter 5**, and its proposed role in deprotonation discussed in **Section 6.2.1.2**. Based on the literature, three potential acceptors for the proton have been proposed near the S1 site: periplasmic water, the hydroxyl group of the residue S219, and the carboxyl group of the residue D160 (Javelle *et al.*, 2004; Khademi *et al.*, 2004; Ishikita and Knapp, 2007). The former can be excluded, as if a liberated proton was accepted by periplasmic water the proton would not be translocated and thus no current would be observed. To investigate the role of these residues (**Figure 3.9**), we combined *in vivo* yeast complementation with *in vitro* SSME

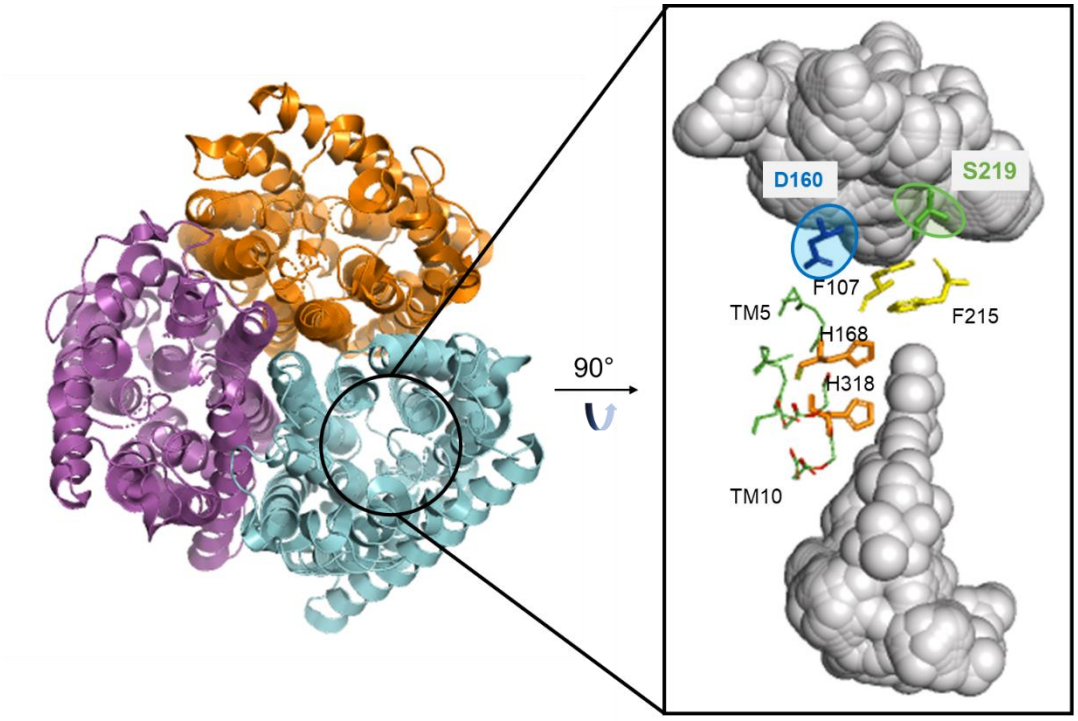

Figure 3.9 Residues Implicated in Deprotonation View of the AmtB trimer from the periplasm, with each monomer represented in purple, orange, or cyan. The pore region a single monomer is expanded, with the water-accessible volume represented in grey. Conserved residues are represented in ball and stick, with S219 (green), and D160 (blue) highlighted.

3.8.1 *S219 is Not Essential* for AmtB Activity

As an initial test, AmtB^{S219A} was expressed in triple-*mepΔ S. cerevisiae* deprived of its endogenous ammonium transporters. As this strain is deprived of its endogenous ammonium transporters, it is unable to grow on ammonium as a sole nitrogen source. If AmtB is expressed in these cells, it complements the activity of the native transporters, restoring the ability to utilise ammonium. When expressed in this system, equivalent growth is observed for WT AmtB and AmtB^{S219A} using ammonium as the sole nitrogen source (**Figure 3.10C**). Methylammonium (MeA) is toxic to *S. cerevisiae,* and can inhibit growth at external concentrations of 100 mM (Marini *et al.*, 1994). However, it has been demonstrated that inactive variants of Mep1 granted resistance to MeA toxicity (Marini *et al.*, 1994). As such, it would be expected that WT AmtB and any active variant would inhibit growth of *S. cerevisiae* on media supplemented with MeA, whilst inactive variants would support growth. As expected, no growth is observed in complemented *S. cerevisiae* grown on MeA-supplemented media. This demonstrates that even in the absence of S219, AmtB is able to complement the function of the endogenous yeast transporters and facilitate uptake of both ammonium and MeA.

Next, the activity of purified AmtB^{S219A} reconstituted in liposomes was quantified using SSME. While a 200 mM ammonium pulse elicited a transient current with a maximum amplitude of 3.38 nA in WT AmtB, a current of only 1.86 nA was measured for AmtB^{S219A} (**Figure 3.10B**). This shows that the transporter retains activity, but the translocation cycle has been impacted. To verify transportation, transient currents at LPR 5:1 and 10:1 were compared. The amplitude depended on the concentration, increasing from 1.8 nA at LPR 10 to 2.5 nA at LPR 5 (**Figure 3.11A**). In addition, the decay rate also correlated to LPR (**Figure 3.11A**). Further, the catalytic constants (*Km*) of AmtB^{S219A} and WT AmtB are comparable (0.8 *vs* 1 mM respectively) (**Figure 3.11B**). Taken together, this demonstrates that AmtB^{S219A} is able to complete the translocation cycle, albeit with a reduction in amplitude due to the disruption of the S1 binding site. Therefore, it is unlikely to be involved in the deprotonation of NH_4^+

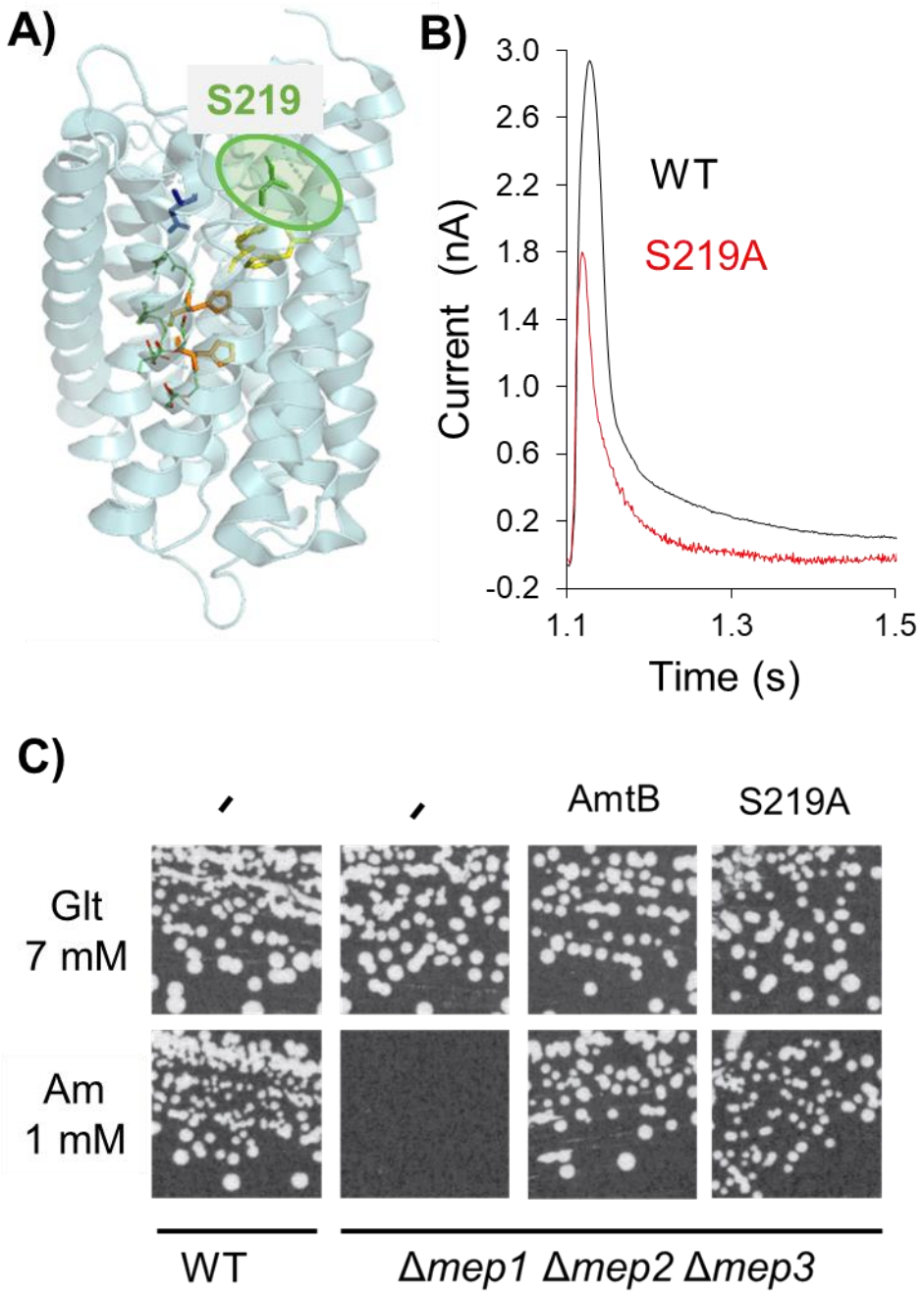

Figure 3.10 S219 is not essential. A) Cartoon representation of AmtB, highlighting substitution site B) Yeast complementation after 5 days of growth on minimal media supplemented with either 7 mM glutamate (Glt) or 1 mM $(NH_4)_2SO_4$ (Am) C) Representative traces following a 200 mM ammonium pulse for WT AmtB (black) and $AmtB^{S219A}$ (red) at LPR 10.

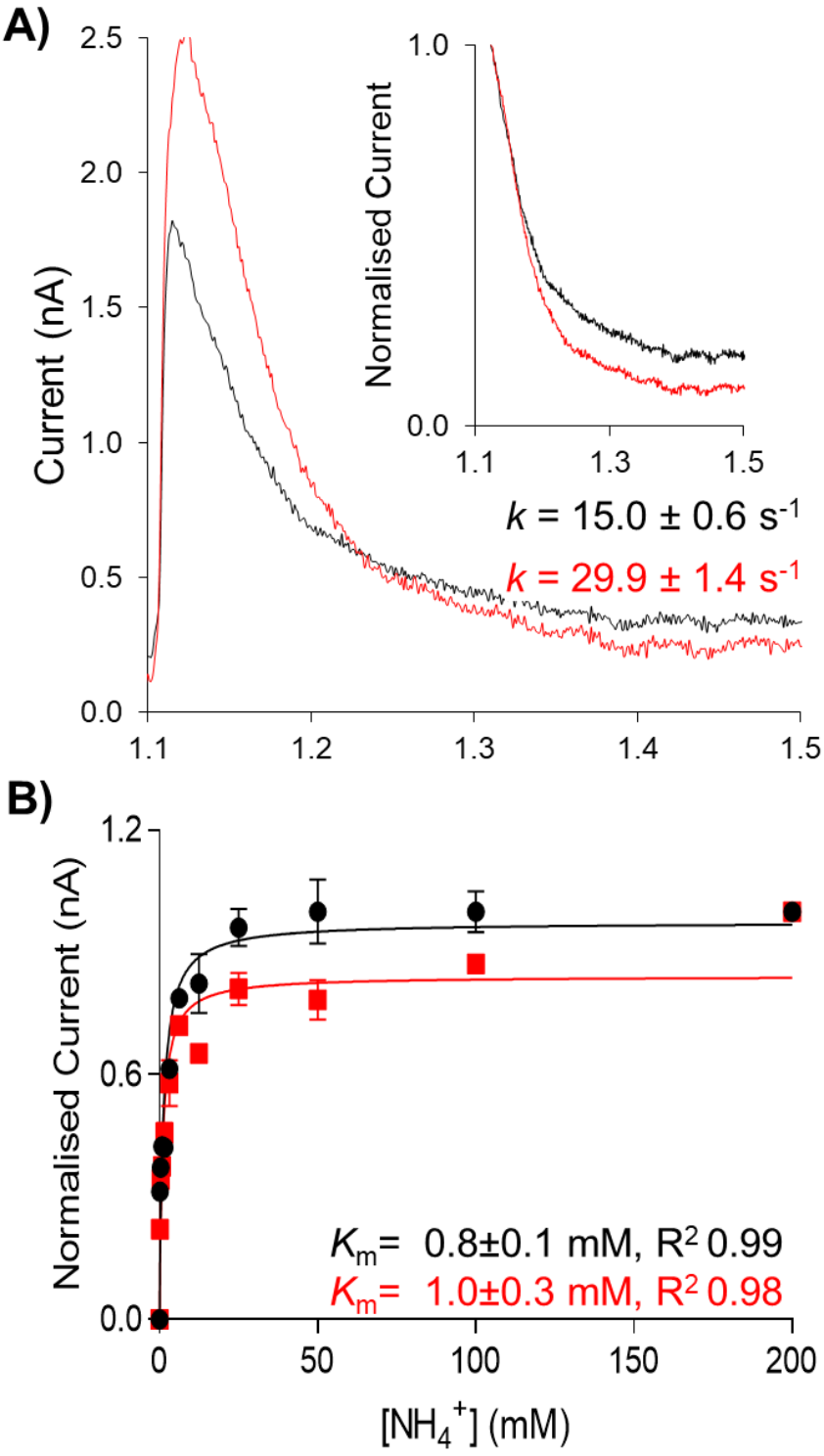

Figure 3.11 AmtB^{S219A} Retains WT Activity: A) Representative traces following a 200 mM ammonium pulse for AmtB^{S219A} at LPR 10 (black) and LPR 5 (red). B) Kinetics for WT AmtB (black) and AmtB^{S219A} (red) at LPR 10 using NH_4^+. Maximum amplitudes have been normalised to 1.0 for comparison**.** Data points represent mean ± SD.

3.8.2 D160 is Essential for AmtB Activity

Having excluded periplasmic water molecules and S219 as potential proton acceptors, the same set of experiments were repeated using $AmtB^{D160A}$.

$AmtB^{D160A}$ did not restore growth in triple-*mepΔ S.* cerevisiae (**Figure 3.12A**), suggesting that the variant cannot replace the function of endogenous ammonium transporters and is thus inactive. However, when measured *via* SSME, a 200 mM ammonium pulse yielded a transient current with a maximum of 0.63 nA. Whilst this is ~5-fold lesser than that measured for WT AmtB, the observation of a current implied some residual activity (**Figure 3.12B**). Comparison of currents at different LPR reveals that the decay rate is completely unaffected LPR (**Figure 3.13A**), implying that the residual current observed is merely due to a protein-substrate interaction instead of describing the complete translocation cycle activity. This is supported by the fact that the *Km* of $AmtB^{D160A}$ increased 70-fold compared to the WT (**Figure 3.13B**). Therefore, whilst a protein-specific electrogenic interaction is taking place, likely at the binding site, $AmtB^{D160A}$ is no longer able to transport ammonium.

Following this, I measured the activity $AmtB^{D160E}$ with the goal of ascertaining if D160's importance is solely due to electrostatic interactions between its carboxylic function and NH_4^+ in the S1 site. If this were the case, it would be expected that a substitution of D for E would conserve the activity of AmtB, as the carboxylic function is retained. However, when expressed in triple-*mep*Δ *S. cerevisiae*, the cells failed to grow, indicating that $AmtB^{D160E}$ failed to replace the activity of the endogenous Mep transporters (**Figure 3.14A**). Electrogenic activity, triggered by a 200 mM ammonium pulse, yielded a reduced maximum current of 1.42 nA compared to the 3.38 nA observed for the WT (**Figure 3.14B**). As with $AmtB^{D160A}$ the decay rate of the current was unaffected by changes in liposomal LPR, hence this residual current represents binding of NH_4^+ to the proteins and not a full translocation cycle (**Figure 3.15A**). Additionally, it was impossible to confidently determine a catalytic constant

(K_m) for AmtB^{D160E} as saturation was not reached, even after an ammonium pulse of 200 mM (**Figure 3.15B**).

These results exclude S219 as an essential facilitator of deprotonation, whilst supporting a key role for the highly conserved D160. It is clear that D160 plays a central role in the transport mechanism as opposed to having a strictly structural role as speculated previously (Khademi *et al.*, 2004). Moreover, the fact that the D to E variation at position 160 impairs ammonium transport *via* AmtB indicates that the D160 residue does not only show electrostatic interaction with NH_4^+ at the S1 site but is also likely involved in the translocation mechanism in *a hitherto* unknown fashion.

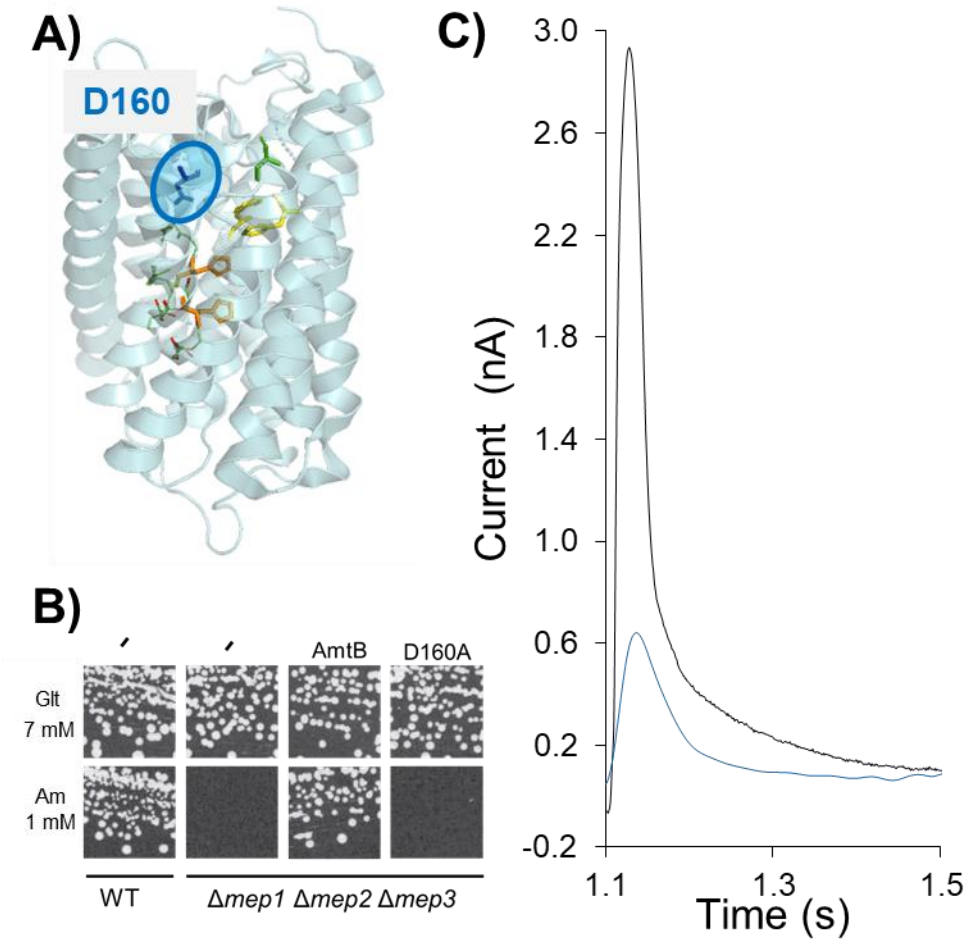

Figure 3.12 D160 is Essential A) Crystal structure of monomer with key residues represented. D160 is highlighted in blue. B) Yeast complementation after 5 days of growth on minimal media supplemented with either 7 mM glutamate (Glt) or 1 mM $(NH_4)_2SO_4$. C) Representative traces following a 200 mM ammonium pulse for WT AmtB (black) and $AmtB^{D160A}$ (blue) at LPR 10

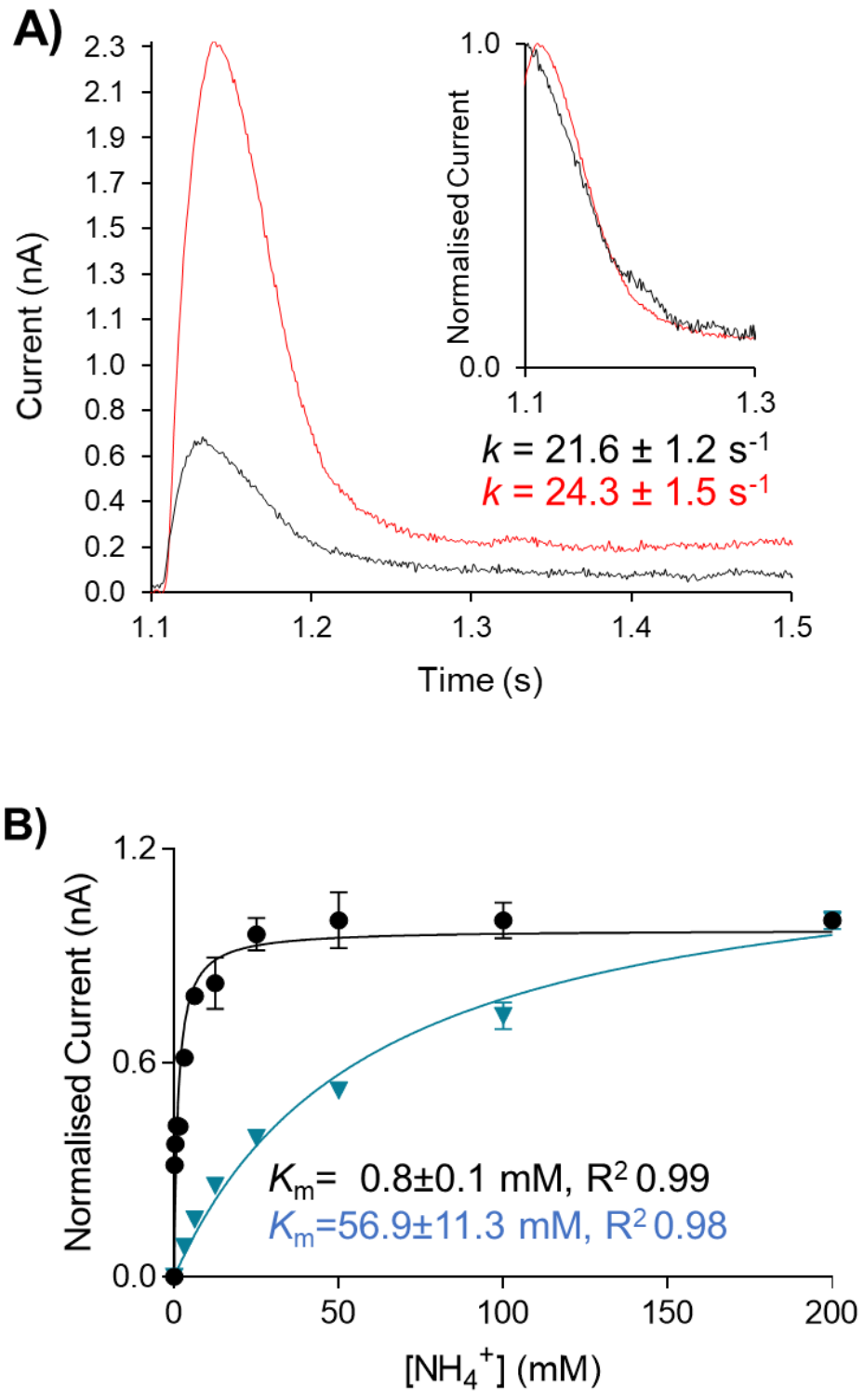

Figure 3.13 AmtB^{D160A} Activity is Abolished: A) Representative traces following a 200 mM ammonium pulse for AmtB^{D160A} at LPR 10 (black) and LPR 5 (red). B) Kinetics for WT AmtB (black) and AmtB^{D160A} (blue) at LPR 10 using NH_4^+. Maximum amplitudes have been normalised to 1.0 for comparison. Data points represent mean ± SD.

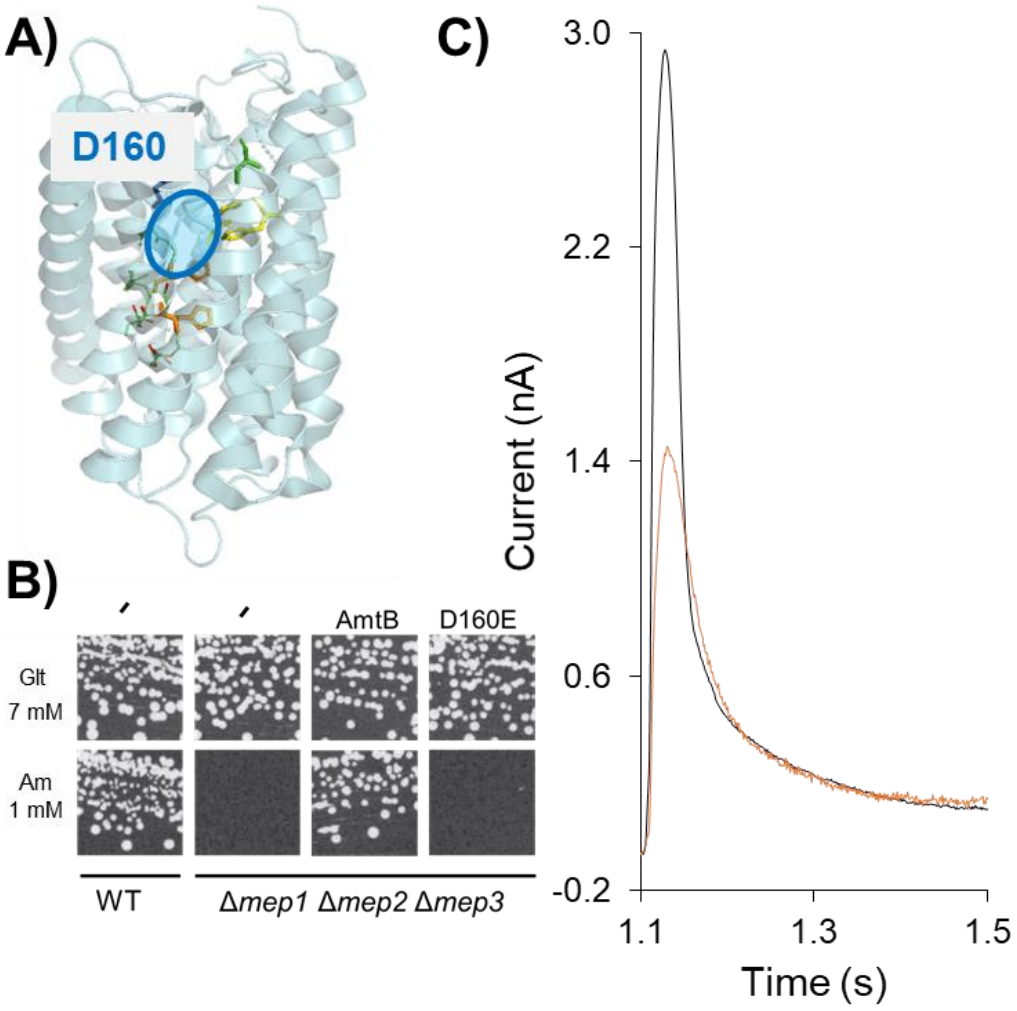

Figure 3.14 D160E Does Not Restore Activity A) Crystal structure of monomer with key residues represented. D160 is highlighted in blue. B) Yeast complementation after 5 days of growth on minimal media supplemented with either 7 mM glutamate (Glt) or 1 mM $(NH_4)_2SO_4$. C) Representative traces following a 200 mM ammonium pulse for WT AmtB (black) and $AmtB^{D160E}$ (orange) at LPR 10

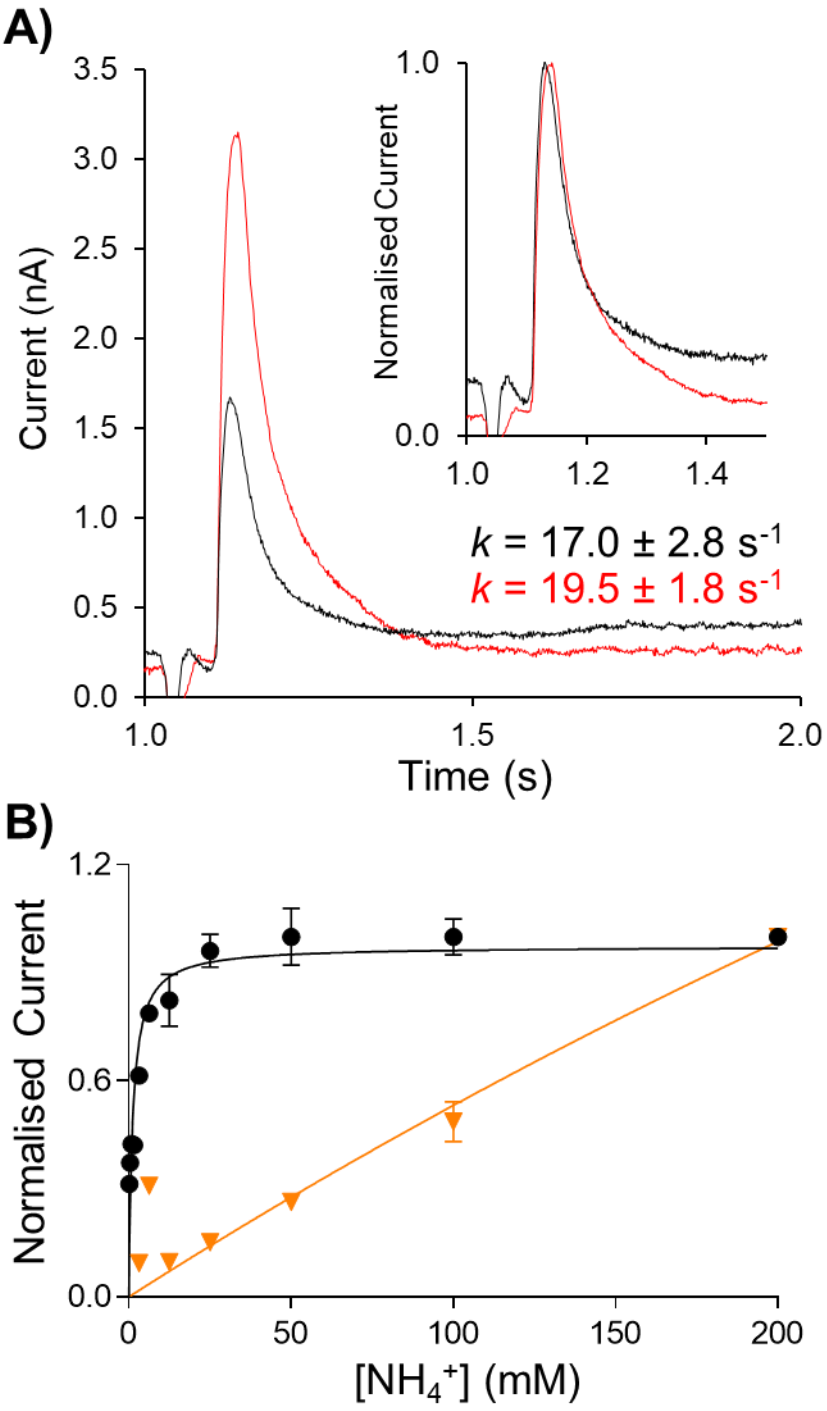

Figure 3.15 AmtB^{D160E} Activity is Abolished: A) Representative traces following a 200 mM ammonium pulse for AmtB^{D160E} at LPR 10 (black) and LPR 5 (red). B) Kinetics for WT AmtB (black) and AmtB^{D160E} (orange) at LPR 10 using NH_4^+. Maximum amplitudes have been normalised to 1.0 for comparison. Data points represent mean ± SD.

3.9 Discussion

3.9.1 AmtB is an Electrogenic Transporter

As stated in the introduction, there is a long standing debate over the substrate transported by Amt/Mep/Rh proteins (NH_4^+ vs. NH_3) as well as the mechanism of the transport, thus whether AmtB activity is electrogenic or electroneutral. The results obtained *via* SSME provide a three-fold support of electrogenic activity. The transient current observed with proteoliposomes containing AmtB is more than 10-fold greater than the signal measured in empty liposomes. The decay rate of the observed current is LPR-dependant, demonstrating that the current represents translocation and not simply a protein-substrate interaction. Finally, the selectivity profile observed with SSME mirrors the previously described selectivity of AmtB, where it is permeable to NH_4^+ but not K^+ or Na^+ (Javelle *et al.*, 2008).

These results correlate well with observations made by Wacker *et al,* who previously applied SSME technology to Amt1 from *A. fulgidus*. They also reported direct observation of selective, electrogenic ammonium transport mediated by the Amt protein (Wacker *et al.*, 2014). This suggests that electrogenic transport could be a conserved feature of Amt proteins, and raises questions about the universality of the transport mechanism across the Amt/Mep/Rh family. Currently, there is conflicting evidence about regarding the electrogenicity of select Mep and Rh proteins, but no published reports on these proteins featuring SSME (Ludewig, Von Wiren and Frommer, 2002; Westhoff *et al.*, 2002; Neuhauser, Dynowski and Ludewig, 2009; Neuhäuser, Dynowski and Ludewig, 2014). Characterisation of the activity of the subfamilies *via* SSME would prove useful in understanding mechanistic conservation within the Amt/Mep/Rh family.

3.9.2 MeA is a Poor Substrate Analogue

MeA has been used extensively in the field as a tool for investigating and characterising AmtB and other members of the Amt/Mep/Rh superfamily. As a result, much of the work throughout this thesis will be discussed within the context of data obtained *via* MeA-based assays. However, my results clearly show that MeA is a poor substrate analogue, and thus is not well-suited for characterisation of AmtB. When investigating the role of the twin-His motif (which is highly conserved in the pore of Amt/Mep/Rh proteins) and aromatic residues in AmtB activity, Hall and Kustu observed comparable doubling times on low NH_3 media, suggesting that the mutations had minimal impact on activity (Hall and Kustu, 2011). Despite this, Hall and Kustu also reported significant variation in MeA uptake activity (ranging from <5–1,300% of wild type) between the WT and mutants. Thus it is clear that MeA-uptake activity does not necessarily correlate with the true activity of AmtB. This is highlighted by Wang ***et al's*** observation that some single His variants (in both AmtB and *Sc*Mep2) were unable to uptake MeA, but retained their ability to grow on minimal media supplemented with 1 mM NH_4^+ as a sole nitrogen source (Wang *et al.*, 2013). Whilst these studies highlighted the potential limitations of MeA as a substrate analogue, they did so in the context of variant proteins – with the latter suggesting the discrepancy was due to substitutions widening the central pore enough to permit translocation of ammonium but not MeA. My results demonstrate that this issue is not an emergent property of substitutions in the protein, but rather an inherent feature of AmtB. This is supported by a comparison of my results with those obtained by Wacker *et al*. Whilst my results are largely in agreement with Wacker *et al*. there is a key difference. Wacker *et al* observed minimal discrimination between ammonium and MeA in their experiments, with mean peak amplitudes of 2.1 and 1.8 nA respectively (Wacker *et al.*, 2014). In contrast, AmtB displays a higher selectivity for ammonium than MeA, with a ~5-fold higher signal obtained for the former. Given the high similarity between the structures of AmtB and Amt1, this stark difference in discrimination is unexpected and extended studies are needed to

clarify this point (Khademi *et al.*, 2004; Andrade *et al.*, 2005). This revelation necessitates careful evaluation of any information derived from MeA-based assays and will be considered in the discussions throughout this thesis. It also highlights the power of SSME, as it permits usage of the true substrate and thus enables interrogation of the mechanism in finer detail. Having established this, I can move on to discuss my results in the context of specific mechanistic aspects of AmtB, starting with deprotonation.

3.9.3 Deprotonation

My results demonstrate that AmtB is electrogenic, thus it must either; transport solvated NH_4^+ directly, facilitate symport of NH_4^+ and H^+, or dissociate NH_4^+, into NH_3 and H^+, and transport these fragments separately through the protein. As stated, the hydrophobic nature of the translocation pore represents a thermodynamic barrier against charge translocation (Khademi *et al.*, 2004; Zheng *et al.*, 2004). Due to this, it is improbable that NH_4^+ could be transported, whereas NH_3 would be able to pass unhindered. Free energy calculations concur that permeation of NH_3 through the pore is energetically favourable, often having comparable energetics to water, whilst direct charge translocation is translocation is near impossible (Zheng *et al.*, 2004; Wang *et al.*, 2012; Baday *et al.*, 2013). However, Boogerd *et al* calculated that transport of NH_3 alone would be insufficient to support observed growth in *E. coli* (Boogerd *et al.*, 2011). Therefore, it is likely that NH_4^+ is deprotonated shortly after binding at the S1 site.

Deprotonation has been proposed previously, including when reporting the crystal structures. Khademi noted that when bound to the S1 site, the pKa of NH_4^+ decreased below 6, favouring the deprotonation of ammonium into ammonia. Khademi and co-workers used an assay which monitored the pH-sensitive fluorescence 5-carboxy fluorescein loaded into AmtB proteoliposomes. When mixed with ammonium chloride the internal pH increased, suggesting an influx of NH_3 into the proteoliposomes. In addition,

the rate of pH change was 10-fold greater in AmtB proteoliposomes (115.6 ± 13.2 s^{-1}) compared to empty liposomes (12.8 ± 0.7 s^{-1}), demonstrating that influx was mediated by AmtB. Based on this, they concluded that the proton was released into the periplasm following deprotonation and neutral NH_3 translocated (Khademi *et al.*, 2004). However, despite extensive efforts, a subsequent study was unable to replicate the rapid alkalisation rates reported by Khademi *et al* and instead found no significant difference between AmtB-proteoliposomes and empty proteoliposomes (Javelle *et al.*, 2007). This lack of reproducibility requires that the results of Khademi *et al*'s original assay be considered with caution and scepticism.

Zheng *et al* similarly discussed deprotonation and stressed that dissociation of the proton back into the periplasm would be essential (Zheng *et al.*, 2004). More recently, Ariz *et al* used relative depletion of 15N compared to 14N to provide support for deprotonation as a shared characteristic of Amt/Mep/Rh proteins, however they did not reach a conclusion regarding the fate of the proton (Ariz *et al.*, 2018). My results demonstrate that AmtB is not able to translocate a proton in the absence of NH_4^+, and that the current induced by AmtB activity is generated by specific deprotonation of the substrate and subsequent H^+ translocation.

As the proton is not exiting into the periplasmic space, it must be accepted by a residue within AmtB. I investigated two potential proton acceptors: S219 and D160. The first was proposed based on computational modelling, which predicted that S219 could accept a proton after coordinating NH_4^+ at the S1 site (Ishikita and Knapp, 2007). However, this hypothesis is discounted by my results: if S219 played a role in deprotonation, its substitution should have a large impact on the activity of AmtB. Instead, I observed no measurable change in activity, indicating that S219 is not essential. D160 is the other candidate for a proton acceptor, due to its proximity to the S1 site, high conservation, and prior evidence of functional importance (Javelle *et al.*, 2004; Wang *et al.*, 2011). I have demonstrated that D160 is strictly essential, as AmtB activity is abolished when substituted to alanine, but also to glutamic acid. If D160 fulfilled a purely structural role, the latter mutation would be expected to

retain the same activity. Thus it seems clear that D160 plays an essential role in the translocation mechanism in AmtB, and whilst a role in deprotonation cannot be proven – the results here provide initial support.

3.9.4 Importance of the S1 binding site:

Prior investigation into the AmtB binding site by Javelle *et al* revealed that $AmtB^{S219A}$ retained similar activity to the WT in MeA uptake assays (Javelle *et al.*, 2008). In fact, they observed a higher transport activity in $AmtB^{S219A}$, leading the authors to conclude that the S1 binding site represented a well in the free energy profile that limited transport rate. In contrast, I observed ~2-fold decrease in maximum transient current compared to the WT. This discrepancy is unsurprising as, highlighted in **Section 1.8.2**, I have demonstrated that MeA is a poor substrate analogue in the characterisation of AmtB. For example, it is possible that $AmtB^{S219A}$ has a lesser discrimination between NH_4^+ and MeA, and thus gives the ersatz impression of increased activity. In addition, the *Km* of AmtB and $AmtB^{S219A}$ are comparable, suggesting that the rate-limiting step is not at the S1 binding site, but further along the translocation pathway.

Deprotonation, or the subsequent translocation of H^+, could represent the true rate-limiting step of the AmtB-mediated NH_4^+ transport. Potential mean force (PMF) calculations carried out by Bostick and Brooks into NH_4^+ and NH_3 conduction in AmtB, suggest that deprotonation occurs between the S1 and S2 sites (Bostick and Brooks, 2007). This supports the concept of the rate limiting step laying below the S1 site, but also gives further credence to D160 playing a role in deprotonation.

Regardless, these results make it clear that ammonium binding at S1 is not the rate limiting step for transport, therefore it cannot be a high affinity binding site. It is important to note however, that in many of these experiments the concentration of ammonium exceeds what might be encountered in the wild, and that the affinity of S1 may become physiologically relevant under limited

ammonium conditions. Previous work by Javelle *et al,* in which AmtB was co-crystallised in the presence of thallium, can help address this possibility. Javelle *et al* observed densities around the S1 site, indicating binding, but the occupancy was a ~10% in the crystal lattice (Javelle *et al.*, 2008). This is low, and suggests that the S1 site is not a high affinity recruitment site. In addition, the Ishikita and Knapp's hypothesis that S219 facilitates deprotonation (Ishikita and Knapp, 2007) is formally ruled out by the results of this work (**Section 1.8.1**). Further, Giulia Tamburrino, from the laboratory of Prof. Ulrich Zachariae, our collaborator at the University of Dundee, simulated the residence time of NH_4^+ and K^+ in the S1 site, and found that both followed a similar profile, appearing to follow diffusion dynamics rather than a peak (personal communication). Again, this suggests that S1 is not a high affinity binding site. As a result, further investigation is required to understand the true role of S219, and the S1 site, in AmtB-mediated transport. The current hypothesis in our lab is that the S1 maintains a niche electrostatic microenvironment that lowers the pKa of ammonium, thus favouring deprotonation (Dr. Arnaud Javelle, personal communication).

3.9.5 Role of D160

Conservation of D160 within the Amt/Mep/Rh family, combined with a loss of MeA uptake in D160A variants lead to the view that the D160 played a mechanistic role (Thomas and Mullins, 2000; Javelle *et al.*, 2004). Due to the proximity of D160 to the S1 site, it is tempting to assume that its role is associated with binding. In the crystal structure, the carboxy group of D160 is buried too deeply in the pore to directly contact an ammonium ion in the binding site (Khademi *et al.*, 2004). However, later molecular dynamic simulations (MDS) predicted that the carboxyl group of D160 would be available for interaction with NH_4^+ (Luzhkov *et al.*, 2006). Whilst the results presented here do not disprove a role in binding, they strongly suggest that binding is not the only role for D160. The effects of D160 substitution are starkly different to

substitution of S219 – a core residue in coordinating NH_4^+ at the S1 site. In the case of S219A, the rate of transport is seemingly unaffected – whilst D160 substitution results in complete abolition transport activity. This suggests a distinct functional role compared to S219. Interestingly, *in vivo* experiments previously demonstrated that $AmtB^{D160A}$ was inactive in the transport of MeA, but found that $AmtB^{D160E}$ retained 70% activity (compared to the WT). This discrepancy is difficult to explain directly, however it is notable that in *in vivo* experiments $AmtB^{D160E}$ does not complement ammonium uptake in yeast, nor does it transport MeA.

Taken together, these results demonstrate an essential functional role for D160 in AmtB-mediated NH_4^+ transport. Whilst the true nature of this role is unclear, my data supports a hypothesis that D160 is involved in a deprotonation step that precedes separate translocation of NH_3 and H^+. No matter the means of deprotonation, the fate of the proton after this step is currently unclear. As such, I sought to identify potential proton transfer pathways in and determine how the proton is translocated in AmtB. This will be presented in **Chapter 4.**

Chapter 4:

Mechanistic Model and the Twin-His Motif

Chapter 4: Mechanistic Model and Twin-His Motif

Aims and Objectives

Computational and experimental studies have suggested that deprotonation of NH_4^+ is likely to be a major step in ammonium transport (Wang *et al.*, 2012; Ariz *et al.*, 2018). The results presented in the previous chapter make it clear that AmtB is electrogenic. Thus the electrogenicity is likely due to translocation of H^+ following deprotonation of NH_4^+, however it is unclear from the crystal structure how this translocation could occur. In this chapter, I present a dynamic polar network across AmtB that could form a transfer pathway for the translocation of H^+ and investigate key residues involved in maintaining this pathway.

Objectives:

1. Apply molecular dynamic simulations (MDS) to reveal potential pathways for proton translocation through the hydrophobic pore of AmtB.
2. Validate the simulated pathway *via in vitro* SSME assays
3. Identify and characterise substitutions of residues involved in proton translocation

4.1 Introduction

Computational and experimental studies have suggested that deprotonation is a key step in the mechanism of AmtB (Wang *et al.*, 2012; Ariz *et al.*, 2018). However, it remains unclear how a proton would be translocated through the protein. The crystal structures show no clear pathway for proton conductance, and the phenylalanine gate and hydrophobic central pore both present potential barriers for movement of charged molecules (Khademi *et al.*, 2004). However, even “open pore” variants, wherein the phenylalanine gate is

removed, have been reported to be impermeable to H^+ (Javelle *et al.*, 2008). As such, it was initially hypothesised that following deprotonation, the liberated H^+ was released into the periplasm. However, this is incompatible with the observation of electrogenic activity, and suggests that the proton is translocated via a *hitherto* unknown mechanism.

Molecular dynamic simulations carried out by Baday *et al* suggested that a discrete chain of water molecules can form near the twin-His motif, parallel to the pore (Baday *et al.*, 2013). The presence of water at this position however, has yet to be confirmed and the relevance of this predicated chain is unclear. In theory, this chain could function as a water wire, enabling H^+ conduction through a Grotthuss mechanism, in which a single H^+ "hops" from one water molecule to the next in rapid succession. However, it is unclear how H^+ could reach this chain as it is buried deep in the pore, thus leaving an incomplete pathway. Therefore, to understand the fate of H^+ following deprotonation, it is imperative to identify a complete pathway for proton conduction, from the periplasmic to the cytoplasmic side of the protein, and demonstrate its role in AmtB-mediated electrogenic activity.

Part of this has been the subject of a paper published in the journal *eLife* and is presented in **Appendix A**):

Gordon Williamson, Giulia Tamburrino, Adriana Bizior, Mélanie Boeckstaens, Gaëtan Dias Mirandela, Marcus G Bage, Andrei Pisliakov, Callum M Ives, Eilidh Terras, Paul A Hoskisson, Anna Maria Marini, Ulrich Zachariae, and Arnaud Javelle. (2020) '**A two-lane mechanism for selective biological ammonium transport**', *eLife*. Edited by N. Ben-Tal. eLife Sciences Publications, Ltd, 9, p. e57183.

4.2 Molecular Dynamic Simulations Reveal Two Interconnected Water Wires

In order to identify potential polar networks within AmtB, collaborators from the laboratory of Prof. Ulrich Zachariae at the University of Dundee performed atomistic molecular dynamic simulations of AmtB in mixed lipid bilayers. This initially revealed hydration in the pore, connecting the twin-His motif to the cytoplasmic side of the pore (cytoplasmic water wire -CWW- **Figure 4.1**). The stabilisation of this wires seems to depend on the respective protonation state of the twin-His motif: H168 donor, with the proton on Nδ for H168 and on Nε for H318 (DE); and H168 acceptor (ED), with the proton on Nε for H168 and on Nδ for H318 (**Figure 4.2**). The CWW is particularly stabilized in the DE twin-His tautomeric state, where the occupancy is 79% on average with at least three water molecules over the course of the simulations. As previously observed, the CWW develops in the early stages of the simulations (Lamoureux, Klein and Bernèche, 2007) (**Figure 4.3**)**.**

Crucially, the simulations revealed the presence of a second, previously unidentified, water wire opening around the residue D160 near the S1 binding site and extending to the twin-His motif (periplasmic water wire – PWW- **Figure 4.1**). In comparison to the CWW, the PWW develops over a longer timescale and shows greater fluctuations thus is less stable (**Figure 4.3**).

The PWW and CWW are connected by the H168, which forms a bridge that links the two chains. Whilst neither water wire is wide enough to permit movement of solvated NH_4^+, water molecules and histidine side-chains are often hallmarks of efficient proton transfer in proteins (Wraight, 2006). Such features have been noted in the M2 proton channel of Influenza A (Acharya *et al.*, 2010), the D-channel of Cytochrome Oxidase C (Ghane *et al.*, 2018), and the channels formed by the ionophoric antibiotic gramicidin A (Pomès and Roux, 2002). Thus, the water wires could represent a complete pathway for proton translocation from the periplasm to the cytoplasm, following deprotonation. In this model, the central twin-His motif would assume two important roles: 1) linking the periplasmic and cytoplasmic water wires to allow

the conduction of H^+, 2) Prevent the formation of a continuous channel. This ensures selectivity, as the presence of a continuous water-filled channel could allow passage of hydrated ions.

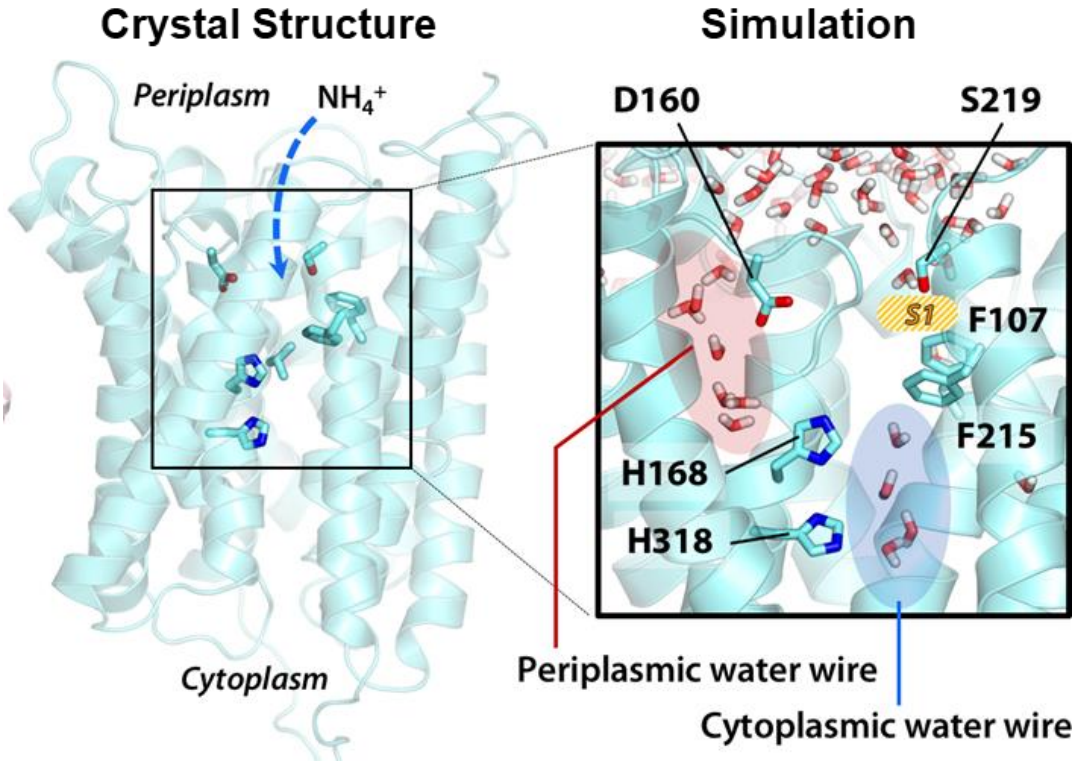

Figure 4.1 Formation of the two water wires in AmtB. Extended atomistic simulations show a hydration pattern across the protein, in which cytoplasmic and periplasmic water wires, connected via H168, form a continuous pathway for proton transfer from the S1 NH_4^+ sequestration region to the cytoplasm. Adapted from (Williamson *et al.*, 2020).

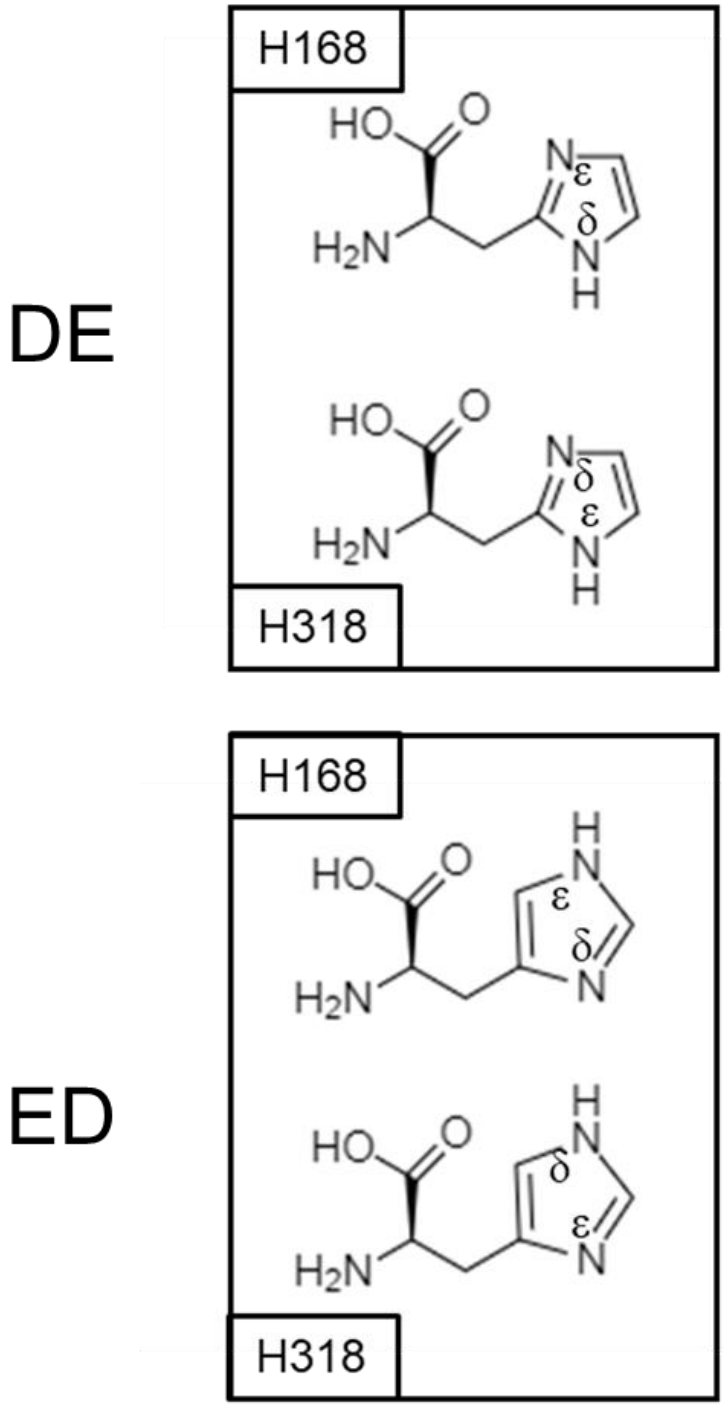

Figure 4.2: H168 and H318 Configurations. Simplified view of the configurations of H168 and H318. The top panel shows the DE configuration, with the protonated Nδ of H168 pointing toward the unprotonated Nδ of H318. The bottom panel shows the ED configuration, in which the protonation flips and the protonated N δ of H318 points toward the unprotonated N δ of H168.

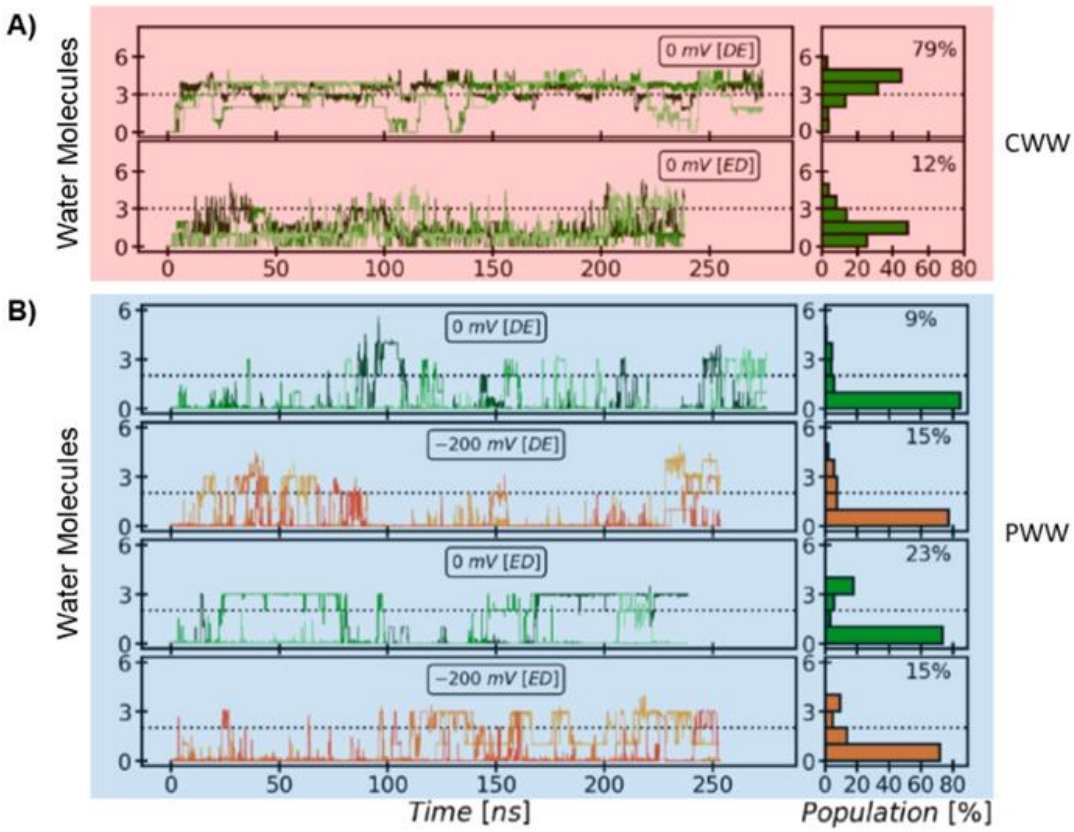

Figure 4.3 Evolution and occupancy of A) Cytoplasmic Water Wire and B) Periplasmic Water Wire using molecular dynamic simulations. The CWW is particularly stabilized in the DE twin-His tautomeric state, where the occupancy is 79% on average with at least three water molecules over the course of our simulations. The periplasmic water wire evolves on a slower time scale than the CWW and shows greater fluctuations. It is stabilized by the ED twin-His tautomeric state, where 23% occupancy of the PWW with three water molecules or more is observed. Stably occupied states are seen after ~25 ns simulated time. Adapted from (Williamson *et al.*, 2020).

4.3 Water Wires Are Functionally Important for AmtB

To experimentally test if the water wires are essential for the proton conduction during AmtB transport cycle, we made use of the reduced deuteron mobility of heavy water D_2O. Because deuterons have twice the mass of a proton and the strength of a bond is increased, proton mobility is reduced by 30% for each D_2O molecule compared to H_2O (Wiechert and Beitz, 2017). As the polar network of water identified by MDS comprise more than 3 water molecules, AmtB activity should be abolished if tested in the presence of D_2O only. To test this, an SSME-based assay was devised, wherein all buffers used to prepare the proteoliposomes and SSME sensors were done using D_2O instead of H_2O. No current was observed following a 200 mM ammonium pulse under these conditions, indicating that the presence of D_2O abolished AmtB activity compared to the same assay carried out with H_2O based solutions (**Figure 4.4**) As a control to ensure that the loss of activity wasn't merely the result of damage to the protein, D_2O sensors were rinsed with H_2O-based solutions and the measurements repeated. By saturating the protein with water, the D_2O in the water wires should be replaced with H_2O and restore electrogenic activity. Indeed, after rinsing the sensor prepared in D_2O with water, AmtB re-gained 100% of its activity measured by SSME (**Figure 4.4**), showing that the presence of D_2O did not affect the protein itself nor impact the integrity of proteoliposome. Further calculations suggested that H^+ transfer between the water molecules in the PWW and CWW is possible and could occur with high rates (the highest energy barrier is ~18 kJ/mol in the cytoplasmic wire near the twin-His motif; Table 4.1). Taken together, the experimental and computational data demonstrate that the water wires in AmtB underpin its activity.

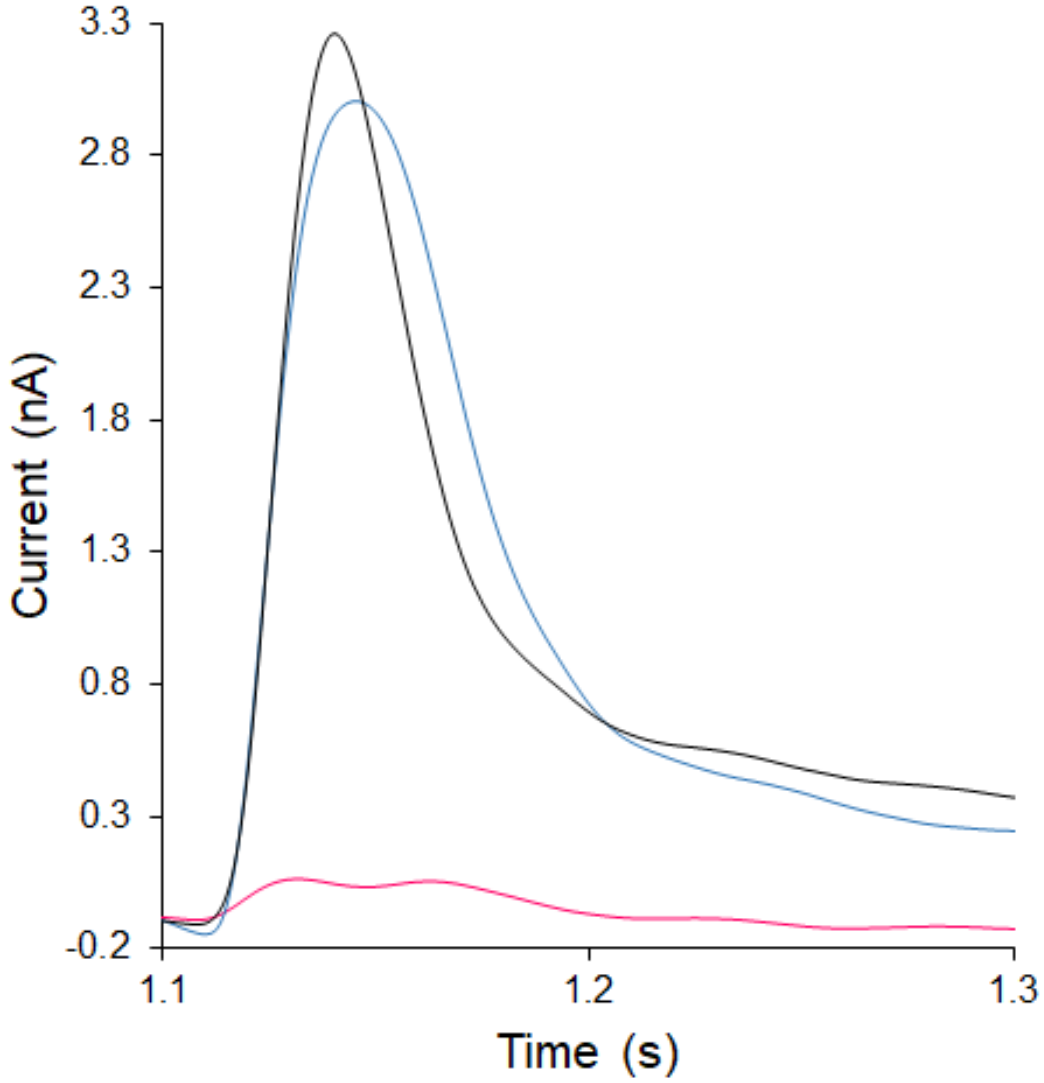

Figure 4.4: D_2O abolishes electrogenic activity of AmtB. Transient currents measured following a 200 mM ammonium pulse on sensors prepared with solutions containing either H_2O (black) or D_2O (magenta). Subsequently, the D_2O sensors were rinsed with H_2O-solutions and measured again (blue).

Table 4.1: Free Energies of proton translocation through cytoplasmic and periplasmic water wires.

			z (Ä)	Free energy (kJ/mol)
(bulk)	Periplasmic Water Wire	Water1	14.7	0.0
		Water2	12.7	8.7
		Water3	10.7	15.0
		Water4	8.3	14.4
		Water5	6.1	7.5
D160		Water6	5.4	11.0
		Water7	3.2	
		Water8	0.6	
H168				
	Cytoplasmic Water Wire	Water9	-0.4	17.3
		Water10	-0.8	14.4
		Water11	-3.2	12.1
H318		Water12	-5.1	13.8

*The vertical coordinate (z) was calculated relative to the position of H168. Positions of the sidechains of D160, H168, and H318 with respect to the periplasmic and cytoplasmic water wires are indicated in the leftmost column.

4.4 Purification of Twin-His Variants

The predicted roles of the twin-His motif would make it essential in the proposed transport mechanism. Therefore, a collection of twin-His variants were purified and characterised in order to understand the functional role of the motif. These variants will be presented throughout this chapter and were purified and inserted into proteoliposomes as described previously (**Section 2.4**). Like the WT, all variants purified with an elution peak observed at ~11 mL in the SEC (**Figure 4.5**). This confirms that the variant AmtB are pure and did not aggregate or destabilise at any point in the purification.

As before, the purified proteins were reconstituted into liposomes to form proteoliposomes for use in SSME. To ensure successful insertion, the proteoliposomes are washed repeatedly and analysed by SDS-PAGE. For all variants, no bands were visible in the supernatant wash samples, and the major bands in the proteoliposome samples were ~130 kDa, as expected of trimeric AmtB (**Figure 4.6**). This confirms that AmtB tolerates substitution of one or both histidines without a deleterious impact on structural integrity.

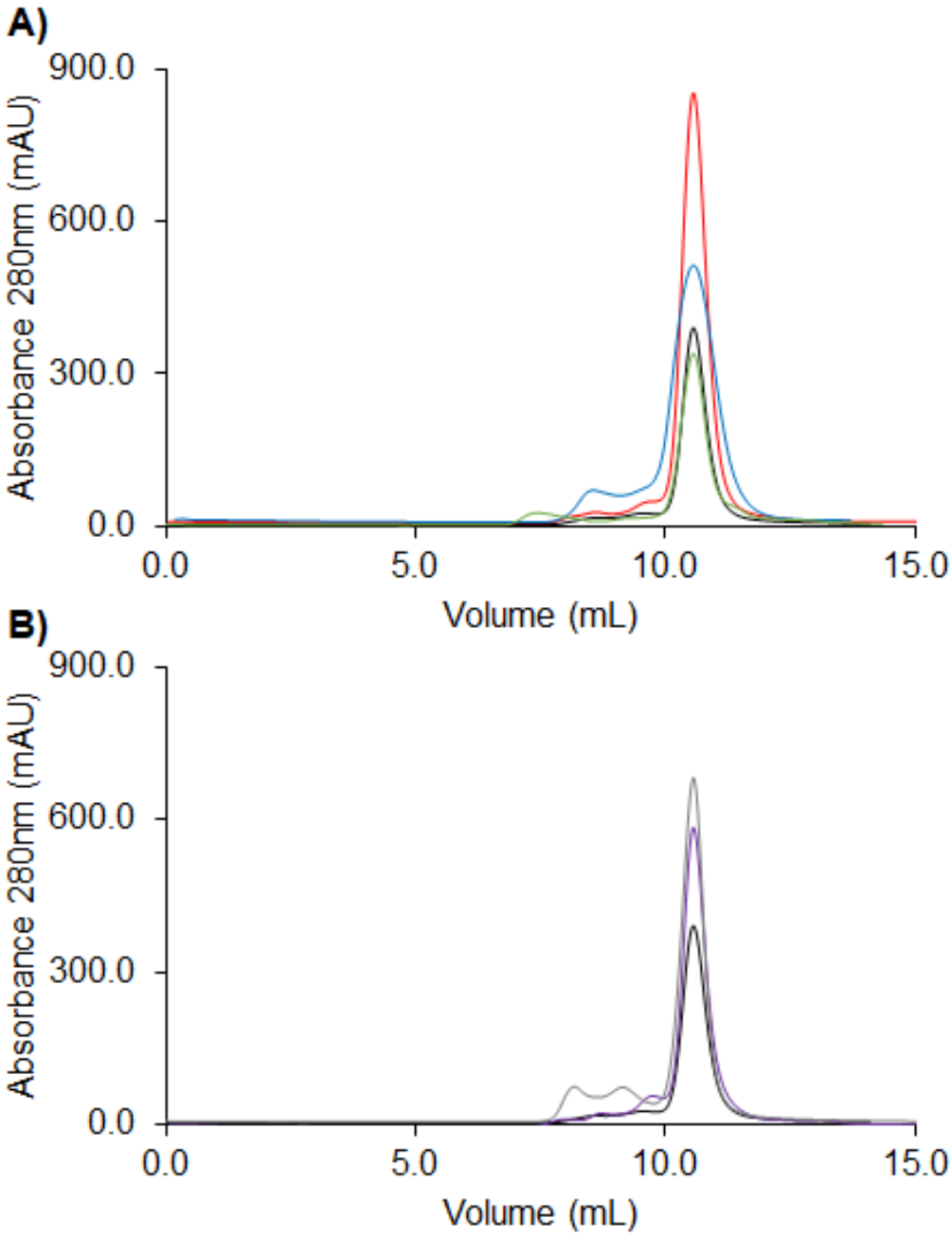

Figure 4.5: Verification of variant AmtB. Size-exclusion chromatogram of *Ec*AmtB solubilised in 0.033% DDM and injected on a Superdex 200 increase 10/300 column. A) WT (black), H168A (red), H318A (blue), H168E (green) B) WT (black), H168A/H318A (purple), S219A/H168A/H318A (grey).

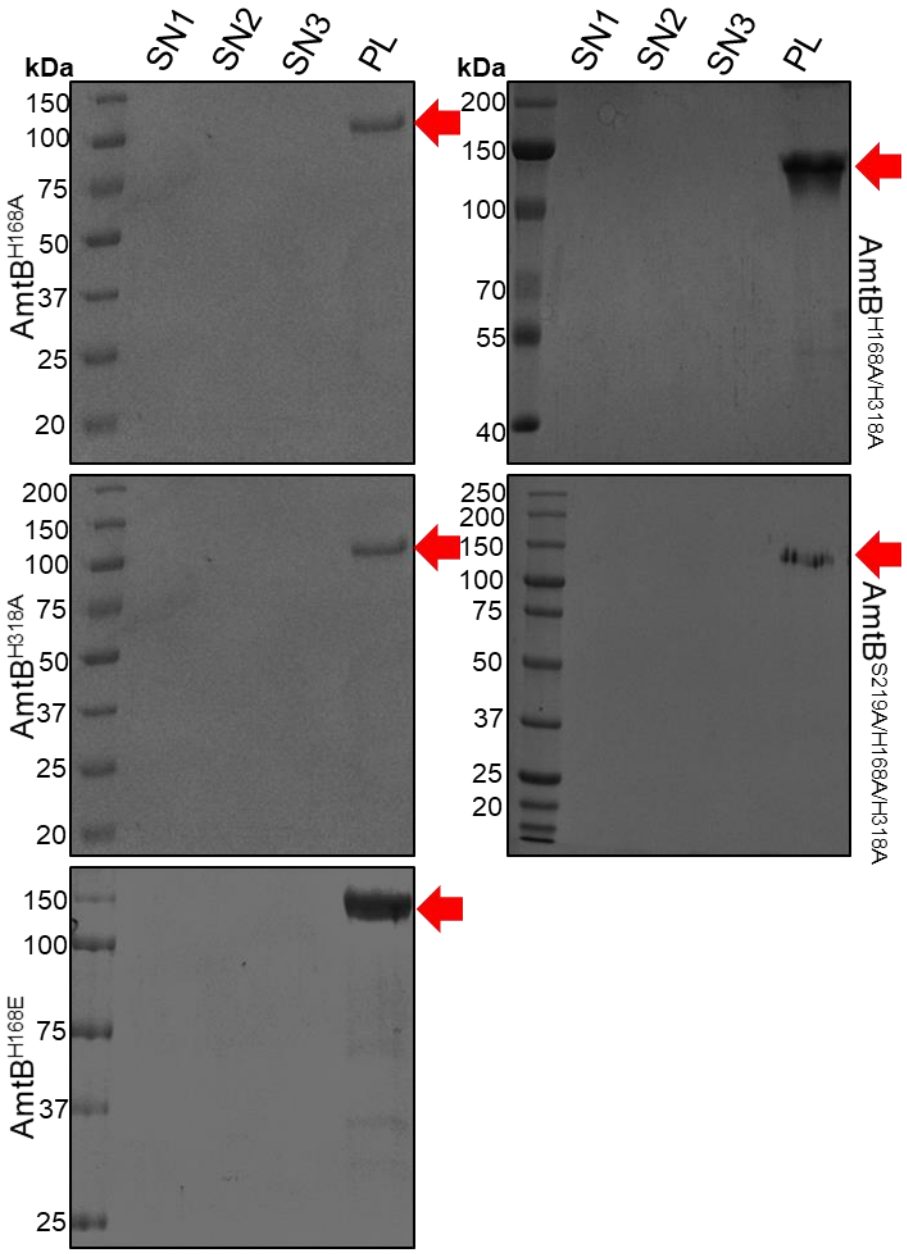

Figure 4.6: Insertion of variant AmtB into proteoliposomes: 10% SDS-PAGE gel monitoring the wash protocol. SN1-3 = supernatant from each wash step, PL is a sample of either AmtB^{H168A} (top-left), AmtB^{H318A}(middle-left), AmtBH^{168E}(bottom-left), AmtB$^{H168A/H318A}$ (top-right), or AmtB$^{S219A/H168A/H318A}$ (middle-right) Polar/POPC 2/1 proteoliposomes at LPR 10. The red arrows indicate regions of 130 kDa, the expected size of AmtB.

4.5 The Twin-His Motif Stabilises the TWW

To determine if the twin-His motif stabilises the water wires, both histidines (H168 and H318) were substituted with alanine and the variant protein characterised. If they fulfil their predicted role, this substitution would be expected to inactive the protein. When expressed in triple-*mep*Δ yeast, $AmtB^{H168A/H318A}$ does not support growth (**Figure 4.7C**), indicating that the protein is incapable of complementing the Mep's ammonium uptake activity. Next proteoliposomes containing variant AmtB were measured via SSME. While a transient current is observed after a 200 mM ammonium pulse, the amplitude is less than half that observed for the WT and the decay rates are not dependent on LPR (**Figure 4.7B**). This suggests that the residual current is the result of an interaction between NH_4^+ and AmtB and not translocation. To verify this, we repeated the experiments with the $AmtB^{S219A/H168A/H318A}$ variant, in which the periplasmic binding site is also disrupted. $AmtB^{S219A/H168A/H318A}$ was unable to complement ammonium uptake in triple-*mep*Δ yeast, but it did not yield a measurable current on SSME (**Figure 4.7B-C**). Taken together, these results demonstrate that the twin-His motif is essential for the transport mechanism, as its removal abolished NH_4^+ transport activity.

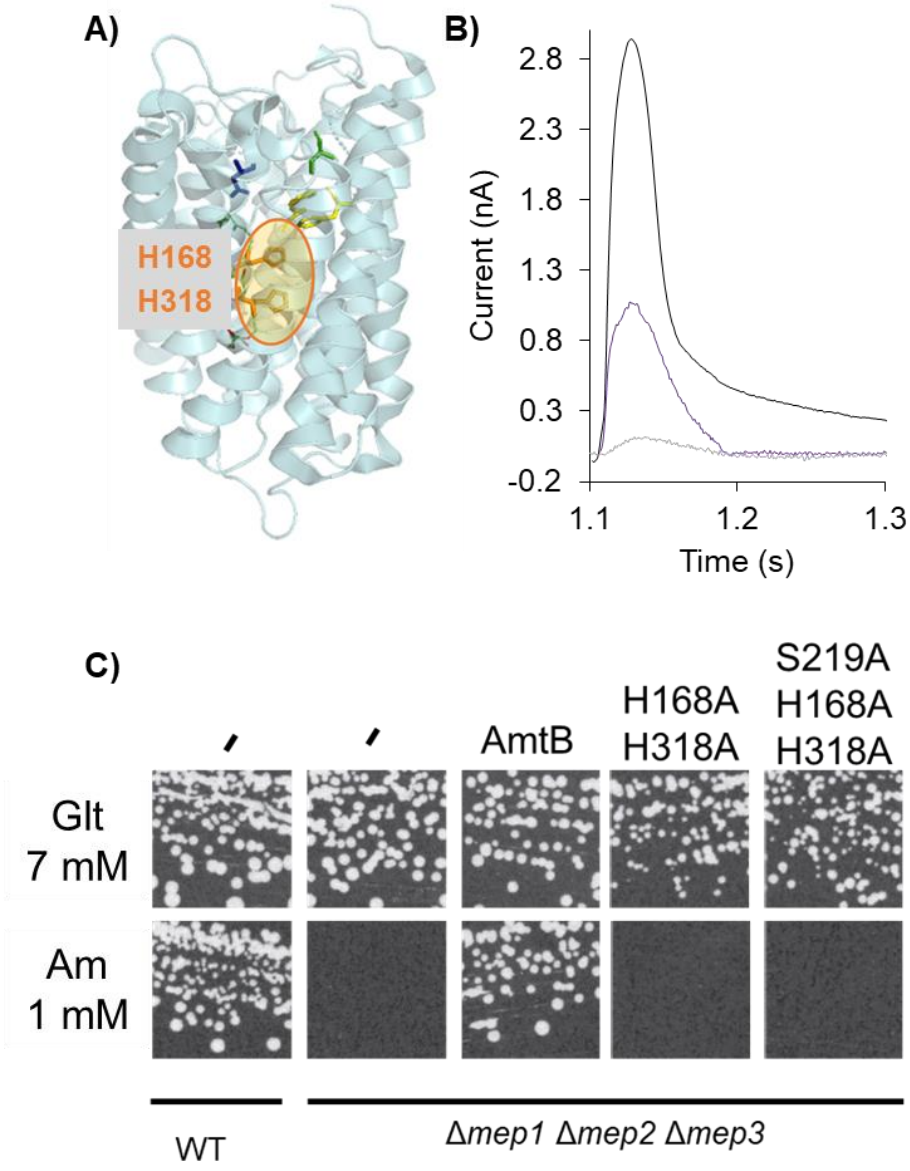

Figure 4.7 Twin-His Motif is essential for AmtB Activity.
A) Cartoon representation of AmtB, highlighting substitution site B) Representative traces following a 200 mM ammonium pulse for WT AmtB (black), AmtB$^{H168A/H318A}$ (red), and AmtB$^{S219A/H168A/H318A}$ (grey) at LPR 10. C) Yeast complementation after 5 days of growth on minimal media supplemented with either 7 mM glutamate (Glt) or 1 mM $(NH_4)_2SO_4$ (Am).

4.6 Single Mutations of Twin-His Motif Are Tolerated

It is unclear if both residues of the of the twin-His motif are required to maintain activity, or if the water wires can be stabilised by just one of the histidines. In order to distinguish if water wire stability was primarily maintained by a single residue of the twin-His motif or was a combined effort, each of the histidines were individually substituted with alanine.

In the single His variant AmtB^{H168A} we unexpectedly observed a 1.5-fold increased current in our SSME recordings (**Figure 4.8B**). Furthermore, triple-*mepΔ* yeast cells expressing AmtB^{H168A} display growth in the presence of low ammonium concentrations (**Figure 4.8C**). Unlike the double twin-His variant AmtB$^{H168A/H318A}$, AmtB^{H168A} retains activity. A previous crystal structure (Javelle *et al.*, 2006) and our MD simulations (**Figure 4.8A**) show increased hydration in the area around A168, which could potentially form a pathway for efficient H^+ transfer or direct translocation of NH_4^+. This pathway could explain why this variant complements growth in yeast and retains activity on SSME, while AmtB^{H168AH318A} does not. Notably, the NH_4^+ translocation activity was not saturable in the concentration range [12.5-200 mM] for AmtB^{H168A} (**Figure 4.9B),** suggesting a reduction in NH_4^+ affinity in this variant or a switch to a channel-like type of activity.

Similarly, AmtB^{H318A} restored growth in triple-*mepΔ* yeast, indicating that it is active in ammonium transport (**Figure 4.10C**). As with AmtB^{H168A}, a transient current was observed following a 200 mM ammonium pulse, with a maximum amplitude ~2-fold lower than that of the WT (**Figure 4.10B**). The decay rate of the transient current was LPR dependent (**Figure 4.11A**), confirming that AmtB^{H318A} retains translocation activity. AmtB^{H318A} activity was also not saturable in the [12.5-200 mM] concentration range (**Figure 4.11B**), suggesting that substitution of either histidine has a large effect on the kinetics of AmtB.

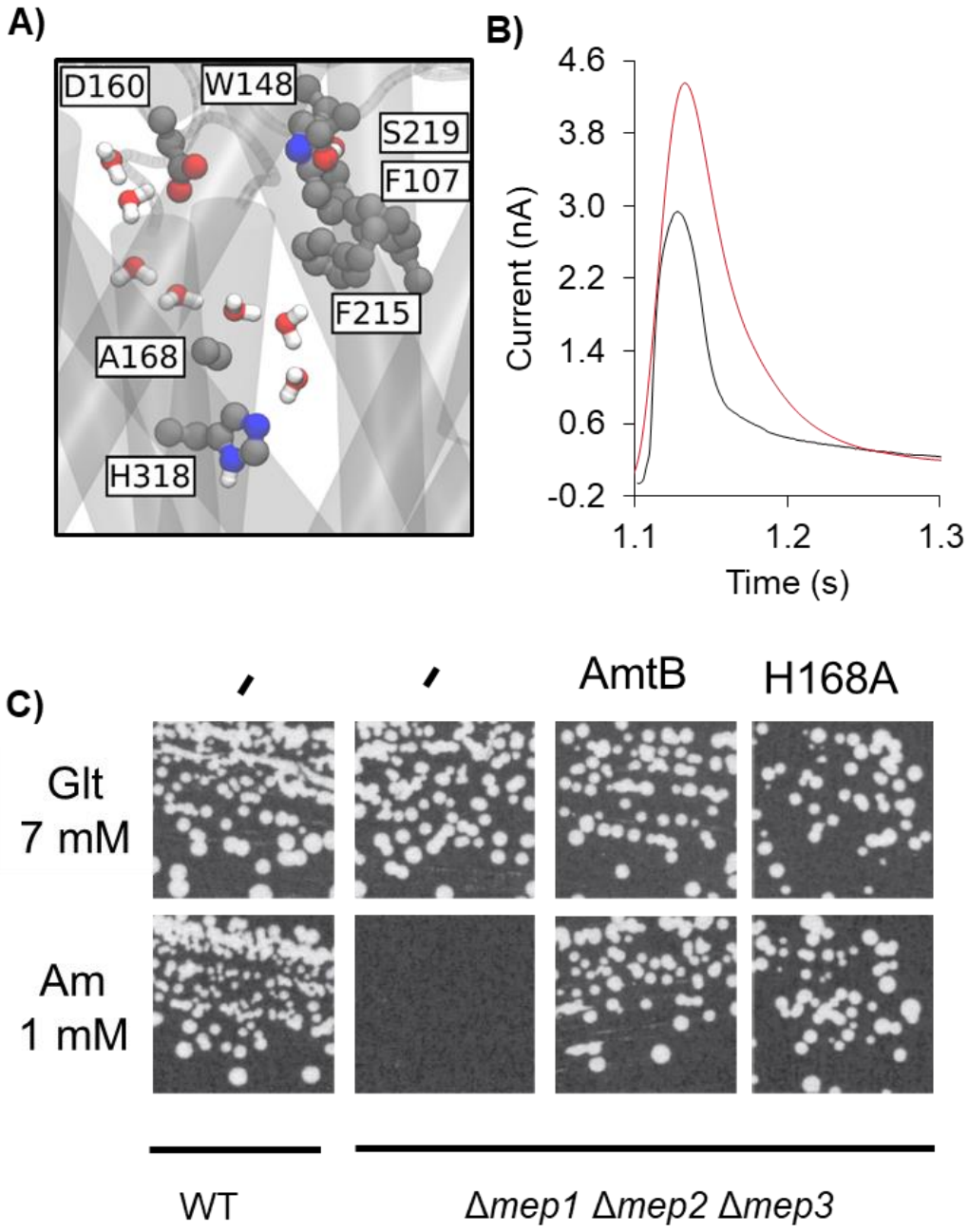

Figure 4.8 AmtB^{H168A} retains activity. A) Crystal structure of AmtB^{H168A}, as reported by Javelle *et al.*, 2006 B) Representative traces following a 200 mM ammonium pulse for WT AmtB (black), AmtB^{H168A} (red) at LPR 10. C) Yeast complementation after 5 days of growth on minimal media supplemented with either 7 mM glutamate (Glt) or 1 mM $(NH_4)_2SO_4$ (Am).

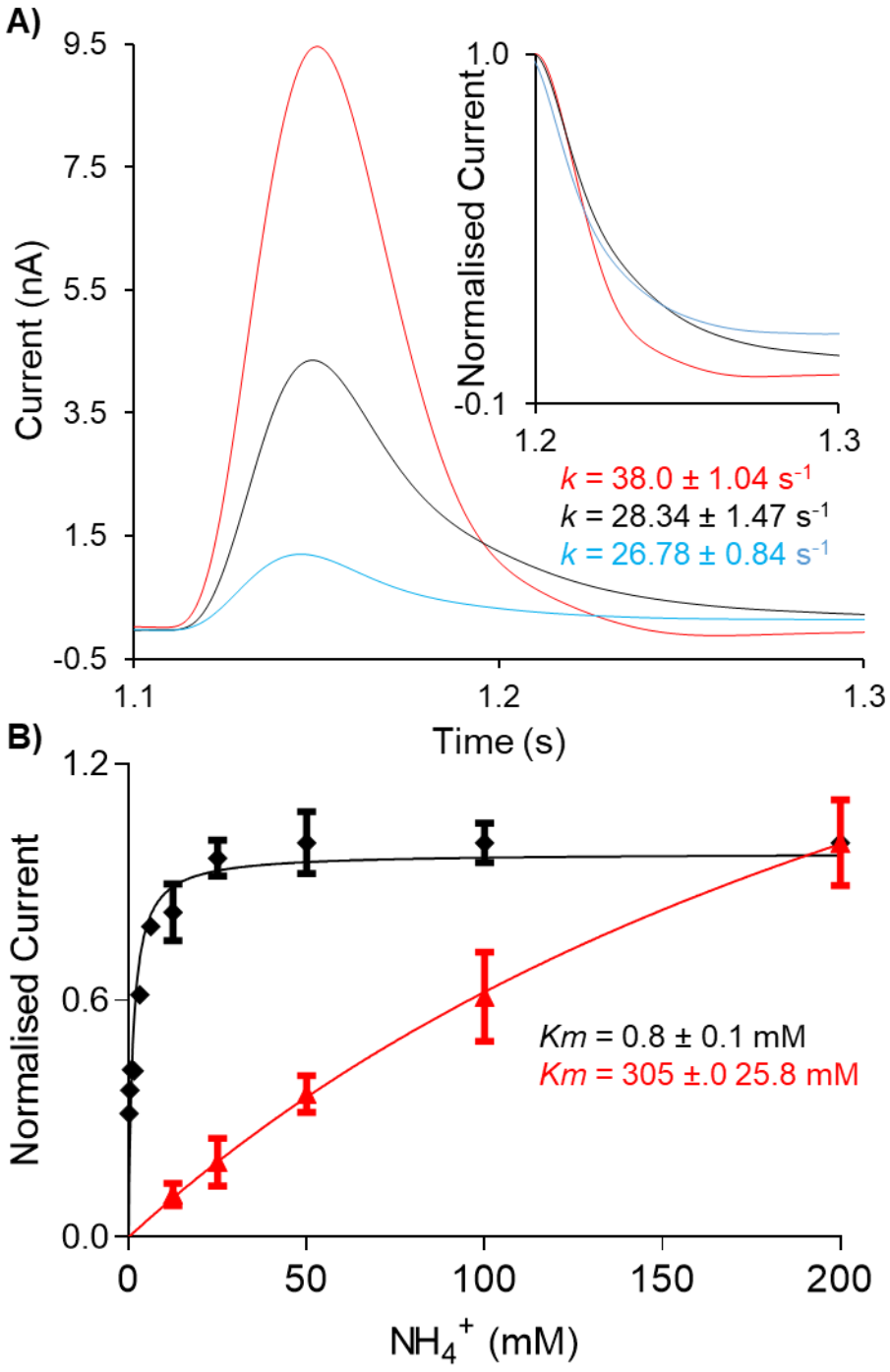

Figure 4.9 AmtB^{H168A} Characterisation. A) Transient currents following a 200 mM NH_4^+ pulse with AmtB^{H168A} reconstituted into Polar/POPC 2/1 proteoliposomes at a LPR of 5:1 (red), 10:1 (black), or 50:1 (blue). B) Kinetics for WT AmtB (black) and AmtB^{H168A} (red) at LPR 10 using NH_4^+. Maximum amplitudes have been normalised to 1.0 for comparison. Data points represent mean ± SD.

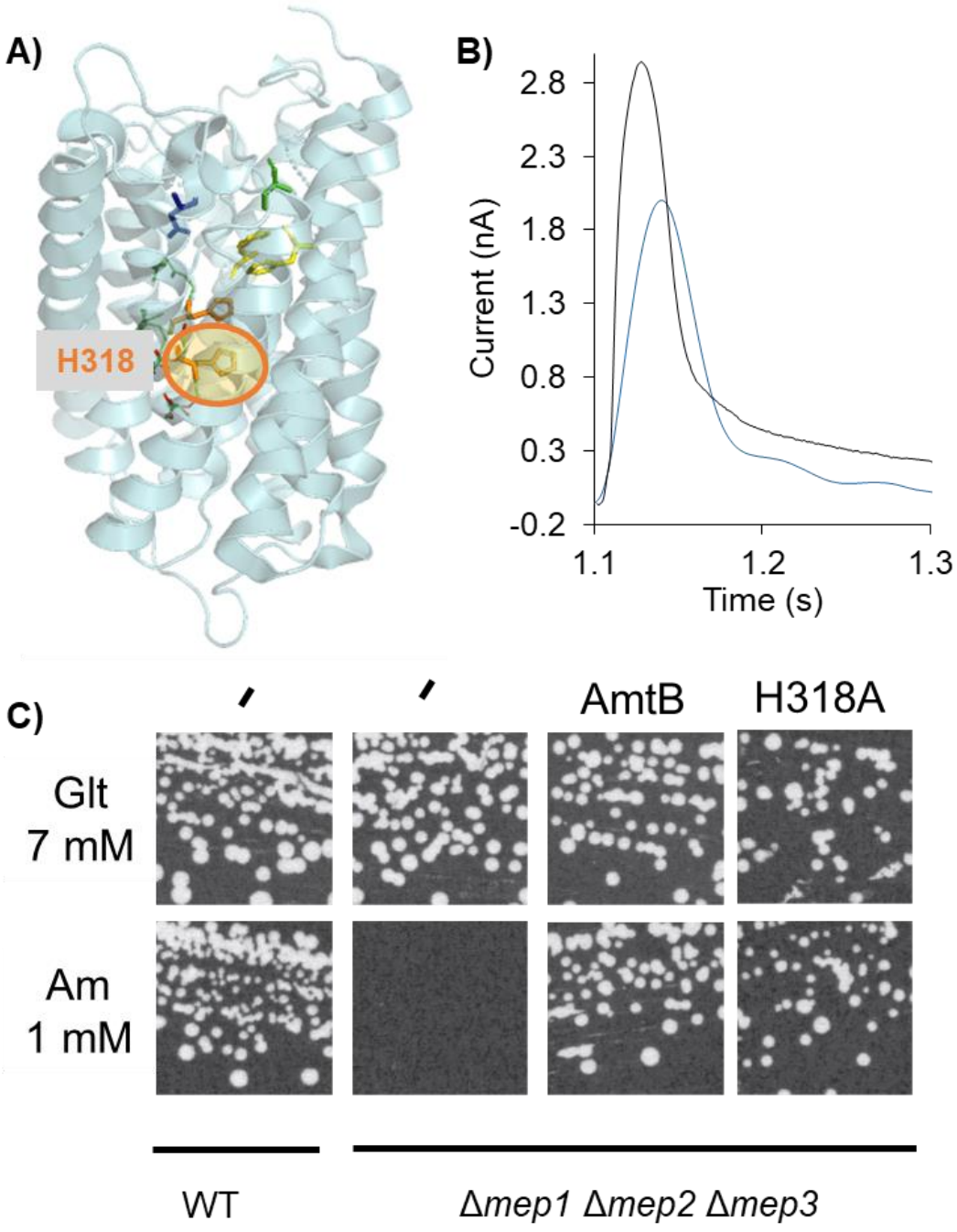

Figure 4.10 AmtB^{H318A} retains activity. A) Cartoon representation of AmtB, highlighting substitution site B) Representative traces following a 200 mM ammonium pulse for WT AmtB (black), AmtB^{H318A} (blue) at LPR 10. C) Yeast complementation after 5 days of growth on minimal media supplemented with either 7 mM glutamate (Glt) or 1 mM $(NH_4)_2SO_4$ (Am).

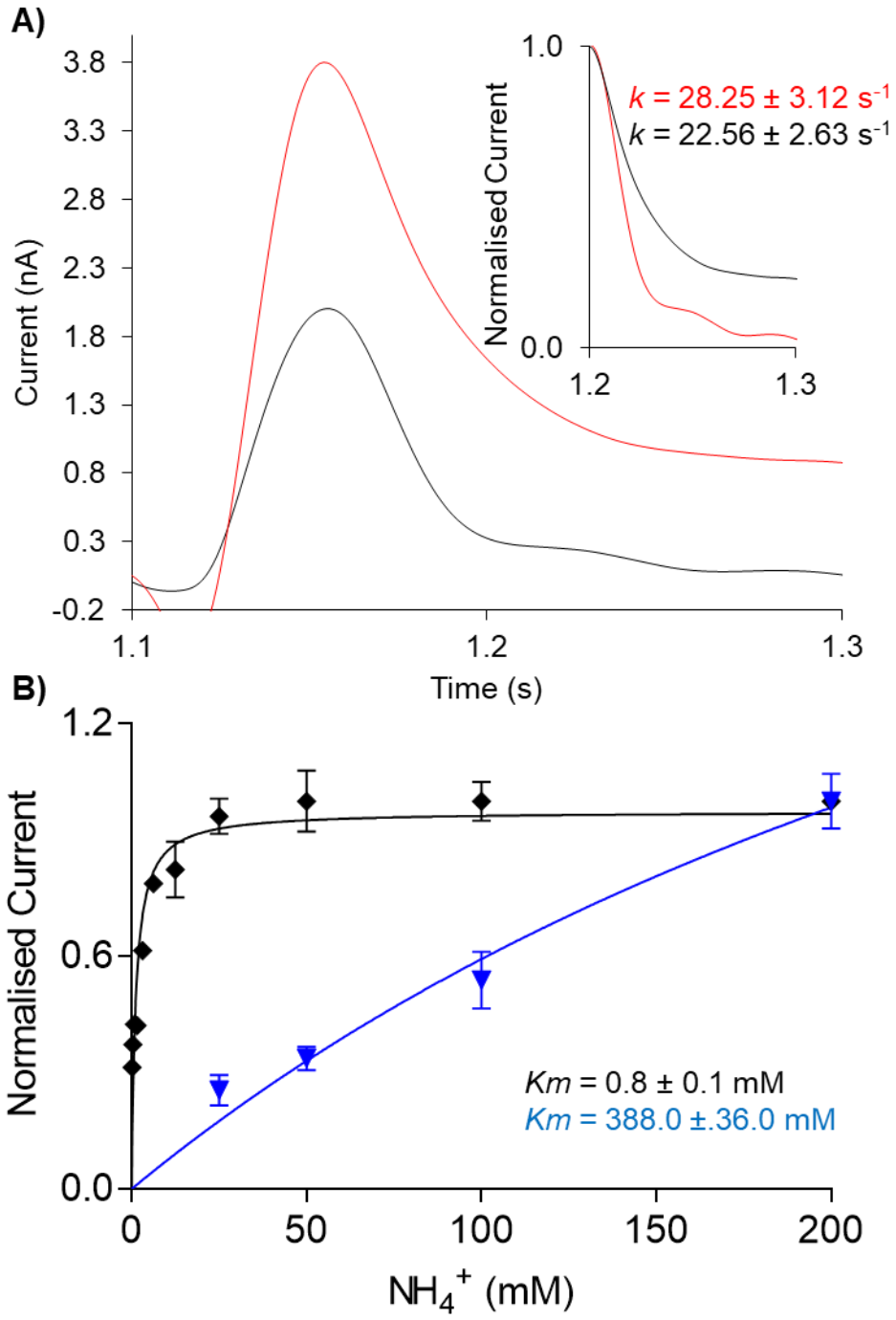

Figure 4.11 AmtB^{H318A} Characterisation. A) Transient currents following a 200 mM NH_4^+ pulse with AmtB^{H318A} reconstituted into Polar/POPC 2/1 proteoliposomes at a LPR of 5:1 (red), 10:1 (black), or 50:1 (blue). B) Kinetics for WT AmtB (black) and AmtB^{H318A} (blue) at LPR 10 using NH_4^+. Maximum amplitudes have been normalised to 1.0 for comparison. Data points represent mean ± SD.

4.7 Rare H168 Variant is Super-active

Whilst the twin-His motif is highly conserved, in some fungal Mep proteins the first histidine (H168) is replaced with glutamic acid (E). In light of this, and the surprising tolerance of single histidine substitutions, we wanted to assess any phenotypical changes in this variant.

Existing crystal structures of $AmtB^{H168E}$ show that the region around E168 has increased hydration (**Figure 4.12A**) (Javelle *et al.*, 2006). This would maintain a pathway for proton translocation, therefore $AmtB^{H168E}$ should retain activity. Expression in triple-*mepΔ* yeast using ammonium as the sole nitrogen source yielded unexpected results. There was also no growth on the typical concentration range of NH_4^+ (1-3 mM), which would ordinarily suggest inactivity (**Figure 4.12C**). However, no growth is observed on media supplemented with MeA, which is toxic to yeast, implying that the transporter is still able to uptake MeA. This suggests that $AmtB^{H168E}$ is active, but is experiencing toxicity in NH_4^+ supplemented media. When the experiment was repeated over a lower NH_4^+ concentration range (0.1 – 0.5 mM), the growth phenotype was restored, with equivalent to the WT observed at the lowest concentrations (**Figure 4.12C**). This suggests that the observed cytotoxicity is due to super-activity of $AmtB^{H168E}$. To confirm this, a transient current was measured following a 200 mM ammonium pulse. The measurements revealed that a 5-fold increase in current amplitude compared to the WT (**Figure 4.12B**) and a strongly LPR dependent decay rate, confirming that the $AmtB^{H168E}$ variant is super-active.

These findings suggest that the additional charge introduced by the H168E substitution further stabilizes the periplasmic and cytoplasmic water wires, raising proton transfer rates, and resulting in a large increase in activity. The drastically increased activity of this variant is, however, not tolerated by all cell types.

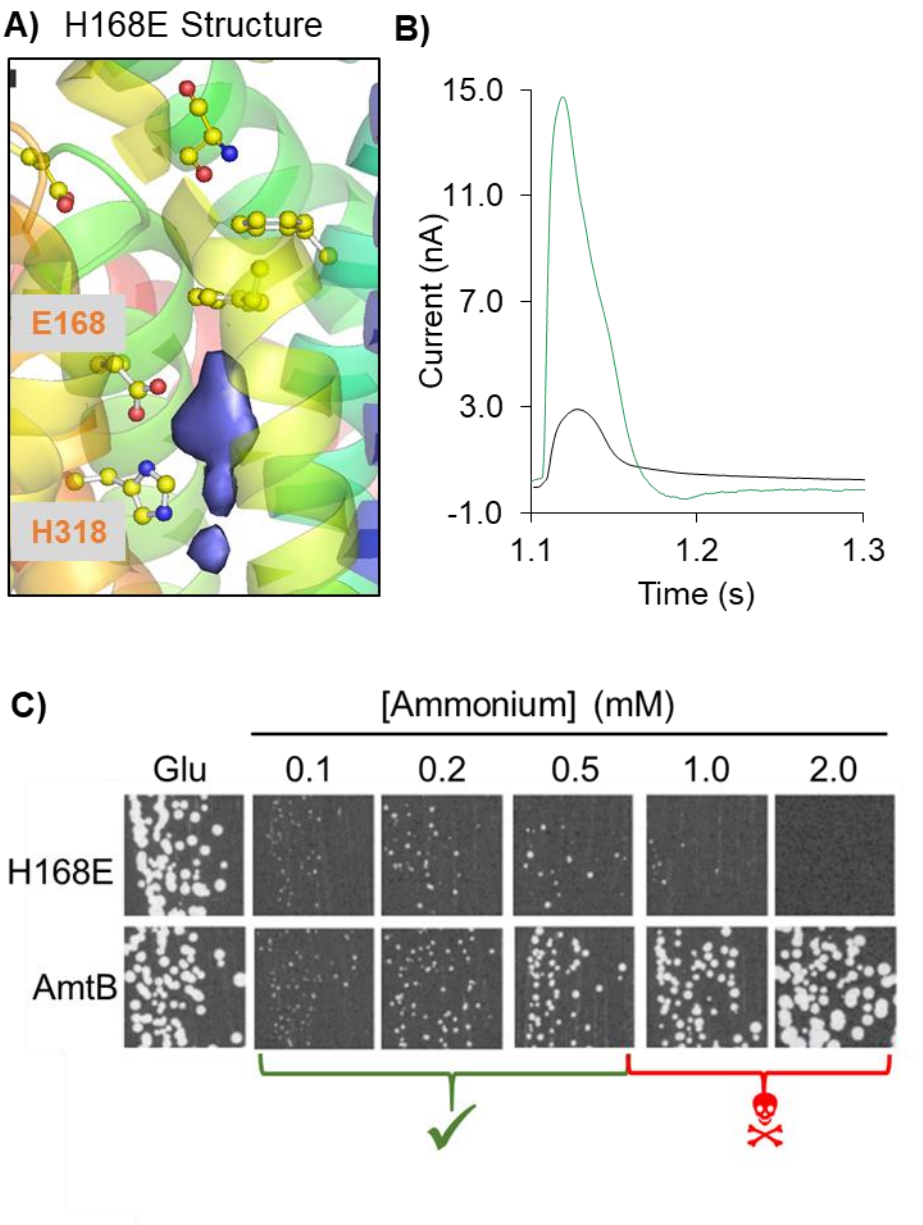

Figure 4.12 AmtB^{H168E} is Super-Active A) Crystal structure of AmtBH168E showing increased hydration. B) Representative traces following a 200 mM ammonium pulse for WT AmtB (black), AmtB^{H318E} (green) at LPR 10. C) Yeast complementation test of WT AmtB compared to AmtB^{H168E}. Growth on minimal medium supplemented with glutamate (Glt) (7 mM) or [ammonium] (0.1-2 mM) as sole nitrogen source. No complementation was observed for AmtB^{H168E} in medium containing more than 1 mM ammonium.

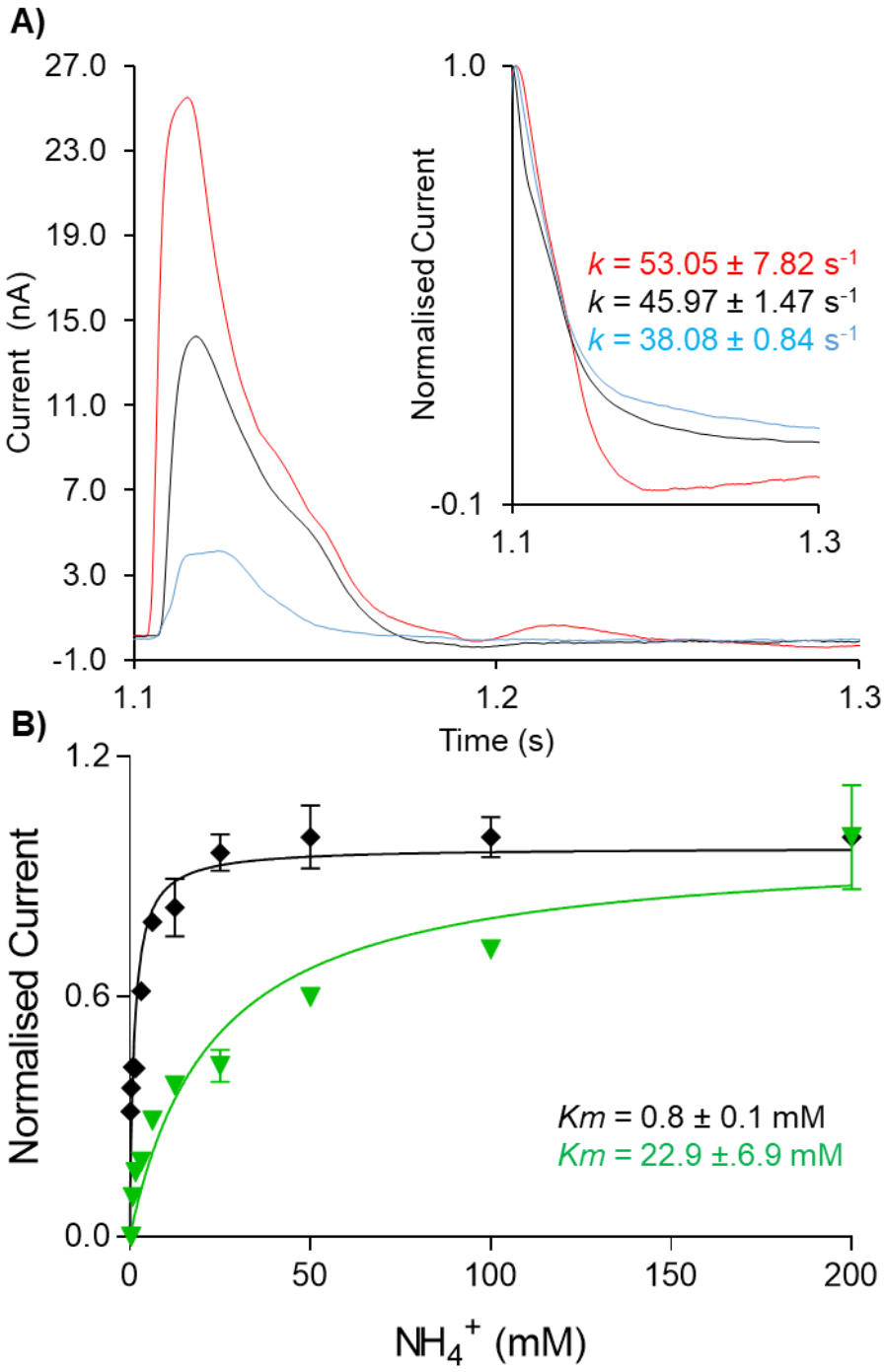

Figure 4.13 AmtB^{H168E} Characterisation. A) Transient currents following a 200 mM NH_4^+ pulse with AmtB^{H168E} reconstituted into Polar/POPC 2/1 proteoliposomes at a LPR of 5:1 (red), 10:1 (black), or 50:1 (blue). B) Kinetics for WT AmtB (black) and AmtBH168E (green) at LPR 10 using NH_4^+. Maximum amplitudes have been normalised to 1.0 for comparison. Data points represent mean ± SD.

4.8 Revised Model of Electrogenic Ammonium Transport

A new model for the mechanism of electrogenic ammonium transport emerges from our findings (**Figure. 4.14**). After deprotonation of NH_4^+ at the periplasmic side, a previously enigmatic polar conduction route enables H^+ transfer into the cytoplasm. A parallel pathway, lined by hydrophobic groups within the protein core, facilitates the simultaneous transfer of uncharged NH_3, driven by concentration differences. On the cytoplasmic face, the pH of the cell interior leads to recombination to NH_4^+. The major kinetic barrier to transport occurs for H^+ transfer across the twin-His motif, which bridges the water chains and creates a complete pathway through the protein. I propose that this mechanism is conserved amongst the electrogenic members of the Amt/Mep/Rh family

Calculation of the energetics of NH_3 transfer, carried out by our collaborators, reveal that NH_3 permeation through the hydrophobic pore of AmtB experiences a maximum energy barrier of ~10 kJ/mol (**Figure 4.15**). Since both energy barriers for H^+ transfer along the water chains and NH_3 permeation are relatively small, either initial deprotonation or proton transfer across the twin-His motif could be rate-limiting for overall NH_4^+ transport. Since we find a strongly increased activity for the H168E variant, I conclude that the transport rate of AmtB is determined by the rate of H^+ transfer across the twin-His motif.

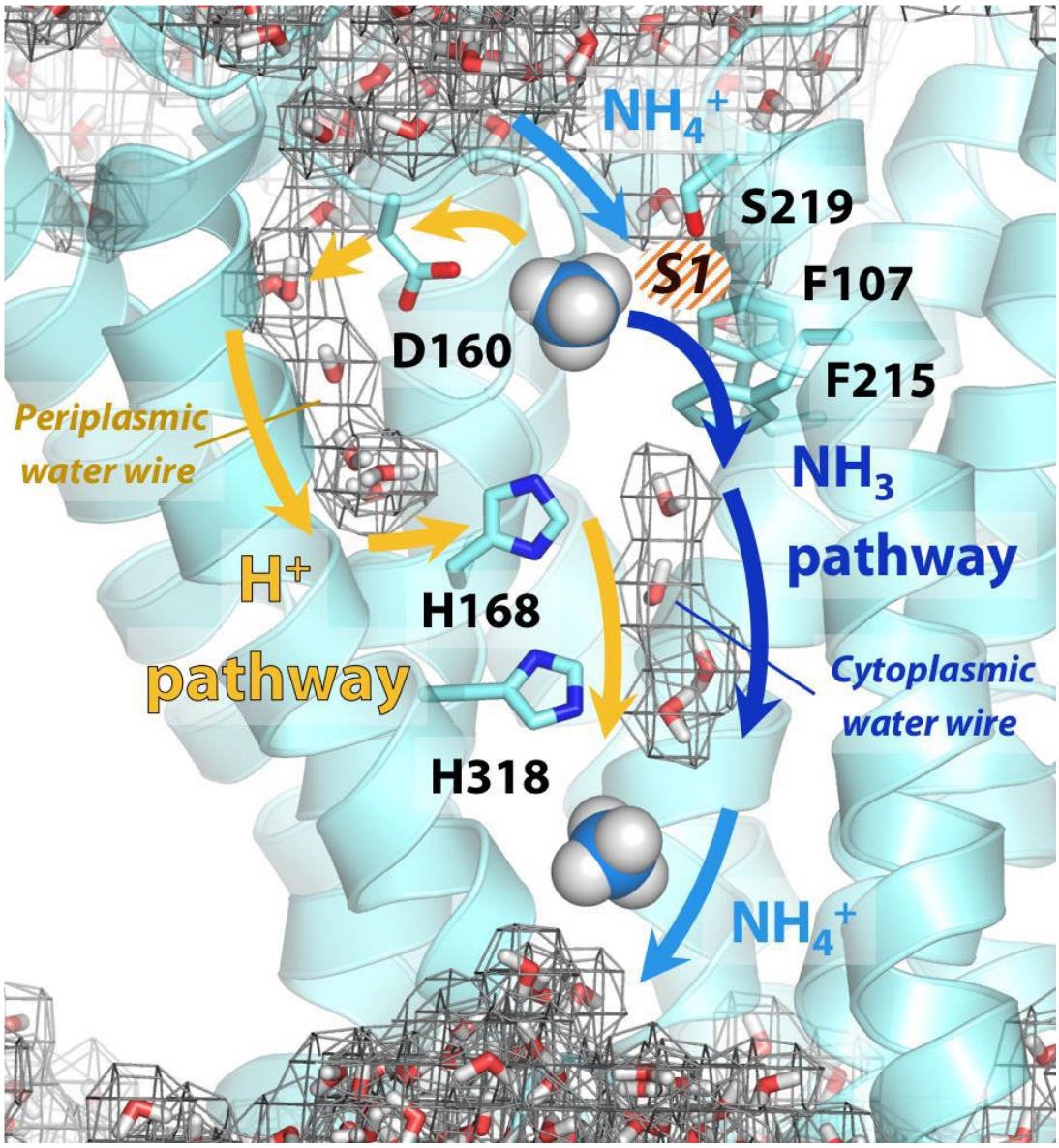

Figure 4.14: Mechanism of electrogenic NH_4^+ translocation in AmtB. NH_4^+ binds at the S1 site, is deprotonated, and the fragments translocated via separate pathways. NH_3 moves directly through the hydrophobic pore, whilst H^+ travels through the periplasmic and cytoplasmic water wires via a Grotthuss mechanism.

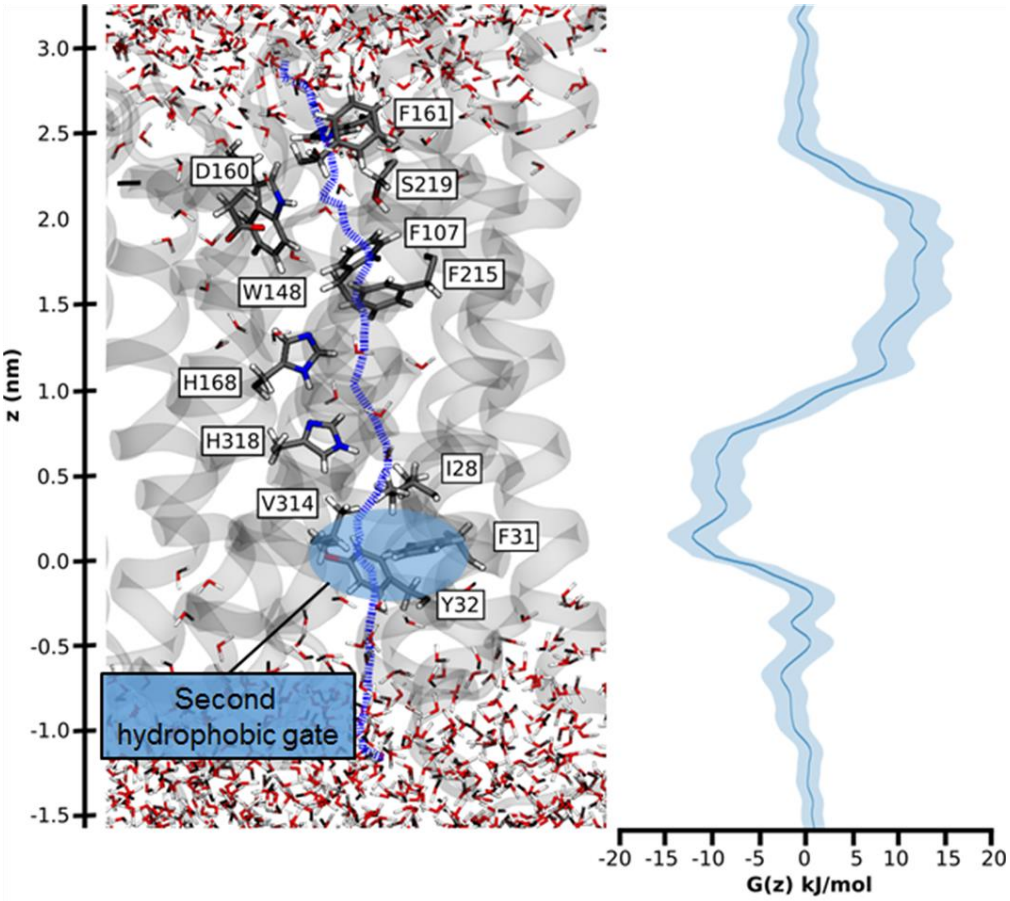

Figure 4.15: **Hydrophobic pathway and energetics for NH3 translocation in AmtB**. We probed an optimal pathway for NH_3 transfer during our PMF calculations (left, purple dash trajectory) in the presence of both the PWW and CWW. The pathway from the periplasm to the cytoplasm traverses the hydrophobic gate region (F107 and F215), crosses the cavity next to the twin-His motif (H168 and H318) occupied by the CWW, and continues across a second hydrophobic region (I28, V314, F31, Y32) before entering the cytoplasm. The energetics of transfer on this pathway (right, blue curve) show that NH_3 translocation experiences a moderate energy barrier during traversal of the periplasmic hydrophobic gate region (~10 kJ/mol, near F107 and F215).

4.9 Discussion

4.9.1 Assessing the Novel Model

The model of AmtB-mediated NH_4^+ transport presented here unifies the conflicting structural and functional observations, without undermining established work in the field. Specifically, it provides a rationale for the observation of charge translocation (Mirandela *et al.*, 2019) despite the hydrophobic pore identified in the initial crystal structures. As mentioned previously, following reports of the first crystal structure of AmtB many concluded that the protein was a simple NH_3 channel (Khademi *et al.*, 2004). However, when re-examined in the light of new information, this structure can support other hypotheses. For example, in addition to the S1 binding site, Khademi *et al* observed several densities (allocated S2-S4) within the pore parallel to the twin-His motif. Given their hypothesis, they interpreted these as NH_3 binding at different stages of translocation. However, at 1.35Å a molecule of H_2O and NH_3 are not readily distinguished, thus the densities are equally likely to be water molecules. Importantly, these densities are observed in the pore with or without the substrate present, hence they should be water (Zheng *et al.*, 2004; Javelle *et al.*, 2006, 2008). In fact, a later molecular dynamic simulation study revealed a chain of water molecules in this position (Lamoureux, Klein and Bernèche, 2007). The positions of these water molecules matches those observed in molecular dynamics simulations of the cytoplasmic water wire.

At the time, this didn't affect a shift in mechanistic understanding because the CWW alone would be insufficient for proton conduction. However, the revelation of an additional water wire linking the periplasm to the twin-His motif creates a previously unknown but complete proton translocation pathway, enabling new interpretations. Unlike the CWW, the PWW has never been observed in AmtB crystal structures. This is likely due to the lower frequency of the PWW, making the densities less likely to be captured in the crystal

structure. Additionally, the PWW evolves on a much slower timescale and stably occupied states are only seen after ~25 ns simulated time. Since earlier simulations studying the internal hydration of AmtB were shorter (Wang *et al.*, 2012) this may explain why the PWW has not been described previously. Finally, it is currently unknown if the PWW is constantly evolving and collapsing or if there a condition to trigger/stabilise the PWW. For example, it may only stabilise upon substrate binding and, if so, this would again lessen the likelihood of it being visible during crystallisation.

4.9.2 Validating Role of Twin-His

Our results demonstrate that AmtB activity is affected by the disruption of the twin-His motif. This corroborates previous functional evidence that implicated the twin-His motif in the translocation cycle (Javelle *et al.*, 2006; Wang *et al.*, 2013), and provides an explanation for those observations. Wang *et al.* employed yeast complementation assays to demonstrate that a double substitution of the twin-His motif to alanine would not be tolerated, but a single substitution (of either residue) would restore ammonium transport activity in yeast. In our model, this can be explained by simultaneous substitution of H168 and H318 dismantling the water wires, thus abolishing transporter activity. In contrast, hydration in the pore around A168 increases, creating a continuous water wire through the protein, thereby allowing activity.

Our findings also elucidate the mechanistic reason underlying the twin-His motif's essentiality, as previously demonstrated (Javelle *et al.*, 2006). Whilst $AmtB^{H168A}$ and $AmtB^{H318A}$ both retain activity, neither substitution has been observed naturally. The specific conversation of histidines in this position suggests a strong evolutionary pressure to retain them, and thus a vital role in transport. This is likely due to the significant impact of H168 and H318 substitutions on the transporter's substrate selectivity. Of note, is the complete absence of the twin-His motif in RhD and RhCE, human rhesus proteins which have lost transporter activity and evolved structural and immunological roles

in erythrocytes (Burton and Anstee, 2008). Taken together, the remarkable conservation of the twin-His motif can be explained by its specific role in the mechanism of AmtB/Mep/Rh proteins.

4.9.3 Cytotoxicity of H168E

Currently, the H168E substitution found in some fungal species is the only common natural twin-His substitution reported in the literature. Previously, methylammonium uptake has been used to demonstrate that this variant retains activity (Javelle *et al.*, 2006; Hall and Kustu, 2011). In addition, Boeckstaens *et al.* reported that the equivalent mutation in *S. cerevisiae* Mep2 (H194E) is able to transport both ammonium and methylammonium (Boeckstaens, André and Marini, 2008). Interestingly, the complementation efficiency of *Sc*Mep2^{H194E} in triple-*mepΔ S. cerevisiae* was greater than WT *Sc*Mep2, and methylammonium uptake increased 3-fold (Boeckstaens, André and Marini, 2008). These results are consistent with my observations of super-activity of AmtB^{H168E} compared to the WT.

When expressed in triple-*mepΔ S. cerevisiae* the super-activity of H168E resulted in toxicity at NH_4^+ concentrations >0.5 mM. Ammonium toxicity in *S. cerevisiae* has been reported previously, by Hess *et al,* who observed ammonium toxicity in yeast grown in chemostats (Hess *et al.*, 2006). Initially, this toxicity was only observed under potassium limitation, but Hess *et al* reported toxicity occurred even in high potassium conditions if native ammonium transporters were overexpressed (Hess *et al.*, 2006).

If a similar outcome occurs as a result of H168E substitution, then a strong selective pressure against the substitution would be expected. However, the toxicity we observe is likely not the case in the physiological environment. Normally, *S. cerevisiae* can regulate expression of its 3 Mep proteins to exert finer control over ammonium uptake. This regulation is in response to nitrogen limitation, with mRNA transcripts for *MEP1* low when cells are grown on 20 mM, but high when the concentration is reduced to 500 µM (Marini *et al.*, 1994).

AmtB itself is also impacted by ammonium concentration, with an ammonium shock of 50 µM enough to trigger interaction with GlnK, a PII signal protein integral to nitrogen metabolism in *E. coli* (Javelle *et al.*, 2004). In our system, however, AmtB is expressed from a plasmid and thus the *S. cerevisiae* is unable to regulate its expression. This results in the NH_4^+ concentration exceeding the capacity of *S. cerevisiae* to utilise it, and thus toxicity. In conclusion, the seemingly aberrant H168E substitution is explained by our model. However, why H168E has been observed naturally, but H168A and H318A have not remains unclear. Whilst they all retain ammonium transport activity, it is possible that they have different impacts on the mechanism or selectivity. This will be explored in **Chapter 5**.

Chapter 5:

Mechanism of Ammonium-selectivity in the pore of AmtB

Chapter 5: Mechanism of Ammonium-selectivity in the pore of AmtB

Aims and Objectives

The twin-His motif is highly conserved throughout the Amt/Mep/Rh superfamily, with the only notable exception in certain classes of Mep proteins. Due to this conservation it is expected that the motif would be mechanistically important (Khademi *et al.*, 2004; Zheng *et al.*, 2004; Javelle *et al.*, 2006). However, the results presented in **Chapter 4** clearly demonstrate that one or both residues of the twin-His motif can be substituted without an injurious impact on the structure or the activity of the protein. In this chapter, I present evidence that the twin-His motif plays an essential role in maintaining the selectivity of AmtB toward ammonium.

Objectives:

1. Apply molecular dynamic simulations (MDS) to predict the correlation between hydrophobicity and hydration of the pore.
2. Characterise the impact of altering the hydrophobicity of the pore on AmtB activity using *in vitro* SSME measurements and *in vivo* yeast complementation tests.
3. Identify the mechanism underlying changes in selectivity.

5.1 Introduction

The remarkable conservation of the twin-His motif within the Amt/Mep/Rh superfamily has fuelled expectations of vital mechanistic or structural importance (Zheng *et al.*, 2004). Early experimental evidence supported the hypothesis that the twin-His motif was essential for substrate conduction, with Javelle *et al.* demonstrating that substitution of one or both of the residues greatly diminished [^{14}C]-methylammonium uptake activity (Javelle *et al.*, 2006). Later work however, revealed that H168 and/or H318 can be substituted with acidic residues while still supporting growth at low NH_4^+ concentrations (Hall

and Kustu, 2011). My results in **Chapter 4** corroborate the latter findings, and raise a key question regarding why these residues are so highly conserved if they are demonstrably non-essential. Further work by Hall *et al* suggested that a double-substitution of H168D/H318E can result in a loss of selectivity, enabling transport of potassium (Hall and Yan, 2013). If true, this could hint at the real basis of twin-His conservation and implicates hydrophobicity of the pore in the selectivity of AmtB. As such, it is imperative to better understand the impact of such substitutions on the structure of the pore and characterise the selectivity of twin-His variants *via* SSME.

5.2 Purification of Twin-His Variants

The purification of many of the variants discussed throughout this chapter are presented in results chapter 4 (**Section 4.4**). Additional variants ($AmtB^{H168D/H318E}$ and $AmtB^{H318E}$) were purified and inserted into proteoliposomes as described previously (**Section 2.3.1**). Like the WT, these variants purified as a trimer on size exclusion chromatography with an elution peak observed at ~11 mL (**Figure 5.1**). This shows that the variant AmtB did not aggregate or become destabilised during the purification process.

The purified proteins were inserted into Polar/POPC 2/1 liposomes to form proteoliposomes for use in SSME. To verify that insertion was successful, the proteoliposomes were washed repeatedly and analysed by SDS-PAGE. For each variant, bands were only observed in the proteoliposome lane, with major band matching that of trimeric AmtB (**Figure 5.2**). This confirms that the $AmtB^{H168D/H318E}$ and $AmtB^{H318E}$ variants retain the structural integrity exhibited by the WT AmtB.

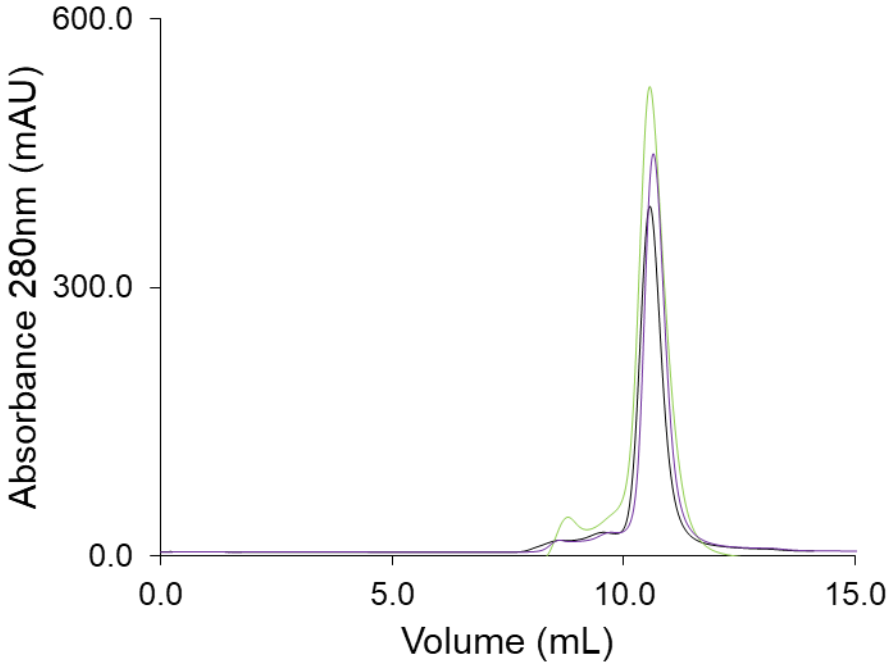

Figure 5.1 Size-Exclusion Chromatography analysis of AmtB twin-His variant. Size-exclusion chromatogram of AmtB solubilised in 0.033% DDM and injected on a Superdex 200 Increase 10/300 column. Traces represent either WT AmtB (black), $AmtB^{H168D/H318E}$ (purple) or $AmtB^{H318E}$ (green).

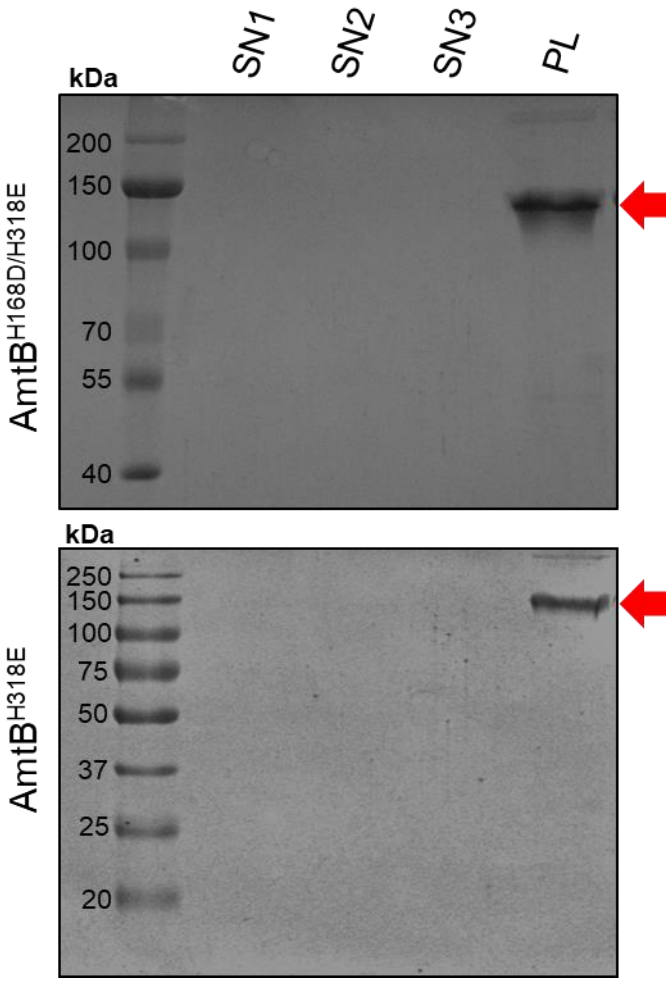

Figure 5.2 Insertion of variant AmtB into proteoliposomes: 10% SDS-PAGE gel monitoring the wash protocol. SN1-3 = supernatant from each wash step, PL is a sample of either AmtB$^{H168D/H318E}$ (top), AmtB^{H318E}(bottom) Polar/POPC 2/1 proteoliposomes at LPR 10. The red arrows indicate regions of 130 kDa, the expected size of AmtB

5.3 Altering Hydrophobicity Does Not Impact Activity

The dramatically altered activity observed in the singe-histidine variants implied that altering hydrophobicity of the pore has a large impact on AmtB. Therefore, molecular dynamics simulations of twin-His variants were carried out to identify other potentially impactful variants. These simulations predicted that in AmtB$^{H168D/H318E}$, wherein both twin-His motif residues are substituted with charged residues, the central pore would be destabilised and flood with water (**Figure 5.3**). If accurate, this would represent a significant change from the ordered structure seen in simulations of WT AmtB. In principle, a flooded pore in AmtB$^{H168D/H318E}$ would allow a complete pathway for proton translocation so would retain activity. However, the loss of the discrete water chains would be expected to impact its ability to act as a specific transporter, and enable transport of competing ions.

AmtB$^{H168D/H318E}$ restored growth when expressed in triple-*mepΔ* yeast, confirming that the variant remained active in ammonium transport when expressed in yeast (**Figure 5.4C**). In addition, a current was observed following an NH_4^+ pulse on SSME, albeit with a ~2-fold reduction in the maximum amplitude of the current (**Figure 5.4B**). Both the maximum amplitude and decay constant of this current were LPR-dependent, confirming that it is due to translocation and not only NH_4^+-protein interaction (**Figure 5.5A**). Unlike WT AmtB, activity was not saturable over the 0.39-200 mM ammonium concentration range. In fact, AmtB$^{H168D/H318E}$ kinetics cannot be described according to the Michaelis-Menten model but are linear (**Figure 5.5B**). This suggests that AmtB$^{H168D/H318E}$ no longer acts as a specific transporter, but that the mechanism has switched to function more like a channel.

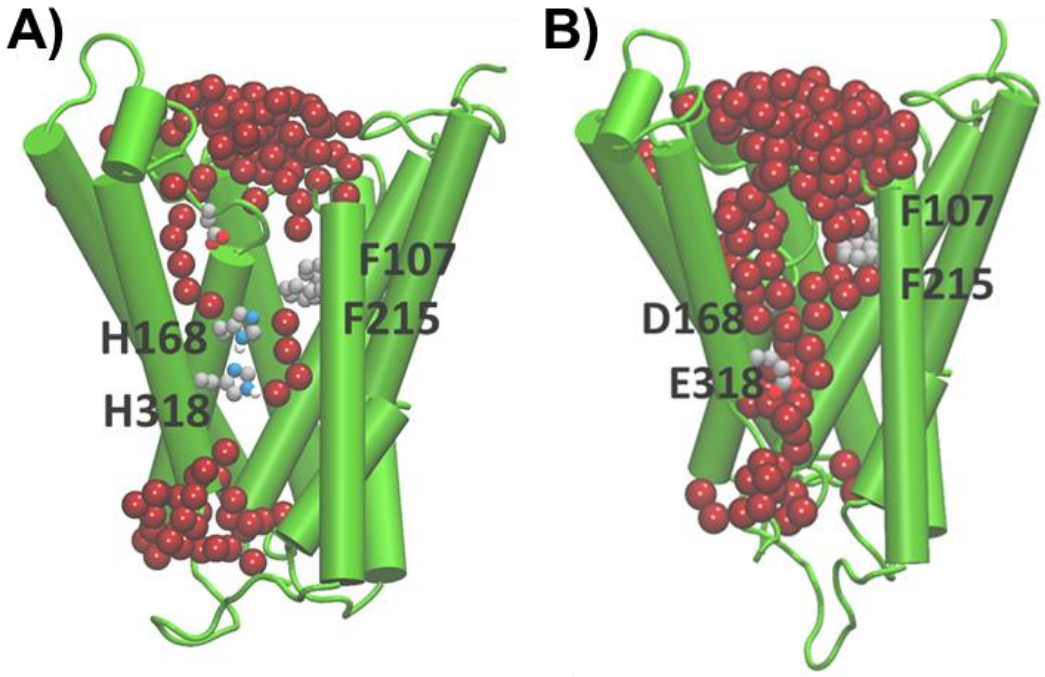

Figure 5.3 Molecular dynamic simulation of AmtB. Comparison of simulations of (A) WT AmtB and (B) AmtB$^{H168D/H318E}$ The simulations highlight a single monomer with the helices displayed as green cylinders and water molecules represented by red spheres. While WT AmtB has two ordered chains of water molecules, the pore of AmtB^{H168DH318E} is flooded with water. These simulations were run by Giulia Tamburrino as part of her PhD research.

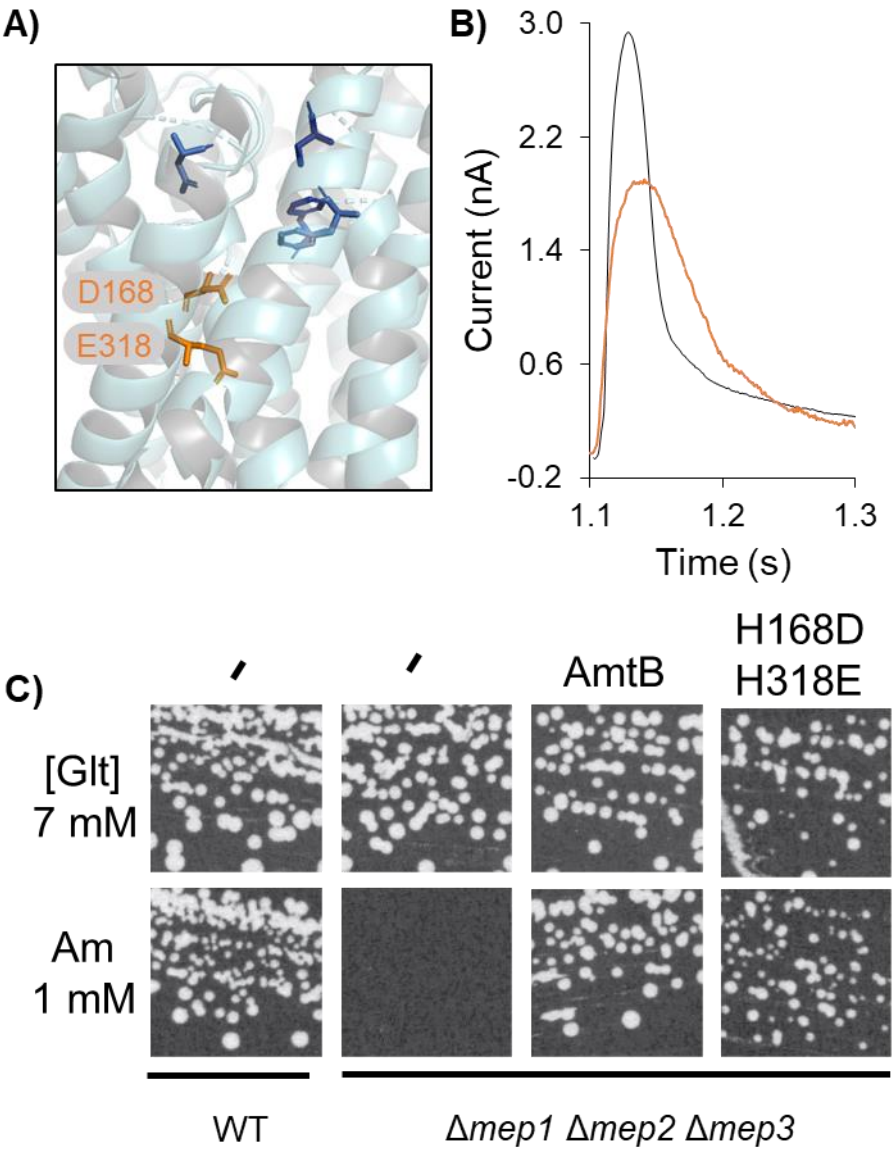

Figure 5.4 AmtB$^{H168D/H318E}$ retains activity. A) Cartoon representation of AmtB, highlighting substitution site B) Representative traces following a 200 mM ammonium pulse for WT AmtB (black), AmtB$^{H168D/H318E}$ (orange) at LPR 10. C) Yeast complementation after 5 days of growth on minimal media supplemented with either 7 mM glutamate (Glt) or 1 mM $(NH_4)_2SO_4$ (Am)

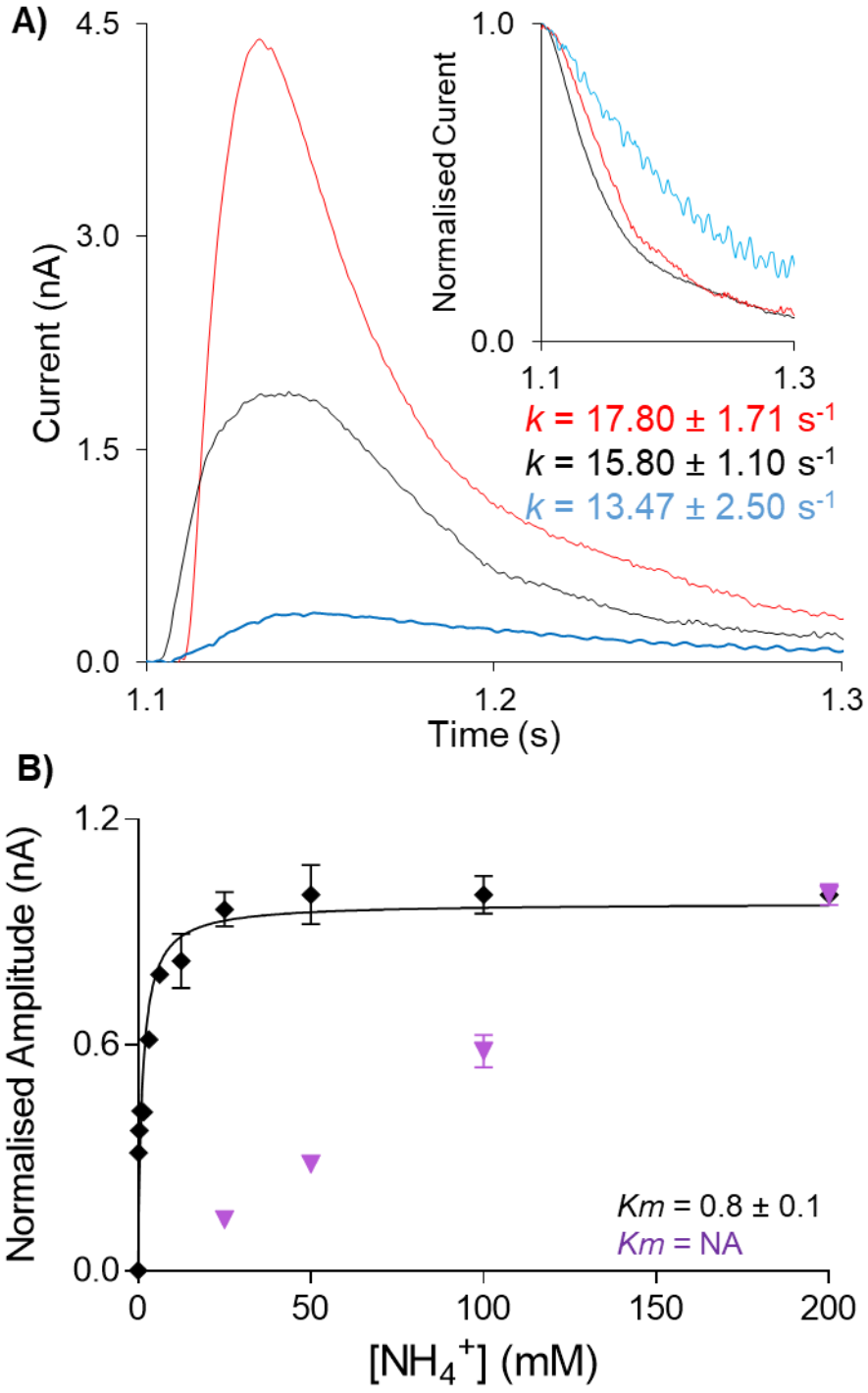

Figure 5.5 AmtB$^{H168D/H318E}$ Characterisation. A) Transient currents following a 200 mM NH_4^+ pulse with AmtB$^{H168D/H318E}$ reconstituted into Polar/POPC 2/1 proteoliposomes at a LPR of 5:1 (red), 10:1 (black), or 50:1 (blue). B) Kinetics for WT AmtB (black) and AmtB$^{H168D/H318E}$ (purple) at LPR 10 using NH_4^+. Maximum amplitudes have been normalised to 1.0 for comparison. Data points represent mean ± SD.

5.4 Selectivity is impaired in AmtB$^{H168D/H318E}$

Having confirmed that AmtB$^{H168D/H318E}$ can transport ammonium, the next step was to determine if the variant retained selectivity against competing ions. Indeed, if the pore has flooded and become a continuous water channel, then there is nothing to selectively prevent the movement of small hydrated ions. To test this, the SSME experiments were repeated using K^+ as a substrate.

A 200 mM K^+ pulse triggered a transient current in AmtB$^{H168D/H318E}$, whilst no current was recorded following the same pulse in WT AmtB (**Figure 5.6A**). The amplitude and decay time of these currents strongly depended on LPR (**Figure 5.7A**). In addition, WT AmtB and AmtB$^{H168D/H318E}$ were expressed in a *S. cerevisiae* strain lacking its three endogenous *Mep (*NH_4^+*)* and two *Trk (*K^+*)* transporters. This strain is unable to grow on media with a limited concentration of K^+. Expression of AmtB$^{H168D/H318E}$ complemented this growth defect, whilst WT AmtB did not. (**Figure 5.6A**). This demonstrates that AmtB$^{H168D/H318E}$ lost its selectivity toward NH_4^+ and transports K^+ to a degree sufficient to support growth of *S. cerevisiae.*

The K^+ translocation activity was not saturable over a 12.5-200 mM K^+ concentration range and revealed a linear concentration-response relationship (**Figure 5.7B**). Taken together, these results demonstrate that AmtB$^{H168D/H318E}$ translocates K^+ across the membrane, hence that this substitution within the twin-His motif has abolished AmtB selectivity for NH_4^+.

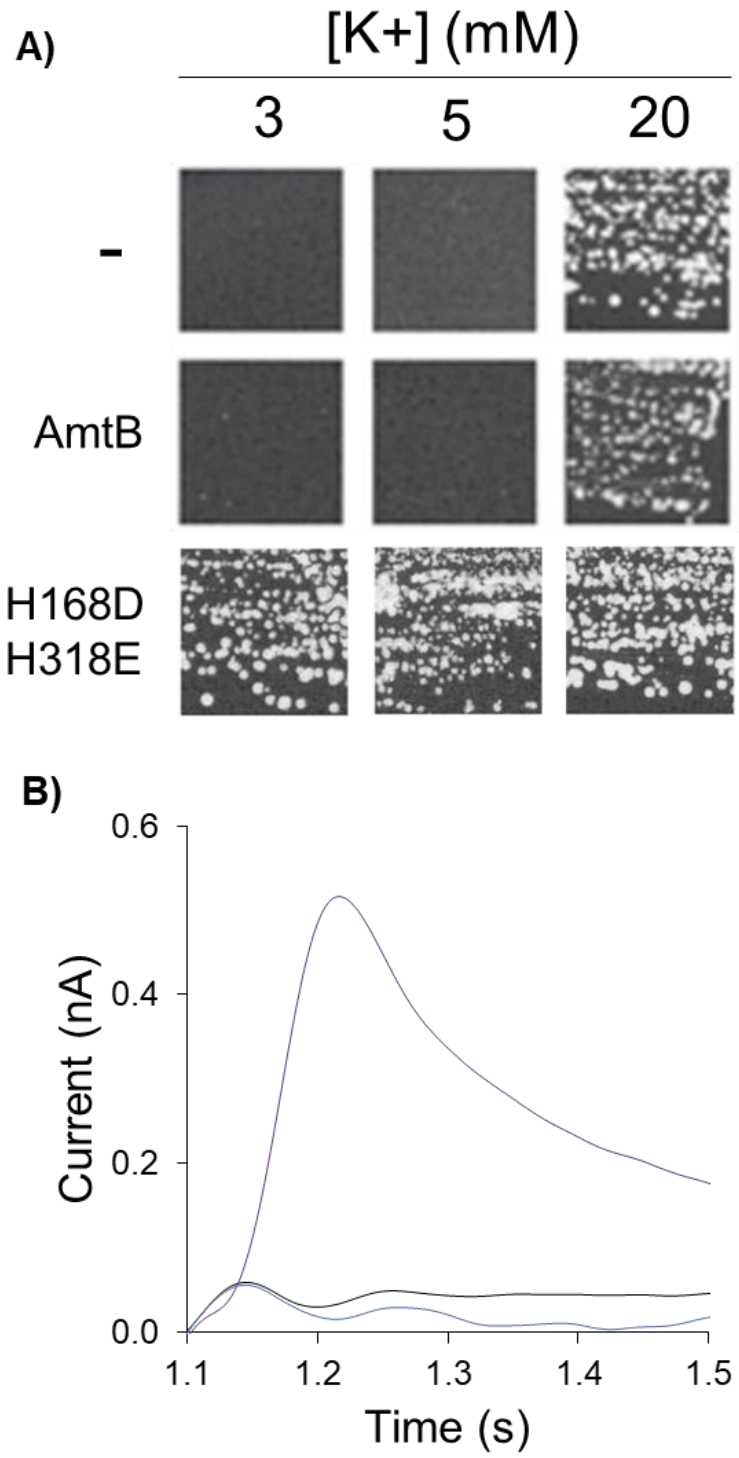

Figure 5.6 AmtB$^{H168D/H318E}$ Loses Selectivity. A) Yeast complementation after 5 days of growth on minimal media supplemented with either 3 mM, 5 mM, 20 mM KCl B) Representative traces following a 200 mM potassium pulse for WT AmtB (black), AmtB$^{H168D/H318E}$ (purple) at LPR 10, or empty liposomes (blue).

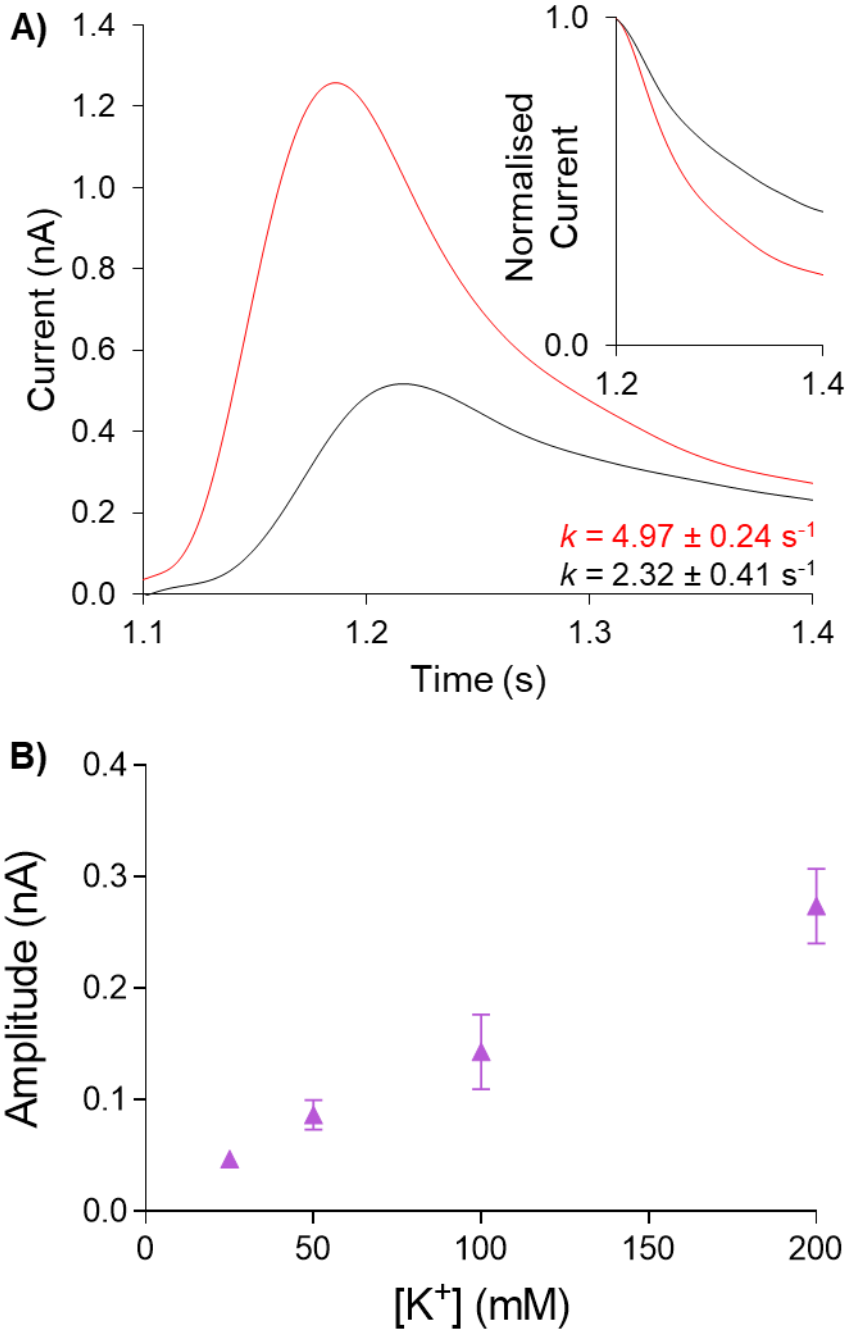

Figure 5.7 AmtB$^{H168D/H318E}$ Loses Selectivity A) Transient currents following a 200 mM K^+ pulse with AmtB$^{H168D/H318E}$ reconstituted into Polar/POPC 2/1 proteoliposomes at a LPR of 5:1 (red), 10:1 (black), or 50:1 (blue). B) Kinetics for AmtB$^{H168D/H318E}$ (purple) at LPR 10 using K^+. Data points represent mean ± SD.

5.5 Single His Variants Lose Selectivity

The relationship between the twin-His motif and selectivity is unclear. Whilst the loss of selectivity observed in AmtB$^{H168D/H318E}$ appears to be due to flooding of the pore, the impact of single variants on selectivity must also be investigated. From previous work, we know that the activity of AmtB$^{H168A/H318A}$ is abolished, whilst the single variants AmtB^{H168A} and AmtB^{H318A} retain activity. Therefore, to determine if selectivity is governed by a single histidine or a combination of both, the selectivity of AmtB^{H168A} and AmtB^{H318A} were characterised.

Both AmtB^{H168A} and AmtB^{H318A} variants restore the growth defect of *S. cerevisiae* lacking its three endogenous *Mep (*NH_4^+*)* and two *Trk (*K^+*)* transporters, whilst the WT and AmtB$^{H168A/H318A}$ do not (**Figure 5.8**). This demonstrates that AmtB^{H168A} and AmtB^{H318A} have both lost selectivity and permit translocation of K^+. In addition, when measured on SSME, a 200 mM K^+ pulse triggered a current in both single variants (**Figure 5.8**). In each case, the amplitude and decay of the currents were LPR dependent (**Figure 5.9A and 5.10A**), demonstrating that the activity is due to translocation and not protein-substrate interaction. Interestingly, measuring activity across a 12.5-200 mM potassium concentration range in both variants resulted in linear kinetics with no saturable activity (**Figure 5.9B and 5.10B**). This demonstrates that AmtB-mediated K^+ translocation is not facilitated in a transporter-like manner, and suggests the AmtB^{H168A} and AmtB^{H318A} variants are acting like channels.

Taken together it is clear that removal of either residue of the twin-His motif disrupts AmtB sufficiently to impair selectivity and permit permeation of other cations. This potentially explains why AmtB^{H168A} and AmtB^{H318A} have not been observed in nature, despite their retained activity. In the physiological setting, selectivity is paramount as uncontrolled entry of potassium or other cations would disrupt homeostasis and prove fatal to the cells.

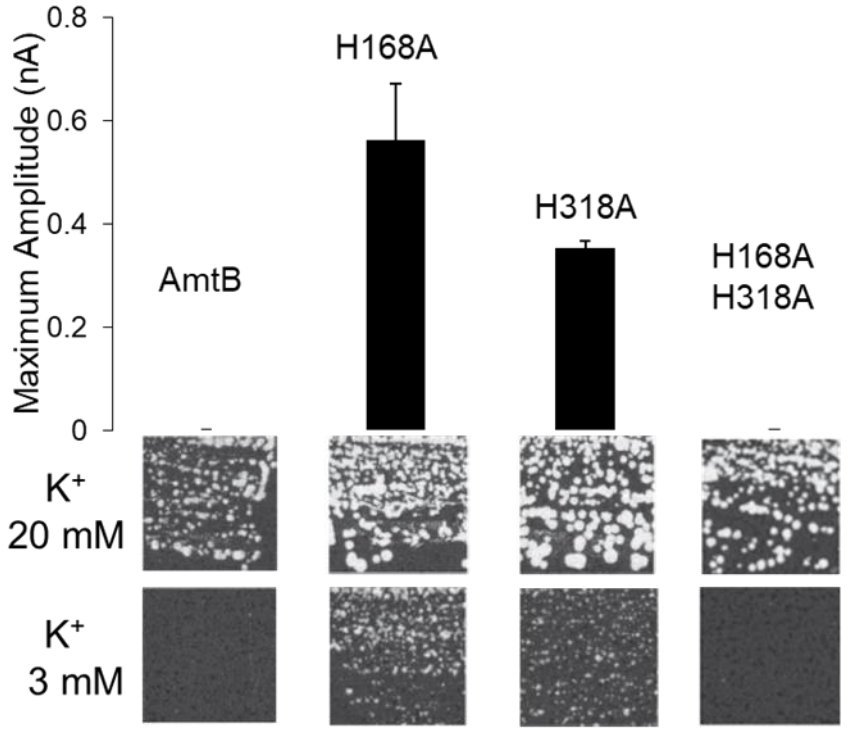

Figure 5.8 Potassium Transport in Single-His Variants Maximum amplitude of the transient current measured using SSME after a 200 mM potassium pulse. Bars represent mean measurements from eight sensors from two independent protein purification batches, with three measurements recorded for each sensor (means ± SD). *Lower panels*: yeast complementation test (strain #228, *mep1Δ mep2Δ mep3Δ trk1Δ trk2Δ leu2 ura3)* using media supplemented with 20 mM or 3 mM KCl.

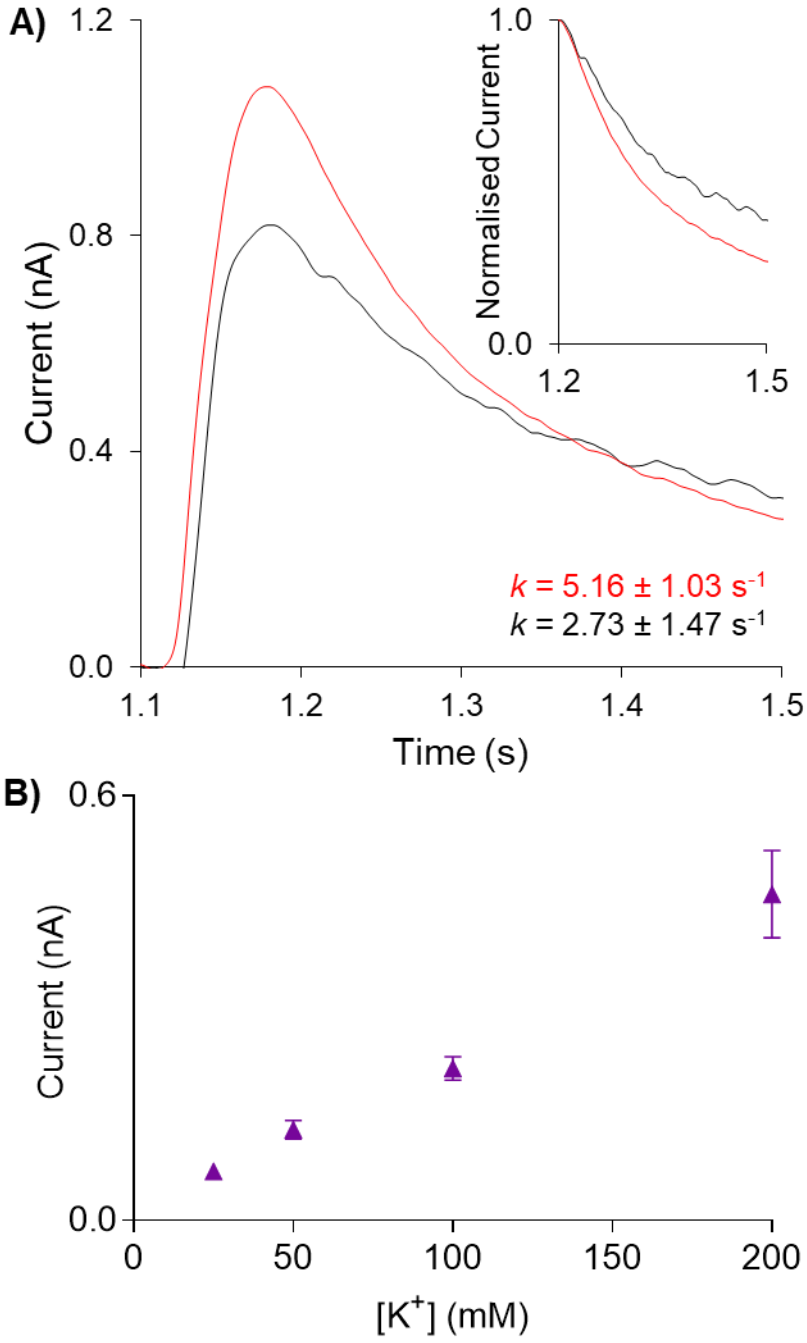

Figure 5.9 AmtB^{H168A} Loses Selectivity. A) Transient currents following a 200 mM K^+ pulse with AmtB^{H168A} reconstituted into Polar/POPC 2/1 proteoliposomes at a LPR of 5:1 (red), 10:1 (black), or 50:1 (blue). B) Kinetics for AmtB^{H168A} (purple) at LPR 10 using K^+. Data points represent mean ± SD.

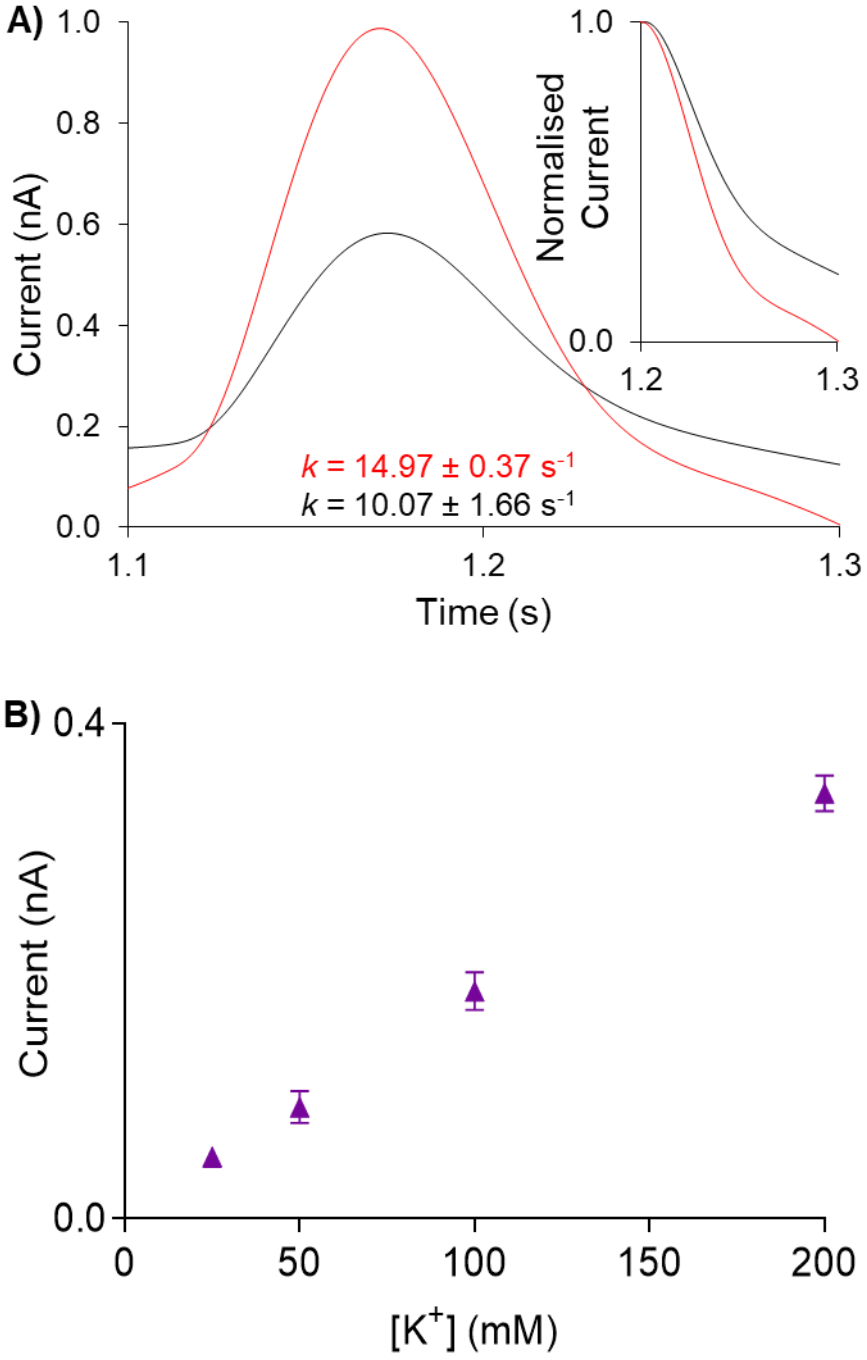

Figure 5.10 AmtB^{H318A} Loses Selectivity. A) Transient currents following a 200 mM K^+ pulse with AmtB^{H318A} reconstituted into Polar/POPC 2/1 proteoliposomes at a LPR of 5:1 (red), 10:1 (black), or 50:1 (blue). B) Kinetics for AmtB^{H318A} (purple) at LPR 10 using K^+. Data points represent mean ± SD.

5.6 Acidic Single-His Variants Retain Selectivity

It is clear that substitutions within the twin-His motif significantly impact activity and/or selectivity in AmtB. This raises questions regarding the substitution of the upper histidine to glutamic acid, as reported naturally occurring in some fungal Mep proteins (Javelle *et al.*, 2006; Boeckstaens, André and Marini, 2008). In addition, the results presented in **Section 4.7** demonstrate that, in AmtB, a H168E substitution results in super-activity. Given that it is tolerated where other mutations are not, I hypothesised that a AmtB^{H168E} variant retained selectivity.

As an initial test, AmtB^{H168E} was expressed in triple-Δ*mep*, *trkΔ S. cerevisiae*, which exhibits a growth defect on low potassium media. Both AmtB^{H168E} and WT AmtB fail restore growth in this *S. cerevisiae* strain, suggesting that neither permit permeation of potassium (**Figure 5.11A**). To confirm this, AmtB^{H168E} proteoliposomes were measured via SSME. No current was observed following a 200 mM K^+ pulse, indicating that AmtB^{H168E} did not transport K^+ and that there was no electrogenic interaction between K^+ and the protein (**Figure 5.11B**).

Given that the double variant (AmtB$^{H168D/H318E}$) loses selectivity, despite also featuring acidic residues, the selectivity of the individual variants was tested in the same way. When expressed in triple-*mepΔ*, *trkΔ S. cerevisiae,* AmtB^{H168D} does not restore growth in potassium limited conditions (**Figure 5.11A**), suggesting that it does not permit potassium influx. In addition, a 200 mM K^+ pulse did not trigger any measurable current, demonstrating that AmtB^{H168D} was not transporting K^+. When expressed in triple-*mepΔ S. cerevisiae,* no growth was observed over the typical concentration range of NH_4^+ (1-3 mM), but growth was restored when repeated at lower NH_4^+ concentrations (0.1 – 1 mM) (**Figure 5.12A**). The mechanism underlying this toxicity is unclear, but uncontrolled expression of Mep1 and Mep3 have previously been shown to induce ammonium toxicity in *S. cerevisiae* (Hess *et al.*, 2006), thus it is probable that the yeast is simply overwhelmed by the unregulated influx of

NH_4^+. In addition, very high amplitudes were observed following a 200 mM NH_4^+ pulse on SSME (**Figure 5.12B**) This suggests that, like $AmtB^{H168E}$, $AmtB^{H168D}$ is super-active in ammonium transport.

Finally, substitution of H318 with glutamate appears to abolish activity. When expressed in triple-*mepΔ S. cerevisiae,* $AmtB^{H318E}$ failed to restore growth, indicating that it is inactive (**Figure 5.13A**). Whilst exposure to a 200 mM $NH4^+$ *via* SSME does elicit distinct LPR-dependent transient currents the decay rate is unaffected by LPR (**Figure 5.13B**), indicating that the variant is inactive. Together, these results show that $AmtB^{H168E}$ and $AmtB^{H168D}$ retain both activity and selectivity, whilst other single-his variants result in either inactivity or a loss of selectivity. For ease of reading, the activity of these variants across different substrates and techniques has been summarised in **Table 5.1**.

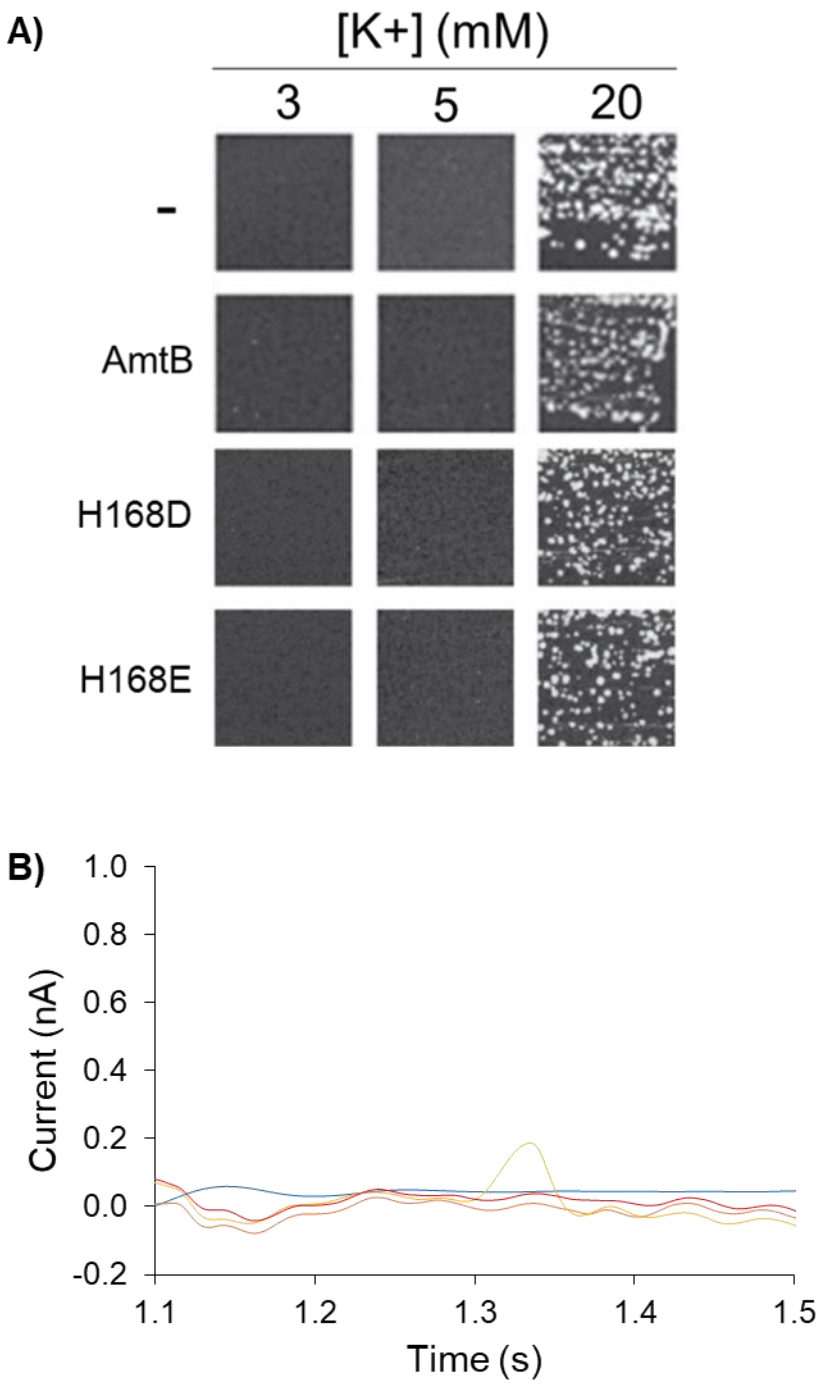

Figure 5.11 Single His Variants Retain Selectivity. A) Yeast complementation test after 5 days of growth on minimal media supplemented with either 3 mM, 5 mM, 20 mM KCl B) Representative traces following a 200 mM potassium pulse for AmtB^{H168D} (yellow), AmtB^{H168E} (orange), or AmtB^{H318E} (red) at LPR 10, or empty liposomes (blue).

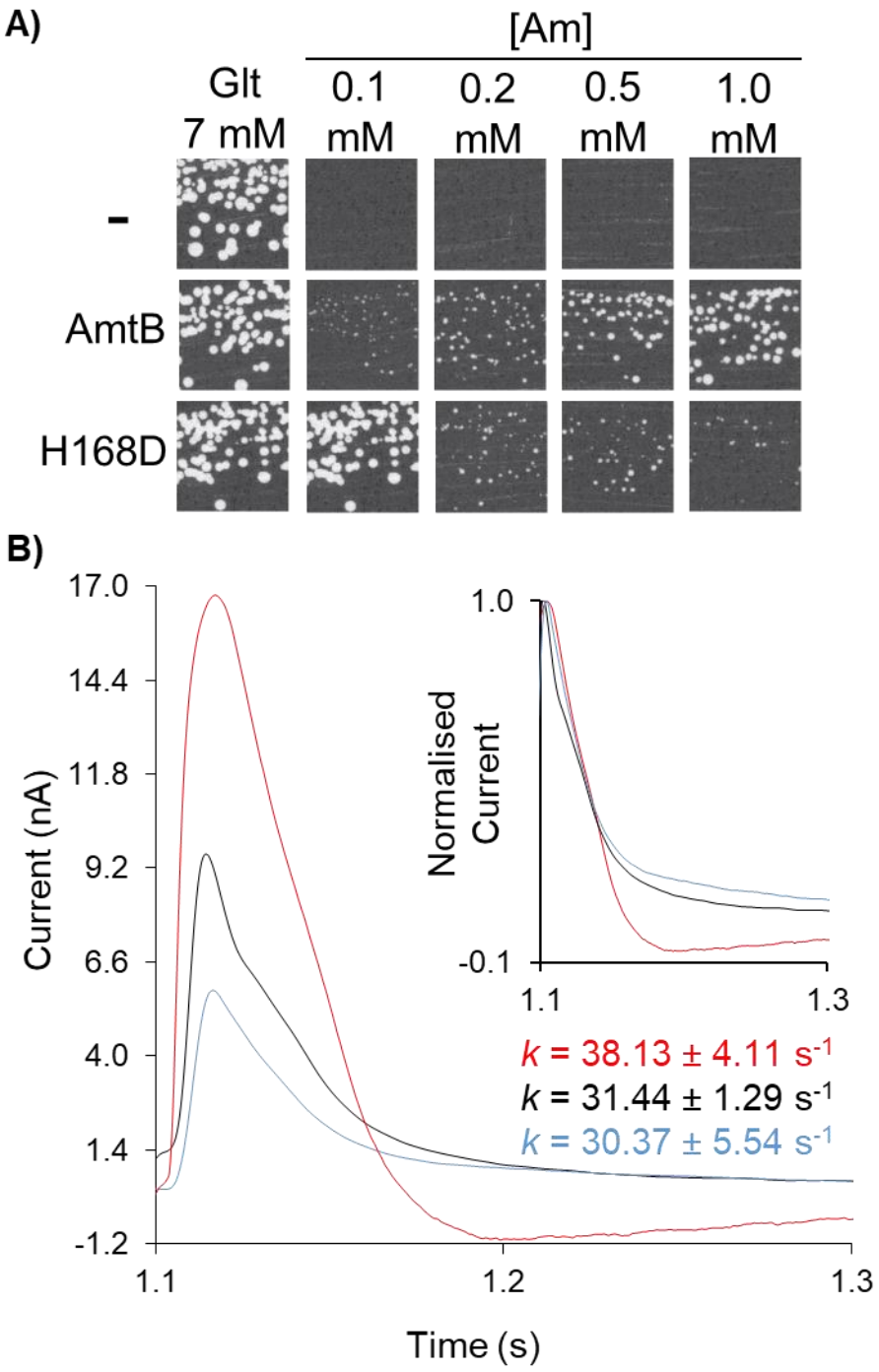

Figure 5.12 AmtB^{H168D} is Super-Active. A) Yeast complementation after 5 days of growth on minimal media supplemented with either 7 mM glutamate (glt) or 1 mM $(NH_4)_2SO_4$ (Am). B) Transient currents following a 200 mM NH_4^+ pulse with AmtB^{H168D} reconstituted into Polar/POPC 2/1 proteoliposomes at a LPR of 5:1 (red), 10:1 (black), or 50:1 (blue).

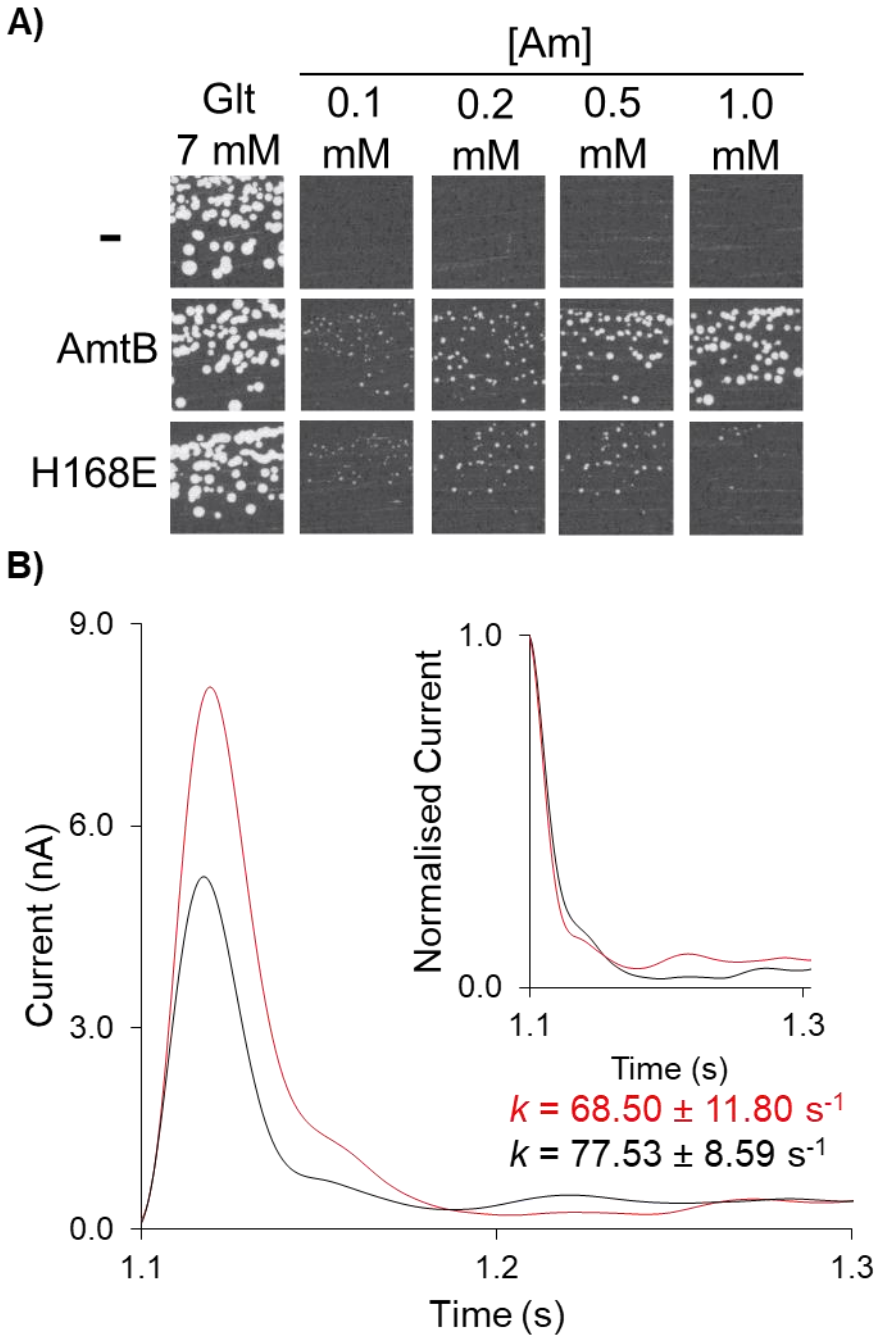

Figure 5.13 AmtB^{H318E} is Inactive A) Yeast complementation after 5 days of growth on minimal media supplemented with either 7 mM glutamate (Glt) or 1 mM $(NH_4)_2SO_4$ (Am). B) Transient currents following a 200 mM NH_4^+ pulse with AmtB^{H318E} reconstituted into Polar/POPC 2/1 proteoliposomes at a LPR of 5:1 (red) or 10:1 (black).

Table 5.1: Activity of Twin-His variants

	NH_4^+		MeA		K^+	
Variant	*in vitro*	*in vivo*	*in vitro*	*in vivo*	*in vitro*	*in vivo*
H168A	Y	Y	Y	Y	Y	Y
H318A	Y	Y	Y	Y	Y	Y
H168A/H318A	N	N	N	N	N	N
H168D	Y	Y	Y	Y	N	N
H168E	Y	Y	Y	Y	N	N
H318E	N	N	N	N	N	N
H168D/H318E	Y	Y	Y	Y	Y	Y

*MeA = Methylammonium
**Green/Y indicates a positive result, while Red/N indicates a negative result.
***_In vitro_ refers to a 200 mM pulse of the relevant substrate at LPR 5, 10, and 50. _In vivo_ refers to complementation in triple-_mepΔ trkΔ S. cerevisiae._

5.7 Methylammonium Transport in Twin-His Variants

Due to significant impact mutations within the twin-His motif can clearly have on the selectivity of AmtB, the activity of these variants with MeA (an ammonium analogue) was measured. Transient currents were observed for all twin-His variants following a 200 mM MeA pulse (**Figure 5.14**). The results of this mirror those obtained with ammonium, albeit with lower amplitudes: $AmtB^{H168D}$ and $AmtB^{H168E}$ appear to be super-active compared to the WT (9-fold and 12-fold increase in amplitude respectively), while the variants which lose selectivity ($AmtB^{H168D/H318E}$, $AmtB^{H168A}$, and $AmtB^{H318A}$) have comparable maximum amplitudes. In each case, the amplitude and decay of the observed currents was dependent on LPR, suggesting that the variants are active. Notably, high maximum amplitudes were observed when measuring with $AmtB^{H318E}$, which is inactive in ammonium transport. However, the decay rate of these currents was unaffected by LPR, suggesting that it is inactive and the amplitude is merely result of a protein-substrate interaction.

As with previous SSME experiments, yeast complementation was carried out in parallel. While the experimental procedure is unchanged, different interpretation is required. Whilst MeA has classically been used as an ammonium analogue, it is actually toxic to yeast and inhibits growth at high external concentrations (Roon *et al.*, 1975; Boeckstaens, André and Marini, 2008). As a result, if a MeA-transporting protein (such as WT AmtB) is expressed in triple-*mepΔ S. cerevisiae* the yeast will grow on media supplemented with glutamate, but will not grow on media supplemented with glutamate and MeA. When the collection of twin-His variants were expressed in triple-*mepΔ S. cerevisiae,* the results were as expected, all variants permitted growth in the glutamate control media, but only $AmtB^{H318E}$ supported growth in the media supplemented with glutamate and 100 mM MeA (**Figure 5.14**). This confirms that $AmtB^{H318E}$ is inactive and, by extension, that the other variants are active in MeA transport regardless of whether or not they retained selectivity against potassium. The activity of these variants is summarised in **Table 5.1**.

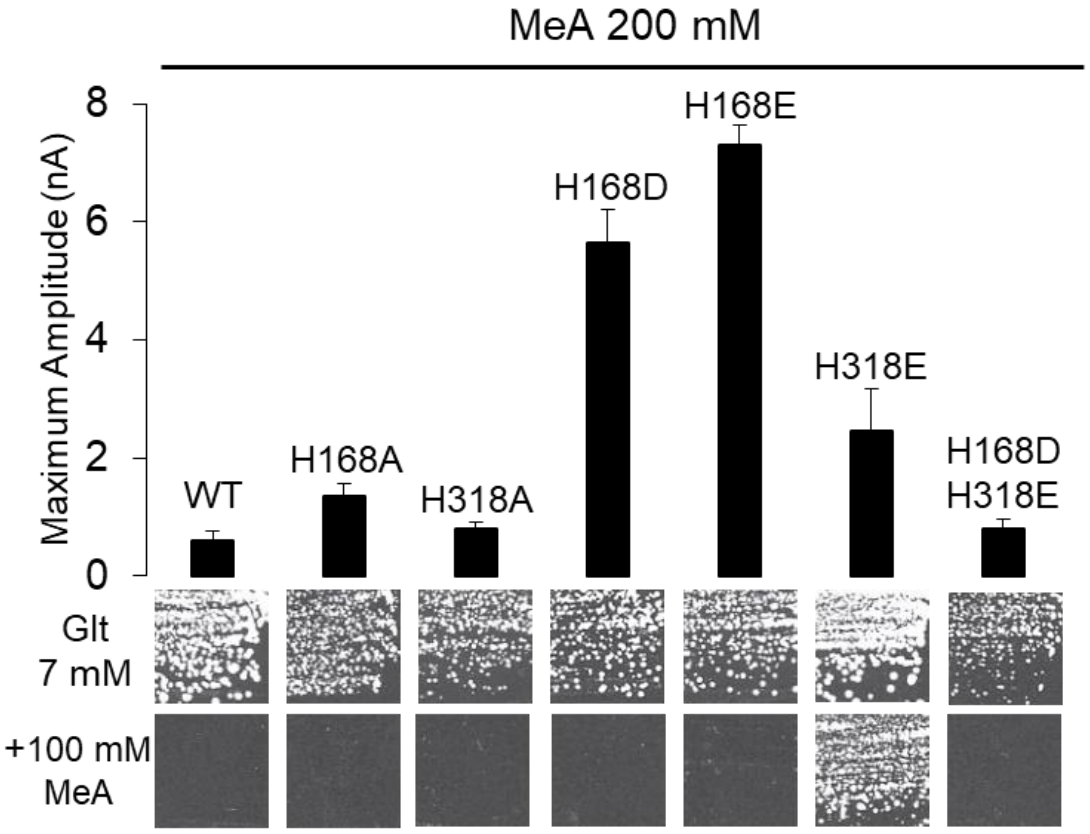

Figure 5.14 Methylammonium Transport in Twin-His Variants Maximum amplitude of the transient current measured using SSME after a 200 mM MeA pulse. Bars represent mean measurements from eight sensors from two independent protein purification batches, with three measurements recorded for each sensor (means ± SD). *Lower panels*: yeast complementation test (strain 31019b, *mep1Δ mep2Δ mep3Δ ura3)* using media supplemented with 7 mM glutamate (Glt) or 7 mM glutamate and 100 mM methylammonium (+100 mM MeA).

5.8 Stabilisation of Water Wires is Required to Ensure Selectivity

Many of the variants presented throughout this thesis are functionally active ammonium transporters, but lose their selectivity ($AmtB^{H168A}$, $AmtB^{H318A}$, and $AmtB^{H168D/H318E}$). However, $AmtB^{H168D}$ and $AmtB^{H168E}$ retain both ammonium transport activity and their ammonium-selectivity. On the surface, it is unclear what governs the difference of substitution on activity. However, based on the flooded pore observed in simulated $AmtB^{H168D/H318E}$ (**Section 5.3**), it is possible that substitutions differentially disturb the water wires within AmtB, and by extension, disrupt the mechanism described in **Section 4.8**.

To determine whether the water wires were disrupted in the variants, each variant was subjected to a D_2O-based SSME assay. Because deuterons have twice the mass of a proton and the strength of a bond is increased, proton mobility is reduced by 30% for each D_2O molecule compared to H_2O (Wiechert and Beitz, 2017). If the water wires are intact and remain part of the transport mechanism, replacement of H_2O with D_2O should result in complete abolishment of current when measured on SSME. If, however, the wires are disrupted or the mechanism altered, then D_2O shouldn't affect the observed current following a 200 mM ammonium pulse.

The response to D_2O substitution appeared to correlate to the selectivity (or lack thereof) of the variant. $AmtB^{H168E}$ responded to D_2O substitution in the same manner as WT AmtB: the current observed following a 200 mM NH_4^+ is diminished in D_2O compared to H_2O (**Figure 5.15**). Unlike WT AmtB, the current is not completely abolished (instead reduced ~4-fold). This demonstrates that the proton translocation remains part of the transport mechanism in $AmtB^{H168E}$.

The non-selective variants ($AmtB^{H168A}$, $AmtB^{H318A}$, and $AmtB^{H168D/H318E}$) yielded quite different results. In each case, the amplitude of the current observed following a 200 mM NH_4^+ pulse was comparable between D_2O- and H_2O-based sensors (**Figure 5.16**). Notably, the decay rate was also comparable between conditions. This suggests that these variants directly

transport hydrated NH_4^+ (and K^+) independently of proton translocation via the water wires. If so, substitution within the twin-His motif does not merely impair selectivity, but may govern a switch in the transport mechanism of AmtB from a transporter- to a channel-like activity, where NH_4^+ is transported in its hydrated form.

Taken together, these results demonstrate that the twin-His motif is an essential functional element of AmtB's transport mechanism and governs selectivity against competing cations (**Figure 5.17**).

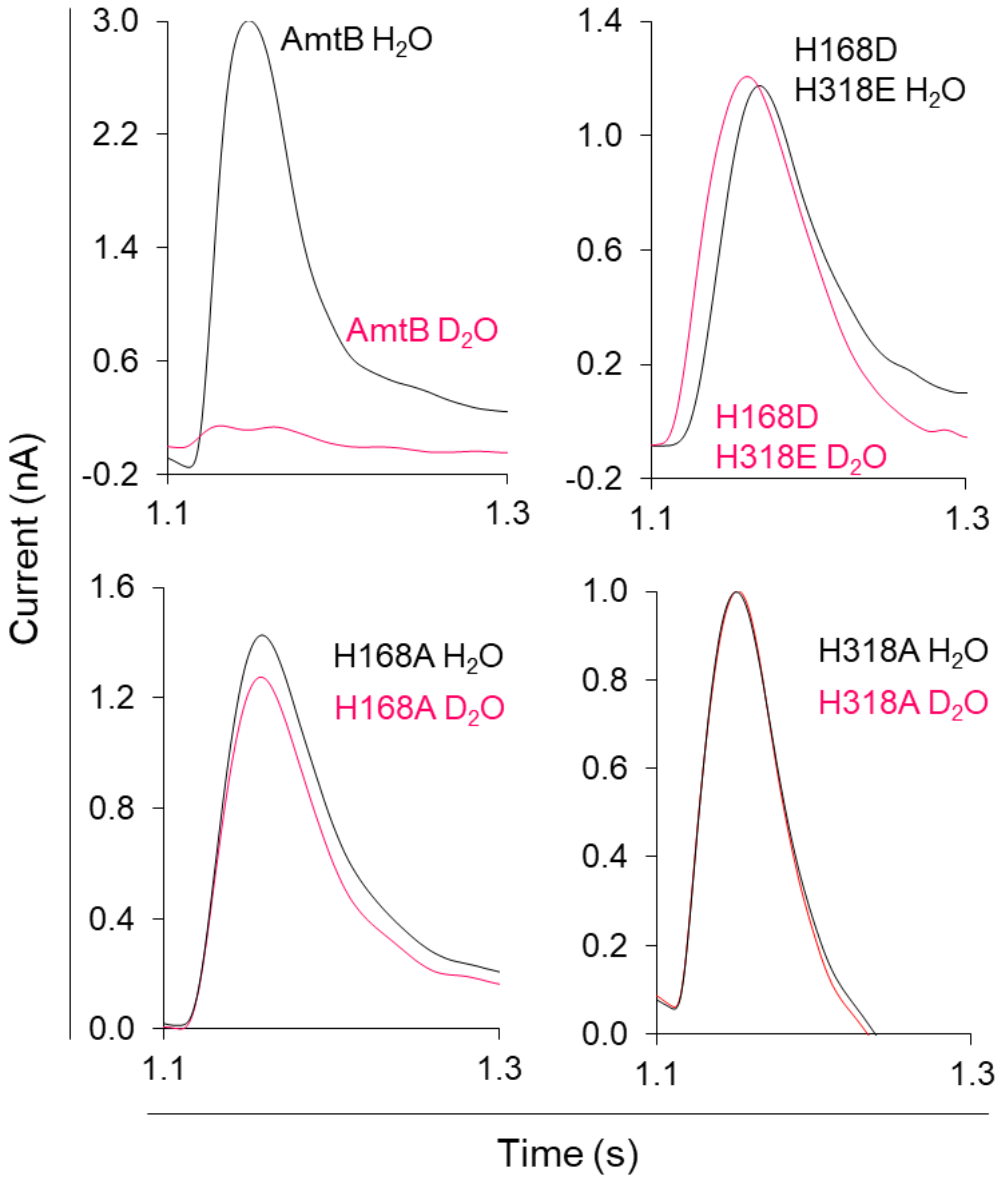

Figure 5.15: Non-selective Histidine Variants Are Unaffected by D_2O Transient currents measured using SSME following a 200 mM ammonium pulse on sensors prepared with solutions containing either H_2O (black) or D_2O (magenta).

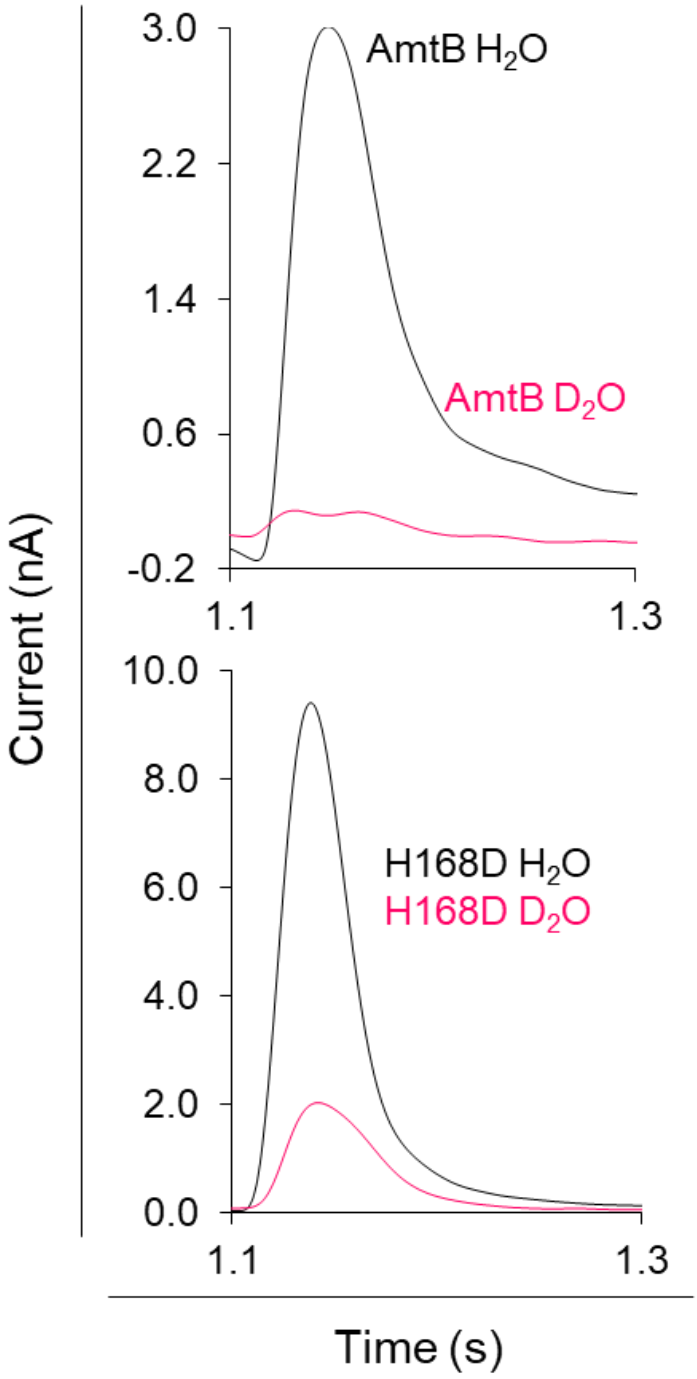

Figure 5.16: **Activity of Selective Histidine Variants is reduced in D_2O** Transient currents measured using SSME following a 200 mM ammonium pulse on sensors prepared with solutions containing either H_2O (black) or D_2O (magenta).

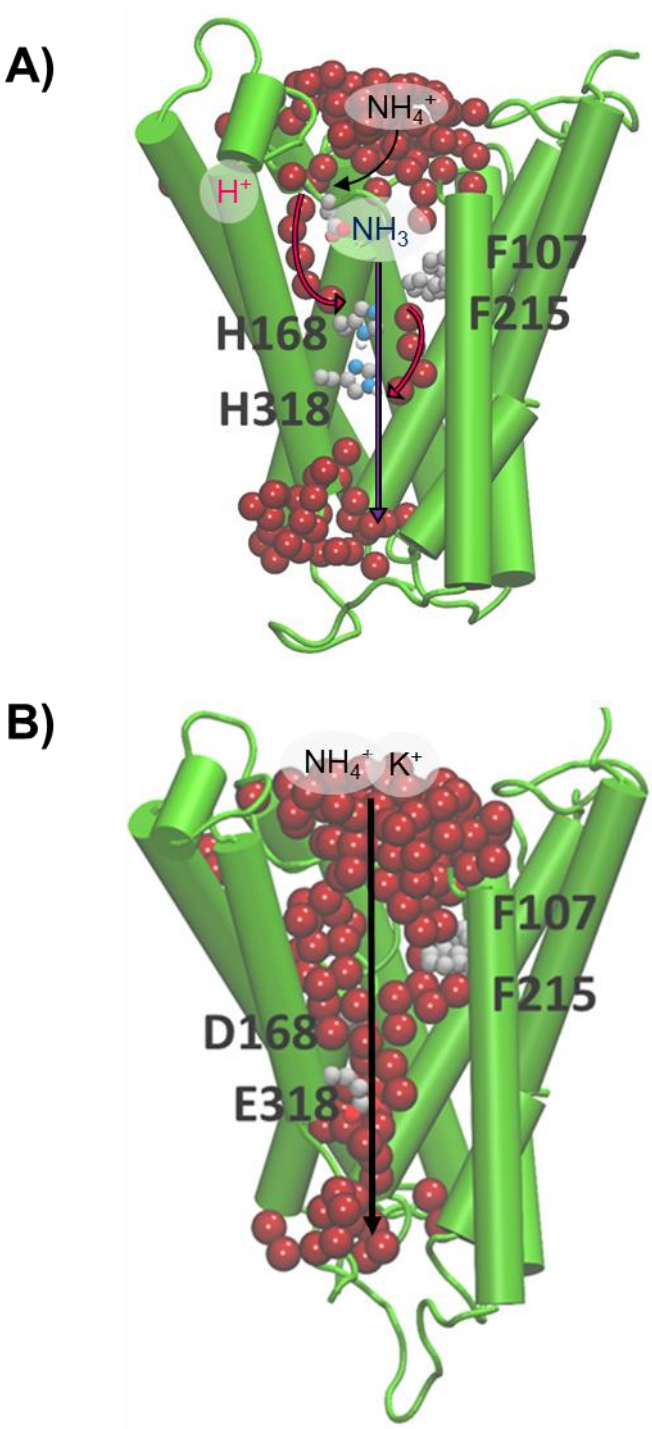

Figure 5.17: Schematic Comparison of Transport in A) WT AmtB and B) AmtB$^{H168D/H318E}$ A) Following sequestration of NH_4^+ at the periplasmic face, NH_4^+ is deprotonated and H^+ and NH_3 follow two separated pathways to the cytoplasm (magenta arrows depict the pathway for H^+ transfer, dark blue arrows for NH_3) facilitated by the presence of two internal water wires. B) Due to the increased hydration within the pore periplasmic NH_4^+, and K^+, are translocated directly through the central pore to the cytoplasm.

5.9 Discussion

5.9.1 Novel Selectivity Mechanism

Our findings define a novel mechanism which allows ionisable molecules that are typically charged in solution to be selectively and efficiently transported across a highly hydrophobic environment like the AmtB/Rh pore (**Figure 5.17A**). This adds a new principle by which selectivity against competing ions can be achieved. Classical mechanisms include size-exclusion, wherein the protein region which interacts with the substrate is of a precise or limited size. Thus larger molecules are sterically blocked from being transported (Kopec *et al.*, 2018). This can be seen in acid sensing ion channels (ASICs), where the size of the channel pore changes at different pH, permitting dynamic ion selectivity (Baconguis and Gouaux, 2012). Within a solution, ions interact with the solvent and become surrounded by a concentric ring of solvent. Prior to transport this shell has to be stripped away. The strength of the interactions holding the ring together will vary depending on the central ion, with stronger bonds requiring more energy to break. This can be exploited to enforce selectivity, with proteins able to desolvate certain ions but not others (Kopec *et al.*, 2018). Potassium channels combine these two principles in order to allow potassium ions to pass, while blocking smaller sodium ions. Prior to passing through the selectivity filter, the hydration shell of K^+ must first be stripped. This is achieved by carbonyl oxygen atoms which line the interior of the selectivity filter and mimic the waters of hydration, desolvating K^+ and allowing it to enter the channel (Zhou *et al.*, 2001). Competing Na^+ are slightly smaller and thus unable to coordinate with these oxygen atoms. As a result, they remain their hydrated shell and are not translocated across the membrane (Zhou *et al.*, 2001).

These mechanisms, however, do not explain the selectivity we observe in AmtB and *Ne*Rh50 as K^+ and Na^+ have similar ionic radii and charge to NH_4^+.

Instead, the mechanism we propose exploits the fact that NH_4^+ can be deprotonated, whilst monovalent cations cannot.

It is likely that similar mechanisms centred on cycling protonation states could be employed by other biological transport systems. For example, a thematically similar mechanism was recently proposed for the Formate-nitrite (FNT) family of weak-acid transporters (Wiechert and Beitz, 2017). In this case, the substrate is anionic so is neutralised by protonation to allow it to bypass hydrophobic constrictions prior to entering the cell. This was initially demonstrated using FocA from *Salmonella typhimurium* and FNT from *Plasmodium falciparum*, and shown to be conserved in the *Entamoeba histolytica* homologue FNT, suggesting that this mechanism is conserved across the family (Helmstetter *et al.*, 2019).

5.9.2 Twin-His Motif is Key to Maintaining Selectivity

The results presented in this chapter suggest a role for the twin-His motif in maintaining selectivity against competing ions in AmtB. In doing so, it offers a rationale for the notable conservation of the motif within the Amt/Mep/Rh family. The loss of selectivity and onset of potassium permeability previously observed (Hall and Yan, 2013), is corroborated by both the SSME and yeast complementation growth test. Hall and Yan focussed on acidic residues, and speculated that they altered the permeability profile of AmtB by changing the hydrophilicity of the pore (Hall and Yan, 2013). However, in this chapter I have demonstrated that non-polar substitutions in the twin-His motif can also elicit potassium permeability. Thus whilst equivalent growth was observed in triple-*mep*Δ yeast expressing the WT or potassium-permeable variants, it appears the presence of both histidine residues is critical. Permeability to K^+ in AmtB proteins would undermine the ionic homeostasis of *E. coli* cells and disrupt membrane potentials, which depend on maintaining K^+ gradients. In addition, Amt proteins are expressed in response to nitrogen limitation conditions (low NH_4^+: K^+ ratio), where the loss of NH_4^+ selectivity would be detrimental to nitrogen uptake (Pedro-Roig *et al.*, 2013). Taken together, these results

demonstrate that the twin-His motif, which is highly conserved amongst members of the family, is an essential functional element in the transport mechanism, preventing the transport of competing cations, whilst providing a pathway for proton transfer by bridging the periplasmic and the cytoplasmic water wires.

5.9.3 Twin-His governs Mechanistic Switch

Whilst the mechanistic importance of the twin-His motif appears to lie in maintaining selectivity, substitution within the twin-His motif impacts the overall mechanism of AmtB-mediated ammonium transport. Simultaneous removal of both residues completely abolishes transport activity in SSME, corroborating observations by (Javelle *et al.*, 2006). Interestingly, Javelle *et al* also demonstrated <10% methylammonium-uptake activity for the single variants $AmtB^{H168A}$ and $AmtB^{H318A}$. This contrasts later observations that $AmtB^{H168A}$ and $AmtB^{H318A}$ could restore growth in triple-*mepΔ S. cerevisiae* (Wang *et al.*, 2012) and my results, which suggests the single variants are tolerated without issue. On the surface, these observations appear difficult to reconcile as there is no clear rationale for why single His mutants would be active, but a double mutant inactive. In the context of our model, these results could be explained by the different impact these substitutions have on the neighbouring water wires and the overall hydrophobicity of the pore. Specifically, removal of both histidines would prevent the twin-His motif from bridging the water wires and thus a complete translocation pathway through the protein fails to form. In contrast, the existing crystal structure for $AmtB^{H168A}$ reveals increased hydration around A168 (Javelle *et al.*, 2006), which could permit passage of hydrated ions.

My results demonstrate changes in the mechanism are also seen when the twin-His motif is replaced with acidic residues. Initially, *in vivo* experiments revealed that replacing one or both histidines with glutamic or aspartic acid, resulted in a loss of methylammonium accumulation compared to the WT

(Javelle *et al.*, 2006). However, later work demonstrated that whilst methylammonium accumulation was reduced, the doubling time of *E. coli* expressing variant AmtB was unaffected suggesting that acidic substitutions could be accommodated (Hall and Kustu, 2011). This discrepancy is likely due to the fact that methylammonium is a poor substrate analogue for ammonium. My results demonstrated that most polar substitutions (H168D, H168E, and H168D/H318E) were able to restore growth in triple-*mepΔ S. cerevisiae*, indicating ammonium transport activity. Whilst these variants all retained activity, $AmtB^{H168D/H318E}$ was alone in having markedly altered kinetics compared to the WT. Combined with the results of the D_2O based assays, which reveal that proton-hopping is not a feature of transport in the variant, it is clear that while $AmtB^{H168DH318E}$ and WT AmtB both conduct NH_4^+, they do so via distinctly different mechanism.

Chapter 6:

General Discussion and Future Work

Chapter 6: General Discussion and Future Work

6.1 Summary

Through my PhD, I successfully developed and utilised a combinatorial approach to characterise the activity of the *E. coli* ammonium transporter AmtB, and revealed new insights into its mechanism.

Initially, I utilised Solid Supported Membrane Electrophysiology (SSME) to characterise the activity, selectivity and kinetics of WT AmtB (**Chapter 3**). This provided a foundational understanding of the assay, and permitted investigation into the role of deprotonation in the mechanism of AmtB.

Following on from this, I combined, with the help of our collaborators, *in vitro* SSME, *in vivo* yeast complementation, and *in silico* molecular dynamic simulations (MDS) to identify and explore potential transfer routes for H^+ across AmtB (**Chapter 4**). In doing so, I revealed the presence of two ordered water wires embedded within the pore of AmtB, linked by the highly conserved twin-His motif. Assays exploiting the altered proton mobility between H_2O and D_2O revealed that proton transfer along these wires via the Grotthuss reaction was a feature of the electrogenic activity observed for AmtB. In addition, substitutions that were predicted to disrupt these wires resulted in a complete loss of activity. These observations form the basis for our novel model, wherein NH_4^+ is deprotonated, with NH_3 and H^+ separately translocated.

Finally, in the context of this mechanistic model, I provided a rationale for the proposed functional importance of the twin-His motif (**Chapter 5**). Disruption of the motif had a demonstrable effect on the kinetic of ammonium transport and, crucially, had a deleterious impact on the ability of AmtB to prevent permeation of competing ions, resulting in a loss of selectivity.

Overall, this work has provided a novel model of AmtB-mediated electrogenic ammonium transport which reconciles historically conflicting observations in the field. In addition, it offers insight into the functional importance of some

highly conserved residues within AmtB, and potentially other members of the Amt/Mep/Rh family.

6.2 General Discussion

6.2.1 Deprotonation Site

Whilst deprotonation was discussed in **Chapter 3**, this was done in the context of deprotonation at the S1 binding site. In the past, authors have proposed that deprotonation occurs deeper within the protein's pore, which I will discuss in the context of my results.

6.2.1.1 Phe-Gate

The potential function of the highly conserved dyad of phenylalanine (F107 and F215 in AmtB) within the pore of Amt/Mep/Rh proteins has remained enigmatic. Positioned immediately after the S1 binding site, the stacked phenyl rings of F107 and F215 form a constriction that blocks access to the pore from the S1 site (Khademi *et al.*, 2004; Zheng *et al.*, 2004). These rings would have to move to permit access to the pore, but appear in the closed state in all AmtB crystal structures.

Some authors have posited that the Phe-gate is involved in deprotonation. Either as a deprotonation facilitator, or as a shuttle for a proton liberated from NH_4^+ at the S1 site. Molecular dynamic simulations examining the hydration of ammonium within the pore suggested that ammonium could be deprotonated or reprotonated at F107 (Bostick and Brooks, 2007). However, *in vivo* work since demonstrated that F107 can be removed without a loss of [^{14}C]-methylammonium uptake activity, but substitution of F215 abolished activity (Javelle *et al.*, 2008; Hall and Kustu, 2011). This allows F107 to be eliminated as a candidate for deprotonation, whilst supporting the authors' conclusion that F215 is essential role for substrate conduction (Javelle *et al.*, 2008). Following substitution of F215 with a series of other residues (H, L, Q, S, and W) Javelle *et al* concluded that its importance was due to a specific role of the phenyl ring, possibly in deprotonation. Interestingly, further exploration into this by Hall and

Kustu revealed that simultaneous substitution of F215 and W148 with L, did not abolish activity suggesting a more complex, but less essential, role (Hall and Kustu, 2011). In the context of the model presented in this thesis, deprotonation by F215 seems unlikely, as NH_4^+ must deprotonated in the vicinity of the S1 site in order for the proton to be shuttled into the cytoplasmic water wire.

Interestingly, (Javelle *et al.*, 2008) reported that a double variant (F107A/F215A) was also inactive, whilst preliminary data (**Figure 6.1**) obtained via SSME shows measureable electrogenic activity for this variant. Thus, it is possible that F215A may yet retain activity, albeit at a very low level. This could be tested using the same SSME-assays presented here, which use the true substrate and have a higher sensitivity.

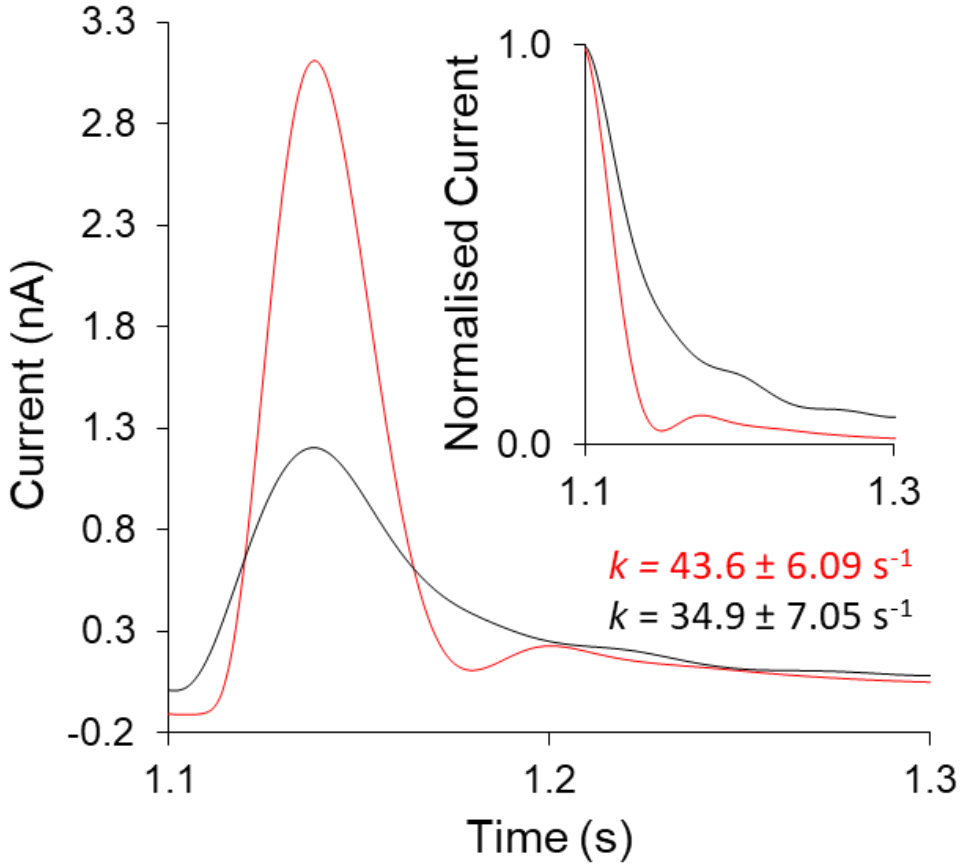

Figure 6.1 AmtB$^{F107A/F215A}$ Has Electrogenic Activity Representative traces following a 200 mM ammonium pulse on AmtB$^{F107A/F215A}$ reconstituted into Polar/POPC 2/1 liposomes at LPR 10 (black) and LPR 5 (red).

6.2.1.2 Twin-His Motif

When reporting the initial crystal structures of AmtB, both groups speculated that deprotonation might occur at the first histidine of the twin-His motif (Khademi *et al.*, 2004; Zheng *et al.*, 2004). However, Zheng *et al* noted that deprotonation via this system would require a path for the proton to return to the aqueous phase. Subsequent work highlighting the conservation and clear functional importance of H168 (and the twin-His motif as a whole) lent initial support to this idea (Zheng *et al.*, 2004; Javelle *et al.*, 2006) and mean force calculations were also used to support H168-mediated deprotonation (Lamoureux, Klein and Bernèche, 2007).

In particular, early *in vivo* studies supported this hypothesis, as they reported $AmtB^{H168A}$ and $AmtB^{H318A}$ were deficient in MeA-uptake compared to the WT (Javelle *et al.*, 2006). Later work however, demonstrated that both variants were able to restore growth in triple-*mepΔ S. cerevisiae*, showing that neither is strictly essential for ammonium uptake activity (Wang *et al.*, 2013). This discrepancy is likely due to the different substrate used, as my results presented in **Section 3.6** demonstrate that MeA is a poor substrate analogue.

My results further suggest that H168 is an unlikely site for deprotonation, as it can be substituted without a loss of activity in either *in vivo* or *in vitro* assays. Specifically, the H168E variant of AmtB results in super-activity without an apparent change in the mechanism (**Section 4.7**). Notably, $AmtB^{H168E}$ was the only variant tested by Javelle *et al* to retain even residual MeA-uptake activity (~20%) compared to the WT corroborating that it is more active than other variants (Javelle *et al.*, 2006). In contrast, substitution of D160 with alanine completely abolished ammonium transport activity. This corroborates a hypothesis formed by Lin *et al*, whose molecular dynamic simulations predicated that D160 played a critical role in deprotonation of NH_4^+ at the S1 site, and that it would be well-positioned to shuttle the proton onto a potential transfer pathway (Lin, Cao and Mo, 2009)

Taken together, it is clear that the twin-His motif's role in AmtB-mediated ammonium transport is important, but not essential. Thus it appears more probable that the twin-His motif's importance is not related to deprotonation, but rather is tied to maintenance of selectivity.

6.2.2 Twin-His Motif in Maintaining Selectivity

The results presented in **Chapter 3** clearly demonstrate that substitutions within the twin-His motif can lead to permeability to potassium ions. Specifically, $AmtB^{H168A}$, $AmtB^{H318A}$, and $AmtB^{H168D/H318E}$ could transport both NH_4^+ and K^+. In contrast, both $AmtB^{H168D}$ and $AmtB^{H168E}$ retain NH_4^+ activity without sacrificing selectivity. This is consistent with previous characterisation of Mep1/3-like proteins, which do not transport K^+ despite their first histidine naturally being replaced with glutamate (Boeckstaens, André and Marini, 2008). Recent work demonstrated that variant AMT1;2 and AMT2 from *Ariadopsis thaliana* with substitutions in the twin-His motif are also able to transport K^+ (Ganz *et al.*, 2020). Contrasting observations in AmtB and Mep1/3, replacement of the first histidine with glutamate in AMT2 resulted in a loss of selectivity. Additionally, Ganz *et al* reported that substitution of the second histidine in either AMT1;2 or AMT2 with an acid residue also resulted in K^+ transport. This is a significantly different phenotype from that observed in the AmtB equivalent ($AmtB^{H318E}$), which was inactive in both NH_4^+ and K^+ transport (**Section 5.6**). Together, these observations reinforce the important role the twin-His motif plays in maintaining selectivity and demonstrate that it is held throughout the Amt/Mep/Rh. However, it is also clear that the impact of specific twin-His mutations differ across the Amt/Mep/Rh family suggesting either mechanistic differences, or the existence of additional selectivity barriers in some family members.

6.2.3 Universality of Mechanism across Amt/Mep/Rh Family

The broad structural conservation across the Amt/Mep/Rh superfamily suggests that they would share a similar mechanism. Specifically, the residues of great mechanistic importance to our proposed model (D160, H168, and H318) are highly conserved, suggesting that other family members utilise the same mechanism. Our preliminary results for *Ne*Rh50, a phylogenetically distant homolog of AmtB, demonstrate that *Ne*Rh50 is electrogenic and strongly selective for NH_4^+, providing initial support for a conserved mechanism (**Section 6.3.3.2**). In addition, other groups have reported electrogenic activity in other Amt/Mep/Rh members including; Amt1 and Amt3 from *Archaeoglobus fulgidus*, Amt1;1 from *Lycopersicon esculentum,* and mouse Rhbg (Ludewig, Von Wiren and Frommer, 2002; Nakhoul, 2004; Wacker *et al.*, 2014). Widespread adoption of this mechanism is sensible as in normal environmental conditions ammonium will predominate as NH_4^+, therefore it is likely that most systems will scavenge NH_4^+ rather than NH_3. However, it is important to note that attempts to been made to characterise multiple Amt/Mep/Rh proteins, and electroneutral activity has been reported for a number of proteins (summarised in **Table 6.1**) Notably, protein isoforms within a single species have been characterised as having different activity. For example, of the transporting Rhesus proteins in humans (RhAG, RhBG, and RhCG), only RhAG appears to be electrogenic, whilst RhBG and RhCG are both reported to be electroneutral (Mouro-Chanteloup *et al.*, 2010; Ripoche *et al.*, 2011; Caner *et al.*, 2015). A similar split is seen in *A. thaliana* AMT proteins and *S. cerevisiae* Mep proteins, suggesting that the family possesses more than one mechanism and, if so, there may be an advantage to maintaining multiple mechanisms (Boeckstaens, André and Marini, 2008).

As a result, it is necessary to further investigate the universality of the mechanism throughout the family. We have shown that single mutations have profound effects on phenotype, thus it is difficult to predict the phenotype of other family members based on sequence alone. In addition, the Amt/Mep/Rh have evolved to fulfil diverse physiological roles, so it is possible that individual

members have altered mechanisms. The Mep1, Mep2, and Mep3 proteins in *S. cerevisiae* are highly similar but have differing substrate affinities and transport capacities (Marini *et al.*, 1997). In addition, Mep2 has developed a transceptor function, being implicated in signalling the dimorphic transition of pathogenic yeast to a pseudohyphal form (Lorenz and Heitman, 1998). The mechanism underlying this signalling is *hitherto* unknown, but one hypothesis is that Mep2's transport mechanism differs from its homologs Mep1/3 and this is what instigates the signalling cascade (Brito *et al.*, 2020). In a similar vein, of the five Rhesus isoforms in humans, only three (RhAG, RhBG, RhCG) are transport competent and are expressed in different tissues (Cherif-Zahar *et al.*, 2007). Whilst structurally similar, the remaining two isoforms (RhD and RhCE) do not transport and instead carry the antigen used in conjunction with ABO blood-type testing (Avent and Reid, 2000). Thus, further work must be done to fully understand the universality of the Amt/Mep/Rh transport mechanism, as the family might possess multiple mechanisms.

Table 6.1: Mechanism of Amt/Mep/Rh proteins

Protein	Mechanism	Technique	References
*Ec*AmtB	Electrogenic	SSME	(Ariz *et al.*, 2018) (Williamson *et al.*, 2020) (Mirandela *et al.*, 2019)
*At*AMT1;1	Electrogenic	Expression in *Xenopus* oocytes	(Loqué *et al.*, 2009)
*At*AMT1;2	Electrogenic	Expression in *Xenopus laevis* oocytes	(Neuhauser *et al.*, 2007)
*At*AMT2	Electroneutral	Expression in *Xenopus laevis* oocytes	(Neuhauser, Dynowski and Ludewig, 2009)
Af-AMT1	Electrogenic	SSME	(Wacker *et al.*, 2014)
Af-AMT3	Electrogenic	SSME	(Wacker *et al.*, 2014)
*Le*Amt1;1	Electrogenic	Expression in *Xenopus laevis* oocytes	(Ludewig, Von Wiren and Frommer, 2002)
*Sc*Mep1	Electrogenic	Expression in *Xenopus laevis* oocytes	(Brito *et al.*, 2020)
*Sc*Mep2	Electroneutral	Expression in *Xenopus laevis* oocytes	(Brito *et al.*, 2020)
*Ne*Rh50	Electrogenic	SSME	(Williamson *et al.*, 2020)
*Mm*Rhbg	Electrogenic	Expression in *Xenopus laevis* oocytes	(Nakhoul, 2004)
*Hs*RhAG	Electrogenic	Expression in *Xenopus laevis* oocytes	(Caner *et al.*, 2015)
*Hs*RhBG	Electroneutral	Expression in *Xenopus laevis* oocytes	(Caner *et al.*, 2015)
*Hs*RhCG	Electroneutral	i) Expression in *Xenopus laevis* oocytes ii) Stopped-flow Spectrophotometry	(Caner *et al.*, 2015) (Ripoche *et al.*, 2011) (Mouro-Chanteloup *et al.*, 2010)

6.3 Future Work

6.3.1 Further Work in AmtB

6.3.1.1 Structural Confirmation of Water Wires

The cytoplasmic water wire (CWW) and periplasmic water wire (PWW) presented in this work are central to the novel mechanistic model I propose. Whilst the existence of the CWW is supported by previous structural and functional investigation of the pore hydration in AmtB (Javelle *et al.*, 2006; Lamoureux *et al.*, 2007). In contrast, there is currently no structural evidence for the existence of the PWW. As discussed in **Section 4.2** the PWW forms later in the simulation and generally has a lower occupancy compared to the CWW, which could explain the current difficulty of observing the PWW in AmtB.

Our simulations also revealed defined physical location for the water molecules of the PWW (Williamson *et al.*, 2020). Thus, it would be possible to use Pan-Dataset Density Analysis (PanDDA) to attempt to validate the low occupancy binding sites of the PWW. Traditionally, binding sites would be identified by comparing the X-ray structure of a protein crystallised in the presence and absence of the substrate, however the difference between these states can be overwhelmed by experimental noise. The PanDDA method analyses a series of datasets of the ground-state and the changed-state of the target protein, enabling it to better identify, and eliminate, the source of background noise yielding a far greater contrast at ligand binding sites (Pearce *et al.*, 2017). The Javelle group has thus planned a collaboration with Prof. Martin Walsh at Diamond Light Source to use this method to further study the water wires in AmtB. The experimental procedure will comprise the collection and average over a large set of data (typically >50) from a batch of high quality AmtB crystals. A new data collection strategies and the ability of Diamond's MX beamlines to collect the best data to the highest resolution to provide the best possible model of AmtB will be used. With the automation developed at Diamond, data acquisition from many crystals will take on the order of hours.

This data would then be analysed via PanDDA methodology. In addition to structural information about the PWW, this analysis could provide further insight into the CWW and the long-standing debate around structural movement, particularly of the Phe-gate, in activity within the pore. Finally, our MD simulations and experimental results suggest that the inactivity in $AmtB^{D160A}$ and $AmtB^{H168A/H318A}$ is due to an absence of the PWW (**Section 3.8.2 and Section 4.5**). PanDDA analysis of these variants would allow the connection between AmtB activity and pore hydration to be established and explored.

6.3.1.2 Energetics of Proton Translocation

A key feature of the mechanism proposed in this thesis is the initial deprotonation of NH_4^+, prior to separate translocation of the resultant fragments. Thus, it is essential that further study be carried out to understand the energetics and pathway of proton transfer through AmtB. Quantum mechanical and pKa calculations could help ascertain whether electrostatic interactions between NH_4^+ and the residues within the binding site decreases the pKa to create a favourable environment for deprotonation. In addition, empirical valence bond (EVB) calculations could help visualise the transfer of a proton from D160 to the further quantum mechanical and pKa calculations could also help ascertain whether electrostatic interactions between NH_4^+ and the residues within the binding site decreases the pKa to create a favourable environment for deprotonation. Such calculations could be carried out in collaboration with Prof. Ulrich Zachariae of the University of Dundee and would represent a landmark use of EVB calculations to elucidate mechanistic details of a biological transporter.

6.3.2 Conservation of Mechanism

While this work has primarily focused on the mechanism within *E. coli* AmtB, the results provide insights across the Amt/Mep/Rh family. Crucially, whether the mechanism proposed here is conserved throughout the Amt/Mep/Rh family remains unclear.

In general, conservation, or the lack thereof, of the mechanism could inform our understanding of how this ubiquitous superfamily has evolved over time. Currently, the published literature regarding Amt/Mep/Rh is insightful but limited. Future studies could be conducted by characterising and comparing the mechanisms of a selection of Amt, Mep, and Rhesus proteins via assays similar to those used in this work might reveal distinct mechanistic groups within the family, as suggested for plant Amt1 and Amt2 subfamily (Neuhauser, Dynowski and Ludewig, 2009; Neuhäuser, Dynowski and Ludewig, 2014).

Additionally, the methods outlined within this thesis could form the foundation of studies targeting specific members of the Amt/Mep/Rh family. Two notable candidates for such studies include; Mep2 from *Saccharomyces cerevisiae*, due to its role in fungal pathogenicity; and the Rhesus proteins due to their involvement in human pathophysiology. Throughout my PhD I carried out some preliminary work with Mep2 from *Saccharomyces cerevisiae* and Rh50 from *Nitrosomonas europaea.*

6.3.2.1 *Saccharomyces cerevisiae* Mep2

As outlined in the introduction, Mep2 has been identified as the trigger of pseudohyphal growth: a dimorphic transition associated with the virulence of some fungal pathogens (**Section 3.4.2**, Lorenz and Heitman, 1998). It is unclear if Mep2 initiates this signal cascade by complexing with a partner signalling protein and or if it is a function of Mep2 transport activity (van den Berg *et al.*, 2016; Brito *et al.*, 2020). Thus far, no candidates have been

proposed as transduction factors in a signalling complex, so the latter hypothesis seems more likely. It is possible that the three Mep isoforms employ different mechanisms to achieve ammonium transport, and that such a difference is what allows Mep2 to act as a trigger.

To investigate this, I collaborated with the Marini group from the free University of Brussels, to attempt to purify and characterise the *S. cerevisiae* Mep2 via SSME. Despite initial issues with protein yield and aggregation during the purification process, I successfully purified and inserted *Sc*Mep2 into (*E. coli* Polar Lipids/POPC 2/1) liposomes, ready for measurement on the SURFE^{2}R (**Figure 6.2**). Initial SSME measurements following a pulse a 200 mM ammonium pulse elicited a transient current with an amplitude of 0.3 nA, compared to 3.0 nA for WT AmtB and no current for empty liposomes (**Figure 6.3**). This suggests that Mep2 is electrogenic, though further work, including repeat measurements at different LPR, is required to verify this. Dr Mélanie Boeckstaens, in collaboration with Prof. Von Wirén obtained preliminary data of Mep1 and Mep2 activity when expressed in *Xenopus* oocytes (Ariz *et al.*, 2018). In line with my SSME results, this data showed that Mep2 was not associated with a measurable current, whilst Mep1 elicited a clear current. Thus it would be of interest to measure the activity of Mep1, and the final isoform Mep3, on SSME. In doing so, it would be possible to uncover any large-scale difference in the mode or mechanism of transport between the three proteins, and thus have a foundation for explaining the transceptor function of Mep2.

Prior to any further work, the purification process has to be optimised further to allow for higher-yield purification of *Sc*Mep1 and *Sc*Mep2, such that a single batch can consistently be reconstituted into liposomes at LPRs of 5, 10, and 50. This would enable comparisons between the decay rate of the three LPRs and a clearer insight into transport. Secondly, if electrogenic transport is observed then Mep protein should be subjected to the D_2O-based assay presented in **Section 4.3**. This would reveal whether or not a Grothuss mechanism is involved in its mechanism and, by extension, provide initial evidence of a potential conserved mechanism.

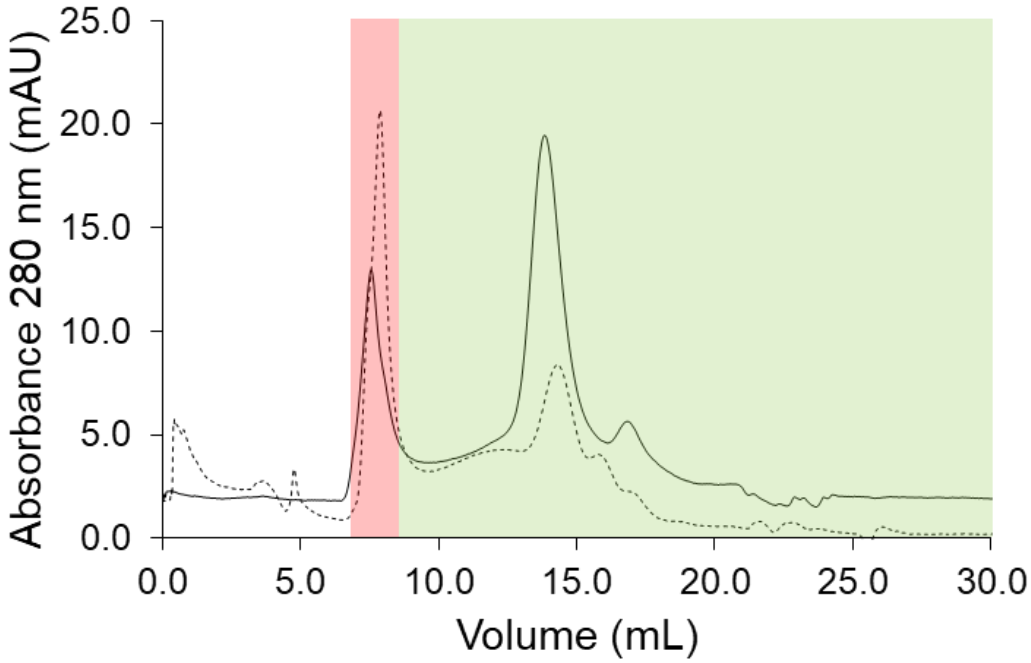

Figure 6.2: Size-exclusion Chromatography of Mep2. Comparison of sample chromatograms from initial (dashed line) and buffer-optimised (solid line) purifications of Mep2. The peak highlighted by the red region of the chromatogram eluted at the void volume (~7 mL) of the Superose 6 10/300 column used. The green region indicates the running volume of the column and the elution profile of the protein.

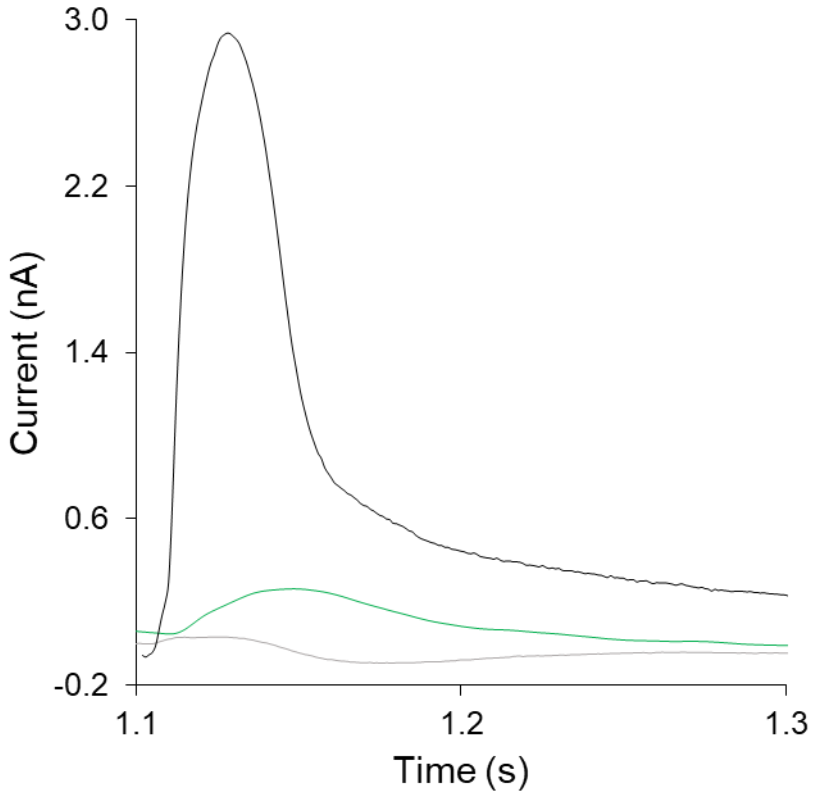

Figure 6.3 Mep2 is Electrogenic. Representative traces following a 200 mM ammonium pulse for WT AmtB (black), Mep2 (green) at LPR 10, and empty Polar/POPC 2/1 proteoliposomes (grey).

6.3.2.2 *Nitrosomonas europaea* Rh50

The human rhesus proteins are involved in a number of vital processes, including maintenance of acid-base homeostasis to preventing toxic build-up of ammonium in erythrocytes (Garvin, Burg and Knepper, 1988). Due to their importance, it is unsurprising that Rh mutation has been associated with various pathologies, ranging from anaemias to depression (Hadley and Kumpel, 1993; Lozano and Cid, 2003; Verma *et al.*, 2008; Bruce *et al.*, 2009). In some instances, the link between specific mutations and clinical symptoms has been made (Biver *et al.*, 2008; Bourgeois *et al.*, 2018), but the enigmatic mechanism of Rh proteins inhibits an understanding of how the mutation manifests the malfunction.

Towards the end of my PhD, I purified and characterised Rh50 from the bacterium *Nitrosomonas europaea* as a preliminary move towards enhancing our understanding of the mechanism of Rh proteins and their role in pathophysiology. *Ne*Rh50 was chosen for multiple reasons; as a bacterial protein, it can be heterologously expressed in *E. coli* and can be purified with a near-identical workflow as AmtB (0.033% DDM is replaced with 0.09% LDAO). In addition, it is structurally highly similar to human Rh, having been used as a scaffold for a model of the human RhCG and retaining a number of residues associated with disease in humans (Lupo *et al.*, 2007; Cartron *et al.*, 2009; Gruswitz *et al.*, 2010).

My preliminary work confirmed a number of facts regarding Rh50 activity and provides a foundation work. When expressed in triple-*mepΔ S. cerevisiae* Rh50 restores growth, indicating that it can facilitate ammonium uptake (**Figure 6.4**). Additionally, SSME characterisation revealed that this ammonium transport activity is electrogenic and that Rh50 retains selectivity against potassium (**Figure 6.4**). In addition, Rh50 activity can be described by the Michaelis-Menten model in a similar fashion to AmtB, suggesting that it is also a transporter and not a channel (**Figure 6.5**). Notably, the Km for Rh50 is, like AmtB, in the mM range. Finally, the transient current observed following

a 200 mM ammonium pulse is completely abolished in D_2O (**Figure 6.6**). This implicates proton hopping as a feature of the mechanism, as I previously demonstrated in AmtB, suggesting a conserved mechanism (**Section 4.3**).

This work is currently being continued and expanded by Miss Adriana Bizior, a PhD student in the Javelle group. The main goal of her work will be to generate a collection of *Ne*Rh50 variants, including equivalents to mutants presented throughout this work and mutants associated with disease in humans. It is hoped that her work will provide insights into the mechanism of Rh50 and the causative link between functional alteration and pathophysiology.

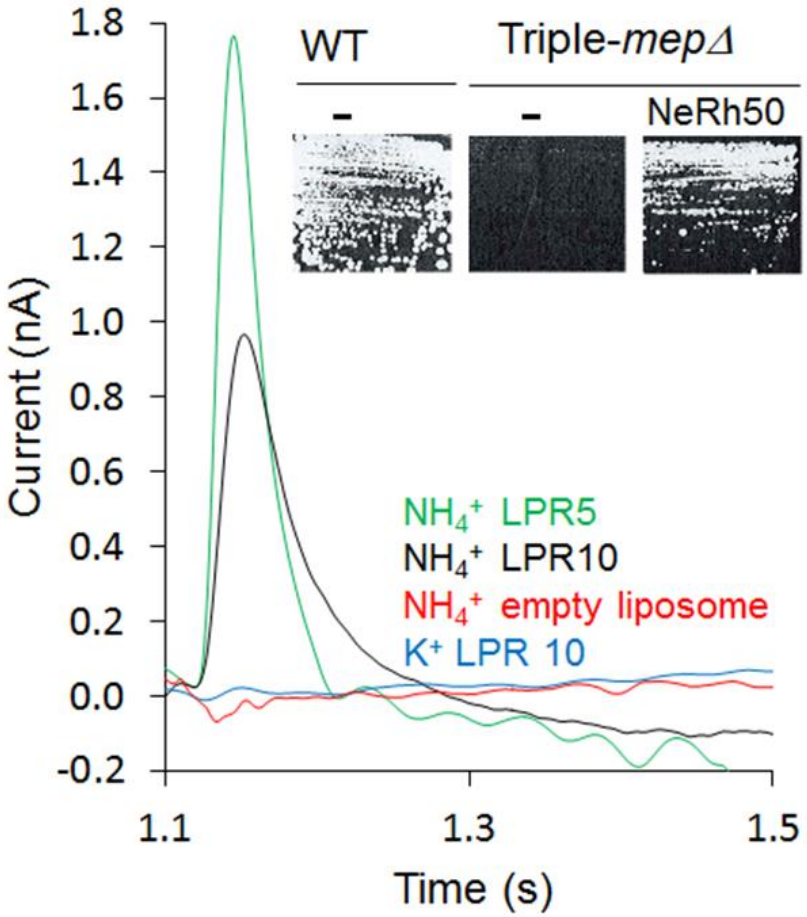

Figure 6.4 Characterization of the activity of *Ne*Rh50.Representative traces following a 200 mM pulse (ammonium or potassium) in Rh50-containing proteoliposomes at LPR 5 (green) or LPR 10 (black), or empty liposomes (red). Insert: Yeast complementation by *Ne*Rh50 (strain 31019b, *mep1Δ mep2Δ mep3Δ ura3*) on minimal medium supplemented with 3 mM ammonium as sole nitrogen source.

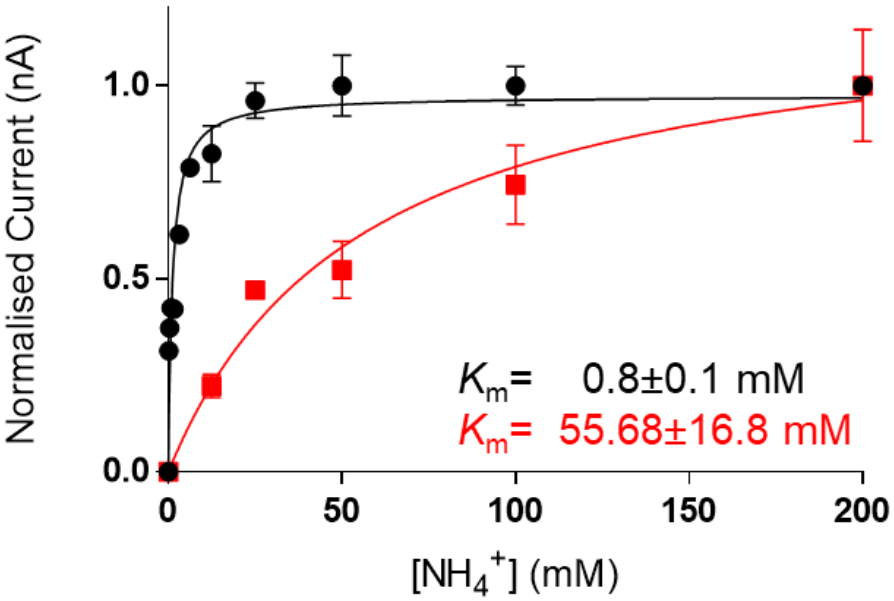

Figure 6.5 Rh50 Kinetics Characterisation Kinetics for WT AmtB (black) and Rh50 (red) at LPR 10 using NH_4^+. Maximum amplitudes have been normalised to 1.0 for comparison

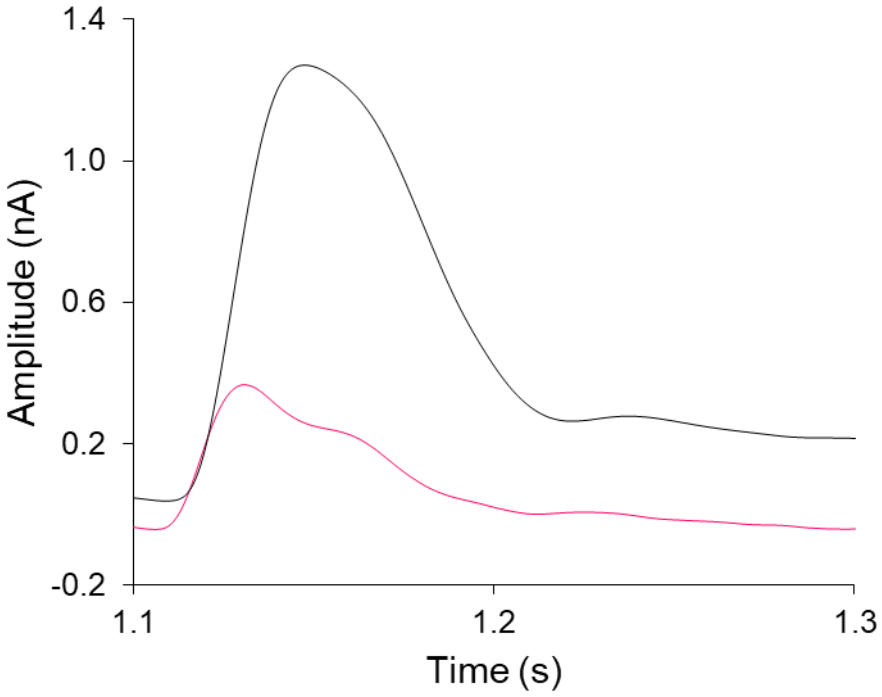

Figure 6.6 D_2O abolishes electrogenic activity of Rh50. Transient currents measured following a 200 mM ammonium pulse on sensors prepared with solutions containing either H_2O (black) or D_2O (magenta).

Chapter 7: References

Acharya, R., Carnevale, V., Fiorin, G., Levine, B. G., Polishchuk, A. L., Balannik, V., Samish, I., Lamb, R. A., Pinto, L. H., DeGrado, W. F. and Klein, M. L. (2010) 'Structure and mechanism of proton transport through the transmembrane tetrameric M2 protein bundle of the influenza A virus', *Proceedings of the National Academy of Sciences*, 107(34), pp. 15075–15080.

Andrade, S. L., Dickmanns, A., Ficner, R. and Einsle, O. (2005) 'Crystal structure of the archaeal ammonium transporter Amt-1 from *Archaeoglobus fulgidus*', *Proceedings of the National Academy of Sciences,*102(42), pp. 14994–9.

Andrade, S. L., Dickmanns, A., Ficner, R. and Einsle, O. (2005) 'Expression, purification and crystallization of the ammonium transporter Amt-1 from Archaeoglobus fulgidus', *Acta Crystallographica Section F: Structural Biology and Crystallization Communications*, 61(9), pp. 861–863.

Andrade, S. L., and Einsle, O. (2007) 'The Amt/Mep/Rh family of ammonium transport proteins.', *Molecular membrane biology*, 24(5–6), pp. 357–365.

Ariz, I., Boeckstaens, M., Gouveia, C., Martins, A. P., Sanz-Luque, E., Fernández, E., Soveral, G., von Wirén, N., Marini, A. M., Aparicio-Tejo, P. M. and Cruz, C. (2018) 'Nitrogen isotope signature evidences ammonium deprotonation as a common transport mechanism for the AMT-Mep-Rh protein superfamily', *Science Advances*, 4(9), pp. eaar3599.

Avent, N. D. and Reid, M. E. (2000) 'The Rh blood group system: a review.', *Blood*, 95(2), pp. 375–87.

Baconguis, I. and Gouaux, E. (2012) 'Structural plasticity and dynamic selectivity of acid-sensing ion channel-spider toxin complexes.', *Nature*, 489(7416), pp. 400–405.

Baday, S., Wang, S., Lamoureux, G. and Bernèche, S. (2013) 'Different Hydration Patterns in the Pores of AmtB and RhCG Could Determine Their Transport Mechanisms', *Biochemistry*, 52(40), pp. 7091–7098.

Bazzone, A., Barthmes, M. and Fendler, K. (2017) 'Chapter Two - SSM-Based Electrophysiology for Transporter Research', in Ziegler, C. B. T.-M. in E. (ed.) *A Structure-Function Toolbox for Membrane Transporter and Channels*. Academic Press, pp. 31–83.

Benko, P. V., Wood, T. C. and Segel, I. H. (1969) 'Multiplicity and regulation of amino acid transport in *Penicillium chrysogenum*', *Archives of Biochemistry and Biophysics*, 129(2), pp. 498–508.

van den Berg, B., Chembath, A., Jefferies, D., Basle, A., Khalid, S. and Rutherford, J. C. (2016) 'Structural basis for Mep2 ammonium transceptor activation by phosphorylation.', *Nature Communications*, 7(11337), pp. 1-10

Bertani, G. (1951) 'Studies on lysogenesis. I. The mode of phage liberation by lysogenic *Escherichia coli*.', *Journal of Bacteriology*, 62(3), pp. 293–300.

Biswas, K. and Morschhäuser, J. (2005) 'The Mep2p ammonium permease

controls nitrogen starvation-induced filamentous growth in *Candida albicans*', *Molecular Microbiology*, 56(3), pp. 649–669.

Biver, S., Belge, H., Bourgeois, S., Van Vooren, P., Nowik, M., Scohy, S., Houillier, P., Szpirer, J., Szpirer, C., Wagner, C. A., Devuyst, O. and Marini, A. M. (2008) 'A role for Rhesus factor Rhcg in renal ammonium excretion and male fertility.', *Nature*, 456(7220), pp. 339–343.

Blakey, D., Leech, A., Thomas, G. H., Coutts, G., Findlay, K. and Merrick, M. (2002) 'Purification of the *Escherichia coli* ammonium transporter AmtB reveals a trimeric stoichiometry', *Biochemical Journal*, 364(2), pp. 527–535.

Boeckstaens, M., André, B. and Marini, A. M. (2008) 'Distinct transport mechanisms in yeast ammonium transport/sensor proteins of the Mep/Amt/Rh family and impact on filamentation.', *The Journal of Biological Chemistry*, 283(31), pp. 21362–70.

Boogerd, F. C., Ma, H., Bruggeman, F. J., van Heeswijk, W. C., García-Contreras, R., Molenaar, D., Krab, K. and Westerhoff, H. V (2011) 'AmtB-mediated NH_3 transport in prokaryotes must be active and as a consequence regulation of transport by GlnK is mandatory to limit futile cycling of NH_4^+/NH_3', *FEBS Letters*, 585(1), pp. 23–28.

Bostick, D. L. and Brooks, C. L. (2007) 'On the equivalence point for ammonium (de)protonation during its transport through the AmtB channel.', *Biophysical journal*, 92(12), pp. L103-105.

Bourgeois, S., Bounoure, L., Mouro-Chanteloup, I., Colin, Y., Brown, D. and Wagner, C. A. (2018) 'The ammonia transporter RhCG modulates urinary acidification by interacting with the vacuolar proton-ATPases in renal intercalated cells', *Kidney International*, 93(2), pp. 390–402.

Brito, A. S., Neuhäuser, B., Wintjens, R., Marini, A. M. and Boeckstaens, M. (2020) 'Yeast filamentation signaling is connected to a specific substrate translocation mechanism of the Mep2 transceptor', *PLoS Genetics*, 16(2) pp.1-32

Britto, D. T. and Kronzucker, H. J. (2002) 'NH_4^+ toxicity in higher plants: a critical review', *Journal of Plant Physiology*, 159(6), pp. 567–584.

Bruce, L. J., Guizouarn, H., Burton, N. M., Gabillat, N., Poole, J., Flatt, J. F., Brady, R. L., Borgese, F., Delaunay, J. and Stewart, G. W. (2009) 'The monovalent cation leak in overhydrated stomatocytic red blood cells results from amino acid substitutions in the Rh-associated glycoprotein', *Blood*, 113(6), pp. 1350–7.

Burton, N. M. and Anstee, D. J. (2008) 'Structure, function and significance of Rh proteins in red cells.', *Current Opinion in Hematology*, 15(6), pp. 625–630.

Caner, T., Abdulnour-Nakhoul, S., Brown, K., Islam, M. T., Hamm, L. L. and Nakhoul, N. L. (2015) 'Mechanisms of ammonia and ammonium transport by rhesus-associated glycoproteins', *American Journal of Physiology. Cell physiology*. 309(11), pp. C747–C758.

Cartron, J.-P., Callebaut, I., Genetet, S., Le Van Kim, C., Zidi-Yahiaoui, N., Ripoche, P., Colin, Y. and Mouro-Chanteloup, I. (2009) ' Functional analysis of human RhCG: comparison with *E. coli* ammonium transporter reveals similarities in the pore and differences in the vestibule ', *American Journal of Physiology. Cell Physiology*, 297(3), pp. C537–C547.

Cherif-Zahar, B., Durand, A., Schmidt, I., Hamdaoui, N., Matic, I., Merrick, M. and Matassi, G. (2007) 'Evolution and functional characterization of the *RH50* gene from the ammonia-oxidizing bacterium *Nitrosomonas europaea*', *Journal of Bacteriology*, 189(24), pp. 9090–9100.

Conroy, M. J., Jamieson, S. J., Blakey, D., Kaufmann, T., Engel, A., Fotiadis, D., Merrick, M. and Bullough, P. A. (2004) 'Electron and atomic force microscopy of the trimeric ammonium transporter AmtB', *EMBO Reports*, 5(12), pp. 1153–1158.

Coutts, G., Thomas, G., Blakey, D. and Merrick, M. (2002) 'Membrane sequestration of the signal transduction protein GlnK by the ammonium transporter AmtB', *The EMBO Journal*, 21(4), pp. 536–545.

Durant, A. C. and Donini, A. (2019) 'Development of *Aedes aegypti* (Diptera: Culicidae) mosquito larvae in high ammonia sewage in septic tanks causes alterations in ammonia excretion, ammonia transporter expression, and osmoregulation', *Scientific Reports*, 9(1), pp. 1–17.

Elbing, K. and Brent, R. (2002) 'Media Preparation and Bacteriological Tools', *Current Protocols in Molecular Biology*, 59(1), pp. 111-117.

Eyers, S. A., Ridgwell, K., Mawby, W. J. and Tanner, M. J. (1994) 'Topology and organization of human Rh (rhesus) blood group-related polypeptides.', *The Journal of Biological Chemistry*, 269(9), pp. 6417–6423.

Ganz, P., Ijato, T., Porras-Murrilo, R., Stührwohldt, N., Ludewig, U. and Neuhäuser, B. (2020) 'A twin histidine motif is the core structure for high-affinity substrate selection in plant ammonium transporters.', *The Journal of Biological Chemistry*, 295(10), pp. 3362–3370.

Garvin, J. L., Burg, M. B. and Knepper, M. A. (1988) 'Active NH_4^+ absorption by the thick ascending limb.', *The American Journal of Physiology*, 255(2), pp. F57-65.

Gasteiger, E., Hoogland, C., Gattiker, A., Duvand, S., Wilkins, M. ., Appel, R. . and Bairoch, A. (2005) 'Protein Identifiction and Analysis Tools on the ExPASy Server', in Walker, J. M. (ed.) *The Proteomics Protocols Handbook*. Humana Press, pp. 571–607.

Genetet, S., Ripoche, P., Picot, J., Bigot, S., Delaunay, J., Armari-Alla, C., Colin, Y. and Mouro-Chanteloup, I. (2011) 'Human RhAG ammonia channel is impaired by the Phe65Ser mutation in overhydrated stomatocytic red cells', *American Journal of Physiology. Cell Physiology*, 302(2), pp. C419–C428

Ghane, T., Gorriz, R. F., Wrzalek, S., Volkenandt, S., Dalatieh, F., Reidelbach, M. and Imhof, P. (2018) 'Hydrogen-Bonded Network and Water Dynamics in

the D-channel of Cytochrome c Oxidase', *The Journal of Membrane Biology*, 251(3), pp. 299–314.

Gietz, D., St, A., Robin, J. and Schiestl, R. H. (1992) 'Improved Method for high efficiency transformation of intact yeast cells', *Nucleic Acids Research*, 20(6), pp. 1425–1425.

Gimeno, C. J., Ljungdahl, P. O., Styles, C. A. and Fink, G. R. (1992) 'Unipolar cell divisions in the yeast *S. cerevisiae* lead to filamentous growth: Regulation by starvation and *RAS*', *Cell*, 68(6), pp. 1077–1090.

Gruswitz, F., Chaudhary, S., Ho, J. D., Schlessinger, A., Pezeshki, B., Ho, C.-M., Sali, A., Westhoff, C. M. and Stroud, R. M. (2010) 'Function of human Rh based on structure of RhCG at 2.1 Å', *Proceedings of the National Academy of Sciences*, 107(21), pp. 9638–9643.

Häberle, J. (2011) 'Clinical practice: The management of hyperammonemia', *European Journal of Pediatrics*, 170(1), pp. 21–34.

Hackette, S. L., Skye, G. E., Burton, C. and Segel, I. H. (1970) 'Characterization of an ammonium transport system in filamentous fungi with methylammonium-14C as the substrate.', *Journal of Biological Chemistry*, 245(17), pp. 4241–4250.

Hadley, A. G. and Kumpel, B. M. (1993) 'The role of Rh antibodies in haemolytic disease of the newborn.', *Bailliere's Clinical Haematology*, 6(2), pp. 423–444.

Hall, J. A. and Kustu, S. (2011) 'The pivotal twin histidines and aromatic triad of the *Escherichia coli* ammonium channel AmtB can be replaced.', *Proceedings of the National Academy of Sciences*, 108(32), pp. 13270–13274.

Hall, J. A. and Yan, D. (2013) 'The Molecular Basis of K^+ Exclusion by the *Escherichia coli* Ammonium Channel AmtB', *Journal of Biological Chemistry*, 288(20), pp. 14080–14086.

Hanahan, D. (1985) 'DNA Cloning: A Practical Approach', in Glover, D. M. (ed.) *DNA Cloning: A Practical Approach*. McLean: IRL Press, p. 109.

van Heeswijk, W. C., Westerhoff, H. V., Hoving, S., Molenaar, D., Stegeman, B. and Kahn, D. (1996) 'An alternative P(II) protein in the regulation of glutamine synthetase in *Escherichia coli*', *Molecular Microbiology*, 21(1), pp. 133–146.

Helmstetter, F., Arnold, P., Höger, B., Petersen, L. M. and Beitz, E. (2019) 'Formate–nitrite transporters carrying nonprotonatable amide amino acids instead of a central histidine maintain pH-dependent transport', *Journal of Biological Chemistry*, 294(2), pp. 623–631.

Hess, D. C., Lu, W., Rabinowitz, J. D. and Botstein, D. (2006) 'Ammonium toxicity and potassium limitation in yeast', *PLoS Biology*, 4(11), pp. 2012–2023.

ten Hoopen, F., Cuin, T. A., Pedas, P., Hegelund, J. N., Shabala, S.,

Schjoerring, J. K. and Jahn, T. P. (2010) ‘Competition between uptake of ammonium and potassium in barley and *Arabidopsis* roots: molecular mechanisms and physiological consequences.’, *Journal of Experimental Botany*, 61(9), pp. 2303–2315.

Huang, C. H. and Peng, J. (2005) ‘Evolutionary conservation and diversification of Rh family genes and proteins’, *Proceedings of the National Academy of Sciences*, 102(43), pp. 15512–15517.

Ishikita, H. and Knapp, E. (2007) ‘Protonation States of Ammonia/Ammonium in the Hydrophobic Pore of Ammonia Transporter Protein AmtB’, 104(10), pp. 5374–5379.

Javelle, A., Severi, E., Thornton, J. and Merrick, M. (2004) ‘Ammonium sensing in *Escherichia coli*. Role of the ammonium transporter AmtB and AmtB-GlnK complex formation’, *Journal of Biological Chemistry*, 279(10), pp. 8530–8538.

Javelle, A., Lupo, D., Zheng, L., Li, X. D., Winkler, F. K. and Merrick, M. (2006) ‘An unusual twin-His arrangement in the pore of ammonia channels is essential for substrate conductance’, *Journal of Biological Chemistry*, 281(51), pp. 39492–39498.

Javelle, A., Lupo, D., Li, X. D., Merrick, M., Chami, M., Ripoche, P. and Winkler, F. K. (2007) ‘Structural and mechanistic aspects of Amt/Rh proteins’, *Journal of Structural Biology*, 158(3), pp. 472–481.

Javelle, A., Lupo, D., Ripoche, P., Fulford, T., Merrick, M. and Winkler, F. K. (2008) ‘Substrate binding, deprotonation, and selectivity at the periplasmic entrance of the *Escherichia coli* ammonia channel AmtB.’, *Proceedings of the National Academy of Sciences*, 105(13), pp. 5040–5045.

Khademi, S., O’Connell 3rd, J., Remis, J., Robles-Colmenares, Y., Miercke, L. J. and Stroud, R. M. (2004) ‘Mechanism of ammonia transport by Amt/MEP/Rh: structure of AmtB at 1.35 Å’, *Science*, 305(5690), pp. 1587–1594.

Kopec, W., Köpfer, D. A., Vickery, O. N., Bondarenko, A. S., Jansen, T. L. C., de Groot, B. L. and Zachariae, U. (2018) ‘Direct knock-on of desolvated ions governs strict ion selectivity in K^+ channels’, *Nature Chemistry*, 10(8), pp. 813–820.

Laemmli, U. K. (1970) ‘Cleavage of structural proteins during the assembly of the head of bacteriophage T4.’, *Nature*, 227(5259), pp. 680–685.

Lamoureux, G., Klein, M. L. and Bernèche, S. (2007) ‘A stable water chain in the hydrophobic pore of the AmtB ammonium transporter’, *Biophysical Journal*, 92(9), pp. 82–84.

Li, X., Jayachandran, S., Nguyen, H. H. T. and Chan, M. K. (2007) ‘Structure of the *Nitrosomonas europaea* Rh protein’, *Proceedings of the National Academy of Sciences* 104(49), pp. 19279–19284.

Liaw, S. H., Kuo, I. and Eisenberg, D. (1995) ‘Discovery of the ammonium

substrate site on glutamine synthetase, a third cation binding site.', *Protein Science : A Publication of the Protein Society*, 4(11), pp. 2358–2365.

Lin, Y., Cao, Z. and Mo, Y. (2009) 'The Functional Role of Asp160 and the Deprotonation Mechanism of Ammonium in the *Escherichia coli* Ammonia Channel Protein AmtB', *The Journal of Physical Chemistry*, 113(14), pp. 4922–4929.

Livingston, M. D., Bhargav, V. V., Turko, A. J., Wilson, J. M. and Wright, P. A. (2018) 'Widespread use of emersion and cutaneous ammonia excretion in Aplocheiloid killifishes', *Proceedings of the Royal Society B: Biological Sciences*, 285(1884).

Lo, H., Köhler, J. R., DiDomenico, B., Loebenberg, D., Cacciapuoti, A. and Fink, G. R. (2015) 'Nonfilamentous *C . albicans* Mutants Are Avirulent', 90, pp. 939–949.

Loqué, D., Mora, S. I., Andrade, S. L., Pantoja, O. and Frommer, W. B. (2009) 'Pore mutations in ammonium transporter AMT1 with increased electrogenic ammonium transport activity', *Journal of Biological Chemistry*, 284(37), pp. 24988–24995.

Lorenz, M. C. and Heitman, J. (1998) 'Regulators of pseudohyphal differentiation in Saccharomyces cerevisiae identified through multicopy suppressor analysis in ammonium permease mutant strains', *Genetics*, 150(4), pp. 1443–1457.

Lorenz, M. C. and Heitman, J. (1998) 'The MEP2 ammonium permease regulates pseudohyphal differentiation in *Saccharomyces cerevisiae*.', *The EMBO journal*, 17(5), pp. 1236–1247.

Lozano, M. and Cid, J. (2003) 'The clinical implications of platelet transfusions associated with ABO or Rh(D) incompatibility.', *Transfusion Medicine Reviews*, 17(1), pp. 57–68.

Ludewig, U., Von Wirén, N. and Frommer, W. B. (2002) 'Uniport of NH_4^+ by the root hair plasma membrane ammonium transporter *Le*AMT1;1', *Journal of Biological Chemistry*, 277(16), pp. 13548–13555.

Lupo, D., Li, X.-D., Durand, A., Tomizaki, T., Cherif-Zahar, B., Matassi, G., Merrick, M. and Winkler, F. K. (2007) 'The 1.3-Å resolution structure of *Nitrosomonas europaea* Rh50 and mechanistic implications for NH_3 transport by Rhesus family proteins', *Proceedings of the National Academy of Sciences*, 104(49), pp. 19303–19308.

Luzhkov, V. B., Almlof, M., Nervall, M. and Aqvist, J. (2006) 'Computational study of the binding affinity and selectivity of the bacterial ammonium transporter AmtB.', *Biochemistry*, 45(36), pp. 10807–10814.

Maresca, B. and Kobayashi, G. S. (1989) 'Dimorphism in *Histoplasma capsulatum* : a Model for the Study of Cell Differentiation in Pathogenic Fungi', *Microbiological Reviews*, 53(2), pp. 186–209.

Marini, A. M., Matassi, G., Raynal, V., Andre, B., Cartron, J. P. and Chérif-Zahar, B. (2000) 'The human Rhesus-associated RhAG protein and a kidney homologue promote ammonium transport in yeast', *Nature Genetics*, 26(3), pp. 341–344.

Marini, A. M., Urrestarazu, A., Beauwens, R. and André, B. (1997) 'The Rh (rhesus) blood group polypeptides are related to NH_4^+ transporters', *Trends in Biochemical Sciences*, 22(12), pp. 460–461.

Marini, A. M., Vissers, S., Urrestarazu, A. and André, B. (1994) 'Cloning and expression of the *MEP1* gene encoding an ammonium transporter in *Saccharomyces cerevisiae*', *The EMBO Journal*, 13(15), pp. 3456–3463.

Marini, A. M., Soussi-Boudekou, S., Vissers, S. and André, B. (1997) 'A family of ammonium transporters in *Saccharomyces cerevisiae*.', *Molecular and Cellular Biology*, 17(8), pp. 4282–4293.

Marini, A. M., Springael, J. Y., Frommer, W. B. and André, B. (2000) 'Cross-talk between ammonium transporters in yeast and interference by the soybean SAT1 protein', *Molecular Microbiology*, 35(2), pp. 378–385.

Marini, A. M., Boeckstaens, M., Benjelloun, F., Chérif-Zahar, B. and André, B. (2006) 'Structural involvement in substrate recognition of an essential aspartate residue conserved in Mep/Amt and Rh-type ammonium transporters', *Current Genetics*, 49(6), pp. 364–374.

Martinelle, K., Westlund, A. and Häggström, L. (1996) 'Ammonium ion transport - a cause of cell death', *Cytotechnology*, 22(251), pp. 251–254.

McDonald, T. R., Dietrich, F. S. and Lutzoni, F. (2012) 'Multiple horizontal gene transfers of ammonium transporters/ammonia permeases from prokaryotes to eukaryotes: Toward a new functional and evolutionary classification', *Molecular Biology and Evolution*, 29(1), pp. 51–60.

McDonald, T. R. and Ward, J. M. (2016) 'Evolution of Electrogenic Ammonium Transporters (AMTs)', *Frontiers in Plant Science*, 7(352), pp. 1-9.

Mirandela, G. D., Tamburrino, G., Hoskisson, P. A., Zachariae, U. and Javelle, A. (2019) 'The lipid environment determines the activity of the Escherichia coli ammonium transporter AmtB', *FASEB Journal :*, 33(2), pp. 1989–1999.

Miroux, B. and Walker, J. E. (1996) 'Over-production of proteins in *Escherichia coli*: mutant hosts that allow synthesis of some membrane proteins and globular proteins at high levels.', *Journal of Molecular Biology*, 260(3), pp. 289–298.

Mouro-Chanteloup, I., Cochet, S., Chami, M., Genetet, S., Zidi-Yahiaoui, N., Engel, A., Colin, Y., Bertrand, O. and Ripoche, P. (2010) 'Functional reconstitution into liposomes of purified human RhCG ammonia channel.', *PloS One*, 5(1), p. e8921.

Mumberg, D., Müller, R. and Funk, M. (2012) 'Regulatable promoters of *Saccharomyces cerevisiae*: comparison of transcriptional activity and their use

for heterologous expression', *Nucleic Acids Research*, 22(25), pp. 5767–5768.

Nakhoul, N. L., DeJong, H., Abdulnour-Nakhoul, S. M., Boulpaep, E. L., Herring-Smith, K. and Hamm, L. L. (2004) 'Characteristics of renal Rhbg as an NH_4^+ transporter', *Amercian Journal of Physiology: Renal Physiology*, 288(1), pp. F170–F181.

Nakhoul, N. L. and Hamm, L. L. (2004) 'Non-erythroid Rh glycoproteins: A putative new family of mammalian ammonium transporters', *European Journal of Physiology*, 447(5), pp. 807–812.

Neuhäuser, B., Dynowski, M., Mayer, M. and Ludewig, U. (2007) 'Regulation of NH_4^+ Transport by Essential Cross Talk between AMT Monomers through the Carboxyl Tails', *Plant Physiology*, 143(4), pp. 1651–1659.

Neuhäuser, B., Dynowski, M. and Ludewig, U. (2009) 'Channel-like NH_3 flux by ammonium transporter *At*AMT2.', *FEBS letters*, 583(17), pp. 2833–2838.

Neuhäuser, B., Dynowski, M. and Ludewig, U. (2014) 'Switching substrate specificity of AMT/MEP/ Rh proteins', *Channels*, 8(6), pp. 496–502.

Ninnemann, O., Jauniaux, J. C. and Frommer, W. B. (1994) 'Identification of a high affinity NH_4^+ transporter from plants.', *The EMBO journal*, 13(15), pp. 3464–3471.

Pearce, N. M., Krojer, T., Bradley, A. R., Collins, P., Nowak, R. P., Talon, R., Marsden, B. D., Kelm, S., Shi, J., Deane, C. M. and von Delft, F. (2017) 'A multi-crystal method for extracting obscured crystallographic states from conventionally uninterpretable electron density', *Nature Communications*, 8(1), p. 15123.

Pedro-Roig, L., Lange, C., Bonete, M. J., Soppa, J. and Maupin-Furlow, J. (2013) 'Nitrogen regulation of protein-protein interactions and transcript levels of GlnK PII regulator and AmtB ammonium transporter homologs in Archaea', *Microbiologyopen*, 2(5), pp. 826–840.

Pflüger, T., Hernández, C. F., Lewe, P., Frank, F., Mertens, H., Svergun, D., Baumstark, M. W., Lunin, V. Y., Jetten, M. S. M. and Andrade, S. L. (2018) 'Signaling ammonium across membranes through an ammonium sensor histidine kinase', *Nature Communications*, 9(1), pp. 1–11.

Pitts, R. J., Derryberry, S. L., Pulous, F. E. and Zwiebel, L. J. (2014) 'Antennal-Expressed Ammonium Transporters in the Malaria Vector Mosquito *Anopheles gambiae*', *PLoS One*, 9(10), pp. 1-11

Pomès, R. and Roux, B. (2002) 'Molecular mechanism of H^+ conduction in the single-file water chain of the gramicidin channel.', *Biophysical Journal*, 82(5), pp. 2304–2316.

Rath, A., Glibowicka, M., Nadeau, V. G., Chen, G. and Deber, C. M. (2009) 'Detergent binding explains anomalous SDS-PAGE migration of membrane proteins', *Proceedings of the National Academy of Sciences*, 106(6), pp. 1760 LP – 1765.

Reitzer, L. (2003) ‘Nitrogen Assimilation and Global Regulation in *Escherichia coli*’, *Annual Review of Microbiology*, 57(1), pp. 155–176.

Rentsch, D., Laloi, M., Rouhara, I., Schmelzer, E., Delrot, S. and Frommer, W. B. (1995) ‘*NTR1* encodes a high affinity oligopeptide transporter in *Arabidopsis*’, *FEBS Letters*, 370(3), pp. 264–268.

Ripoche, P., Bertrand, O., Gane, P., Birkenmeier, C., Colin, Y. and Cartron, J.-P. (2004) ‘Human Rhesus-associated glycoprotein mediates facilitated transport of NH_3 into red blood cells.’, *Proceedings of the National Academy of Sciences*, 101(49), pp. 17222–17227.

Roon, R. J., Even, H. L., Dunlop, P. and Larimore, F. L. (1975) ‘Methylamine and ammonia transport in *Saccharomyces cerevisiae*’, *Journal of Bacteriology*, 122(2), pp. 502–503.

Rutherford, J. C., Lin, X., Nielsen, K. and Heitman, J. (2008) ‘Amt2 permease is required to induce ammonium-responsive invasive growth and mating in *Cryptococcus neoformans*.’, *Eukaryotic cell*, 7(2), pp. 237–246.

Shannon, R. D. (1976) ‘Revised effective ionic radii and systematic studies of interatomic distances in halides and chalcogenides’, *Acta Crystallographica Section A*, 32(5), pp. 751–767.

Sidey, V. (2016) ‘On the effective ionic radii for ammonium.’, *Acta crystallographica Section B, Structural science, crystal engineering and materials*, 72(Pt 4), pp. 626–633.

Siewe, R. M., Weil, B., Burkovski, A., Eikmanns, B. J., Eikmanns, M. and Krämer, R. (1996) ‘Functional and genetic characterization of the (methyl) ammonium uptake carrier of *Corynebacterium glutamicum*’, *Journal of Biological Chemistry*, 271(10), pp. 5398–5403.

Soupene, E., Lee, H. and Kustu, S. (2002) ‘Ammonium/methylammonium transport (Amt) proteins facilitate diffusion of NH_3 bidirectionally’, *Proceedings of the National Academy of Sciences*, 99(6), pp. 3926–3931.

Studier, F. W. (2005) ‘Protein production by auto-induction in high density shaking cultures.’, *Protein expression and purification*, 41(1), pp. 207–234.

Thomas, G. H. and Mullins, J. G. L. (2000) ‘Membrane topology of the Mep/Amt family of ammonium transporters’, *Molecular Microbiology*, 37, pp. 331–344.

Tremblay, P. L. and Hallenbeck, P. C. (2009) ‘Of blood, brains and bacteria, the Amt/Rh transporter family: Emerging role of Amt as a unique microbial sensor’, *Molecular Microbiology*, 71(1), pp. 12–22.

Verhamme, D. T., Prosser, J. I. and Nicol, G. W. (2011) ‘Ammonia concentration determines differential growth of ammonia-oxidising archaea and bacteria in soil microcosms’, *ISME Journal*, 5(6), pp. 1067–1071.

Verma, R., Holmans, P., Knowles, J. A., Grover, D., Evgrafov, O. V, Crowe, R. R., Scheftner, W. A., Weissman, M. M., DePaulo, J. R., Potash, J. B. and

Levinson, D. F. (2008) ‘Linkage disequilibrium mapping of a chromosome 15q25-26 major depression linkage region and sequencing of *NTRK3*.’, *Biological psychiatry*, 63(12), pp. 1185–9.

Wacker, T., Garcia-Celma, J. J., Lewe, P. and Andrade, S. L. (2014) ‘Direct observation of electrogenic NH_4^+ transport in ammonium transport (Amt) proteins’, *Proceedings of the National Academy of Sciences*, 111(27), pp. 9995–10000.

Wang, J., Fulford, T., Shao, Q., Javelle, A., Yang, H., Zhu, W. and Merrick, M. (2013) ‘Ammonium Transport Proteins with Changes in One of the Conserved Pore Histidines Have Different Performance in Ammonia and Methylamine Conduction’, *PLoS ONE*, 8(5), p. e62745.

Wang, L., Lai, L., Ouyang, Q. and Tang, C. (2011) ‘Flux Balance Analysis of Ammonia Assimilation Network in *E. coli* Predicts Preferred Regulation Point’, *PLoS ONE*, 6(1), p. e16362.

Wang, S., Orabi, E. A., Baday, S., Bernèche, S. and Lamoureux, G. (2012) ‘Ammonium transporters achieve charge transfer by fragmenting their substrate’, *Journal of the American Chemical Society*, 134(25), pp. 10419–10427.

Westhoff, C. M., Ferreri-Jacobia, M., Mak, D. O. D. and Kevin Foskett, J. (2002) ‘Identification of the erythrocyte Rh blood group glycoprotein as a mammalian ammonium transporter’, *Journal of Biological Chemistry*, 277(15), pp. 12499–12502.

Wiechert, M. and Beitz, E. (2017) ‘Mechanism of formate–nitrite transporters by dielectric shift of substrate acidity’, *The EMBO Journal*, 36(7), pp. 949–958.

Williamson, G., Tamburrino, G., Bizior, A., Boeckstaens, M., Dias Mirandela, G., Bage, M., Pisliakov, A., Ives, C. M., Terras, E., Hoskisson, P. A., Marini, A.-M., Zachariae, U. and Javelle, A. (2020) ‘A two-lane mechanism for selective biological ammonium transport’, *eLife*, 9, pp. e57183.

Winkler, F. K. (2006) ‘Amt/MEP/Rh proteins conduct ammonia’, *European Journal of Physiology*, 450, pp. 701–707.

von Wirén, N. and Merrick, M. (2004) ‘Regulation and function of ammonium carriers in bacteria, fungi, and plants’, in *Molecular Mechanisms Controlling Transmembrane Transport*. Berlin, Heidelberg: Springer Berlin Heidelberg, pp. 95–120.

Wraight, C. A. (2006) ‘Chance and design-Proton transfer in water, channels and bioenergetic proteins’, *Biochimica et Biophysica Acta - Bioenergetics*, 1757(8), pp. 886–912.

Zheng, L., Kostrewa, D., Bernèche, S., Winkler, F. K. and Li, X. D. (2004) ‘The mechanism of ammonia transport based on the crystal structure of AmtB of *Escherichia coli*’, *Proceedings of the National Academy of Sciences*, 101(49), pp. 17090–17095.

Zhou, Y., Morais-Cabral, J. H., Kaufman, A. and MacKinnon, R. (2001) ‘Chemistry of ion coordination and hydration revealed by a K^+ channel-Fab complex at 2.0 Å resolution.’, *Nature*, 414(6859), pp. 43–48.

Appendices

Appendix A: Publication 1

'A two-lane mechanism for selective biological ammonium transport’

RESEARCH ARTICLE

A two-lane mechanism for selective biological ammonium transport

Gordon Williamson[1†], Giulia Tamburrino[2,3†], Adriana Bizior[1†], Mélanie Boeckstaens[4†], Gaëtan Dias Mirandela[1‡], Marcus G Bage[2,3], Andrei Pisliakov[2,3], Callum M Ives[2], Eilidh Terras[1], Paul A Hoskisson[1], Anna Maria Marini[4], Ulrich Zachariae[2,3]*, Arnaud Javelle[1]*

[1]Strathclyde Institute of Pharmacy and Biomedical Sciences, University of Strathclyde, Glasgow, United Kingdom; [2]Computational Biology, School of Life Sciences, University of Dundee, Dundee, United Kingdom; [3]Physics, School of Science and Engineering, University of Dundee, Dundee, United Kingdom; [4]Biology of Membrane Transport Laboratory, Department of Molecular Biology, Université Libre de Bruxelles, Gosselies, Belgium

Abstract The transport of charged molecules across biological membranes faces the dual problem of accommodating charges in a highly hydrophobic environment while maintaining selective substrate translocation. This has been the subject of a particular controversy for the exchange of ammonium across cellular membranes, an essential process in all domains of life. Ammonium transport is mediated by the ubiquitous Amt/Mep/Rh transporters that includes the human Rhesus factors. Here, using a combination of electrophysiology, yeast functional complementation and extended molecular dynamics simulations, we reveal a unique two-lane pathway for electrogenic NH_4^+ transport in two archetypal members of the family, the transporters AmtB from *Escherichia coli* and Rh50 from *Nitrosomonas europaea*. The pathway underpins a mechanism by which charged H^+ and neutral NH_3 are carried separately across the membrane after NH_4^+ deprotonation. This mechanism defines a new principle of achieving transport selectivity against competing ions in a biological transport process.

***For correspondence:**
u.zachariae@dundee.ac.uk (UZ);
arnaud.javelle@strath.ac.uk (AJ)

[†]These authors contributed equally to this work

Present address: [‡]Wellcome Trust Centre for Cell Biology, Michael Swann Building, The King's Buildings, University of Edinburgh, Edinburgh, United Kingdom

Competing interests: The authors declare that no competing interests exist.

Funding: See page 18

Received: 24 March 2020
Accepted: 13 July 2020
Published: 14 July 2020

Reviewing editor: Nir Ben-Tal, Tel Aviv University, Israel

Introduction

The transport of ammonium across cell membranes is a fundamental biological process in all domains of life. Ammonium exchange is mediated by the ubiquitous ammonium transporter/methyl-ammonium-ammonium permease/Rhesus (Amt/Mep/Rh) protein family. The major role of bacterial, fungal, and plant Amt/Mep proteins is to scavenge ammonium for biosynthetic assimilation, whereas mammals are thought to produce Rh proteins in erythrocytes, kidney, and liver cells for detoxification purposes and to maintain pH homeostasis (***Biver et al., 2008***; ***Huang and Ye, 2010***). In humans, Rh mutations are linked to pathologies that include inherited hemolytic anemia, stomatocytosis, and early-onset depressive disorder (***Huang and Ye, 2010***). Despite this key general and biomedical importance, so far, no consensus on the pathway and mechanism of biological ammonium transport has been reached.

High-resolution structures available for several Amt, Mep and Rh proteins show a strongly hydrophobic pore leading towards the cytoplasm (***Andrade et al., 2005***; ***Gruswitz et al., 2010***; ***Khademi et al., 2004***; ***Lupo et al., 2007***; ***van den Berg et al., 2016***). This observation led to the conclusion that the species translocated through Amt/Mep/Rh proteins is neutral NH_3. However, this view has been experimentally challenged, first for some plant Amt proteins (***Ludewig et al., 2002***; ***Mayer et al., 2006***; ***McDonald and Ward, 2016***; ***Neuhäuser et al., 2014***), followed by further *in-vitro* studies revealing that the activity of bacterial Amt proteins is electrogenic (***Mirandela et al.,***

2019; Wacker et al., 2014). Taken together, these findings renewed a long-standing debate on the mechanism by which a charged molecule is translocated through a hydrophobic pore and how selectivity for NH_4^+ over competing ions is achieved.

Here, we reveal the pathways, mechanism, and key determinants of selectivity of electrogenic ammonium transport in Amt and Rh proteins, unifying the diverse observations that led to these seemingly incompatible suggestions. The transport mechanism is underpinned by the separate transfer of H^+ and NH_3 on a unique two-lane pathway following NH_4^+ sequestration and deprotonation. This mechanism ensures that ammonium – which occurs mainly in protonated form in the aqueous phase – is efficiently translocated across the membrane, while maintaining strict selectivity against K^+, a monovalent cation of similar size. This previously unobserved principle is likely to form a new paradigm for the electrogenic members of the Amt/Mep/Rh family. Similar mechanisms may be utilized by other membrane transporters to facilitate the selective translocation of pH-sensitive molecules.

Results and discussion

AmtB and NeRh50 activity is electrogenic

Motivated by our finding that the activity of *Escherichia coli* AmtB is electrogenic (Mirandela et al., 2019), we first investigated the transport mechanism of the Rh50 protein from *Nitrosomonas europaea* (NeRh50). Rh and Amt proteins are distant homologs, and thus a functional distinction between both subfamilies has been proposed (Huang and Ye, 2010). The architecture of NeRh50 is highly representative of Rh proteins (Gruswitz et al., 2010; Lupo et al., 2007) which have been repeatedly reported to serve as electroneutral NH_3 or CO_2 gas channels (Cherif-Zahar et al., 2007; Hub et al., 2010a; Li et al., 2007; Lupo et al., 2007; Weidinger et al., 2007). The activity of purified NeRh50 reconstituted into liposomes was quantified using Solid-Supported Membrane Electrophysiology (SSME) (Bazzone et al., 2017) experiments, where we recorded a NH_4^+-selective current (Figure 1) with a decay rate that is strongly dependent on the lipid-to-protein ratio (LPR; Table 1, Figure 1—figure supplement 1). Expressed in a *Saccharomyces cerevisiae* triple-mepΔ strain, deprived of its three endogenous Mep ammonium transporters, NeRh50 complemented the growth defect on minimal medium containing ammonium as sole nitrogen source (Figure 1). The electrogenic transport activity observed for NeRh50 and AmtB may suggest a common transport mechanism amongst the distant Amt and Rh proteins, but more experiments are needed to conclusively confirm this. Also, the NH_4^+ selectivity of both transporters further highlighted the question of how these proteins achieve selective charge translocation through their hydrophobic pore.

Two interconnected water wires form an H^+ translocation pathway in AmtB

We next made use of the most substantive body of structural information available for the archetypal ammonium transporter AmtB from *E. coli* and its variants to decipher the molecular mechanism of electrogenic NH_4^+ transport (Dias Mirandela et al., 2018). Computational (Wang et al., 2012) and experimental studies (Ariz et al., 2018) have suggested that deprotonation of NH_4^+ is likely to be a major step in ammonium transport. We therefore aimed to identify dynamic polar networks across AmtB that could form a transfer pathway through the protein for the translocation of H^+, coming from NH_4^+ deprotonation. AmtB forms homotrimers in the cytoplasmic membrane, in which each monomer exhibits a potential periplasmic NH_4^+ binding region (S1) near residue D160, followed by a strongly hydrophobic pore leading towards the cytoplasm (Figure 2A; Khademi et al., 2004). Two highly conserved histidine residues, H168 and H318, protrude into the lumen, forming the family's characteristic 'twin-His' motif (Javelle et al., 2006). The only variation in the twin-His motif in members of the Amt/Mep/Rh family is in numerous fungal Mep transporters where the first His, corresponding to H168, is replaced by a Glu (Javelle et al., 2006). The general conservation pattern in the AmtB pore, as analysed with ConSurf (Ashkenazy et al., 2016), is shown in Figure 2—figure supplement 1.

To locate potential polar transfer routes, we performed atomistic molecular dynamics (MD) simulations of AmtB in mixed lipid bilayers. The simulations initially showed hydration of part of the putative hydrophobic NH_3 pathway from the twin-His motif to the cytoplasm (cytoplasmic water wire –

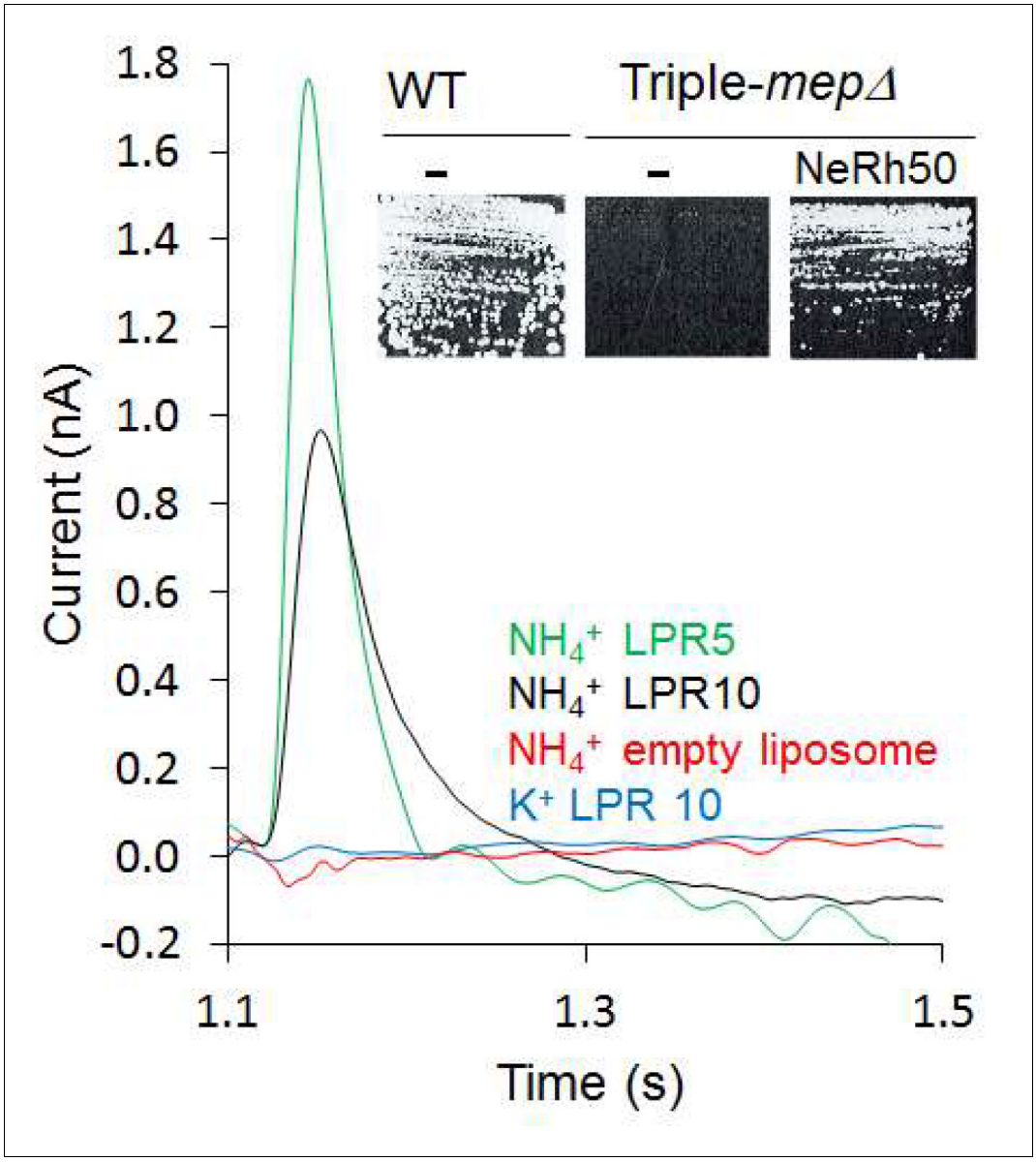

Figure 1. Characterization of the activity of NeRh50. Transient current measured using SSME after a 200 mM pulse (ammonium or potassium). *Insert:* Yeast complementation by NeRh50 (strain 31019b, *mep1Δ mep2Δ mep3Δ ura3*) on minimal medium supplemented with 3 mM ammonium as sole nitrogen source.
The online version of this article includes the following source data and figure supplement(s) for figure 1:

Source data 1. Characterization of the activity of NeRh50.
Figure supplement 1. Characterization of the activity of NeRh50.

CWW; ***Figure 2A***), confirming previous observations (***Lamoureux et al., 2007***). Notably, a new observation we made over longer simulation timescales is the presence of a previously unidentified second water-filled channel (periplasmic water wire - PWW). The PWW spans from residue D160 near the S1 region to the central twin-His motif (***Figure 2A***) and is formed both in simulations without and with applied membrane voltage V_m (***Figure 2A*** - ***Figure 2—figure supplement 2***; V_m in *E. coli* ~ −140 mV [***Felle et al., 1980***]).

As the protonation pattern of the twin-His motif has been found to play a role in the hydration of the protein (***Ishikita and Knapp, 2007***), two different tautomeric states of the twin-His motif were systematically probed in the simulations. The tautomeric state in which H168 is protonated on its N_δ and H318 is protonated on its N_ε atom is referred to as 'DE', while 'ED' terms the twin-His

Table 1. Decay time constants (s^{-1}) of transient currents triggered after an ammonium or potassium pulse of 200 mM in proteoliposomes containing AmtB at various LPR*.

	NH_4^+		K^+	
Variant	**LPR 10**	**LPR 5**	**LPR 10**	**LPR 5**
AmtB-WT	13.4 ± 1.5	18.7 ± 1.0	NC	NC
D160A	21.6 ± 1.2	24.3 ± 1.5	NC	NC
D160E	17.03 ± 2.84	19.53 ± 1.8	NC	NC
H168A H318A	29.5 ± 2.1	29.8 ± 2.6	NC	NC
S219A H168A H318A	NC	NC	NC	NC
H168A	28.3 ± 1.5	38.0 ± 1.0	2.7 ± 0.5	5.2 ± 1.0
H318A	22.56 ± 2.63	28.25 ± 3.1	10.07 ± 1.7	15.64 ± 2.1
NeRh50	24.0 ± 1.7	39.0 ± 3.6	NC	NC

*NC: No transient current recorded.

The online version of this article includes the following source data for Table 1:

Source data 1. Decay time constants (s^{-1}) of transient currents triggered after an ammonium or potassium pulse of 200 mM measured by SSME.

configuration where H168 is protonated on N_ε and H318 is protonated on N_δ (***Figure 2A***- ***Figure 2—figure supplement 2***, ***3***, ***4***). Formation of the CWW is observed to occur within a few nanoseconds at the beginning of each simulation. In the DE tautomeric state, the cytoplasmic pocket of each subunit almost continuously remains occupied by 3–4 water molecules for the rest of the simulation (***Figure 2A*** - ***Figure 2—figure supplement 2***, ***3***, ***4***; data for 0 mV membrane voltage). In the ED state, greater fluctuations in the number of water molecules in the chain are seen, and the average occupancy is decreased. Using a cut-off value of three water molecules per subunit, a complete water chain is present during 79% of the simulations in the DE state, and only during 12% of the simulated time in the ED state. The PWW is generally more transiently occupied than the cytoplasmic channel; however, we record up to 23% occupancy with at least three water molecules when the histidine sidechains are in the ED tautomeric state (***Figure 2A*** - ***Figure 2—figure supplement 2***, ***3***, ***4***).

Both water wires are connected via the twin-His motif, which bridges the aqueous chains, while preventing the formation of a continuous water channel in the simulations. Although neither the CWW nor the PWW are sufficiently wide to allow the transfer of solvated NH_4^+, water molecules and histidine side chains could serve as efficient pathways to facilitate proton transfer in proteins (***Acharya et al., 2010***). As shown in ***Figure 2—figure supplement 1***, the key residues that line both water wires in AmtB are highly conserved in the family.

The interconnected water wires are functionally essential to AmtB activity

To experimentally test if the water wires are essential for proton conduction during the AmtB transport cycle, we made use of the reduced deuteron mobility of heavy water D_2O. Because deuterons have twice the mass of a proton and the bond strength is increased, the deuteron mobility is reduced by 30% for each D_2O molecule compared to normal water (***Wiechert and Beitz, 2017***). Since the polar network of water we identified involves more than three water molecules (***Figure 2A***), AmtB should be nearly inactive if tested in the presence of D_2O. Indeed, we found that in an SSME-based assay where all buffers used to prepare the proteoliposomes and SSM sensors were made using D_2O, AmtB activity was completely abolished compared to buffer containing water (***Figure 2B***). After rinsing the sensor prepared in D_2O with water, AmtB re-gained 100% of its activity measured by SSME, showing that the presence of D_2O did not affect the protein itself or the integrity of the proteoliposomes (***Figure 2B***). Further calculations suggested that H^+ transfer between the water molecules is possible both within the PWW and CWW and could occur with high rates (the highest energy barrier is ~18 kJ/mol in the cytoplasmic wire near the twin-His motif; ***Table 2***). Taken together, the experimental and computational data suggest that proton transfer between water

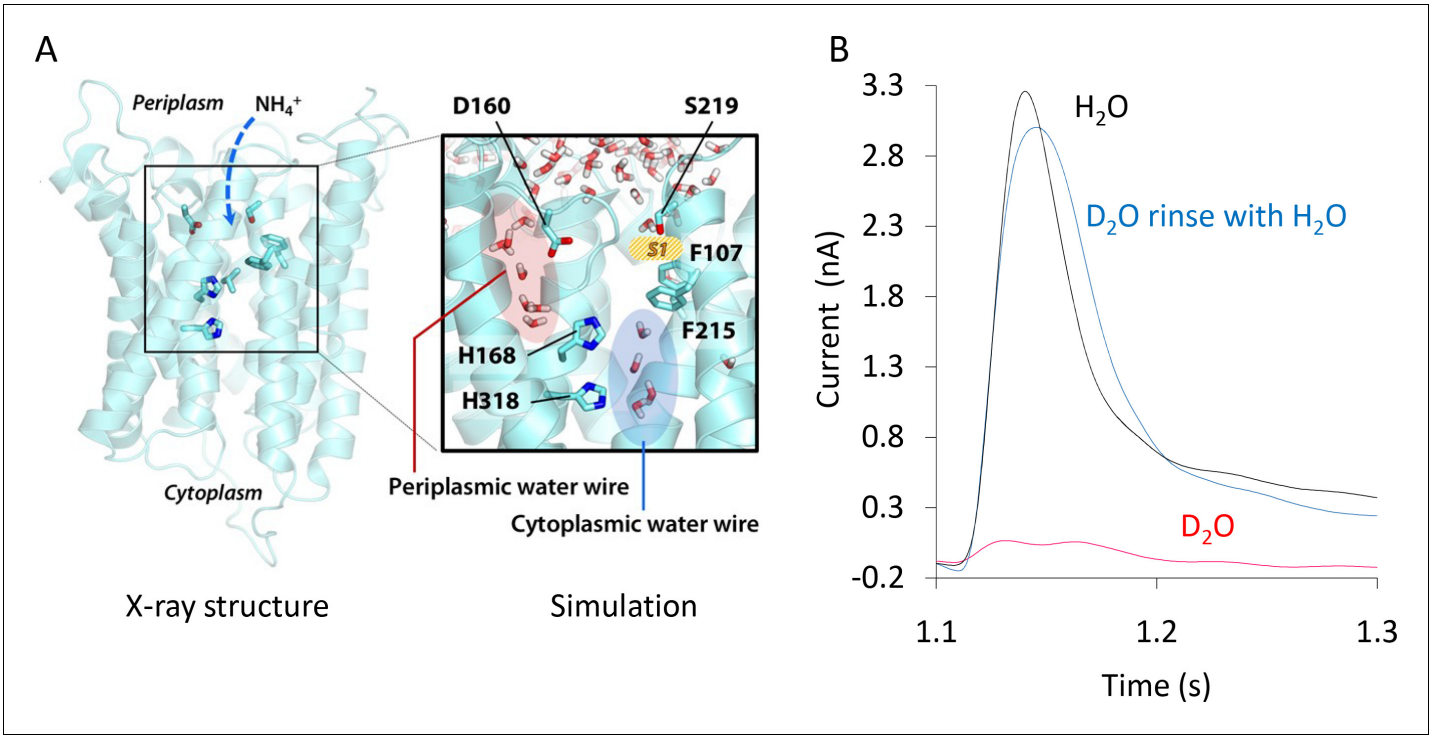

Figure 2. Formation and functionality of the periplasmic (PWW) and cytoplasmic (CWW) water wires in AmtB. (**A**) Extended atomistic simulations show a hydration pattern across the protein, in which cytoplasmic and periplasmic water wires, connected via H168, form a continuous pathway for proton transfer from the S1 NH_4^+ sequestration region to the cytoplasm. (**B**) Transient currents measured following a 200 mM ammonium pulse on sensors prepared with solutions containing either H_2O (black) or D_2O (red). D_2O sensors were rinsed with H_2O solutions and subsequently exposed to another 200 mM ammonium pulse (blue).

The online version of this article includes the following source data and figure supplement(s) for figure 2:

Source data 1. Functionality of the periplasmic (PWW) and cytoplasmic (CWW) water wires in AmtB.
Figure supplement 1. Evolutionary conservation of the proton and hydrophobic pathways for H^+ and NH_3 translocation in AmtB.
Figure supplement 2. Evolution and occupancy of the Periplasmic Water Wire (PWW).
Figure supplement 3. Evolution and occupancy of the Cytoplasmic Water Wire (CWW).
Figure supplement 4. The DE and ED twin-His motif configurations.

molecules, most likely the PWW and CWW detected in the simulations, may underpin the electrogenic activity of AmtB.

AmtB activity is not driven by the proton motive force

In the absence of ammonium, a proton pulse did not trigger a discernible current and additionally, in the presence of ammonium, an inward-orientated pH gradient did not increase AmtB activity (***Figure 3***). These findings suggest that there is no H^+-dependent symport activity of AmtB, showing instead that AmtB is not able to translocate a proton in the absence of NH_4^+, and indicating that the current induced by AmtB activity is generated by specific deprotonation of the substrate and subsequent H^+ translocation. Furthermore, they show that AmtB cannot act as an uncoupler, which raises the question of proton selectivity and the coupling between NH_3 and H^+ transfer (***Boogerd et al., 2011***; ***Maeda et al., 2019***). Our current data suggest that the PWW is transiently occupied and that its occupancy is strongly dependent on the particular state and conformation of D160, since even a D to E conservative change abolished presence of the PWW (***Figure 4A***). Any disruption of the PWW will, in turn, impede the capability of AmtB to transfer H^+. The functionally relevant conformation and protonation state of D160 that stabilize the PWW is likely to be coupled to the presence of a charged substrate binding near S1, thereby linking substrate binding and deprotonation to H^+ transfer.

Table 2. Free energies for proton translocation through the cytoplasmic and periplasmic water wires and neighboring water molecules (bulk)*.

			Z (Å)	Free energy (kJ/mol)
(bulk)	Peripl. water wire	wat1	14.7	0.0
		wat2	12.7	8.7
		wat3	10.7	15.0
		wat4	8.3	14.4
		wat5	6.1	7.5
D160		wat6	5.4	11.0
		wat7	3.2	14.4
		wat8	0.6	18.5
H168				
	cytopl. water wire	wat9	−0.4	17.3
		wat10	−0.8	14.4
		wat11	−3.2	12.1
H318		wat12	−5.1	13.8

*The vertical coordinate z was calculated relative to the position of the sidechain of H168. Positions of the sidechains of D160, H168 and H318 with respect to the periplasmic and cytoplasmic water wires are indicated in the left column.

The residue D160 is essential to stabilize the PWW

As the PWW is formed near the sidechain of D160, an invariant residue in the Amt/Mep/Rh superfamily (***Marini et al., 2006***; ***Thomas et al., 2000***), we further investigated the role of this residue in ensuring PWW and CWW stability by simulating the AmtB D160A and D160E mutants. Both mutants were stable on the time scale of our simulations and we did not detect major rearrangements in the protein. Moreover, all the elution profiles of the purified WT and variants proteins obtained by analytical size exclusion chromatography, before and after solubilization of the proteoliposomes in 2% DDM, were identical, showing a single monodisperse peak eluting between 10.4–10.6 ml (***Figure 4—figure supplement 1***). Taken together, these results suggest that major structural re-arrangements in the mutants are unlikely to occur. The simulations revealed no difference in the formation of the CWW in the D160A and D160E variants compared to the WT, however the formation of the PWW is almost completely abolished in the presence of these mutations (***Figure 4A***).

We then expressed wild-type AmtB as well as the D160A and D160E mutants in *S. cerevisiae* triple-*mep*Δ. Using ammonium as the sole nitrogen source, we found that cells expressing the mutants failed to grow, showing that $AmtB^{D160A}$ or $AmtB^{D160E}$ are unable to replace the function of the endogenous Mep transporters (***Figure 4B***).

The activity of the purified variants reconstituted into liposomes was next quantified using SSME. Electrogenic transport activity, triggered by a 200 mM ammonium pulse, led to a transient current with a maximum amplitude of 3.38 nA in AmtB, while $AmtB^{D160A}$ and $AmtB^{D160E}$ displayed reduced maximum currents of 0.63 nA and 1.42 nA respectively (***Figure 4B***, ***Figure 4—figure supplement 2***). Importantly, the lifetime of currents in both variants was unaffected by changes in liposomal LPR, and therefore the small transient current accounts for the binding of a NH_4^+ to the proteins and not a full translocation cycle (***Table 1***, ***Figure 4—figure supplement 2***; ***Bazzone et al., 2017***). Additionally, it was impossible to determine with confidence a catalytic constant (K_m) for both variants since no clear saturation was reached, even after an ammonium pulse of 200 mM (***Figure 4C***). These results thus demonstrate that $AmtB^{D160A}$ and $AmtB^{D160E}$ are transport-deficient. Our data show that residue D160 plays a central role in the transport mechanism as opposed to having a strictly structural role as previously suggested (***Khademi et al., 2004***). Moreover, the fact that the conservative D to E variation at position 160 impairs ammonium transport via AmtB indicates that D160 does not only show electrostatic interaction with NH_4^+ at the S1 site but is also involved in the translocation mechanism by stabilizing the PWW.

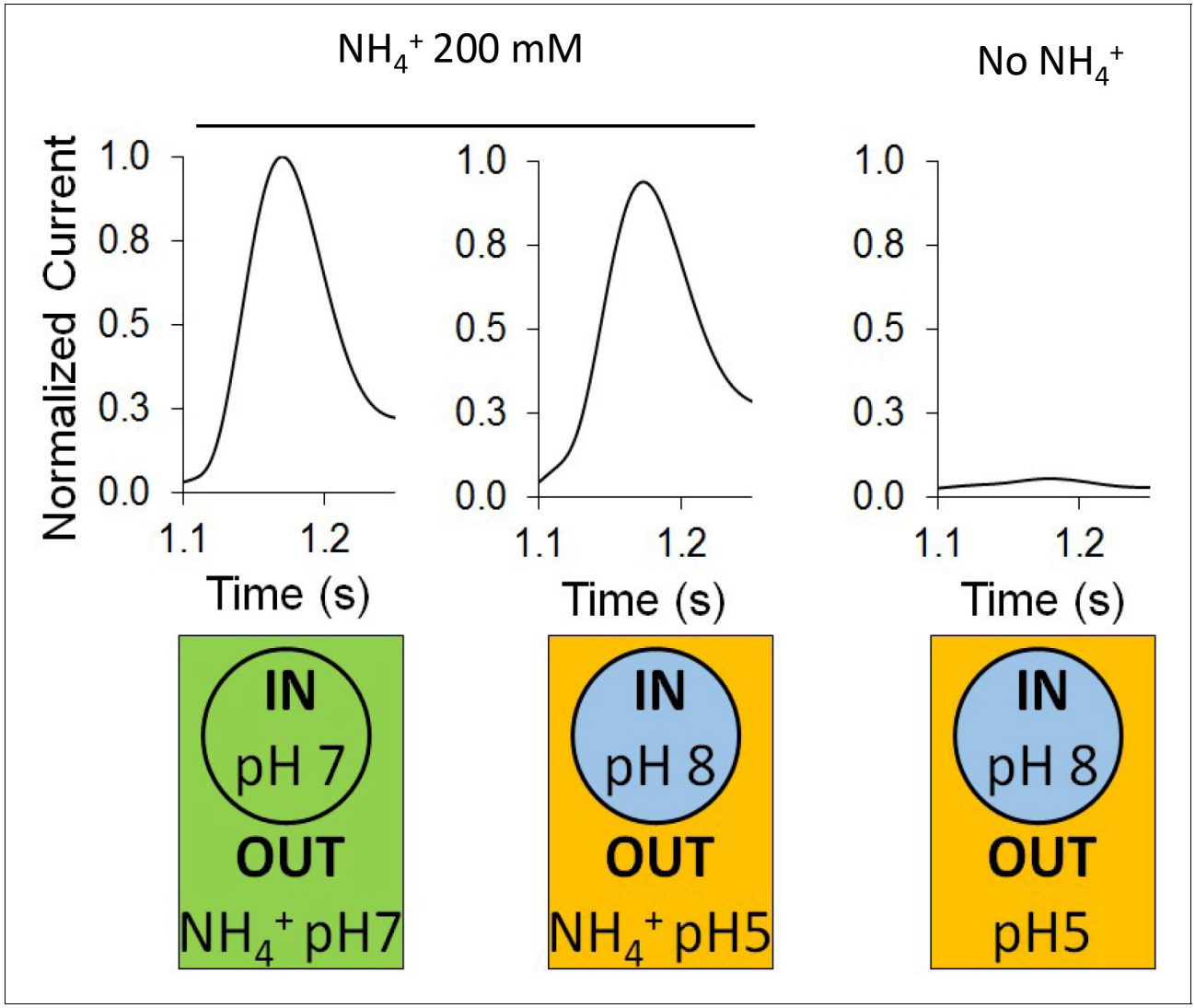

Figure 3. Effect of a proton gradient on AmtB activity. The transient currents were measured using SSME following an ammonium pulse of 200 mM at pH 7 (left) or under an inwardly directed pH gradient in the presence (center) or absence (right) of ammonium. eight sensors from two independent protein purification batches were measured, with three measurements recorded for each sensor. Single representative traces were chosen to visualize the results. Each sensor was measured in the order pH (in/out) 7/7, 8/5, 8/5 (this time without NH_4^+), and finally 7/7 again to be sure that the signals do not significantly decrease with time. The data are normalized against the measurements done at pH7 in/out for each sensor.
The online version of this article includes the following source data for figure 3:

Source data 1. Effect of a proton gradient on AmtB activity.

AmtB switches from transporter to channel-like activity in the absence of the 'twin-His' motif

The CWW and PWW are connected via the twin-His motif, which bridges the aqueous chains, while preventing the formation of a continuous water channel in the simulations (***Figure 2A***). We therefore next probed if the twin-His motif enables proton transfer between the two water wires by recording the activities of twin-His variants. Expressed in *S. cerevisiae* triple-*mep*Δ, $AmtB^{H168A/H318A}$ did not support cell growth on low ammonium (***Figure 5A***). *In-vitro* SSME measurements with this variant displayed LPR-independent current decay rates (***Figure 5A***, ***Figure 5—figure supplement 1***, ***Table 1***), showing that the residual current is caused by the association of NH_4^+ to AmtB without further transport. No current was recorded for the triple mutant $AmtB^{S219A/H168A/H318A}$, in which binding at the periplasmic face was further altered, confirming that the residual current reflects NH_4^+ interaction near S1 (***Figure 5—figure supplement 1***). The double-His mutant $AmtB^{H168A/H318A}$ is

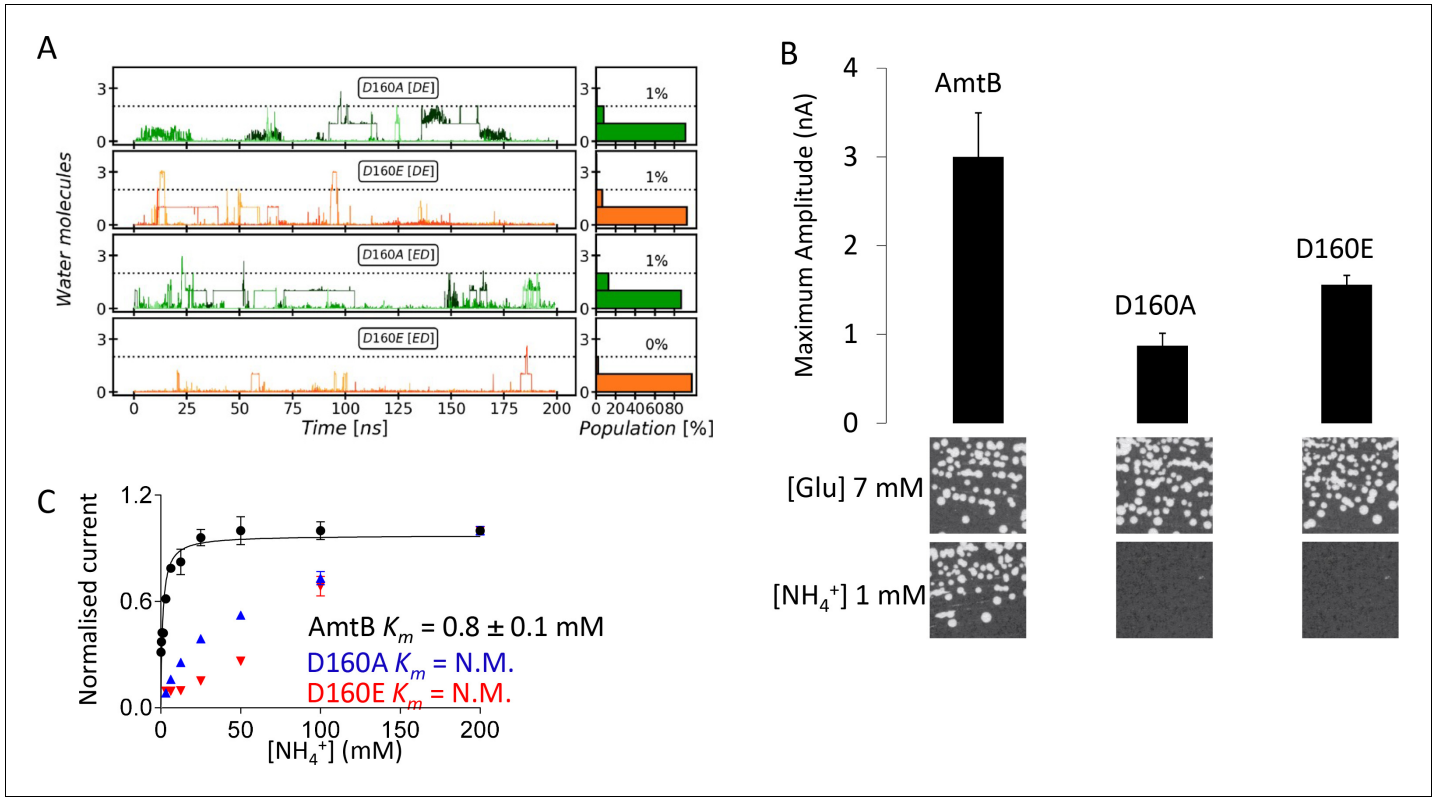

Figure 4. Effect of D160 substitutions. (**A**) The Periplasmic Water Wire (PWW) in the D160A and D160E variants. We observe no significant occupancy of the PWW above the threshold of at least three water molecules in the D160A and D160E AmtB variants, irrespective of the tautomeric protonation states of H168 and H318 (DE or ED, see Materials and method section). (**B**) *Upper panel:* maximum amplitude of the transient current measured using SSME following a 200 mM ammonium pulse. Eight sensors from two independent protein purification batches were measured, with three measurements recorded for each sensor (means ± SD). *Lower panel*: yeast complementation test (strain 31019b, *mep1Δ mep2Δ mep3Δ ura3*) using 7 mM Glutamate (Glu) or 1 mM ammonium as a sole nitrogen source. The growth tests have been repeated twice. (**C**) Kinetics analysis of the transport of ammonium. The maximum amplitudes recorded after a 200 mM ammonium pulse have been normalized to 1.0 for comparison. N.M.: Non Measurable. eight sensors from two independent protein purification batches were measured, with three measurements recorded for each sensor (means ± SD).
The online version of this article includes the following source data and figure supplement(s) for figure 4:

Source data 1. Effect of D160 substitutions on AmtB activity measured by SSME.
Figure supplement 1. Size Exclusion Chromatography analysis of AmtB.
Figure supplement 2. Characterization of the activity and specificity of AmtB variants.

thus able to interact with NH_4^+ but cannot transport the substrate across the membrane. This supports our previous structural analysis showing that the CWW in the pore of the double-His mutant $AmtB^{H168A/H318A}$ is absent (***Javelle et al., 2006***).

By contrast, the two single histidine-to-alanine substitutions in the twin-His motif unexpectedly produced an LPR-dependent current in our SSME recordings (***Figure 5A***, ***Figure 5—figure supplement 1***, ***Table 1***). Furthermore, triple-*mep*Δ yeast cells expressing these variants were able to grow in the presence of low ammonium concentrations (***Figure 5A***). Our previous crystal structure (***Javelle et al., 2006***) and our MD simulations (***Figure 5—figure supplement 2***) show increased hydration in the area around A168, which could potentially form a pathway for direct translocation of NH_4^+ without a deprotonation step. To test this hypothesis, we measured the activity of $AmtB^{H168A}$ and $AmtB^{H318A}$ in D_2O conditions, as described above. Crucially, the activity of both variants measured in the presence or absence of D_2O was similar (***Figure 5B***), in contrast to native AmtB where no activity was recorded in D_2O (***Figure 2B***), showing that proton transfer between water molecules is not a key mechanistic feature in the activity of the mutants. Additionally, the translocation of NH_4^+ is not saturable in the tested concentration range [12.5–200 mM] for $AmtB^{H168A}$ and $AmtB^{H318A}$ (***Figure 5C***). Summarizing, these results suggest that AmtB switches from transporter- to channel-like activity in the absence of the twin-His motif, directly translocating hydrated

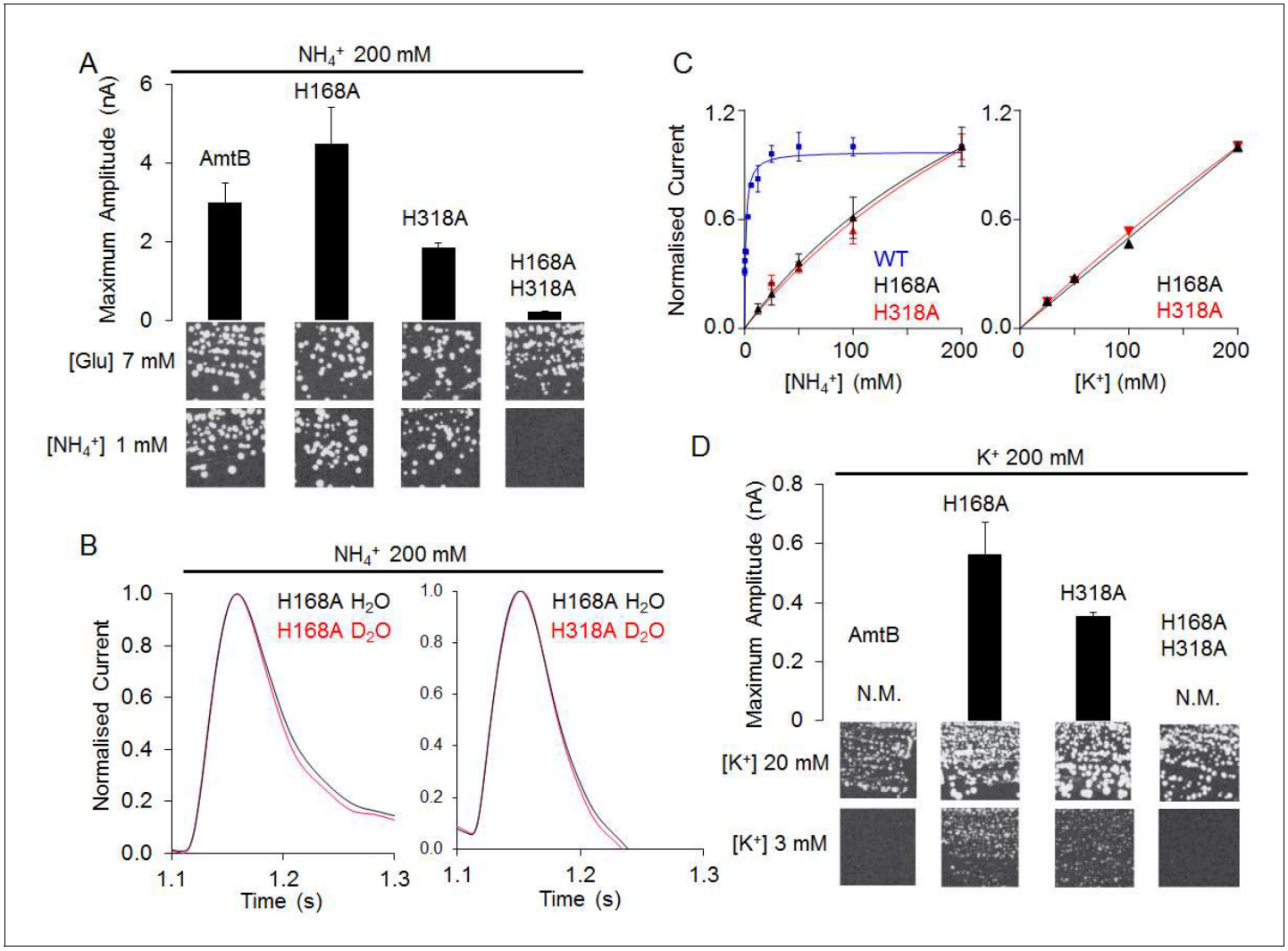

Figure 5. The AmtB^{H168A} and AmtB^{H318A} lose their specificity toward ammonium. (**A**) *Upper panels:* maximum amplitude of the transient current measure using SSME after a 200 mM ammonium pulse. Eight sensors from two independent protein purification batches were measured, with three measurements recorded for each sensor (means ± SD). *Lower panels*: yeast complementation test (strain 31019b, *mep1Δ mep2Δ mep3Δ ura3*) using 7 mM Glutamate (Glu) or 1 mM ammonium as a sole nitrogen source. The growth tests have been repeated twice. (**B**) Transient currents measured using SSME following a 200 mM ammonium pulse on sensors prepared with solutions containing either H_2O (black) or D_2O (red). The maximum amplitudes recorded after a 200 mM ammonium pulse on sensor prepared in H_2O have been normalized to 1.0 for comparison. eight sensors from two independent protein purification batches were measured, with three measurements recorded for each sensor (means ± SD). (**C**) Kinetics analysis of the transport of NH_4^+ (or K^+ in AmtB^{H168A} (black), AmtB^{H318A} (red) and WT-AmtB (bleu, only for NH_4^+, as no signal was measurable with K^+). The maximum amplitudes recorded after a 200 mM NH_4^+ or K^+ pulse have been normalized to 1.0 for comparison. Eight sensors from two independent protein purification batches were measured, with three measurements recorded for each sensor (means ± SD). (**D**) *Upper panels:* maximum amplitude of the transient current measured using SSME after a 200 mM potassium pulse. N.M. Non Measurable. Eight sensors from two independent protein purification batches were measured, with three measurements recorded for each sensor (means ± SD). *Lower panels*: yeast complementation test (strain #228, *mep1Δ mep2Δ mep3Δ trk1Δ trk2Δ leu2 ura3)* using media supplemented with 20 mM or 3 mM KCl. The growth test has been repeated twice.
The online version of this article includes the following source data and figure supplement(s) for figure 5:

Source data 1. Effect of H168 and/or H318 substitution on AmtB activity and selectivity measured by SSME.
Figure supplement 1. Characterization of the activity and specificity of AmtB variants.
Figure supplement 2. MD simulation of AmtB^{H168A} showing formation of a continuous water wire traversing the central pore region.

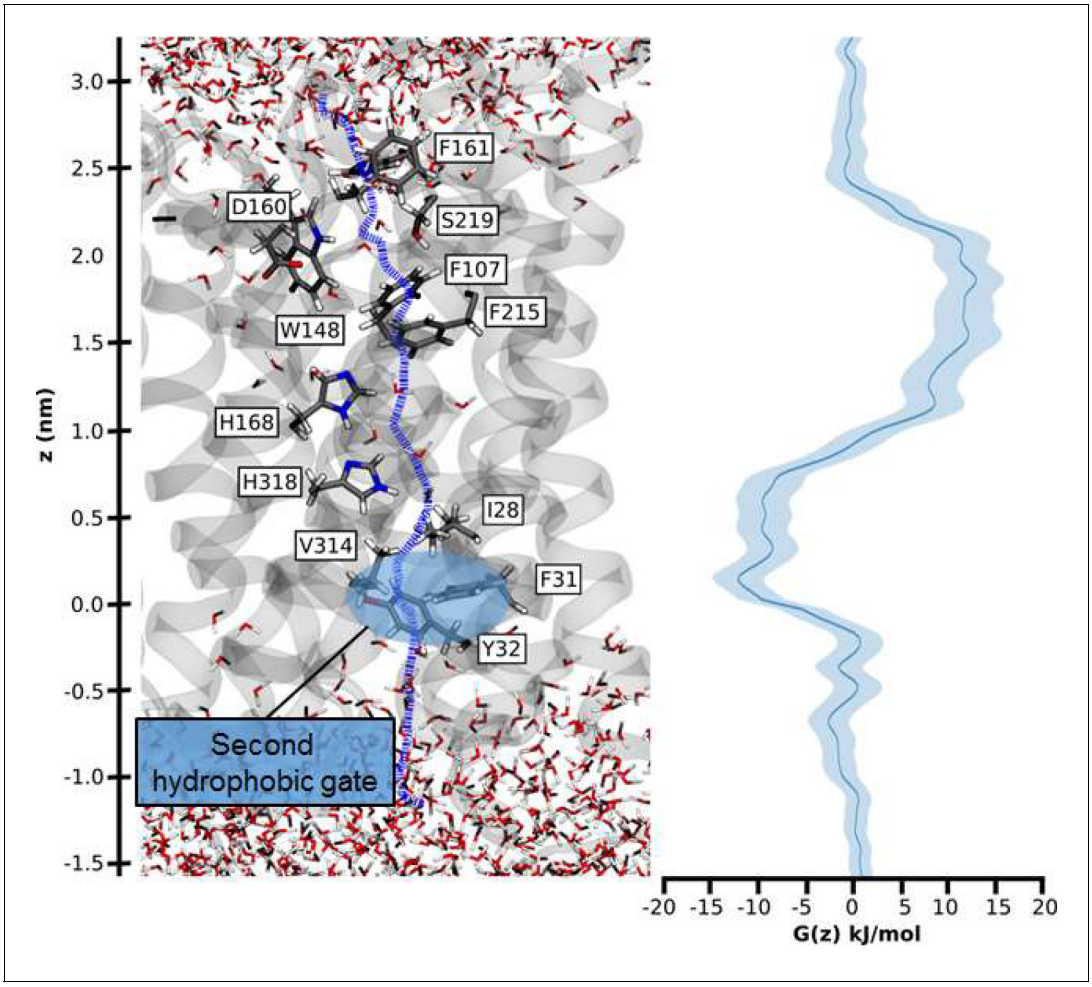

Figure 6. Hydrophobic pathway and energetics for NH_3 translocation in AmtB. We probed an optimal pathway for NH_3 transfer during our PMF calculations (left, purple dash trajectory) in the presence of both the PWW and CWW. The software HOLE (*49*) was used to determine the most likely transfer route. The pathway from the periplasm to the cytoplasm traverses the hydrophobic gate region (F107 and F215), crosses the cavity next to the twin-His motif (H168 and H318) occupied by the CWW, and continues across a second hydrophobic region (I28, V314, F31, Y32) before entering the cytoplasm.

NH_4^+ through the pore. In the wild-types of Amt/Mep/Rh protein family members, the twin-His motif is highly conserved, which shows that transporter, as opposed to channel activity, is mechanistically crucial for the function of these proteins. The only variation seen in naturally occurring sequences is a replacement of the first His by Glu in some fungal Mep proteins (***Javelle et al., 2006***; ***Thomas et al., 2000***). Channel activity is so far only observed for the alanine mutants, not the wild-type. We hypothesized that transport activity might thus be key to ensure ion selectivity of AmtB, since NH_4^+ and K^+ are cations of similar size and hydration energy (***Aydin et al., 2020***).

The twin-His motif interconnects the two water wires to ensure the selectivity of AmtB

Since NH_4^+ was directly translocated in the absence of the twin-his motif and earlier studies implicated a role of the motif in AmtB selectivity (***Ganz et al., 2020***; ***Hall and Yan, 2013***), we repeated our SSME experiments on the $AmtB^{H168A}$ and $AmtB^{H318A}$ variants using the competing K^+ ion as substrate. A 200 mM K^+ pulse triggered currents in both variants, whose decay rates strongly depended on the LPR (***Figure 5D***, ***Table 1***, ***Figure 5—figure supplement 1***). Furthermore, the single His variants, but not native AmtB, complemented the growth defect of a yeast strain lacking its three endogenous ammonium (Mep) and potassium (Trk) transporters when a limited concentration of $K^+$was present (***Figure 5D***). The K^+ translocation activity is not saturable in the substrate range

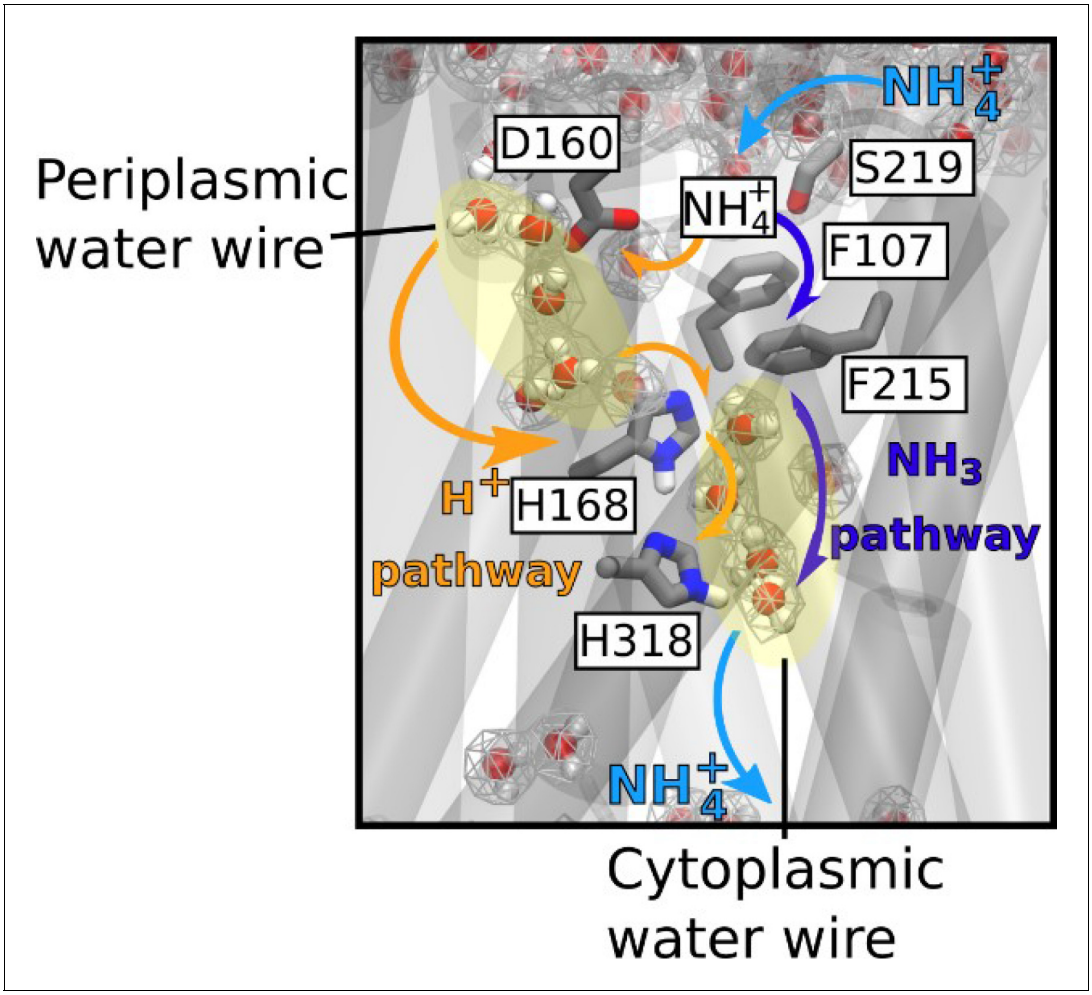

Figure 7. Mechanism of electrogenic NH_4^+ translocation in AmtB. Following sequestration of NH_4^+ at the periplasmic face, NH_4^+ is deprotonated and H^+ and NH_3 follow two separated pathways to the cytoplasm (orange arrows depict the pathway for H^+ transfer, dark blue arrows for NH_3), facilitated by the presence of two internal water wires. NH_3 reprotonation likely occurs near the cytoplasmic exit (***Figure 6***). The hydrated regions within the protein as observed in simulations are highlighted by wireframe representation, crucial residues involved in the transport mechanism are shown as sticks.

[12.5–200 mM] (***Figure 5C***). These results demonstrate that both variants, $AmtB^{H168A}$ and $AmtB^{H318A}$, translocate K^+ ions across the membrane. The substitutions within the twin-His motif thus abolished selectivity for NH_4^+.

The presence of both histidine residues is therefore critical in ammonium transport, since permeability of ammonium transporters for K^+ would compromise ionic homeostasis and disrupt the membrane potential of *E. coli* cells, which crucially depends on maintaining K^+ concentration gradients across the membrane. Moreover, since AmtB is expressed in *E. coli* under nitrogen starvation conditions (low NH_4^+/K^+ ratio), loss of selectivity for NH_4^+ would impede ammonium uptake. Our results thus demonstrate that the twin-His motif, which is highly conserved amongst members of the family, is an essential functional element in the transport mechanism, preventing the transport of competing cations, whilst providing a pathway for proton transfer by bridging the periplasmic and the cytoplasmic water wires.

NH_3 permeation through the hydrophobic pore

Umbrella sampling free-energy calculations were performed to establish the rate limiting step of NH_4^+ transport. Our calculations show that NH_3 translocation experiences only a moderate energy barrier (~10 kJ/mol) at the periplasmic hydrophobic constriction region (F107 and F215) (***Figure 6***). The starting points of the sampling windows were determined from the centers of HOLE calculations

(*Smart et al., 1996*), optimizing the pathway of NH_3 translocation across the pore. A possible influence from this selection regarding the pathway was further reduced by allowing the molecule to move freely perpendicular to the pore axis within a radius of 5 Å in addition to extensive sampling; however, residual bias from window selection cannot be completely excluded. From the free energy profile of NH_3 translocation, we identified a shallow binding site below the twin-His motif (~5 kJ/mol). This is followed by a second hydrophobic region (I28, V314, F31 and Y32) that forms a small energy barrier between this binding site and the cytoplasmic exit. The increased residence time of NH_3 within this energy minimum suggests that reprotonation to NH_4^+, caused by the cytoplasmic pH, occurs in this region (*Figure 6*). Since both energy barriers for H^+ transfer along the water chains and NH_3 permeation are relatively small, we concluded that either initial deprotonation or proton transfer across the twin-His motif could be rate-limiting for overall NH_4^+ transport.

Conclusion

A new model for the mechanism of electrogenic ammonium transport therefore emerges from our findings (*Figure 7*). After deprotonation of NH_4^+ at the periplasmic side, a previously undiscovered polar conduction route enables H^+ transfer into the cytoplasm. A parallel pathway, lined by hydrophobic groups within the protein core, facilitates the simultaneous transfer of uncharged NH_3, driven by concentration differences. On the cytoplasmic face, the pH of the cell interior leads to recombination to NH_4^+, most likely near a second hydrophobic gate (*Figure 6*). The twin-His motif, which bridges the water chains constitutes the major selectivity gate for NH_4^+ transport preventing K^+ flow. We propose that this mechanism is conserved amongst the electrogenic members of the Amt/Mep/Rh family. Importantly, two RhAG polymorphisms associated to the overhydrated stomatocytosis human syndrome have also acquired the ability to transport K^+. Thus, deciphering the transport mechanism of two archetypal members of the family such as AmtB and NeRh50 could bring new insights to the understanding of substrate specificity determinants in Rh proteins in the context of human diseases (*Bruce et al., 2009*).

Our findings define a new mechanism, by which ionizable molecules that are usually charged in solution are selectively and efficiently transported across a highly hydrophobic environment like the AmtB/Rh pore. Alongside size-exclusion and ion desolvation (*Kopec et al., 2018*), it adds a new principle by which selectivity against competing ions can be achieved. Other biological transport systems, like the formate/nitrite transporters, may share similar mechanisms involving deprotonation-reprotonation cycles (*Wiechert and Beitz, 2017*).

Materials and methods

Key resources table

Reagent type (species) or resource	Designation	Source or reference	Identifiers	Additional information
Gene (*Escherichia coli*)	AmtB	*Zheng et al., 2004*	Uniprot: C3TLL2	
Gene (*Nitrosomonas europea*)	Rh50	*Lupo et al., 2007*	Uniprot Q82 × 47	
Strain, strain background (*Escherichia coli*)	C43 (DE3)	*Miroux and Walker, 1996*		Chemically competent cells
Strain, strain background (*Escherichia coli*)	GT1000	*Javelle et al., 2004*		Chemically competent cells
Recombinant DNA reagent	pET22b (+)	Novagen	Cat# - 69744	
Recombinant DNA reagent	pDR195	*Rentsch et al., 1995*	Addgene - 36028	High copy yeast expression vector
Recombinant DNA reagent	pAD7	*Cherif-Zahar et al., 2007*		pESV2-RH50$(His)_6$

Continued on next page

Continued

Reagent type (species) or resource	Designation	Source or reference	Identifiers	Additional information
Recombinant DNA reagent	p426MET25	***Mumberg et al., 1994***		
Recombinant DNA reagent	PZheng	***Zheng et al., 2004***		pET22b-AmtB$(His)_6$
Recombinant DNA reagent	pGDM2	This study		pET22b-AmtB $(His)_6^{H168AH318A}$
Recombinant DNA reagent	pGDM4	This study		pET22b-AmtB$(His)_6^{D160A}$
Recombinant DNA reagent	pGDM5	This study		pET22b-AmtB$(His)_6^{D160E}$
Recombinant DNA reagent	pGDM6	This study		pET22b-AmtB $(His)_6^{S219AH168AH318A}$
Recombinant DNA reagent	pGW2	This study		pET22b-AmtB$(His)_6^{H168A}$
Recombinant DNA reagent	pGDM9	This study		pDR195-AmtB$(His)_6^{D160A}$
Recombinant DNA reagent	pGDM10	This study		pDR195-AmtB$(His)_6^{D160E}$
Recombinant DNA reagent	pGDM12	This study		pDR195-AmtB $(His)_6^{H168AH318A}$
Recombinant DNA reagent	pGDM13	This study		pDR195-AmtB $(His)_6^{S219AH168AH318A}$
Recombinant DNA reagent	pGW7	This study		pDR195-AmtB$(His)_6^{H168A}$
Sequence-based reagent	$AmtB^{S219A}$ F	IDT	PCR Primer (Mutagenesis)	GGTGGCACCGTGGTGGATAT TAACGCCGCAATC
Sequence-based reagent	$AmtB^{D160A}$ F	IDT	PCR Primer (Mutagenesis)	CTCACGGTGCGCTGGCCTTCG CGGGTGGCACC
Sequence-based reagent	$AmtB^{D160E}$ F	IDT	PCR Primer (Mutagenesis)	CTCACGGTGCGCTGGAGTTCG CGGGTGGCACC
Sequence-based reagent	$AmtB^{H168A}$ F	IDT	PCR Primer (Mutagenesis)	GGTGGCACCGTGGTGGCCATT AACGCCGCAATC
Sequence-based reagent	$AmtB^{H318A}$ F	IDT	PCR Primer (Mutagenesis)	TGTCTTCGGTGTGGCCGGCGT TTGTGGCATT
Sequence-based reagent	AmtB XhoI	IDT	PCR primer	AGTCCTCGAGATGAAGATAGC GACGATAAAA
Sequence-based reagent	AmtB BamHI	IDT	PCR primer	AGTCGGATCCTCACGCGTTAT AGGCATTCTC
Sequence-based reagent	P5'NeRh	IDT	PCR primer	GCCACTAGTATGAGTAAACAC CTATGTTTC
Sequence-based reagent	P3'NeRh	IDT	PCR primer	GCCGAATTCCTATCCTTCTGA CTTGGCAC
Peptide, recombinant protein	$AmtB(His)_6$	This study		purified from *E. coli* C43 (DE3) cells
Peptide, recombinant protein	$AmtB(His)_6^{D160A}$	This study		purified from *E. coli* C43 (DE3) cells
Peptide, recombinant protein	$AmtB(His)_6^{D160E}$	This study		purified from *E. coli* C43 (DE3) cells
Peptide, recombinant protein	$AmtB(His)_6^{H168AH318A}$	This study		purified from *E. coli* C43 (DE3) cells

Continued on next page

Continued

Reagent type (species) or resource	Designation	Source or reference	Identifiers	Additional information
Peptide, recombinant protein	AmtB $(His)_6^{S219AH168AH318A}$	This study		purified from *E. coli* C43 (DE3) cells
Peptide, recombinant protein	$AmtB(His)_6^{H168A}$	This study		purified from *E. coli* C43 (DE3) cells
Peptide, recombinant protein	$AmtB(His)_6^{H318A}$	This study		purified from *E. coli* C43 (DE3) cells
Peptide, recombinant protein	*Ne*Rh50$(His)_6$	This study		purified from *E. coli* C43 GT1000 cells
Peptide, recombinant protein	XhoI	Promega	Cat# - R6161	
Peptide, recombinant protein	BamHI	Promega	Cat# - R6021	
Commercial assay or kit	Quikchange XL site-directed mutagensis kit	Agilent Technologies	Cat# 200516	
Chemical compound, drug	n-dodecyl-β-D-maltopyranoside (DDM)	Avanti	Cat#- 850520	
Chemical compound, drug	lauryldecylamine oxide (LDAO)	Avanti	Cat#- 850545	
Chemical compound, drug	*E. coli* Polar Lipids	Avanti	Cat#−100600	
Chemical compound, drug	Phosphotidylcholine (POPC)	Avanti	Cat#−850457	
Software, algorithm	Graphpad Prism software	GraphPad Prism (https://www.graphpad.com)		Version 6.01
Software, algorithm	Origin Pro Software	Origin Labs (https://www.originlab.com)		Origin 2017 Version 94E
Software, algorithm	$SURFE^2R$ Control Software	Nanion (https://www.nanion.de/en/)		V1.5.3.2

Mutagenesis

AmtB mutants were generated using the Quikchange XL site-directed mutagenesis kit (Agilent Technologies), according to the manufacturer's instructions. The primers used for mutagenesis are listed in Key resources table. The template was the *amtB* gene cloned into the plasmid pET22b(+), as previously described (**Zheng et al., 2004**; Key resources table).

AmtB and NeRh50 expression in yeast and complementation test

The different variants of *amtB* were amplified using *amtB* cloned into pET22b(+) (Key resources table) as a template with the primers AmtB XhoI and AmtB BamHI (Key resources table) and then sub-cloned into the plasmids pDR195 (Key resources table). The NeRh50 gene was amplified from *N. europaea* genomic DNA (kind gift from Daniel J. Arp and Norman G. Hommes, Department of Botany and Plant Pathology, Oregon State University, Corvallis, USA) using the primers P5'NeRh and P3'NeRh (Key resources table), and was then cloned into the SpeI and EcoRI restriction sites of the high-copy vector p426Met25 (Key resources table), allowing controlled-expression of NeRh50 by the yeast methionine repressible MET25 promoter.

Saccharomyces cerevisiae strains used in this study are the 31019b strain (*mep1Δ mep2Δ mep3Δ ura3*) and the #228 strain (*mep1Δ mep2Δ mep3Δ trk1Δ trk2Δ leu2 ura3*) (**Hoopen et al., 2010**; **Marini et al., 1997**). The plasmids used in this study are listed in Key resources table. Cell

transformation was performed as described previously (**Gietz et al., 1992**). For growth tests on limiting ammonium concentrations, yeast cells were grown in minimal buffered (pH 6.1) medium and for growth tests on limiting potassium concentrations, a minimal buffered (pH 6.1) medium deprived of potassium salts was used (**Jacobs et al., 1980**). 3% glucose was used as the carbon source and, 0.1% glutamate, 0.1% glutamine or $(NH_4)_2SO_4$ at the specified concentrations were used as the nitrogen sources.

All growth experiments were repeated at least twice.

Protein purification

AmtB(His_6) cloned into the pET22b(+) vector (Key resources table) was overexpressed and purified as described previously (**Zheng et al., 2004**). The plasmid pAD7 (Key resources table) was used to overexpress NeRh50 in the *E. coli* strain GT1000 (**Javelle et al., 2004**). GT1000 was transformed with pAD7 and grown in M9 medium (**Elbing and Brent, 2002**), in which ammonium was replaced by 200 µg/ml glutamine as sole nitrogen source. NeRh50 was purified as described by **Lupo et al., 2007** with minor modifications, namely: the membrane was solubilized using 2% lauryldecylamine oxide (LDAO) instead of 5% *n*-octyl-β-D-glucopyranoside (OG), and 0.09% LDAO was used in place of 0.5% β-OG in the final size exclusion chromatography buffer (50 mL Tris pH 7.8, 100 mL NaCl, 0.09% LDAO).

AmtB and NeRh50 insertion into proteoliposomes

AmtB and NeRh50 were inserted into liposomes containing *E. coli* polar lipids/phosphatidylcholine (POPC) 2/1(wt/wt) as previously described (**Mirandela et al., 2019**). For each AmtB variant, proteoliposomes were prepared at lipid-to-protein ratios (LPRs) of 5, 10, and 50 (wt/wt). The size distribution of proteoliposomes was measured by dynamic light scattering (DLS) using a Zetasizer Nano ZS (Malvern Instruments, Malvern, UK). This analysis showed that the proteoliposomes had an average diameter of 110 nm (**Figure 8**). Proteoliposomes were divided into 100 µL aliquots and stored at −80˚C.

To ensure that all AmtB variants were correctly inserted into the proteoliposomes, the proteoliposomes were solubilized in 2% DDM and the proteins analyzed by size exclusion chromatography using a superdex 200 (10 × 300) enhanced column. The elution profile of all variants and the wild-type were identical, showing a single monodisperse peak eluting between 10.4–10.6 ml (**Figure 4—figure supplement 1**). This demonstrated that all proteins were correctly folded, as trimers, in the proteoliposomes.

Solid supported membrane electrophysiology

To form the solid-supported membrane, 3 mm gold-plated sensors were prepared according to the manufacturer's instructions (Nanion Technologies, Munich, Germany), as described previously (**Bazzone et al., 2017**). Proteoliposomes/empty liposomes were defrosted and sonicated in a sonication bath at 35 W for 1 min, diluted 10 times in non-activating (NA) solution (**Supplementary file 1**), and then 10 µl were added at the surface of the SSM on the sensor. After centrifugation, the sensors were stored at 4˚C for a maximum of 48 hr before electrophysiological measurements. For the D_2O experiments, all the solutions were prepared using D_2O instead of water.

All measurements were made at room temperature (21˚C) using a SURFE^{2}R N1 apparatus (Nanion Technologies, Munich, Germany) with default parameters (**Bazzone et al., 2017**). Prior to any measurements, the quality of the sensors was determined by measuring their capacitance (15–30 nF) and conductance (<5 nS).

For functional measurements at a fixed pH, a single solution exchange protocol was used with each phase lasting 1 s (**Bazzone et al., 2017**). First, non-active (NA) solution was injected onto the sensor, followed by activating (A) solution containing the substrate at the desired concentration and finally NA solution (**Supplementary file 1**).

For the measurements under inwardly orientated pH gradient, a double solution exchange protocol was used (**Bazzone et al., 2017**), in which an additional resting solution phase of 15 min in NA solution at pH 8 was added to the end. The incubation phase adjusts the inner pH of the proteoliposomes to pH 8 and establishes a pH gradient at the beginning of each measurement by pulsing the activation solution at pH 5.

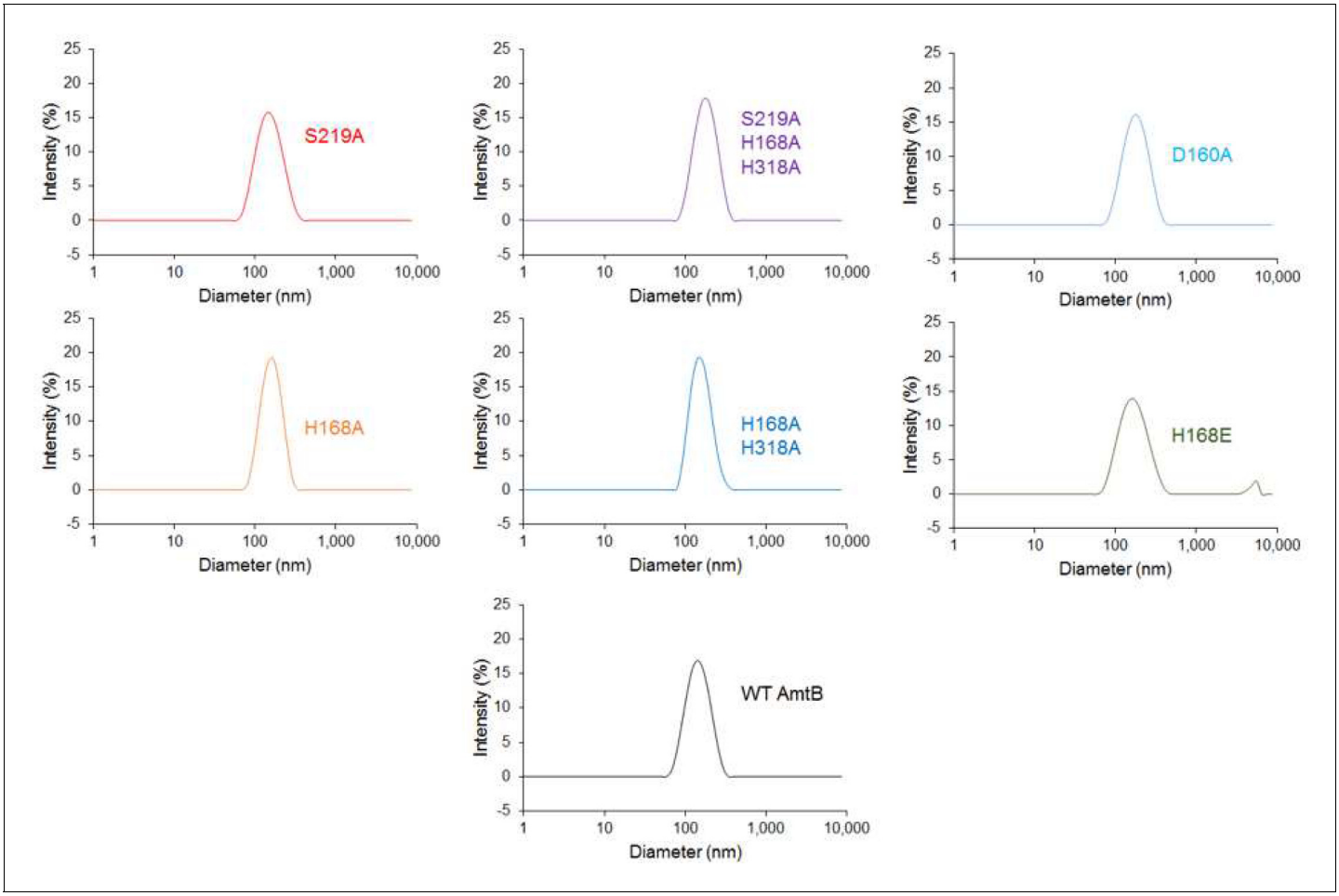

Figure 8. Size distribution of the proteoliposomes containing wild-type and variants of AmtB. Dynamic light scattering was used to determine the number-weighted distribution of liposome sizes in the detection reagent. The distribution was monodisperse, with a mean diameter of 110 nm.

Each sensor was measured in the order pH (in/out) 7/7, 8/5 (with NH_4^+), 8/5 (without NH_4^+), and finally again 7/7 to ensure that the signals do not significantly decrease with time. The data are normalized against the measurements conducted at pH7 in/out for each sensor. All measurements were recorded on 8 sensors from two independent protein purification batches, with 3 measurements recorded for each sensor.

The kinetic parameters were calculated using Graphpad Prism 6 (GraphPad Software, San Diego, California, USA) and fitted according to the Michaelis-Menten equation (Key resources table). Lifetime analysis of the current (decay time of the transient current) was performed to differentiate small pre-steady state currents, which arise due to the binding of a charged species to membrane proteins, from currents reflecting full transport cycles, which show faster decay rates under raised liposomal LPR (***Bazzone et al., 2017***). The decay time of the transient current (***Table 1***) was calculated by fitting the raw transient current data between the apex of the peak and the baseline (after transport) with a non-linear regression using OriginPro 2017 (OriginLab, Northampton, Massachusetts, USA). The regression was done using a one-phase exponential decay function with time constant parameter:

$$y = y_0 = A_1 e^{-x/t_1}$$

The fit was obtained using the Levenberg-Marquardt iteration algorithm, where x and y represent coordinates on the respective axis, y_0 represents the offset at a given point, A represents the amplitude, and t is the time constant.

Molecular Dynamics simulations

The AmtB trimer (PDB code: 1U7G) (**Khademi et al., 2004**) was processed using the CHARMM-GUI web server (**Lee et al., 2016**). Any mutations inserted during the crystallization process were reverted to the wild-type form. The N-termini and C-termini of the subunits were capped with acetyl and N-methyl amide moieties, respectively. The protein was then inserted into a membrane patch of *xy*-dimensions 13 × 13 nm. Unless otherwise specified, a membrane composition of palmitoyl oleoyl phosphatidyl ethanolamine and palmitoyl oleoyl phosphatidyl glycine (POPE/POPG) at a 3:1 ratio was used in order to approximate the composition of a bacterial cytoplasmic membrane. We employed the CHARMM36 forcefield for the protein and counter ions (**Best et al., 2012**). The water molecules were modeled with the TIP3P model (**Jorgensen et al., 1983**). Water bonds and distances were constrained by the Settle method (**Miyamoto and Kollman, 1992**), and all other bonds by the LINCS method (**Hess et al., 1997**). In simulations without ammonium, K^+ and Cl^- ions were added to neutralize the system and obtain a bulk ionic concentration of 250 mM. In simulations with ammonium, K^+ was replaced by NH_4^+. The parameters for NH_4^+ and NH_3 (umbrella sampling simulations) were adapted from **Nygaard et al., 2006**.

After a steepest descent energy minimization, the system was equilibrated by six consecutive equilibration steps using position restraints on heavy atoms of 1000 kJ/mol.nm^2. The first three equilibration steps were conducted in an NVT ensemble, applying a Berendsen thermostat (**Berendsen et al., 1984**) to keep the temperature at 310K. The subsequent steps were conducted under an NPT ensemble, using a Berendsen barostat (**Berendsen et al., 1984**) to keep the pressure at 1 bar. Production molecular dynamics simulations were carried out using a v-rescale thermostat (**Bussi et al., 2007**) with a time constant of 0.2 ps, and a Berendsen barostat with semi-isotropic coupling. A timestep of 2 fs was used throughout the simulations.

In a subset of simulations, we aimed to test the effect of membrane voltage on the internal hydration of AmtB using CompEL. For the CompEL simulations (**Kutzner et al., 2016**), the system was duplicated along the z-axis, perpendicular to the membrane surface. To focus on the physiologically relevant voltage gradient in *E. coli*, that is a negative potential on the inside of the cell of magnitude −140 to −170 mV (**Cohen and Venkatachalam, 2014**), an antiparallel orientation of the two trimers in the double bilayers was used (**Felle et al., 1980**). The final double system consisted of a rectangular box of 13 × 13×20 nm. For the CompEL simulations, 1000 positively charged (either NH_4^+ or K^+) and 1000 negatively charged ions (Cl^-) were added to the system, then the system was neutralized, and the desired ion imbalance established.

The Umbrella Sampling (US) Potential-of-Mean-Force (PMF) calculations (**Torrie and Valleau, 1977**) were set up as described previously by **Hub et al., 2010b**. A snapshot was taken from the simulation of the single bilayer system with the twin-His motif in the DE protonation state and both the CWW and PWW occupied. The pore coordinates were obtained using the software HOLE (**Smart et al., 1996**), removing the solvent and mutating F215 to alanine during the HOLE run only. Starting coordinates for each umbrella window were generated by placing NH_3 in the central x-y coordinate of the pore defined by HOLE at positions every 0.5 Å in the z coordinate. Solvent molecules within 2 Å of the ammonia's N atom were removed. Minimization and equilibration were then re-performed as described above. Unless otherwise stated, position restraints were used for all water oxygen atoms in the CWW with a 200 kJ/mol.nm^2 force constant; while the TIP3 molecules within the lower water wire were not restrained. For the US the N atom of ammonia was position-restrained with a force constant of 1000 kJ/mol.nm^2 on the z axis and a 400 kJ/mol.nm^2 cylindrical flat-bottomed potential with a radius of 5 Å in the x-y plane, as described earlier by **Hub et al., 2010a**. For some US window simulations, the ammonia z-axis restraints were increased and the time step reduced in the equilibration to relax steric clashes between sidechains and ammonia. After equilibration, US simulations were run for 10ns, using the parameters described above (**Lee et al., 2016**) and removing the initial two ns for further equilibration. The PMF profiles were generated with the GROMACS implementation of the weighted histogram analysis method (WHAM) with the periodic implementation (**Hub et al., 2010a**). Further US simulations were performed to as needed to improve sampling in regions of the profile that were not sufficiently sampled. The Bayesian bootstrap method was performed with 200 runs to calculate the standard deviation of the PMF.

Free energy calculations for proton translocation

The free energies for proton translocation were evaluated by protonating the water molecules at different sites along the periplasmic and cytoplasmic water wires. Electrostatic effects in proteins are often treated more effectively using semi-macroscopic models which can overcome the convergence problems of more rigorous microscopic models. Here we used the semi-macroscopic protein dipole/Langevin dipole approach of Warshel and coworkers in the linear response approximation version (PDLD/S-LRA) (***Kato et al., 2006***; ***Sham et al., 2000***). Positions of the water molecules in the PWW and CWW were obtained from the corresponding MD snapshots (***Figure 1***). All PDLD/S-LRA pK_a calculations were performed using the automated procedure in the MOLARIS simulations package (***Lee et al., 1993***) in combination with the ENZYMIX force field. The simulation included the use of the surface-constrained all atom solvent model (SCAAS) (***Warshel and King, 1985***) and the local reaction field (LRF) long-range treatment of electrostatics. At each site, 20 configurations for the charged and uncharged state were generated. The obtained pK_a values were then converted to free energies for proton translocation.

Acknowledgements

Special thanks to Prof. Iain Hunter (Strathclyde Institute of Pharmacy and Biomedical Sciences) for invaluable discussions and help during this project. We also thank Pascale Van Vooren for technical support and Thomas P Jahn for sharing the *triple-mepΔ trk,1,2Δ* yeast strain. Anna Maria Marini is a senior research associate FNRS and WELBIO investigator and thanks the help of FRFS-WELBIO grant ref: CR-2019A-05R.

Additional information

Funding

Funder	Grant reference number	Author
Tenovus	S17-07	Arnaud Javelle
Scottish Universities Physics Alliance		Ulrich Zachariae
Natural Environment Research Council	NE/M001415/1	Paul A Hoskisson
Fonds De La Recherche Scientifique - FNRS	WELBIO grant ref: CR-2019A-05R.	Anna-Maria Marini

The funders had no role in study design, data collection and interpretation, or the decision to submit the work for publication.

Author contributions

Gordon Williamson, Data curation, Formal analysis, Investigation, Methodology, Writing - review and editing; Giulia Tamburrino, Adriana Bizior, Data curation, Formal analysis, Investigation, Writing - review and editing; Mélanie Boeckstaens, Conceptualization, Data curation, Formal analysis, Methodology, Writing - review and editing; Gaëtan Dias Mirandela, Callum M Ives, Data curation, Formal analysis, Investigation; Marcus G Bage, Formal analysis, Investigation; Andrei Pisliakov, Conceptualization, Formal analysis, Methodology, Writing - review and editing; Eilidh Terras, Investigation; Paul A Hoskisson, Formal analysis, Funding acquisition, Writing - review and editing; Anna Maria Marini, Conceptualization, Methodology, Project administration, Writing - review and editing; Ulrich Zachariae, Conceptualization, Formal analysis, Methodology, Writing - original draft, Project administration; Arnaud Javelle, Conceptualization, Data curation, Formal analysis, Supervision, Investigation, Methodology, Writing - original draft, Project administration

Author ORCIDs

Gordon Williamson https://orcid.org/0000-0003-3053-8322
Mélanie Boeckstaens https://orcid.org/0000-0003-1629-7403

Gaëtan Dias Mirandela https://orcid.org/0000-0001-5871-6288
Andrei Pisliakov https://orcid.org/0000-0003-1536-0589
Callum M Ives http://orcid.org/0000-0003-0511-1220
Arnaud Javelle https://orcid.org/0000-0002-3611-5737

Decision letter and Author response
Decision letter https://doi.org/10.7554/eLife.57183.sa1
Author response https://doi.org/10.7554/eLife.57183.sa2

Additional files

Supplementary files

- Supplementary file 1. Supplementary Table 1.
- Transparent reporting form

Data availability

All data generated or analysed during this study are included in the manuscript and supporting files. Source data files have been provided for Figures 1-5 and Table 2. Simulation code is available on GitHub at https://github.com/UZgroup/A-two-lane-mechanism-for-selective-biological-ammonium-transport/ (copy archived at https://github.com/elifesciences-publications/A-two-lane-mechanism-for-selective-biological-ammonium-transport) and the trajectory files are available on Figshare (https://doi.org/10.6084/m9.figshare.12826316).

The following dataset was generated:

Author(s)	Year	Dataset title	Dataset URL	Database and Identifier
Tamburrino G, Zachariae U	2020	Molecular dynamics simulation trajectories, AmtB in twin-His HSD-HSE and HSE-HSD states	https://figshare.com/articles/dataset/Molecular_dynamics_simulation_trajectories_AmtB_in_twin-His_HSD-HSE_and_HSE-HSD_states/12826316	figshare, 10.6084/m9.figshare.12826316

References

Acharya R, Carnevale V, Fiorin G, Levine BG, Polishchuk AL, Balannik V, Samish I, Lamb RA, Pinto LH, DeGrado WF, Klein ML. 2010. Structure and mechanism of proton transport through the transmembrane tetrameric M2 protein bundle of the influenza A virus. *PNAS* **107**:15075–15080. DOI: https://doi.org/10.1073/pnas.1007071107, PMID: 20689043

Andrade SL, Dickmanns A, Ficner R, Einsle O. 2005. Crystal structure of the archaeal ammonium transporter Amt-1 from Archaeoglobus fulgidus. *PNAS* **102**:14994–14999. DOI: https://doi.org/10.1073/pnas.0506254102, PMID: 16214888

Ariz I, Boeckstaens M, Gouveia C, Martins AP, Sanz-Luque E, Fernández E, Soveral G, von Wirén N, Marini AM, Aparicio-Tejo PM, Cruz C. 2018. Nitrogen isotope signature evidences ammonium deprotonation as a common transport mechanism for the AMT-Mep-Rh protein superfamily. *Science Advances* **4**:eaar3599. DOI: https://doi.org/10.1126/sciadv.aar3599, PMID: 30214933

Ashkenazy H, Abadi S, Martz E, Chay O, Mayrose I, Pupko T, Ben-Tal N. 2016. ConSurf 2016: an improved methodology to estimate and visualize evolutionary conservation in macromolecules. *Nucleic Acids Research* **44**:W344–W350. DOI: https://doi.org/10.1093/nar/gkw408, PMID: 27166375

Aydin F, Zhan C, Ritt C, Epsztein R, Elimelech M, Schwegler E, Pham TA. 2020. Similarities and differences between potassium and ammonium ions in liquid water: a first-principles study. *Physical Chemistry Chemical Physics* **22**:2540–2548. DOI: https://doi.org/10.1039/C9CP06163K, PMID: 31942893

Bazzone A, Barthmes M, Fendler K. 2017. SSM-Based electrophysiology for transporter research. *Methods in Enzymology* **594**:31–83. DOI: https://doi.org/10.1016/bs.mie.2017.05.008, PMID: 28779843

Berendsen HJC, Postma JPM, van Gunsteren WF, DiNola A, Haak JR. 1984. Molecular dynamics with coupling to an external bath. *The Journal of Chemical Physics* **81**:3684–3690. DOI: https://doi.org/10.1063/1.448118

Best RB, Zhu X, Shim J, Lopes PE, Mittal J, Feig M, Mackerell AD. 2012. Optimization of the additive CHARMM all-atom protein force field targeting improved sampling of the backbone φ, ψ and side-chain χ(1) and χ(2) dihedral angles. *Journal of Chemical Theory and Computation* **8**:3257–3273. DOI: https://doi.org/10.1021/ct300400x, PMID: 23341755

Biver S, Belge H, Bourgeois S, Van Vooren P, Nowik M, Scohy S, Houillier P, Szpirer J, Szpirer C, Wagner CA, Devuyst O, Marini AM. 2008. A role for rhesus factor rhcg in renal ammonium excretion and male fertility. *Nature* **456**:339–343. DOI: https://doi.org/10.1038/nature07518

Boogerd FC, Ma H, Bruggeman FJ, van Heeswijk WC, García-Contreras R, Molenaar D, Krab K, Westerhoff HV. 2011. AmtB-mediated NH3 transport in prokaryotes must be active and as a consequence regulation of transport by GlnK is mandatory to limit futile cycling of NH4(+)/NH3. *FEBS Letters* **585**:23–28. DOI: https://doi.org/10.1016/j.febslet.2010.11.055, PMID: 21134373

Bruce LJ, Guizouarn H, Burton NM, Gabillat N, Poole J, Flatt JF, Brady RL, Borgese F, Delaunay J, Stewart GW. 2009. The monovalent cation leak in overhydrated stomatocytic red blood cells results from amino acid substitutions in the Rh-associated glycoprotein. *Blood* **113**:1350–1357. DOI: https://doi.org/10.1182/blood-2008-07-171140, PMID: 18931342

Bussi G, Donadio D, Parrinello M. 2007. Canonical sampling through velocity rescaling. *The Journal of Chemical Physics* **126**:014101. DOI: https://doi.org/10.1063/1.2408420, PMID: 17212484

Cherif-Zahar B, Durand A, Schmidt I, Hamdaoui N, Matic I, Merrick M, Matassi G. 2007. Evolution and functional characterization of the RH50 gene from the ammonia-oxidizing bacterium *Nitrosomonas europaea*. *Journal of Bacteriology* **189**:9090–9100. DOI: https://doi.org/10.1128/JB.01089-07, PMID: 17921289

Cohen AE, Venkatachalam V. 2014. Bringing bioelectricity to light. *Annual Review of Biophysics* **43**:211–232. DOI: https://doi.org/10.1146/annurev-biophys-051013-022717, PMID: 24773017

Dias Mirandela G, Tamburrino G, Ivanović MT, Strnad FM, Byron O, Rasmussen T, Hoskisson PA, Hub JS, Zachariae U, Gabel F, Javelle A. 2018. Merging In-Solution X-ray and neutron scattering data allows fine structural analysis of Membrane-Protein detergent complexes. *The Journal of Physical Chemistry Letters* **9**:3910–3914. DOI: https://doi.org/10.1021/acs.jpclett.8b01598, PMID: 29939747

Elbing K, Brent R. 2002. Media preparation and bacteriological tools. *Current Protocols in Molecular Biology* **59**:1. DOI: https://doi.org/10.1002/0471142727.mb0101s59

Felle H, Porter JS, Slayman CL, Kaback HR. 1980. Quantitative measurements of membrane potential in *Escherichia coli*. *Biochemistry* **19**:3585–3590. DOI: https://doi.org/10.1021/bi00556a026

Ganz P, Ijato T, Porras-Murrilo R, Stührwohldt N, Ludewig U, Neuhäuser B. 2020. A twin histidine motif is the core structure for high-affinity substrate selection in plant ammonium transporters. *Journal of Biological Chemistry* **295**:3362–3370. DOI: https://doi.org/10.1074/jbc.RA119.010891, PMID: 31988244

Gietz D, Jean AS, Woods RA, Schiestl RH. 1992. Improved method for high efficiency transformation of intact yeast cells. *Nucleic Acids Research* **20**:1425. DOI: https://doi.org/10.1093/nar/20.6.1425

Gruswitz F, Chaudhary S, Ho JD, Schlessinger A, Pezeshki B, Ho C-M, Sali A, Westhoff CM, Stroud RM. 2010. Function of human Rh based on structure of RhCG at 2.1 A. *PNAS* **107**:9638–9643. DOI: https://doi.org/10.1073/pnas.1003587107

Hall JA, Yan D. 2013. The molecular basis of K+ exclusion by the *Escherichia coli* ammonium channel AmtB. *The Journal of Biological Chemistry* **288**:14080–14086. DOI: https://doi.org/10.1074/jbc.M113.457952, PMID: 23546877

Hess B, Bekker H, Berendsen HJC, Fraaije JGEM. 1997. LINCS: a linear constraint solver for molecular simulations. *Journal of Computational Chemistry* **18**:1463–1472. DOI: https://doi.org/10.1002/(SICI)1096-987X(199709)18:12<1463::AID-JCC4>3.0.CO;2-H

Hoopen Ft, Cuin TA, Pedas P, Hegelund JN, Shabala S, Schjoerring JK, Jahn TP. 2010. Competition between uptake of ammonium and potassium in barley and Arabidopsis roots: molecular mechanisms and physiological consequences. *Journal of Experimental Botany* **61**:2303–2315. DOI: https://doi.org/10.1093/jxb/erq057

Huang C-H, Ye M. 2010. The Rh protein family: gene evolution, membrane biology, and disease association. *Cellular and Molecular Life Sciences* **67**:1203–1218. DOI: https://doi.org/10.1007/s00018-009-0217-x

Hub JS, de Groot BL, van der Spoel D. 2010a. g_wham—A Free Weighted Histogram Analysis Implementation Including Robust Error and Autocorrelation Estimates. *Journal of Chemical Theory and Computation* **6**:3713–3720. DOI: https://doi.org/10.1021/ct100494z

Hub JS, Winkler FK, Merrick M, de Groot BL. 2010b. Potentials of mean force and permeabilities for carbon dioxide, Ammonia, and water flux across a rhesus protein channel and lipid membranes. *Journal of the American Chemical Society* **132**:13251–13263. DOI: https://doi.org/10.1021/ja102133x, PMID: 20815391

Ishikita H, Knapp EW. 2007. Protonation states of Ammonia/ammonium in the hydrophobic pore of Ammonia transporter protein AmtB. *Journal of the American Chemical Society* **129**:1210–1215. DOI: https://doi.org/10.1021/ja066208n, PMID: 17263403

Jacobs P, Jauniaux J-C, Grenson M. 1980. A cis-dominant regulatory mutation linked to the argB-argC gene cluster in *Saccharomyces cerevisiae*. *Journal of Molecular Biology* **139**:691–704. DOI: https://doi.org/10.1016/0022-2836(80)90055-8

Javelle A, Severi E, Thornton J, Merrick M. 2004. Ammonium sensing in *Escherichia coli*. Role of the ammonium transporter AmtB and AmtB-GlnK complex formation. *The Journal of Biological Chemistry* **279**:8530–8538. DOI: https://doi.org/10.1074/jbc.M312399200, PMID: 14668330

Javelle A, Lupo D, Zheng L, Li XD, Winkler FK, Merrick M. 2006. An unusual twin-his arrangement in the pore of Ammonia channels is essential for substrate conductance. *Journal of Biological Chemistry* **281**:39492–39498. DOI: https://doi.org/10.1074/jbc.M608325200, PMID: 17040913

Jorgensen WL, Chandrasekhar J, Madura JD, Impey RW, Klein ML. 1983. Comparison of simple potential functions for simulating liquid water. *The Journal of Chemical Physics* **79**:926–935. DOI: https://doi.org/10.1063/1.445869

Kato M, Pisliakov AV, Warshel A. 2006. The barrier for proton transport in aquaporins as a challenge for electrostatic models: The role of protein relaxation in mutational calculations. *Proteins: Structure, Function, and Bioinformatics* **64**:829–844. DOI: https://doi.org/10.1002/prot.21012

Khademi S, O'Connell J, Remis J, Robles-Colmenares Y, Miercke LJ, Stroud RM. 2004. Mechanism of Ammonia transport by amt/MEP/Rh: structure of AmtB at 1.35 A. *Science* **305**:1587–1594. DOI: https://doi.org/10.1126/science.1101952, PMID: 15361618

Kopec W, Köpfer DA, Vickery ON, Bondarenko AS, Jansen TLC, de Groot BL, Zachariae U. 2018. Direct knock-on of desolvated ions governs strict ion selectivity in K^+ channels. *Nature Chemistry* **10**:813–820. DOI: https://doi.org/10.1038/s41557-018-0105-9

Kutzner C, Köpfer DA, Machtens JP, de Groot BL, Song C, Zachariae U. 2016. Insights into the function of ion channels by computational electrophysiology simulations. *Biochimica Et Biophysica Acta (BBA) - Biomembranes* **1858**:1741–1752. DOI: https://doi.org/10.1016/j.bbamem.2016.02.006, PMID: 26874204

Lamoureux G, Klein ML, Bernèche S. 2007. A stable water chain in the hydrophobic pore of the AmtB ammonium transporter. *Biophysical Journal* **92**:L82–L84. DOI: https://doi.org/10.1529/biophysj.106.102756, PMID: 17351012

Lee FS, Chu ZT, Warshel A. 1993. Microscopic and semimicroscopic calculations of electrostatic energies in proteins by the POLARIS and ENZYMIX programs. *Journal of Computational Chemistry* **14**:161–185. DOI: https://doi.org/10.1002/jcc.540140205

Lee J, Cheng X, Swails JM, Yeom MS, Eastman PK, Lemkul JA, Wei S, Buckner J, Jeong JC, Qi Y, Jo S, Pande VS, Case DA, Brooks CL, MacKerell AD, Klauda JB, Im W. 2016. CHARMM-GUI input generator for NAMD, GROMACS, AMBER, OpenMM, and CHARMM/OpenMM simulations using the CHARMM36 additive force field. *Journal of Chemical Theory and Computation* **12**:405–413. DOI: https://doi.org/10.1021/acs.jctc.5b00935, PMID: 26631602

Li X, Jayachandran S, Nguyen H-HT, Chan MK. 2007. Structure of the *Nitrosomonas europaea* Rh protein. *PNAS* **104**:19279–19284. DOI: https://doi.org/10.1073/pnas.0709710104

Ludewig U, von Wirén N, Frommer WB. 2002. Uniport of NH4+ by the root hair plasma membrane ammonium transporter LeAMT1;1. *Journal of Biological Chemistry* **277**:13548–13555. DOI: https://doi.org/10.1074/jbc.M200739200, PMID: 11821433

Lupo D, Li X-D, Durand A, Tomizaki T, Cherif-Zahar B, Matassi G, Merrick M, Winkler FK. 2007. The 1.3-A resolution structure of *Nitrosomonas europaea* Rh50 and mechanistic implications for NH3 transport by Rhesus family proteins. *PNAS* **104**:19303–19308. DOI: https://doi.org/10.1073/pnas.0706563104

Maeda K, Westerhoff HV, Kurata H, Boogerd FC. 2019. Ranking network mechanisms by how they fit diverse experiments and deciding on *E. coli*'s ammonium transport and assimilation network. *Npj Systems Biology and Applications* **5**:14. DOI: https://doi.org/10.1038/s41540-019-0091-6, PMID: 30993002

Marini AM, Soussi-Boudekou S, Vissers S, Andre B. 1997. A family of ammonium transporters in *Saccharomyces cerevisiae*. *Molecular and Cellular Biology* **17**:4282–4293. DOI: https://doi.org/10.1128/MCB.17.8.4282

Marini AM, Boeckstaens M, Benjelloun F, Chérif-Zahar B, André B. 2006. Structural involvement in substrate recognition of an essential aspartate residue conserved in Mep/Amt and Rh-type ammonium transporters. *Current Genetics* **49**:364–374. DOI: https://doi.org/10.1007/s00294-006-0062-5

Mayer M, Dynowski M, Ludewig U. 2006. Ammonium ion transport by the AMT/Rh homologue LeAMT1;1. *Biochemical Journal* **396**:431–437. DOI: https://doi.org/10.1042/BJ20060051

McDonald TR, Ward JM. 2016. Evolution of electrogenic ammonium transporters (AMTs). *Frontiers in Plant Science* **7**:352. DOI: https://doi.org/10.3389/fpls.2016.00352, PMID: 27066024

Mirandela GD, Tamburrino G, Hoskisson PA, Zachariae U, Javelle A. 2019. The lipid environment determines the activity of the *Escherichia coli* ammonium transporter AmtB. *The FASEB Journal* **33**:1989–1999. DOI: https://doi.org/10.1096/fj.201800782R, PMID: 30211659

Miroux B, Walker JE. 1996. Over-production of proteins *in Escherichia coli*: mutant hosts that allow synthesis of some membrane proteins and globular proteins at high levels. *Journal of Molecular Biology* **260**:289–298. DOI: https://doi.org/10.1006/jmbi.1996.0399, PMID: 8757792

Miyamoto S, Kollman PA. 1992. Settle: An analytical version of the SHAKE and RATTLE algorithm for rigid water models. *Journal of Computational Chemistry* **13**:952–962. DOI: https://doi.org/10.1002/jcc.540130805

Mumberg D, Muller R, Funk M. 1994. Regulatable promoters of *Saccharomyces cerevisiae*: comparison of transcriptional activity and their use for heterologous expression. *Nucleic Acids Research* **22**:5767–5768. DOI: https://doi.org/10.1093/nar/22.25.5767

Neuhäuser B, Dynowski M, Ludewig U. 2014. Switching substrate specificity of AMT/MEP/ Rh proteins. *Channels* **8**:496–502. DOI: https://doi.org/10.4161/19336950.2014.967618, PMID: 25483282

Nygaard TP, Rovira C, Peters GH, Jensen MØ. 2006. Ammonium recruitment and Ammonia transport by *E. coli* Ammonia channel AmtB. *Biophysical Journal* **91**:4401–4412. DOI: https://doi.org/10.1529/biophysj.106.089714, PMID: 17012311

Rentsch D, Laloi M, Rouhara I, Schmelzer E, Delrot S, Frommer WB. 1995. *NTR1* encodes a high affinity oligopeptide transporter in *Arabidopsis*. *FEBS Letters* **370**:264–268. DOI: https://doi.org/10.1016/0014-5793(95)00853-2

Sham YY, Chu ZT, Tao H, Warshel A. 2000. Examining methods for calculations of binding free energies: lra, LIE, PDLD-LRA, and PDLD/S-LRA calculations of ligands binding to an HIV protease. *Proteins: Structure, Function, and Genetics* **39**:393–407. DOI: https://doi.org/10.1002/(SICI)1097-0134(20000601)39:4<393::AID-PROT120>3.0.CO;2-H, PMID: 10813821

Smart OS, Neduvelil JG, Wang X, Wallace BA, Sansom MSP. 1996. HOLE: A program for the analysis of the pore dimensions of ion channel structural models. *Journal of Molecular Graphics* **14**:354–360. DOI: https://doi.org/10.1016/S0263-7855(97)00009-X

Thomas GH, Mullins JGL, Merrick M. 2000. Membrane topology of the Mep/Amt family of ammonium transporters. *Molecular Microbiology* **37**:331–344. DOI: https://doi.org/10.1046/j.1365-2958.2000.01994.x

Torrie GM, Valleau JP. 1977. Nonphysical sampling distributions in Monte Carlo free-energy estimation: Umbrella sampling. *Journal of Computational Physics* **23**:187–199. DOI: https://doi.org/10.1016/0021-9991(77)90121-8

van den Berg B, Chembath A, Jefferies D, Basle A, Khalid S, Rutherford JC. 2016. Structural basis for Mep2 ammonium transceptor activation by phosphorylation. *Nature Communications* **7**:11337. DOI: https://doi.org/10.1038/ncomms11337

Wacker T, Garcia-Celma JJ, Lewe P, Andrade SLA. 2014. Direct observation of electrogenic $NH4^+$ transport in ammonium transport (Amt) proteins. *PNAS* **111**:9995–10000. DOI: https://doi.org/10.1073/pnas.1406409111

Wang S, Orabi EA, Baday S, Bernèche S, Lamoureux G. 2012. Ammonium transporters achieve charge transfer by fragmenting their substrate. *Journal of the American Chemical Society* **134**:10419–10427. DOI: https://doi.org/10.1021/ja300129x, PMID: 22631217

Warshel A, King G. 1985. Polarization constraints in molecular dynamics simulation of aqueous solutions: The surface constraint all atom solvent (SCAAS) model. *Chemical Physics Letters* **121**:124–129. DOI: https://doi.org/10.1016/0009-2614(85)87168-2

Weidinger K, Neuhäuser B, Gilch S, Ludewig U, Meyer O, Schmidt I. 2007. Functional and physiological evidence for a rhesus-type Ammonia transporter in *Nitrosomonas europaea*. *FEMS Microbiology Letters* **273**:260–267. DOI: https://doi.org/10.1111/j.1574-6968.2007.00805.x, PMID: 17608700

Wiechert M, Beitz E. 2017. Mechanism of formate-nitrite transporters by dielectric shift of substrate acidity. *The EMBO Journal* **36**:949–958. DOI: https://doi.org/10.15252/embj.201695776, PMID: 28250043

Zheng L, Kostrewa D, Berneche S, Winkler FK, Li X-D. 2004. The mechanism of ammonia transport based on the crystal structure of AmtB of *Escherichia coli*. *PNAS* **101**:17090–17095. DOI: https://doi.org/10.1073/pnas.0406475101